SELF-FORCE ON POINT PARTICLES IN ORBIT AROUND A SCHWARZSCHILD BLACK HOLE

A Thesis
Presented to
The Faculty of Graduate Studies
of
The University of Guelph

by
ROLAND HAAS

In partial fulfilment of requirements
for the degree of
Doctor of Philosophy
August, 2008

ABSTRACT

SELF-FORCE ON POINT PARTICLES IN ORBIT AROUND A
SCHWARZSCHILD BLACK HOLE

Roland Haas   Advisor:
University of Guelph, 2008   Professor Eric Poisson

We examine the motion of a point scalar or electromagnetic charge in orbit around a
Schwarzschild black hole. As the particle moves it emits radiation and loses energy
and angular momentum to the radiation field. A small part of this radiation backscat-
ters from the curvature of spacetime and returns to the location of the particle. The
interaction of the particle with this radiation gives rise to a self-force acting on the
particle. Initially this self-force appears to be divergent at the position of the parti-
cle. Similar to the situation in quantum field theory, the field close to the particle
requires renormalization, separating a finite physical contribution from the infinite
renormalizable part. One way of handling the divergence in Schwarzschild spacetime
is the mode-sum scheme introduced by Barack and Ori [1, 2]. We apply their scheme
as well as the singular-regular decomposition of Detweiler and Whiting [3] to the
problem at hand. In doing so we calculate what are commonly called the regulariza-
tion parameters A, B, C and D, extending previous work that only included the A,
B and C terms. In the scalar, electromagnetic and gravitational cases we calculate
the regularization parameters for tetrad components of the field gradient, using only
manifestly scalar quantities in the regularization. We also implement a numerical
scheme to calculate the modes of the full retarded field for the scalar and electro-
magnetic cases. The gravitational case is left for future work, but could employ the
same methods. To this end we use the characteristic grid evolution scheme of Price
and Lousto [4, 5]. In the scalar case we implement a fourth order finite-difference
scheme to calculate the retarded field. Our code can handle both circular and highly
eccentric orbits around the black hole. In the electromagnetic case we only implement
a second order accurate scheme to avoid the technical complexities of a fourth-order
accurate code. We examine the influence of the conservative part of the self-force on
the constants of motion along the orbit.

Acknowledgements

I would like to thank my advisor Eric Poisson for his advise and support during the course of my PhD research. Much of this work would have never been completed without his suggestions and help. Thank you, Eric.

I would like to thank the members of my examination committee Eric Poisson, Bernie Nickel, Carlos Lousto, Robert Wickham, and Paul Garrett. Special thanks to my external examiner Carlos Lousto on whose work my numerical method is based.

Finally many thanks to all my fellow students in Guelph who have made my stay here so enjoyable.

This work was made possible by the facilities of the Shared Hierarchical Academic Research Computing Network (SHARCNET:`www.sharcnet.ca`).

Sit up straight

"Piled Higher and Deeper" by Jorge Cham, `www.phdcomics.com`

Ladies and Gentlemen of the 1999 incoming masters program: sit up straight. If I could offer you one tip for the future, sitting up straight would be it.

Get to know your thesis committee members. You never know when they are going to go on sabbatical.

Do not read journal papers. They will only make you feel stupid.

Live in Escondido Village once. But leave before it makes you hard.

Live in Rains once. But leave before it makes you soft.

Don't waste time forwarding emails. Sometimes they're funny, sometimes they're not.

The Ph.D. is long and, in the end, you probably won't earn as much as your friends who didn't go to grad school.

You are not as lazy as you think.

Don't worry about publishing. Or worry, knowing that worrying is as effective as trying to convince your adviser he/she may be wrong.

Nap.

Accept certain inalienable truths: food is not free. Professors will belittle. You too will grow bitter and when you do, you'll fantasize that when you were a master's student food was free and your professors listened to you.

Try to date.

Maybe you'll graduate, maybe you won't. Maybe you'll contribute to society, maybe you won't. Maybe you'll be hooded, maybe you'll drop out and get a life. Whatever you do, don't work too hard. Your thesis topic is half made up. So is everybody else's.

But trust me on sitting up straight.

Contents

List of Tables

List of Figures

WRITING YOUR THESIS OUTLINE   NOTHING SAYS "I'M ALMOST DONE" TO YOUR ADVISOR/ SPOUSE/PARENTS LIKE PRETENDING YOU HAVE A PLAN

STEP 1   Aim for a respectable number of chapters:

THESIS OUTLINE
1.
2.
3.
4.
5.   chapter
6.   #'s
7.

5   = "That's IT??"
6-7 = "Not bad"
8+ = "Are you crazy??"

STEP 2   Fill in the "freebies":

THESIS OUTLINE
1. INTRODUCTION
2. LIT REVIEW
3. METHODOLOGY
4.
5.
6.
7. CONCLUSIONS

You're half way done!

STEP 3   Make up titles for the "meat" chapters:

2. LIT REVIEW
3. METHODOLOGY
4. (THAT STUFF YOU DID YOUR FIRST YEAR)
5. (STUFF YOU'RE SUPPOSED TO BE DOING NOW)
6. (MAKE STUFF UP)
7. CONCLUSIONS

(It'll be years before you actually have to work on that later chapter, and by then your thesis topic will have changed anyway)

STEP 4   Voilá! You just bought yourself another two years

So, how's your thesis going?
i have an outline!

JORGE CHAM © 2006

www.phdcomics.com

"Piled Higher and Deeper" by Jorge Cham, www.phdcomics.com

Chapter 1

Introduction

1.1   Particle motion and self-force

In the test mass limit of general relativity or the test charge limit of electromagnetism the object moves in a fixed background. The influence of the test object on the background is neglected and it moves on a geodesic of the background spacetime. Going beyond the test charge limit, this is no longer true. An electromagnetic or scalar charge moving around a black hole will emit radiation, part of which backscatters to the particle's location and interacts with it. This interaction gives rise to a self-force acting on the particle which dissipates energy and angular momentum. Therefore even in the test *mass* limit a charged object does not move on a geodesic. For an uncharged massive particle similar effects lead to the appearance of a self-force in the context of gravitational perturbation theory. While the particle still moves on a geodesic of the perturbed spacetime generated by it and the central black hole, it moves on an accelerated world line when its motion is described in terms of the background black hole geometry.

In this thesis we calculate the self-force acting on a scalar or electromagnetic charge moving along a prescribed geodesic orbit around a Schwarzschild black hole. This falls short of a full self-consistent calculation of the self-force since we do not let the self-force modify the motion of the particle. Instead the force we calculate should be interpreted as (minus) the force required to counteract the self-force and keep the particle on its geodesic orbit.

1.2 History of self-force calculations

The study of the self-force acting on a point like object is by no means a new field of research. Its roots reach back to the pioneering work of Abraham [6], Lorentz [7] and Dirac [8]. Dirac's work is the first to treat the electron as a point particle and his treatment of the problem forms the basis of the modern treatments. Dirac's results are derived in the context of special relativity. Using energy and momentum balance across a world tube surrounding the electron he derived its equations of motion. His well known result from this consideration is that the regularized self-force acting on the electron is given by

$$m\dot{v}_\mu = ev_\nu f_\mu{}^\nu, \quad f^{\mu\nu} = F_{\text{in}}^{\mu\nu} + \frac{1}{2}(F_{\text{ret}}^{\mu\nu} - F_{\text{adv}}^{\mu\nu}), \tag{1.1}$$

he half-retarded minus half-advanced force. Here m is the particle's mass, v^μ is its four velocity, an overdot denotes derivatives with respect to proper time along the orbit, $F_{\text{in}}^{\mu\nu}$ is the Faraday tensor of the external electromagnetic field and $F_{\text{ret/adv}}$ are the retarded and advanced Faraday tensors of the perturbation (see section 5.2.5).

De Witt and Brehme [9] and Hobbs [10] extended Dirac's treatment to curved spacetime. They find that the half-retarded minus half-advanced force, while finite at the location of the particle, does not give the proper self-force acting on the particle. Instead a tail term encoding contributions from waves travelling within the past light cone appears. The self-force depends, at least in principle, on the entire past history of the particle.

No results for the gravitational self-force were known until Mino, Sasaki and Tanaka [11] and independently Quinn and Wald [12] derived equations, known as the MiSaTaQuWa equations, for the gravitational self-force acting on a point mass. Mino, Sasaki and Tanaka provide two independent derivations. One based on [9] and one based on matched asymptotic expansion. Quinn and Wald's method is built around a set of physically motivated axioms supplementing the usual equations of motion. All three methods yield identical results. Recently several authors [13, 14] have reproduced these results using effective field theory methods and by considering the point particle limit of extended bodies.

The standard formulation of the self-force equations in all three cases requires a split of the retarded field into direct and tail pieces which lacks a physical interpretation as simple and intuitive as the one Dirac gave in his approach. Detweiler and Whiting [3] gave an alternative decomposition of the retarded field into a singular field and a regular remainder, equivalent, but not identical to the older decomposition into direct and tail pieces. Both the singular and the regular fields are solutions to the wave equation. The regular field corresponds to Dirac's radiation field, which is solely responsible for the interaction between the particle and the field.

To employ the MiSaTaQuWa equations in a practical calculation is still a difficult task since they involve Green functions in curved spacetime and an integral over the past history of the particle. Barack and Ori [1] and independently Mino, Nakano and Sasaki [15] developed a practical calculation scheme based on a mode sum decomposition. Calculations of the self-force on infalling massive particles [16] and

frequency domain calculation of the force on scalar particles on a circular orbit around Schwarzschild black holes [17] followed soon afterwards. Detweiler, Messaritaki and Whiting [18] implemented their singular-regular formalism for scalar charges on a circular orbit. Barack and Lousto [19] implemented a time domain code based on [4] to calculate the retarded gravitational perturbation for a particle on circular orbit in Schwarzschild spacetime. Recently Barack and Sago [20] completed the calculation of the gravitational self-force on circular orbits in Schwarzschild. The same group [21] is working towards implementing the mode sum scheme in Kerr spacetime. Alternative methods directly regularizing the Weyl scalars are also under investigation [22].

All the previous works were restricted to self-forces evaluated on circular orbits. This thesis reports work first published in [23, 24], and work to be published that generalizes the calculations to arbitrary geodesic motion around a Schwarzschild black hole. We develop analytical techniques to implement the mode-sum calculation of the self-force, and we develop time-domain numerical techniques to integrate the scalar and electromagnetic wave equations. Combining the ingredients we calculate the scalar and electromagnetic self-force.

1.3 LISA mission

The *Laser Interferometer Space Antenna* is a planned (planned launch date 2018) space-based gravitational wave detector to be operated jointly by ESA and NASA [25]. Its sensitivity band will span the frequency band of $0.1\,\mathrm{mHz} < \nu < 0.1\,\mathrm{Hz}$, complementing Earth based detectors such as LIGO, VIRGO, GEO and TAMA [26] which are typically sensitive to frequencies in the $50\,\mathrm{Hz} < \nu < 4\,\mathrm{kHz}$ band.

LISA consists of three identical spacecrafts that follow the Earth on its orbit lagging behind by 23°. The spacecrafts sit at the vertices of an equilateral triangle whose arms form three Michelson interferometers. The interferometers are used to measure the displacement of test masses within the bodies of the spacecrafts due to the passage of gravitational waves. Since the displacement of the test masses initially scales with the arm length, LISA's increased arm length when compared to Earth based detectors makes it much more sensitive to gravitational waves, raising the signal to noise ratio. Further the comparatively quiet environment in space allows LISA to look for waves in a frequency band forbidden to Earth based detectors due to seismic noise. Sources for LISA include [27] binary white dwarf systems in the Milky Way, massive black hole mergers and finally *extreme mass ratio inspirals* (EMRI) where a solar mass object spirals into a massive black hole. Of these sources the white dwarf binaries are by far the most abundant ones, a fact which is both a blessing and a curse. They form guaranteed sources for LISA, allowing for a fundamental test of the equipment and the existence of gravitational waves. On the other hand, seen from the viewpoint of EMRI's, the white dwarf binary signals are noise that has to be dealt with.

LISA's science goal is the test of Einstein's theory of general relativity. If LISA measures no gravitational waves or waves whose properties differ from those predicted by general relativity, then the theory must be wrong. Beyond just falsifying the theory

LISA will allow for the first time precision measurements of black hole parameters. EMRIs [27] will allow us to map out the spacetime metric of the central object and to determine the mass and angular momentum of the central black hole to one part in 10^4. Similarly the statistical distribution of the binary white dwarf signals will allow us to make deductions about the distribution of stars in our galaxy.

1.4   Motivation

The inspiral and capture of solar-mass compact objects by supermassive black holes is one of the most promising and interesting sources of gravitational radiation to be detected by LISA. Such a system consists of a supermassive black hole of mass $10^4 \, M_\odot - 10^6 \, M_\odot$, such as the ones found at the centre of galaxies, which is orbited by a small, compact $1 \, M_\odot - 10 \, M_\odot$ object, such as a neutron star or a small black hole. These systems form if a star in the halo surrounding the central black hole of a galaxy is driven from its orbit by interacting with nearby stars and enters an inspiralling orbit towards the black hole. During its inspiral the small object serves as a probe for the local spacetime geometry. Information about it is encoded in the waves that are emitted by the system which can therefore be used can be used to map out the spacetime. This reconstruction of the spacetime parameters becomes more accurate the longer the observed wavetrain is, that is the longer the systems emits waves that lie within LISA's window of sensitivity. For an extreme mass ratio system we expect to see about 10^5 wave cycles per year, which is sufficient to accurately pin down the parameters describing the central black hole.

In order to detect the weak EMRI signal in the noisy LISA data stream a hierarchical search algorithm whose final stage consists of a matched filtering has been proposed [28]. This last phase requires accurate templates which are convoluted with the data stream. If there is a high degree of correlation, then a signal due to a system matching the parameters that were used to generate the template is present in the data, with high probability. For this parameter extraction to be possible, however, the template must stay in phase with the waveform throughout the inspiral, requiring very accurate templates. Due to the small mass ratio between the star and the central black hole, a perturbative analysis that treats the compact object as a point mass can be employed to reach this accuracy.

In such a treatment the motion of the particle is described in the background spacetime of the *unperturbed* central black hole. In this description the particle no longer moves on a geodesic as it did in the perturbed spacetime. Instead its failure to move on a geodesic is interpreted as the effect of a self-force acting on the particle. The self-force is responsible for the particle's losses of energy and angular momentum, which will drive the inspiral towards the black hole.

Any self-consistent calculation of the inspiral and the waveforms emitted during the inspiral has to take this self-force into account. Neglecting it, an observer at infinity would detect energy and angular momentum in the gravitational waves without the source losing equal amounts of energy and angular momentum, violating conservation statements. Also, for parameter extraction purposes the predicted waveforms

would quickly run out of phase with the real waves.

Of the various methods to generate templates discussed in [29, 30] only the wave-forms calculated by directly involving the self-force are able to achieve this accuracy. Waveforms generated by other methods (for example energy balance arguments) are useful for detection, but cannot be used for parameter extraction. Therefore a practical calculation of the motion governed by the MiSaTaQuWa equation and the waves generated by it are of great astrophysical interest.

1.5   This thesis

This thesis is part of the ongoing effort to provide waveform templates for LISA which include the effects of the self-force. Including these effects is crucial in any scheme that aims to extract black hole parameters from the experimental data. The holy grail is the calculation of the waveforms generated by a point mass in orbit around a Kerr black hole including the influence of its self-force. So far this has proved to be an elusive goal, although there is now a concerted effort by several groups to the tackle first steps towards a concrete calculation of the self-force in the Kerr spacetime [20, 31, 22].

Rather than trying to solve the problem directly, in this thesis we retreat to the technically simpler problem of a point particle of mass m endowed with a scalar or electric charge q orbiting a Schwarzschild black hole of mass M; the particle emits scalar or electromagnetic radiation, and it is affected by a scalar or electromagnetic self-force. We implement for the first time a complete calculation of the self-force on fixed geodesic orbits. We use the regularization procedure of [1, 2] to calculate regularization parameters for the three cases of a scalar charge, an electric charge and a small mass. We solve the scalar and electromagnetic wave equations using a second- or fourth-order finite-difference scheme based on [4, 5].

Since the particle motion is prescribed a priory, we do not implement a full self-force calculation that lets the force modify the motion of the particle. Instead the force we calculate should be interpreted as (minus) the force necessary to keep the particle on the geodesic orbit, to counteract the action of the self-force. For the electromagnetic and scalar fields considered here, this can always be achieved by imagining some external non-electromagnetic or non-scalar agent to provide this force. For gravity such an approach invariable leads to the occurrence of a "strut", a conical singularity in spacetime which is responsible for the required force.

Nevertheless we can use our results to draw conclusions on the physical effect of the self-force, since the departure from the given geodesic to accelerated motion is a slow process occurring on timescales of the order of a radiation reaction time.

We find that the self-force generically dissipates energy and angular momentum as expected, and we find that the radial part of the self-force points away from the black hole. In fact, for the scalar case Diaz-Rivera, Messaritaki, Whiting and Detweiler [32] showed that the effect of the conservative self-force is to move the innermost stable orbit closer to the black hole. We perform a similar analysis for eccentric orbits of an electromagnetic charge. We find that the effect of the conservative piece of the

self-force is important.

1.6   Organization

Chapter 2 introduces the theoretical concepts which this work is based on. We do not aim to give a thorough treatment of the topics covered; instead we give just enough information to understand the origin of the formulae used in this thesis. We begin with a short review of bi-tensors in curved spacetime. We introduce Synge's world function $\sigma(x, x')$, the parallel propagator $g^{\alpha'}{}_{\beta}(x, x')$ and methods to covariantly expand bi-tensors around a point x. In this we follow the treatment in [33]. We further introduce the concept of retarded and advanced Green functions in curved spacetime and derive a formal expression for the singular field of the particle.

Chapter 3 contains our first set of results, regularization parameters for a particle on arbitrary geodesic orbits of Schwarzschild spacetime. To meet this goal we find an expansion of the singular field around the position of the particle. We display results for the three cases of scalar, electromagnetic and gravitational fields. In appendix E we also outline the changes required to accommodate an accelerated world line and display regularization parameters for this case too.

Chapter 4 describes the numerical methods we used to calculate the modes of the scalar and electromagnetic fields, respectively. In the first part of the chapter we describe the second and fourth-order finite-difference finite-difference schemes that were used in the scalar case. In the second part we introduce the second-order finite-difference schemes that were used in the electromagnetic case. We implement schemes to calculate either the vector potential A_α or the Faraday tensor $F_{\alpha\beta}$. The first method closely parallels the treatment necessary for gravity, while the second serves as an independent test of the numerical method. We also present results of numerical tests of the convergence properties of our code.

Chapter 5 contains our main results for the scalar and electromagnetic self-forces. We calculate each self-force for selected orbits and verify that analytical and numerical calculations tie into each other as expected. We also display results for the effect of the conservative self-force on the orbital parameters in the electromagnetic case.

Chapter 6 gives some concluding remarks and suggests future projects.

Appendix A reviews the symbols used in the thesis and further appendices contain technical results that need not be presented in the main text.

What your research supposedly looks like:

Data → Data Acquisition

Prototype ← Controller ← Computer
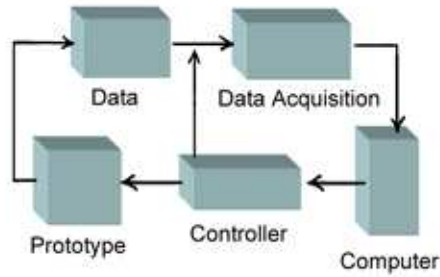
Figure 1. Experimental Diagram

What your research *actually* looks like:

Figure 2. Experimental Mess

JORGE CHAM © 2008

WWW.PHDCOMICS.COM

"Piled Higher and Deeper" by Jorge Cham, `www.phdcomics.com`

Chapter 2

Theoretical framework

In this section we introduce the methods and concepts used in the remainder of the thesis. Almost all of the material in this section can be found in [33].

2.1 Bi-tensors in curved spacetime

When dealing with Green functions in curved spacetime, as we will do later in this section, it is advantageous to introduce the concept of *bi-tensors*, tensor valued functions of two coordinates x and $\bar{x}$ as done in [33]. Such a function can have different tensorial structures at the two points, for example it can be a vector at x but a scalar at $\bar{x}$. We use this fact extensively in our calculation. We will require that x and $\bar{x}$ are in a normal neighbourhood of each other, implying that for any two points there is a unique geodesic

$$\beta : \lambda \mapsto z^\mu(\lambda) \tag{2.1}$$

parametrized by an affine parameter λ which links links them together as indicated in Fig. 2.1.

2.1.1 Synge's world function

A particularly useful bi-tensor is Synge's world function $\sigma(x, \bar{x})$, which is numerically equal to half the squared geodesic distance between x and $\bar{x}$. In terms of the tangent vector $t^\mu \equiv \frac{\mathrm{d}z^\mu}{\mathrm{d}\lambda}$ along the (unique) geodesic linking the two points, the world function
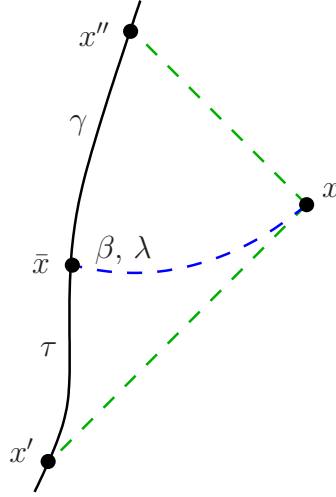
Figure 2.1: World line γ of the particle and geodesic β linking the field point x off the world line with the point $\bar{x}$ on the world line. Also shown are the retarded x' and advanced points x''.

can be written as

$$\sigma(x, \bar{x}) = \frac{1}{2}(\lambda_1 - \lambda_0) \int_{\lambda_0}^{\lambda_1} g_{\mu\nu} t^\mu t^\nu \, d\lambda = \frac{1}{2}\varsigma(\lambda_1 - \lambda_0)^2 \,, \tag{2.2}$$

where $z(\lambda_0) = \bar{x}$, $z(\lambda_1) = x$ and

$$\varsigma \equiv g_{\mu\nu} t^\mu t^\nu = \pm 1, 0 \,, \tag{2.3}$$

along spacelike, timelike and null geodesics respectively.

Derivatives of the world function

Since σ is a bi-scalar distinct derivatives with respect to x and $\bar{x}$ can be defined,

$$\sigma_\alpha \equiv \frac{\partial \sigma}{\partial x^\alpha} \,, \quad \sigma_{\bar{\alpha}} \equiv \frac{\partial \sigma}{\partial x^{\bar{\alpha}}} \,. \tag{2.4}$$

Here and in the following, unbarred indices α, β, ... refer to tensors at x while barred indices $\bar{\alpha}$, $\bar{\beta}$, ... refer to tensors at $\bar{x}$. Indices μ, ν, ... refer to a generic point on the geodesic. Similar to the first derivatives defined in Eq. (2.4) higher derivatives of any order can be defined; for example

$$\sigma_{\alpha\beta\bar{\gamma}} \equiv \nabla_{\bar{\gamma}} \nabla_\beta \nabla_\alpha \sigma \,, \tag{2.5}$$

which is a two-tensor at x and a (dual-)vector at $\bar{x}$.

Poisson [33] derives an expression linking the derivative of $\sigma(x, \bar{x})$ to the tangent vector of the geodesic linking x and $\bar{x}$, his Eqs. (55) and (56). They read

$$\sigma_\alpha = (\lambda_1 - \lambda_0) t_\alpha \,, \tag{2.6a}$$

and

$$\sigma_{\bar{\alpha}} = -(\lambda_1 - \lambda_0)t_{\bar{\alpha}}\,. \tag{2.6b}$$

Up to the factor involving the difference in the affine parameter, σ_α and $\sigma_{\bar{\alpha}}$ are the tangent vectors along the geodesic at x or $\bar{x}$.

Interestingly, we can express the world function in terms of its derivatives. Comparing Eq. (2.2) and Eqs. (2.6a), (2.6b) it is easy to see that

$$g^{\alpha\beta}\sigma_\alpha\sigma_\beta = 2\sigma\,, \quad \text{and} \quad g^{\bar{\alpha}\bar{\beta}}\sigma_{\bar{\alpha}}\sigma_{\bar{\beta}} = 2\sigma\,. \tag{2.7}$$

We will use this relationship extensively in section 2.2.1 to derive coincidence limits for σ and its derivatives.

2.1.2 Parallel propagator

A tensor $T^\mu{}_\nu$ of arbitrary index structure is said to be parallel transported along a geodesic β if along β

$$T^\mu{}_{\nu;\lambda}t^\lambda = 0\,. \tag{2.8}$$

Its behaviour along the geodesic is completely described by the action of the parallel propagator $g^\alpha{}_{\bar{\alpha}}$ defined in terms of the change of an arbitrary vector parallel transported from $\bar{x}$ to x

$$v^\alpha \equiv g^\alpha{}_{\bar{\alpha}}v^{\bar{\alpha}}\,. \tag{2.9}$$

This is well defined as a linear map from vectors at $\bar{x}$ to vectors at x since the parallel transport equation (2.8) is linear. Similarly, a parallel propagator transporting vectors from x to $\bar{x}$ can be defined via

$$v^{\bar{\alpha}} \equiv g^{\bar{\alpha}}{}_\alpha v^\alpha\,. \tag{2.10}$$

Clearly parallel transporting a vector from x to $\bar{x}$ and back to x is an identity operation that does not change the vector. Hence

$$g^\alpha{}_{\bar{\alpha}}g^{\bar{\alpha}}{}_\beta = \delta^\alpha{}_\beta\,, \quad \text{and} \quad g^{\bar{\alpha}}{}_\alpha g^\alpha{}_{\bar{\alpha}} = \delta^{\bar{\alpha}}{}_{\bar{\beta}}\,. \tag{2.11}$$

Similarly the parallel propagator itself is parallel transported along the geodesic, so

$$g^{\bar{\alpha}}{}_{\alpha;\beta}t^\beta = g^{\bar{\alpha}}{}_{\alpha;\bar{\beta}}t^{\bar{\beta}} = 0\,, \quad g^\alpha{}_{\bar{\alpha};\beta}t^\beta = g^\alpha{}_{\bar{\alpha};\bar{\beta}}t^{\bar{\beta}} = 0\,. \tag{2.12}$$

This property becomes obvious if one considers (for a parallel transported vector v^μ)

$$0 = v^\alpha{}_{;\beta}t^\beta = \left(g^\alpha{}_{\bar{\alpha}}v^{\bar{\alpha}}\right)_{;\beta}t^\beta = g^\alpha{}_{\bar{\alpha};\beta}t^\beta v^{\bar{\alpha}}\,, \tag{2.13}$$

which yields the proposition since v^μ is arbitrary.

Note that these properties can be formally proved using a tetrad $e^{(\mu)}{}_\alpha$ parallel transported along the geodesic and writing the parallel propagator as

$$g^\alpha{}_{\bar{\alpha}} = e^{(\mu)}{}_\alpha e^{\bar{\alpha}}{}_{(\mu)} \tag{2.14}$$

in terms of the tetrad and its dual [33].

2.2 Covariant expansion of bi-tensors

Since we are eventually interested in an expansion of the (scalar, electromagnetic and gravitational) fields around a base point $\bar{x}$, we need expansions of bi-tensors that are similar to Taylor expansions in flat spacetime. Given that $\sigma_{\bar{\alpha}}$ is the closest thing to a distance vector $(x - \bar{x})^\alpha$, we seek an expansion in terms of $\sigma_{\bar{\alpha}}$.

2.2.1 Coincidence limits

In finding expansions for bi-tensors around $\bar{x}$ we will require the values of the tensor and its derivatives at coincidence $x = \bar{x}$, which we denote by

$$[T_{\mu\nu}(x, \bar{x})] \equiv \lim_{x \to \bar{x}} T_{\mu\nu}(x, \bar{x}) \,. \tag{2.15}$$

Further we need expressions for the coincidence limits of $\sigma_{\bar{\alpha}}$ and its derivatives as well as $g^\alpha{}_{\bar{\alpha}}$ and its derivatives. These are derived in [33] by continued differentiations of Eqs. (2.7), (2.12) and careful use of Synge's rule

$$[\sigma_{\dots\bar{\alpha}}] = [\sigma_{\dots}]_{;\bar{\alpha}} - [\sigma_{\dots\alpha}] \,, \tag{2.16}$$

where "$\cdots$" is any combination of barred and unbarred indices. A proof of Synge's rule can be found in [33].

Clearly, from Eqs. (2.2), (2.6a), (2.6b), the world function and its first derivatives vanish at coincidence

$$[\sigma] = 0 \,, \quad [\sigma_\alpha] = 0 \,, \quad \text{and} \quad [\sigma_{\bar{\alpha}}] = 0 \,. \tag{2.17}$$

The remaining coincidence limits are

$$[\sigma_{\alpha\beta}] = g_{\bar{\alpha}\bar{\beta}} \,, \tag{2.18a}$$

$$[\sigma_{\alpha\bar{\beta}}] = [\sigma_\alpha]_{;\bar{\beta}} - [\sigma_{\alpha\beta}] = -g_{\bar{\alpha}\bar{\beta}} \,, \tag{2.18b}$$

$$[\sigma_{\bar{\alpha}\bar{\beta}}] = [\sigma_{\bar{\alpha}}]_{;\bar{\beta}} - [\sigma_{\bar{\alpha}\beta}] = g_{\bar{\alpha}\bar{\beta}} \,, \tag{2.18c}$$

and

$$[\sigma_{\bar{\alpha}\beta}] = [\sigma_{\beta\bar{\alpha}}] = -g_{\bar{\alpha}\bar{\beta}} \,. \tag{2.18d}$$

As well as

$$[\sigma_{\alpha\beta\gamma}] = [\sigma_{\alpha\beta\bar{\gamma}}] = [\sigma_{\alpha\bar{\beta}\bar{\gamma}}] = [\sigma_{\bar{\alpha}\bar{\beta}\bar{\gamma}}] = 0 \,. \tag{2.19}$$

Finally using

$$\sigma_{\alpha\beta\gamma\delta} = \sigma^\varepsilon{}_{\alpha\beta\gamma\delta}\sigma_\varepsilon + \sigma^\varepsilon{}_{\alpha\beta\gamma}\sigma_{\varepsilon\delta} + \sigma^\varepsilon{}_{\alpha\beta\delta}\sigma_{\varepsilon\gamma} + \sigma^\varepsilon{}_{\alpha\beta\beta}\sigma_{\varepsilon\beta}$$
$$+ \sigma^\varepsilon{}_{\alpha\beta}\sigma_{\varepsilon\gamma\delta} + \sigma^\varepsilon{}_{\alpha\gamma}\sigma_{\varepsilon\beta\delta} + \sigma^\varepsilon{}_{\alpha\delta}\sigma_{\varepsilon\beta\gamma} + \sigma^\varepsilon{}_\alpha\sigma_{\varepsilon\beta\gamma\delta} \,, \tag{2.20}$$

the coincidence limits for $\sigma_{\alpha\beta\gamma\delta}$ are

$$[\sigma_{\alpha\beta\gamma\delta}] = -\frac{1}{3}\left(R_{\bar{\alpha}\bar{\gamma}\bar{\beta}\bar{\delta}} + R_{\bar{\alpha}\bar{\delta}\bar{\beta}\bar{\gamma}}\right) \,, \tag{2.21a}$$

$$[\sigma_{\alpha\beta\gamma\bar{\delta}}] = \frac{1}{3}\left(R_{\bar{\alpha}\bar{\gamma}\bar{\beta}\bar{\delta}} + R_{\bar{\alpha}\bar{\delta}\bar{\beta}\bar{\gamma}}\right) \,, \tag{2.21b}$$

$$[\sigma_{\alpha\beta\bar{\gamma}\bar{\delta}}] = -\frac{1}{3}\left(R_{\bar{\alpha}\bar{\gamma}\bar{\beta}\bar{\delta}} + R_{\bar{\alpha}\bar{\delta}\bar{\beta}\bar{\gamma}}\right) \,, \tag{2.21c}$$

$$[\sigma_{\alpha\bar{\beta}\bar{\gamma}\bar{\delta}}] = -\frac{1}{3}\left(R_{\bar{\alpha}\bar{\beta}\bar{\gamma}\bar{\delta}} + R_{\bar{\alpha}\bar{\gamma}\bar{\beta}\bar{\delta}}\right) \,, \tag{2.21d}$$

and

$$\left[\sigma_{\bar{\alpha}\bar{\beta}\bar{\gamma}\bar{\delta}}\right] = -\frac{1}{3}\left(R_{\bar{\alpha}\bar{\gamma}\bar{\beta}\bar{\delta}} + R_{\bar{\alpha}\bar{\delta}\bar{\beta}\bar{\gamma}}\right). \tag{2.21e}$$

The last coincidence limit we require is for $\sigma_{\alpha\beta\gamma\delta\varepsilon}$ obtainable from taking four derivatives of Eq. (2.7). It is slightly easier to consider taking one additional derivative of Eq. (2.20) using the fact that at coincidence any terms containing σ_α and $\sigma_{\alpha\beta\gamma}$ vanish and a term $\sigma_{\alpha\beta}$ turns into the metric. Doing so we find

$$0 = \left[\sigma_{\varepsilon\alpha\beta\gamma\delta}\right] + \left[\sigma_{\alpha\delta\beta\gamma\varepsilon}\right] + \left[\sigma_{\alpha\gamma\beta\delta\varepsilon}\right] + \left[\sigma_{\alpha\beta\gamma\delta\varepsilon}\right], \tag{2.22}$$

and eventually after invoking Ricci's identity, the symmetries of the Riemann tensor and Synge's rule as done in [33] we find

$$\left[\sigma_{\alpha\beta\gamma\delta\varepsilon}\right] = -\frac{1}{4}\Big(R_{\bar{\alpha}\bar{\varepsilon}\bar{\beta}\bar{\gamma};\bar{\delta}} + R_{\bar{\alpha}\bar{\varepsilon}\bar{\beta}\bar{\delta};\bar{\gamma}} + R_{\bar{\alpha}\bar{\delta}\bar{\beta}\bar{\gamma};\bar{\varepsilon}} + R_{\bar{\alpha}\bar{\delta}\bar{\varepsilon};\bar{\gamma}} \\ + R_{\bar{\alpha}\bar{\gamma}\bar{\beta}\bar{\delta};\bar{\varepsilon}} + R_{\bar{\alpha}\bar{\gamma}\bar{\beta}\bar{\varepsilon};\bar{\delta}}\Big), \tag{2.23a}$$

$$\left[\sigma_{\alpha\bar{\beta}\gamma\delta\varepsilon}\right] = -\frac{1}{12}\Big(R_{\bar{\alpha}\bar{\delta}\bar{\gamma}\bar{\varepsilon};\bar{\beta}} + R_{\bar{\alpha}\bar{\varepsilon}\bar{\gamma}\bar{\delta};\bar{\beta}}\Big) + \frac{1}{4}\Big(R_{\bar{\alpha}\bar{\beta}\bar{\gamma}\bar{\delta};\bar{\varepsilon}} + R_{\bar{\alpha}\bar{\beta}\bar{\gamma}\bar{\delta};\bar{\varepsilon}}\Big) \\ + \frac{1}{4}\Big(R_{\bar{\alpha}\bar{\beta}\bar{\gamma}\bar{\varepsilon};\bar{\delta}} + R_{\bar{\alpha}\bar{\varepsilon}\bar{\gamma}\bar{\beta};\bar{\delta}}\Big), \tag{2.23b}$$

$$\left[\sigma_{\alpha\bar{\beta}\bar{\gamma}\delta\varepsilon}\right] = \frac{1}{12}\Big(R_{\bar{\alpha}\bar{\varepsilon}\bar{\delta}\bar{\gamma};\bar{\beta}} + R_{\bar{\alpha}\bar{\gamma}\bar{\delta}\bar{\varepsilon};\bar{\beta}}\Big) + \frac{1}{12}\Big(R_{\bar{\alpha}\bar{\varepsilon}\bar{\delta}\bar{\beta};\bar{\gamma}} + R_{\bar{\alpha}\bar{\beta}\bar{\delta}\bar{\varepsilon};\bar{\gamma}}\Big) \\ - \frac{1}{4}\Big(R_{\bar{\alpha}\bar{\beta}\bar{\delta}\bar{\gamma};\bar{\varepsilon}} + R_{\bar{\alpha}\bar{\gamma}\bar{\delta}\bar{\beta};\bar{\varepsilon}}\Big), \tag{2.23c}$$

$$\left[\sigma_{\alpha\bar{\beta}\bar{\gamma}\bar{\delta}\varepsilon}\right] = -\frac{1}{12}\Big(R_{\bar{\alpha}\bar{\beta}\bar{\varepsilon}\bar{\gamma};\bar{\delta}} + R_{\bar{\alpha}\bar{\gamma}\bar{\varepsilon}\bar{\beta};\bar{\delta}}\Big) - \frac{1}{12}\Big(R_{\bar{\alpha}\bar{\delta}\bar{\varepsilon}\bar{\gamma};\bar{\beta}} + R_{\bar{\alpha}\bar{\delta}\bar{\varepsilon}\bar{\gamma};\bar{\beta}}\Big) \\ - \frac{1}{12}\Big(R_{\bar{\alpha}\bar{\delta}\bar{\varepsilon}\bar{\beta};\bar{\gamma}} + R_{\bar{\alpha}\bar{\beta}\bar{\varepsilon}\bar{\delta};\bar{\gamma}}\Big), \tag{2.23d}$$

$$\left[\sigma_{\alpha\bar{\beta}\bar{\gamma}\bar{\delta}\bar{\varepsilon}}\right] = -\frac{1}{3}\Big(R_{\bar{\alpha}\bar{\beta}\bar{\gamma}\bar{\delta};\bar{\varepsilon}} + R_{\bar{\alpha}\bar{\gamma}\bar{\beta}\bar{\delta};\bar{\varepsilon}}\Big) + \frac{1}{12}\Big(R_{\bar{\alpha}\bar{\beta}\bar{\varepsilon}\bar{\gamma};\bar{\delta}} + R_{\bar{\alpha}\bar{\gamma}\bar{\varepsilon}\bar{\beta};\bar{\delta}}\Big) \\ + \frac{1}{12}\Big(R_{\bar{\alpha}\bar{\delta}\bar{\varepsilon}\bar{\gamma};\bar{\beta}} + R_{\bar{\alpha}\bar{\gamma}\bar{\varepsilon}\bar{\delta};\bar{\beta}}\Big) + \frac{1}{12}\Big(R_{\bar{\alpha}\bar{\delta}\bar{\varepsilon}\bar{\beta};\bar{\gamma}} + R_{\bar{\alpha}\bar{\beta}\bar{\varepsilon}\bar{\delta};\bar{\gamma}}\Big), \tag{2.23e}$$

and

$$\left[\sigma_{\bar{\alpha}\bar{\beta}\bar{\gamma}\bar{\delta}\varepsilon}\right] = -\frac{1}{4}\Big(R_{\bar{\alpha}\bar{\gamma}\bar{\beta}\bar{\delta};\bar{\varepsilon}} + R_{\bar{\alpha}\bar{\delta}\bar{\beta}\bar{\gamma};\bar{\varepsilon}}\Big) - \frac{1}{4}\Big(R_{\bar{\alpha}\bar{\varepsilon}\bar{\beta}\bar{\gamma};\bar{\delta}} + R_{\bar{\alpha}\bar{\gamma}\bar{\beta}\bar{\varepsilon};\bar{\delta}}\Big) \\ - \frac{1}{4}\Big(R_{\bar{\alpha}\bar{\varepsilon}\bar{\beta}\bar{\delta};\bar{\gamma}} + R_{\bar{\alpha}\bar{\delta}\bar{\beta}\bar{\varepsilon};\bar{\gamma}}\Big). \tag{2.23f}$$

Analogous expressions for the parallel propagator are found by starting from Eq. (2.12). It is found that

$$\left[g^\alpha{}_{\bar{\beta}}\right] = \delta^{\bar{\alpha}}{}_{\bar{\beta}}, \tag{2.24a}$$

$$\left[g^\alpha{}_{\bar{\beta};\gamma}\right] = \left[g^\alpha{}_{\bar{\beta};\bar{\gamma}}\right] = 0, \tag{2.24b}$$

$$\left[g^\alpha{}_{\bar{\beta};\gamma\delta}\right] = -\left[g^\alpha{}_{\bar{\beta};\gamma\delta}\right] = \left[g^\alpha{}_{\bar{\beta};\bar{\gamma}\delta}\right] = -\left[g^\alpha{}_{\bar{\beta};\bar{\gamma}\bar{\delta}}\right] = -\frac{1}{2}R^{\bar{\alpha}}{}_{\bar{\beta}\bar{\gamma}\bar{\delta}}, \tag{2.24c}$$

11

and

$$\left[g^{\alpha}{}_{\bar{\beta};\gamma\delta\varepsilon}\right] = -\frac{1}{3}\left(R^{\bar{\alpha}}{}_{\bar{\beta}\bar{\gamma}\bar{\delta};\bar{\varepsilon}} + R^{\bar{\alpha}}{}_{\bar{\beta}\bar{\gamma}\bar{\varepsilon};\bar{\delta}}\right),$$

$$\left[g^{\alpha}{}_{\bar{\beta};\gamma\delta\bar{\varepsilon}}\right] = -\frac{1}{6}R^{\bar{\alpha}}{}_{\bar{\beta}\bar{\gamma}\bar{\delta};\bar{\varepsilon}} + \frac{1}{3}R^{\bar{\alpha}}{}_{\bar{\beta}\bar{\gamma}\bar{\varepsilon};\bar{\delta}},$$

$$\left[g^{\alpha}{}_{\bar{\beta};\gamma\bar{\delta}\bar{\varepsilon}}\right] = \frac{1}{6}\left(R^{\bar{\alpha}}{}_{\bar{\beta}\bar{\gamma}\bar{\delta};\bar{\varepsilon}} + R^{\bar{\alpha}}{}_{\bar{\beta}\bar{\gamma}\bar{\varepsilon};\bar{\delta}}\right), \tag{2.24d}$$

$$\left[g^{\alpha}{}_{\bar{\beta};\bar{\gamma}\bar{\delta}\bar{\varepsilon}}\right] = \frac{1}{6}\left(R^{\bar{\alpha}}{}_{\bar{\beta}\bar{\gamma}\bar{\delta};\bar{\varepsilon}} R^{\bar{\alpha}}{}_{\bar{\beta}\bar{\gamma}\bar{\varepsilon};\bar{\delta}}\right).$$

2.2.2 Expansion of Bi-tensors

We have to expand the bi-tensor $T_{\bar{\alpha}\bar{\beta}}(x,\bar{x})$ around the base point $\bar{x}$. Since both indices are barred, $T_{\bar{\alpha}\bar{\beta}}$ is a scalar at x. An expansion of the form

$$T_{\bar{\alpha}\bar{\beta}} = A_{\bar{\alpha}\bar{\beta}} + A_{\bar{\alpha}\bar{\beta}\bar{\gamma}}\sigma^{\bar{\gamma}} + \frac{1}{2}A_{\bar{\alpha}\bar{\beta}\bar{\gamma}\bar{\delta}}\sigma^{\bar{\gamma}}\sigma^{\bar{\delta}} + \frac{1}{6}A_{\bar{\alpha}\bar{\beta}\bar{\gamma}\bar{\delta}\bar{\varepsilon}}\sigma^{\bar{\gamma}}\sigma^{\bar{\delta}}\sigma^{\bar{\varepsilon}} + \dots, \tag{2.25}$$

where the coefficients $A_{\bar{\alpha}\bar{\beta}}$ etc. are functions of the base point $\bar{x}$ only, can then be found [33]. The coefficients are found be evaluating Eq. (2.25) and its derivatives at coincidence. Doing so the coefficients read

$$A_{\bar{\alpha}\bar{\beta}} = \left[T_{\bar{\alpha}\bar{\beta}}\right], \tag{2.26a}$$

$$A_{\bar{\alpha}\bar{\beta}\bar{\gamma}} = \left[T_{\bar{\alpha}\bar{\beta};\bar{\gamma}}\right] - A_{\bar{\alpha}\bar{\beta};\bar{\gamma}}, \tag{2.26b}$$

$$A_{\bar{\alpha}\bar{\beta}\bar{\gamma}\bar{\delta}} = \left[T_{\bar{\alpha}\bar{\beta};\bar{\gamma}\bar{\delta}}\right] - A_{\bar{\alpha}\bar{\beta};\bar{\gamma}\bar{\delta}} - 2A_{\bar{\alpha}\bar{\beta}\bar{\gamma};\bar{\delta}}, \tag{2.26c}$$

and

$$A_{\bar{\alpha}\bar{\beta}\bar{\gamma}\bar{\delta}\bar{\varepsilon}} = \left[T_{\bar{\alpha}\bar{\beta};\bar{\gamma}\bar{\delta}\bar{\varepsilon}}\right] - A_{\bar{\alpha}\bar{\beta};\bar{\gamma}\bar{\delta}\bar{\varepsilon}} - 3A_{\bar{\alpha}\bar{\beta}\bar{\gamma};\bar{\delta}\bar{\varepsilon}} - 3A_{\bar{\alpha}\bar{\beta}\bar{\gamma}\bar{\delta};\bar{\varepsilon}}. \tag{2.26d}$$

Our expressions for the coefficients differ slightly from those found in [33] in that we have made use of the fact that the indices $\bar{\gamma}$, $\bar{\delta}$, and $\bar{\varepsilon}$ can be freely moved around since they are contracted with copies of $\sigma^{\bar{\alpha}}$, as well as symmetries of the Riemann tensor.

We next have to expand the bi-tensor $T_{\alpha\bar{\beta}}(x,\bar{x})$ around the base point $\bar{x}$. Since only one index is barred, $T_{\bar{\alpha}\beta}$ is a vector at x. Repeating the procedure outlined in [33] we define an auxiliary tensor $\tilde{T}_{\bar{\alpha}\bar{\beta}} \equiv g^{\alpha}{}_{\bar{\alpha}}T_{\alpha\bar{\beta}}$ to which the procedure of outlined above can be applied. We find expansion coefficients

$$B_{\bar{\alpha}\bar{\beta}} = \left[T_{\alpha\bar{\beta}}\right], \tag{2.27a}$$

$$B_{\bar{\alpha}\bar{\beta}\bar{\gamma}} = \left[T_{\alpha\bar{\beta};\bar{\gamma}}\right] - B_{\bar{\alpha}\bar{\beta};\bar{\gamma}}, \tag{2.27b}$$

$$B_{\bar{\alpha}\bar{\beta}\bar{\gamma}\bar{\delta}} = \left[T_{\alpha\bar{\beta};\bar{\gamma}\bar{\delta}}\right] - B_{\bar{\alpha}\bar{\beta};\bar{\gamma}\bar{\delta}} - 2B_{\bar{\alpha}\bar{\beta}\bar{\gamma};\bar{\delta}} \tag{2.27c}$$

and

$$B_{\bar{\alpha}\bar{\beta}\bar{\gamma}\bar{\delta}\bar{\varepsilon}} = \left[T_{\alpha\bar{\beta};\bar{\gamma}\bar{\delta}\bar{\varepsilon}}\right] - B_{\bar{\alpha}\bar{\beta};\bar{\gamma}\bar{\delta}\bar{\varepsilon}} - 3B_{\bar{\alpha}\bar{\beta}\bar{\gamma};\bar{\delta}\bar{\varepsilon}} - 3B_{\bar{\alpha}\bar{\beta}\bar{\gamma}\bar{\delta};\bar{\varepsilon}}, \tag{2.27d}$$

which again differ from the expressions displayed in [33] due to our use of the fact that the indices $\bar{\gamma}$, $\bar{\delta}$, and $\bar{\varepsilon}$ can be freely moved around since they are contracted with copies of $\sigma^{\bar{\alpha}}$.

Finally we want to expand the bi-tensor $T_{\alpha\beta}(x, \bar{x})$ around the base point $\bar{x}$. Since no index is barred, $T_{\alpha\beta}$ is a two-tensor at x. Repeating the procedure outlined in [33] to define an auxiliary tensor $\tilde{T}_{\bar{\alpha}\bar{\beta}} \equiv g^{\alpha}{}_{\bar{\alpha}} g^{\beta}{}_{\bar{\beta}} T_{\alpha\beta}$ to which the procedure outlined above can be applied. We find expansion coefficients

$$C_{\bar{\alpha}\bar{\beta}} = [T_{\alpha\beta}] \,, \tag{2.28a}$$

$$C_{\bar{\alpha}\bar{\beta}\bar{\gamma}} = [T_{\alpha\beta;\bar{\gamma}}] - C_{\bar{\alpha}\bar{\beta};\bar{\gamma}} \,, \tag{2.28b}$$

$$C_{\bar{\alpha}\bar{\beta}\bar{\gamma}\bar{\delta}} = [T_{\alpha\beta;\bar{\gamma}\bar{\delta}}] - C_{\bar{\alpha}\bar{\beta};\bar{\gamma}\bar{\delta}} - 2C_{\bar{\alpha}\bar{\beta}\bar{\gamma};\bar{\delta}} \tag{2.28c}$$

and

$$C_{\bar{\alpha}\bar{\beta}\bar{\gamma}\bar{\delta}\bar{\varepsilon}} = [T_{\alpha\beta;\bar{\gamma}\bar{\delta}\bar{\varepsilon}}] - C_{\bar{\alpha}\bar{\beta};\bar{\gamma}\bar{\delta}\bar{\varepsilon}} - 3C_{\bar{\alpha}\bar{\beta}\bar{\gamma};\bar{\delta}\bar{\varepsilon}} - 3C_{\bar{\alpha}\bar{\beta}\bar{\gamma}\bar{\delta};\bar{\varepsilon}} \,, \tag{2.28d}$$

which again differ from the expressions displayed in [33] due to our use of the fact that the indices $\bar{\gamma}$, $\bar{\delta}$, and $\bar{\varepsilon}$ can be freely moved around since they are contracted with copies of $\sigma^{\bar{\alpha}}$.

We note in passing that the main results Eqs. (2.26), (2.27), and (2.28) are identical since the differences that might stem from the presence of the parallel propagator vanish due to the (anti-)symmetry of the Riemann tensor.

2.2.3 Covariant expansions of the world function and the parallel propagator

We now apply the results of section 2.2 to $\sigma_{\alpha\beta}$, $\sigma_{\bar{\alpha}\beta}$ and $\sigma_{\bar{\alpha}\bar{\beta}}$. Using the results in Eqs. (2.17), (2.18), (2.19), (2.21), and (2.23) from section 2.2.1 we find

$$\sigma_{\alpha\beta} = g^{\bar{\alpha}}{}_{\alpha} g^{\bar{\beta}}{}_{\beta} \left(g_{\bar{\alpha}\bar{\beta}} - \frac{1}{3} R_{\bar{\alpha}\bar{\gamma}\bar{\beta}\bar{\delta}} \sigma^{\bar{\gamma}} \sigma^{\bar{\delta}} + \frac{1}{4} R_{\bar{\alpha}\bar{\gamma}\bar{\beta}\bar{\delta};\bar{\varepsilon}} \sigma^{\bar{\gamma}} \sigma^{\bar{\delta}} \sigma^{\bar{\varepsilon}} + O(\varepsilon^4) \right), \tag{2.29a}$$

$$\sigma_{\alpha\bar{\beta}} = g^{\bar{\alpha}}{}_{\alpha} \left(-g_{\bar{\alpha}\bar{\beta}} - \frac{1}{6} R_{\bar{\alpha}\bar{\gamma}\bar{\beta}\bar{\delta}} \sigma^{\bar{\gamma}} \sigma^{\bar{\delta}} - \frac{1}{12} R_{\bar{\alpha}\bar{\gamma}\bar{\beta}\bar{\delta};\bar{\varepsilon}} \sigma^{\bar{\gamma}} \sigma^{\bar{\delta}} \sigma^{\bar{\varepsilon}} + O(\varepsilon^4) \right), \tag{2.29b}$$

$$\sigma_{\bar{\alpha}\bar{\beta}} = g_{\bar{\alpha}\bar{\beta}} - \frac{1}{3} R_{\bar{\alpha}\bar{\gamma}\bar{\beta}\bar{\delta}} \sigma^{\bar{\gamma}} \sigma^{\bar{\delta}} + \frac{1}{12} R_{\bar{\alpha}\bar{\gamma}\bar{\beta}\bar{\delta};\bar{\varepsilon}} \sigma^{\bar{\gamma}} \sigma^{\bar{\delta}} \sigma^{\bar{\varepsilon}} + O(\varepsilon^4) \,. \tag{2.29c}$$

Similarly the results in Eqs.(2.24) allow us to find a covariant expansion for $g^{\bar{\alpha}}{}_{\beta;\gamma}$, the derivative of the parallel propagator

$$g^{\bar{\alpha}}{}_{\beta;\gamma} = g^{\bar{\beta}}{}_{\beta} g^{\bar{\gamma}}{}_{\gamma} \left(-\frac{1}{2} R^{\bar{\alpha}}{}_{\bar{\beta}\bar{\gamma}\bar{\delta}} \sigma^{\bar{\delta}} + \frac{1}{3} R^{\bar{\alpha}}{}_{\bar{\beta}\bar{\gamma}\bar{\delta};\bar{\varepsilon}} \sigma^{\bar{\delta}} \sigma^{\bar{\varepsilon}} + O(\varepsilon^3) \right). \tag{2.30}$$

2.3 Coordinate expansions of world function and the parallel propagator

The results of section 2.2 allow us to express any bi-tensor as a covariant expansion away from the base point $\bar{x}$. This expansion however involves $\sigma_{\bar{\alpha}}$ and $g^{\bar{\alpha}}{}_{\alpha}$ which cannot be further expanded in a covariant manner. In this section we find expressions for these in terms of the coordinate distance $w^{\alpha} \equiv (x - \bar{x})^{\alpha}$.

2.3.1 Coordinate expansion of the world function

We start by recalling Eq. (2.6b) which tells us that $\sigma_{\bar{\alpha}}$ is proportional to the tangent vector along the geodesic joining x and $\bar{x}$. Choosing a parametrization λ such that $\lambda_0 = 0$ at $\bar{x}$ and $\lambda_1 = 1$ at x we find that

$$\sigma_{\bar{\alpha}} \stackrel{*}{=} -t_{\bar{\alpha}} \,, \tag{2.31}$$

where "$\stackrel{*}{=}$" indicates that the equation only holds for a particular parametrization. Next, consider a Taylor expansion of $z^\mu(\lambda)$ along the geodesic around $\bar{x}$. Such an expansion is clearly not covariant, but can be obtained for any given coordinate system, just as the Christoffel symbols are not covariant but can be calculated for any given coordinate system. We have

$$z^\mu(\lambda) = z^\mu(0) + \dot{z}^\mu(0)\lambda + \frac{1}{2}\ddot{z}^\mu(0)\lambda^2 + \frac{1}{6}\dddot{z}^\mu(0)\lambda^3 + \frac{1}{24}z^{(4)\mu}(0)\lambda^4 + O(\lambda^5)\,. \tag{2.32}$$

In this we can eliminate higher derivatives of $\dot{z}^\mu$ in favour of $\dot{z}^\mu$ with the help of the geodesic equation

$$\ddot{z}^\mu + \Gamma^\mu{}_{\nu\lambda}\dot{z}^\nu\dot{z}^\lambda = 0\,, \tag{2.33}$$

where the Christoffel symbols and the four velocity are evaluated at $\bar{x}$. Taking a further derivative of Eq. (2.33) with respect to λ we find

$$0 = \dddot{z}^\mu + 2\Gamma^\mu{}_{\nu\lambda}\dot{z}^\nu\ddot{z}^\lambda + \Gamma^\mu{}_{\nu\lambda,\kappa}\dot{z}^\nu\dot{z}^\lambda\dot{z}^\kappa = \dddot{z}^\mu - \left(2\Gamma^\mu{}_{\nu\lambda}\Gamma^\nu{}_{\kappa\iota}\right)\dot{z}^\lambda\dot{z}^\kappa\dot{z}^\iota\,. \tag{2.34}$$

We introduce coefficients $A^\mu{}_{\nu\lambda}$, $A^\mu{}_{\nu\lambda\kappa}$, and $A^\mu{}_{\nu\lambda\kappa\iota}$ as

$$A^\mu{}_{\nu\lambda} = \Gamma^\mu{}_{\nu\lambda}\,, \tag{2.35a}$$

$$A^\mu{}_{\nu\lambda\kappa} = \left(\Gamma^\mu{}_{\nu\lambda,\kappa} - 2\Gamma^\mu{}_{\iota\nu}\Gamma^\iota{}_{\lambda\kappa}\right)\,, \tag{2.35b}$$

and

$$\begin{aligned}
A^\mu{}_{\nu\lambda\kappa\iota} = \Big(&\Gamma^\mu{}_{\nu\lambda,\kappa\iota} - 4\Gamma^\mu{}_{\rho\nu,\lambda}\Gamma^\rho{}_{\kappa\iota} - 2\Gamma^\mu{}_{\rho\nu}\Gamma^\rho{}_{\lambda\kappa,\iota} - \Gamma^\mu{}_{\nu\lambda,\rho}\Gamma^\rho{}_{\kappa\iota} \\
&+ 2\Gamma^\mu{}_{\rho\sigma}\Gamma^\rho{}_{\nu\lambda}\Gamma^\sigma{}_{\kappa\iota} + 4\Gamma^\mu{}_{\rho\nu}\Gamma^\rho{}_{\sigma\lambda}\Gamma^\sigma{}_{\kappa\iota}\Big)\,,
\end{aligned} \tag{2.35c}$$

in terms of which the Taylor expansion reads

$$\begin{aligned}
z^\mu(\lambda) = {}&z^\mu(0) + \dot{z}^\mu(0)\lambda - \frac{1}{2}A^\mu{}_{\nu\lambda}\dot{z}^\nu(0)\dot{z}^\lambda(0)\lambda^2 - \frac{1}{6}A^\mu{}_{\nu\lambda\kappa}\dot{z}^\nu(0)\dot{z}^\lambda(0)\dot{z}^\kappa(0)\lambda^3 \\
&- \frac{1}{24}A^\mu{}_{\nu\lambda\kappa\iota}\dot{z}^\nu(0)\dot{z}^\lambda(0)\dot{z}^\kappa(0)\dot{z}^\iota(0)\lambda^4 + O(\lambda^5)\,.
\end{aligned} \tag{2.36}$$

Letting $\lambda \to 1$ we find for the coordinate difference

$$w^\alpha \stackrel{*}{=} \dot{z}^{\bar{\alpha}} - \frac{1}{2}A^{\bar{\alpha}}{}_{\bar{\beta}\bar{\gamma}}\dot{z}^{\bar{\beta}}\dot{z}^{\bar{\gamma}} - \frac{1}{6}A^{\bar{\alpha}}{}_{\bar{\beta}\bar{\gamma}\bar{\delta}}\dot{z}^{\bar{\beta}}\dot{z}^{\bar{\gamma}}\dot{z}^{\bar{\delta}} - \frac{1}{24}A^{\bar{\alpha}}{}_{\bar{\beta}\bar{\gamma}\bar{\delta}\bar{\varepsilon}}\dot{z}^{\bar{\beta}}\dot{z}^{\bar{\gamma}}\dot{z}^{\bar{\delta}}\dot{z}^{\bar{\varepsilon}} + O(\lambda^5)\,, \tag{2.37}$$

where all objects on the right hand side are evaluated at $\bar{x}$. Next we invert this relation in order to find $\dot{z}^{\bar{\alpha}}$ as a function of w^{α}. We make an ansatz

$$\dot{z}^{\bar{\alpha}} \overset{*}{=} w^{\alpha} + \frac{1}{2}B^{\alpha}{}_{\beta\gamma}w^{\beta}w^{\gamma} + \frac{1}{6}B^{\alpha}{}_{\beta\gamma\delta}w^{\beta}w^{\gamma}w^{\delta} + \frac{1}{24}B^{\alpha}{}_{\beta\gamma\delta\varepsilon}w^{\beta}w^{\gamma}w^{\delta}w^{\varepsilon} + O(\lambda^5)\,, \quad (2.38)$$

where the $B^{\alpha}{}_{\beta\gamma}$'s are evaluated at $\bar{x}$. After substituting Eq. (2.38) into Eq. (2.37), sorting out the powers of $\dot{z}^{\bar{\alpha}}$ and equating coefficients on both sides, we find

$$B^{\alpha}{}_{\beta\gamma} = \Gamma^{\alpha}{}_{\beta\gamma}\,, \tag{2.39a}$$
$$B^{\alpha}{}_{\beta\gamma\delta} = \Gamma^{\alpha}{}_{\beta\gamma,\delta} + \Gamma^{\alpha}{}_{\mu\beta}\Gamma^{\mu}{}_{\gamma\delta}\,, \tag{2.39b}$$

and

$$B^{\alpha}{}_{\beta\gamma\delta\varepsilon} = \Gamma^{\alpha}{}_{\beta\gamma,\delta\varepsilon} + 2\Gamma^{\alpha}{}_{\mu\beta}\Gamma^{\mu}{}_{\gamma\delta,\varepsilon} + \Gamma^{\alpha}{}_{\mu\nu}\Gamma^{\mu}{}_{\beta\gamma}\Gamma^{\nu}{}_{\delta\varepsilon} + \Gamma^{\alpha}{}_{\beta\gamma,\mu}\Gamma^{\mu}{}_{\delta\varepsilon}\,. \tag{2.39c}$$

2.3.2 Coordinate expansion of the parallel propagator

A very similar approach to the one described in section 2.3.1 is successful in obtaining a coordinate expansion of the parallel propagator. We begin by forming a Taylor expansion of dual vector ω_{μ} parallel transported around $\bar{x}$

$$\omega_{\mu}(\lambda) \overset{*}{=} \omega_{\bar{\alpha}} + \dot{\omega}_{\bar{\alpha}}\lambda + \frac{1}{2}\ddot{\omega}_{\bar{\alpha}}\lambda^2 + \frac{1}{6}\dddot{\omega}_{\bar{\alpha}}\lambda^3 + O(\lambda^4)\,. \tag{2.40}$$

Again we use the geodesic equation to get a handle on the first derivative of ω_{μ}

$$\dot{\omega}_{\bar{\alpha}} - \Gamma^{\bar{\gamma}}{}_{\bar{\alpha}\bar{\beta}}\dot{z}^{\beta}\omega_{\bar{\gamma}} = 0\,, \tag{2.41}$$

and derivatives with respect to λ thereof to get access to the higher derivatives. We find

$$\dot{\omega}_{\bar{\alpha}} = \Gamma^{\bar{\gamma}}{}_{\bar{\alpha}\bar{\beta}}\dot{z}^{\bar{\beta}}\omega_{\bar{\gamma}}\,, \tag{2.42a}$$
$$\ddot{\omega}_{\bar{\alpha}\bar{\beta}} = \left(\Gamma^{\bar{\gamma}}{}_{\bar{\alpha}\bar{\beta},\bar{\delta}} - \Gamma^{\bar{\gamma}}{}_{\bar{\alpha}\bar{\varepsilon}}\Gamma^{\bar{\varepsilon}}{}_{\bar{\beta}\bar{\delta}} + \Gamma^{\bar{\gamma}}{}_{\bar{\beta}\bar{\varepsilon}}\Gamma^{\bar{\varepsilon}}{}_{\bar{\alpha}\bar{\delta}}\right)\dot{z}^{\bar{\beta}}\dot{z}^{\bar{\delta}}\omega_{\bar{\gamma}}\,, \tag{2.42b}$$

and

$$\dddot{\omega}_{\bar{\alpha}\bar{\beta}} = \Big(\Gamma^{\bar{\gamma}}{}_{\bar{\alpha}\bar{\beta},\bar{\delta}\bar{\varepsilon}} - 2\Gamma^{\bar{\gamma}}{}_{\bar{\alpha}\bar{\mu},\bar{\beta}}\Gamma^{\bar{\mu}}{}_{\bar{\delta}\bar{\varepsilon}} - \Gamma^{\bar{\gamma}}{}_{\bar{\alpha}\bar{\beta},\bar{\mu}}\Gamma^{\bar{\mu}}{}_{\bar{\delta}\bar{\varepsilon}} + 2\Gamma^{\bar{\gamma}}{}_{\bar{\beta}\bar{\mu}}\Gamma^{\bar{\mu}}{}_{\bar{\alpha}\bar{\delta},\bar{\varepsilon}} - 2\Gamma^{\bar{\gamma}}{}_{\bar{\mu}\bar{\beta}}\Gamma^{\bar{\mu}}{}_{\bar{\alpha}\bar{\nu}}\Gamma^{\bar{\nu}}{}_{\bar{\delta}\bar{\varepsilon}}$$
$$- \Gamma^{\bar{\gamma}}{}_{\bar{\alpha}\bar{\mu}}\Gamma^{\bar{\mu}}{}_{\bar{\beta}\bar{\delta},\bar{\varepsilon}} + 2\Gamma^{\bar{\gamma}}{}_{\bar{\alpha}\bar{\mu}}\Gamma^{\bar{\mu}}{}_{\bar{\nu}\bar{\beta}}\Gamma^{\bar{\nu}}{}_{\bar{\delta}\bar{\varepsilon}} + \Gamma^{\bar{\gamma}}{}_{\bar{\mu}\bar{\beta},\bar{\delta}}\Gamma^{\bar{\mu}}{}_{\bar{\alpha}\bar{\varepsilon}} - \Gamma^{\bar{\gamma}}{}_{\bar{\mu}\bar{\nu}}\Gamma^{\bar{\nu}}{}_{\bar{\beta}\bar{\varepsilon}}\Gamma^{\bar{\mu}}{}_{\bar{\alpha}\bar{\delta}} \tag{2.42c}$$
$$+ \Gamma^{\bar{\gamma}}{}_{\bar{\mu}\bar{\beta}}\Gamma^{\bar{\mu}}{}_{\bar{\nu}\bar{\delta}}\Gamma^{\bar{\nu}}{}_{\bar{\alpha}\bar{\varepsilon}}\Big)\dot{z}^{\bar{\beta}}\dot{z}^{\bar{\delta}}\dot{z}^{\bar{\epsilon}}\omega_{\bar{\gamma}}\,.$$

Substituting Eq.(2.38) for $\dot{z}^{\bar{\alpha}}$ and sorting out the powers of w^{α} we find

$$g^{\bar{\alpha}}{}_{\beta} = \delta^{\bar{\alpha}}{}_{\beta} + Q^{\bar{\alpha}}{}_{\beta\gamma}w^{\gamma} + \frac{1}{2}Q^{\bar{\alpha}}{}_{\beta\gamma\delta}w^{\gamma}w^{\delta} + \frac{1}{6}Q^{\bar{\alpha}}{}_{\beta\gamma\delta\varepsilon}w^{\gamma}w^{\delta}w^{\varepsilon} + O(\varepsilon^4)\,, \tag{2.43a}$$

where

$$Q^{\bar{\alpha}}{}_{\beta\gamma} = \Gamma^{\bar{\alpha}}{}_{\beta\gamma}\,, \tag{2.43b}$$
$$Q^{\bar{\alpha}}{}_{\beta\gamma\delta} = \Gamma^{\bar{\alpha}}{}_{\beta\gamma,\delta} + \Gamma^{\bar{\alpha}}{}_{\gamma\mu}\Gamma^{\mu}{}_{\beta\delta}\,, \tag{2.43c}$$
$$Q^{\bar{\alpha}}{}_{\beta\gamma\delta\varepsilon} = \Gamma^{\bar{\alpha}}{}_{\beta\gamma,\delta\varepsilon} - \frac{1}{2}\Gamma^{\bar{\alpha}}{}_{\beta\mu,\gamma}\Gamma^{\mu}{}_{\delta\varepsilon} + \frac{1}{2}\Gamma^{\bar{\alpha}}{}_{\beta\gamma,\mu}\Gamma^{\mu}{}_{\delta\varepsilon} + \Gamma^{\bar{\alpha}}{}_{\mu\gamma,\delta}\Gamma^{\bar{\mu}}{}_{\beta\varepsilon} + \Gamma^{\bar{\alpha}}{}_{\mu\gamma}\Gamma^{\mu}{}_{\nu\delta}\Gamma^{\nu}{}_{\beta\varepsilon}\,. \tag{2.43d}$$

All Christoffel symbols in the expressions above are evaluated at the base point $\bar{x}$.

2.4 Singular Green function

We refer the reader to section 12 of [33] for an introduction to the theory of distributions in curved spacetime. We will for the most part simply quote the required results without reproducing all the details.

2.4.1 Scalar field

The scalar field obeys the wave equation

$$g^{\alpha\beta}\nabla_\alpha\nabla_\beta\Phi(x) = -4\pi\rho(x)\,, \tag{2.44}$$

where $\rho(x)$ is a prescribed source. Any Green function of the wave operator satisfies

$$g^{\alpha\beta}\nabla_\alpha\nabla_\beta G(x,\bar{x}) = -4\pi\delta^4(x,\bar{x})\,, \tag{2.45}$$

where $\delta^4(x,\bar{x}) \equiv \delta(x-\bar{x})/\sqrt{-g}$ is a scalarized four dimensional Dirac distribution. Clearly

$$\Phi(x) = \int G(x,\bar{x})\rho(\bar{x})\,\mathrm{d}^4\bar{x} \tag{2.46}$$

is a solution to Eq. (2.44). Different types of Green functions such as retarded or advanced Green functions differ in the boundary conditions that they satisfy, which corresponds to the addition of a homogeneous solution of the wave equation Eq. (2.45). The Green function of physical significance is the retarded one, which has support only on and within the backwards light cone of x. It encodes the correct causal behaviour of the field. For our purposes we will further decompose the retarded Green function into singular and regular pieces according to the singular-regular decomposition of Detweiler and Whiting [3].

In this approach we work in the normal neighbourhood $\mathcal{N}(x)$ around the field point, such that there are unique geodesics linking any two points in the neighbourhood. In the neighbourhood we make the Hadamard ansatz

$$G_\pm(x,\bar{x}) = U(x,\bar{x})\delta_\pm(\sigma) + V(x,\bar{x})\theta_\pm(-\sigma)\,, \tag{2.47}$$

for the retarded $[G_+(x,\bar{x})]$ and advanced $[G_-(x,\bar{x})]$ Green functions. Here $U(x,\bar{x})$ and $V(x,\bar{x})$ are smooth bi-scalars. $\delta_\pm(\sigma)$ and $\theta_\pm(-\sigma)$ are curved spacetime generalizations of Dirac's δ-distribution and Heaviside's step function having support only on the past (upper sign) or future (lower sign) of x, respectively. See [33] for details on their definition. For our purposes it is enough to note that substituting this ansatz into Eq. (2.45) yields differential equations and coincidence conditions on $U(x,\bar{x})$ and $V(x,\bar{x})$ that define them uniquely. In particular we find that

$$U(x,\bar{x}) = \Delta^{1/2}(x,\bar{x})\,, \tag{2.48}$$

where $\Delta(x,\bar{x})$ is the van-Vleck determinant

$$\Delta(x,\bar{x}) \equiv \det\big(-g^{\bar{\alpha}}{}_\alpha(x,\bar{x})\sigma^\alpha{}_{\bar{\beta}}(x,\bar{x})\big)\,. \tag{2.49}$$

We also have

$$[V] = \frac{1}{12}R(\bar{x}),$$

(2.50a)

$$V_{,\alpha}\sigma^{\alpha} + \frac{1}{2}(\sigma^{\alpha}{}_{\alpha} - 1)V = \frac{1}{2}g^{\mu\nu}\nabla_{\mu}\nabla_{\nu}U, \quad \text{on the light cone},$$

(2.50b)

and

$$g^{\mu\nu}\nabla_{\mu}\nabla_{\nu}V = 0,$$

(2.50c)

which determine $V(x, \bar{x})$ anywhere in the normal neighbourhood. The singular Green function G_{S} is defined as

$$G_{\mathrm{S}}(x, \bar{x}) = \frac{1}{2}\Big[G_{+}(x, \bar{x}) + G_{-}(x, \bar{x}) - H(x, \bar{x})\Big],$$

(2.51)

where $H(x, \bar{x})$ is a bi-scalar satisfying the properties H1 – H4 of [33]

$$g^{\mu\nu}\nabla_{\mu}\nabla_{\nu}H(x, \bar{x}) = 0,$$ (H1)

$$H(x, \bar{x}) = H(\bar{x}, x),$$ (H2)

$$H(x, \bar{x}) = G_{+}(x, \bar{x}), \quad \text{if } x \text{ is in the chronological future of } \bar{x}, \quad$$ (H3)

and

$$H(x, \bar{x}) = G_{-}(x, \bar{x}), \quad \text{if } x \text{ is in the chronological past of } \bar{x}. \quad$$ (H4)

With these definitions the singular Green function in the normal neighbourhood is given by

$$G_{\mathrm{S}}(x, \bar{x}) = \frac{1}{2}U(x, \bar{x})\delta(\sigma) - \frac{1}{2}V(x, \bar{x})\theta(\sigma).$$

(2.52)

2.4.2 Electromagnetic field

The procedure to find the singular Green function for the electromagnetic field closely follows the pattern described in section 2.4.1.

The electromagnetic vector potential A_{α} obeys the wave equation [34]

$$g^{\mu\nu}\nabla_{\mu}\nabla_{\nu}A^{\alpha} - R^{\alpha}{}_{\beta}A^{\beta} = -4\pi j^{\alpha},$$

(2.53)

where the Lorenz gauge condition

$$g^{\mu\nu}\nabla_{\mu}A_{\nu} = 0$$

(2.54)

has been imposed and $R^{\alpha}{}_{\beta}$ is the Ricci tensor of the background and j^{α} is a prescribed source. The Green function associated with the wave equation satisfies

$$g^{\mu\nu}\nabla_{\mu}\nabla_{\nu}G^{\alpha}{}_{\bar{\beta}}(x, \bar{x}) - R^{\alpha}{}_{\beta}G^{\beta}{}_{\bar{\beta}}(x, \bar{x}) = -4\pi g^{\alpha}{}_{\bar{\beta}}(x, \bar{x})\delta^{4}(x, \bar{x}).$$

(2.55)

Following the pattern outlined in section 2.4.1 we make an ansatz

$$G^{\alpha}{}_{\pm\bar{\beta}}(x, \bar{x}) = U^{\alpha}{}_{\bar{\beta}}(x, \bar{x})\delta_{\pm}(\sigma) + V^{\alpha}{}_{\bar{\beta}}(x, \bar{x})\theta_{\pm}(-\sigma)$$

(2.56)

valid in the normal neighbourhood $\mathcal{N}(x)$. This, after substitution into Eq. (2.55), yields expressions for $U^\alpha{}_{\bar{\beta}}(x,\bar{x})$ and $V^\alpha{}_{\bar{\beta}}(x,\bar{x})$.

$$U^\alpha{}_{\bar{\beta}}(x,\bar{x}) = g^\alpha{}_{\bar{\beta}}(x,\bar{x})\Delta^{1/2}(x,\bar{x}), \tag{2.57a}$$

$$\left[V^\alpha{}_{\bar{\beta}}\right] = -\frac{1}{2}\left(R^{\bar{\alpha}}{}_{\bar{\beta}} - \frac{1}{6}\delta^{\bar{\alpha}}{}_{\bar{\beta}}\bar{R}\right), \tag{2.57b}$$

$$V^\alpha{}_{\bar{\beta};\gamma}\sigma^\gamma + \frac{1}{2}(\sigma^\gamma{}_\gamma - 2)V^\alpha{}_{\bar{\beta}} = \frac{1}{2}(g^{\mu\nu}\nabla_\mu\nabla_\nu U^\alpha{}_{\bar{\beta}} - R^\alpha{}_\beta U^\beta{}_{\bar{\beta}}), \tag{2.57c}$$
$$\text{on the light cone},$$

and

$$g^{\mu\nu}\nabla_\mu\nabla_\nu V^\alpha{}_{\bar{\beta}} - R^\alpha{}_\beta V^\beta{}_{\bar{\beta}} = 0, \tag{2.57d}$$

which determine $U^\alpha{}_{\bar{\beta}}$, and $V^\alpha{}_{\bar{\beta}}$ uniquely within the normal neighbourhood. The singular Green function is defined analogously to the scalar case as

$$G^\alpha_{\text{S}\bar{\beta}}(x,\bar{x}) = \frac{1}{2}\left[G^\alpha_{+\bar{\beta}}(x,\bar{x}) + G^\alpha_{-\bar{\beta}}(x,\bar{x}) - H^\alpha{}_{\bar{\beta}}(x,\bar{x})\right], \tag{2.58}$$

where $H^\alpha{}_{\bar{\beta}}$ satisfies conditions H1 – H4 analogous to the scalar case. We find

$$G^\alpha_{\text{S}\bar{\beta}}(x,\bar{x}) = \frac{1}{2}U^\alpha{}_{\bar{\beta}}(x,\bar{x})\delta(\sigma) - \frac{1}{2}V^\alpha{}_{\bar{\beta}}(x,\bar{x})\theta(\sigma). \tag{2.59}$$

2.4.3 Gravitational field

The procedure to find the singular Green function for the gravitational perturbation closely follows the pattern described in section 2.4.1.

A small mass m perturbs the background spacetime such that the metric $\hat{g}_{\alpha\beta}$ describing the combined system is given by

$$\hat{g}_{\alpha\beta} = g_{\alpha\beta} + h_{\alpha\beta}, \tag{2.60}$$

where the perturbation $h_{\alpha\beta}$ is "small" compared $g_{\alpha\beta}$. For convenience of notation it is useful to introduce the trace reversed perturbation

$$\gamma_{\alpha\beta} = h_{\alpha\beta} - \frac{1}{2}g^{\mu\nu}h_{\mu\nu}g_{\alpha\beta}. \tag{2.61}$$

Imposing the Lorenz gauge condition

$$g^{\mu\nu}\nabla_\mu\gamma_{\nu\alpha} = 0, \tag{2.62}$$

the trace reversed perturbation satisfies the wave equation [34]

$$g^{\mu\nu}\nabla_\mu\nabla_\nu\gamma^{\alpha\beta} + 2R^\alpha{}_\gamma{}^\beta{}_\delta\gamma^{\gamma\delta} = -16\pi T^{\alpha\beta}, \tag{2.63}$$

where $T^{\alpha\beta}$ is a prescribed source. The Green function associated to the wave operator satisfies

$$g^{\mu\nu}\nabla_\mu\nabla_\nu G^{\alpha\beta}{}_{\bar{\gamma}\bar{\delta}}(x,\bar{x}) + 2R^\alpha{}_\gamma{}^\beta{}_\delta G^{\gamma\delta}{}_{\bar{\gamma}\bar{\delta}}(x,\bar{x}) = -16\pi g^{(\alpha}{}_{\bar{\gamma}}(x,\bar{x})g^{\beta)}{}_{\bar{\delta}}(x,\bar{x})\delta^4(x,\bar{x}). \tag{2.64}$$

Following the pattern outlined in section 2.4.1 we make an ansatz

$$G^{\alpha\beta}_{\pm\ \bar{\gamma}\bar{\delta}}(x,\bar{x}) = U^{\alpha\beta}_{\ \bar{\gamma}\bar{\delta}}(x,\bar{x})\delta_\pm(\sigma) + V^{\alpha\beta}_{\ \bar{\gamma}\bar{\delta}}(x,\bar{x})\theta_\pm(-\sigma) \tag{2.65}$$

valid in the normal neighbourhood $\mathcal{N}(x)$, which, after substitution into Eq. (2.64) yields expressions for $U^{\alpha\beta}_{\ \bar{\gamma}\bar{\delta}}(x,\bar{x})$ and $V^{\alpha\beta}_{\ \bar{\gamma}\bar{\delta}}(x,\bar{x})$.

$$U^{\alpha\beta}_{\ \bar{\gamma}\bar{\delta}}(x,\bar{x}) = g^{(\alpha}_{\ \bar{\gamma}}(x,\bar{x})g^{\beta)}_{\ \bar{\delta}}(x,\bar{x})\Delta^{1/2}(x,\bar{x})\,, \tag{2.66a}$$

$$\left[V^{\alpha\beta}_{\ \bar{\gamma}\bar{\delta}}\right] = \frac{1}{2}\left(R^{\bar{\alpha}}_{\ \bar{\gamma}}{}^{\bar{\beta}}_{\ \bar{\delta}} + R^{\bar{\beta}}_{\ \bar{\gamma}}{}^{\bar{\alpha}}_{\ \bar{\delta}}\right)\,, \tag{2.66b}$$

$$V^{\alpha\beta}_{\ \bar{\gamma}\bar{\delta};\varepsilon}\sigma^\varepsilon + \frac{1}{2}(\sigma^\varepsilon_{\ \varepsilon} - 2)V^{\alpha\beta}_{\ \bar{\gamma}\bar{\delta}} = \frac{1}{2}(g^{\mu\nu}\nabla_\mu\nabla_\nu U^{\alpha\beta}_{\ \bar{\gamma}\bar{\delta}} + 2R^\alpha_{\ \gamma}{}^\beta_{\ \delta}U^{\gamma\delta}_{\ \bar{\gamma}\bar{\delta}})\,, \tag{2.66c}$$
$$\text{on the light cone}\,,$$

and
$$g^{\mu\nu}\nabla_\mu\nabla_\nu V^{\alpha\beta}_{\ \bar{\gamma}\bar{\delta}} + 2R^\alpha_{\ \gamma}{}^\beta_{\ \delta}V^{\gamma\delta}_{\ \bar{\gamma}\bar{\delta}} = 0\,, \tag{2.66d}$$

which determine $U^{\alpha\beta}_{\ \bar{\gamma}\bar{\delta}}$, and $V^{\alpha\beta}_{\ \bar{\gamma}\bar{\delta}}$ uniquely within the normal neighbourhood. The singular Green function is defined analogously to the scalar case as

$$G^{\alpha\beta}_{\text{S}\ \bar{\gamma}\bar{\delta}}(x,\bar{x}) = \frac{1}{2}\left[G^{\alpha\beta}_{+\ \bar{\gamma}\bar{\delta}}(x,\bar{x}) + G^{\alpha\beta}_{-\ \bar{\gamma}\bar{\delta}}(x,\bar{x}) - H^{\alpha\beta}_{\ \bar{\gamma}\bar{\delta}}(x,\bar{x})\right]\,, \tag{2.67}$$

where $H^{\alpha\beta}_{\ \bar{\gamma}\bar{\delta}}$ satisfies conditions H1 – H4 analog to the scalar case. We find

$$G^{\alpha\beta}_{\text{S}\ \bar{\gamma}\bar{\delta}}(x,\bar{x}) = \frac{1}{2}U^{\alpha\beta}_{\ \bar{\gamma}\bar{\delta}}(x,\bar{x})\delta(\sigma) - \frac{1}{2}V^{\alpha\beta}_{\ \bar{\gamma}\bar{\delta}}(x,\bar{x})\theta(\sigma)\,. \tag{2.68}$$

2.5 Singular field

The motion of the particle determines the source terms

$$\rho(x) = q\int_\gamma \delta^4(x,z)\,\mathrm{d}\tau\,, \tag{2.69a}$$

$$j^\alpha(x) = e\int_\gamma g^\alpha_{\ \mu}(x,z)\dot{z}^\mu\delta^4(x,z)\,\mathrm{d}\tau\,, \tag{2.69b}$$

and

$$T^{\alpha\beta}(x) = m\int_\gamma g^\alpha_{\ \mu}(x,z)g^\beta_{\ \nu}(x,z)\dot{z}^\mu\dot{z}^\nu\delta^4(x,z)\,\mathrm{d}\tau \tag{2.69c}$$

that appear in the wave equation for scalar, electromagnetic or gravitational perturbations. Having specified the motion, we use Eq. (2.52), Eq. (2.59), and Eq. (2.68) to calculate the singular part of the scalar, electromagnetic and gravitational fields, which are given by

$$\Phi_\text{S}(x) = \frac{q}{2r}U(x,x') + \frac{q}{2r_\text{adv}}U(x,x'') - \frac{1}{2}q\int_u^v V(x,z)\,\mathrm{d}\tau\,, \tag{2.70a}$$

$$A_\text{S}^\alpha(x) = \frac{e}{2r}U^\alpha_{\ \beta'}(x,x')u^{\beta'} + \frac{e}{2r_\text{adv}}U^\alpha_{\ \beta''}(x,x'')u^{\beta''} - \frac{1}{2}e\int_u^v V^\alpha_{\ \mu}(x,z)u^\mu\,\mathrm{d}\tau\,, \tag{2.70b}$$

and

$$\gamma_{\mathrm{S}}{}^{\alpha\beta}(x) = \frac{2m}{r} U^{\alpha\beta}{}_{\gamma'\delta'}(x,x') u^{\gamma'} u^{\delta'} + \frac{2m}{r_{\mathrm{adv}}} U^{\alpha\beta}{}_{\gamma''\delta''}(x,x'') u^{\gamma''} u^{\delta''}$$
$$- 2m \int_u^v V^{\alpha\beta}{}_{\mu\nu}(x,z) u^{\mu} u^{\nu} \, \mathrm{d}\tau \,. \tag{2.70c}$$

In Eq. (2.70) q, e and m are the charges and mass of the perturbing object, u and v are the retarded and advanced times defined by

$$\sigma(x, z(u)) = \sigma(x, z(v)) = 0 \,, \quad u < v \,, \tag{2.71}$$

u^{μ} is the four velocity along the world line and

$$r \equiv \sigma_{\alpha'}(x, z(u)) u^{\alpha'} \,, \quad r_{\mathrm{adv}} \equiv -\sigma_{\alpha'}(x, z(v)) u^{\alpha''} \tag{2.72}$$

are affine parameter distances on the retarded and advanced light cones of x.

Finally we take one further derivative with respect to x of Eq. (2.70) to find the gradient of the singular field. Here we have to take into account that x and x' or x'' are linked via a null geodesic, so that a variation in x will imply a variation in x' or x'', too. We find

$$\Phi^{\mathrm{S}}{}_{\alpha}(x) = -\frac{q}{2r^2} U(x,x') \partial_{\alpha} r - \frac{q}{2r_{\mathrm{adv}}^2} U(x,x'') \partial_{\alpha} r_{\mathrm{adv}} + \frac{q}{2r} U_{;\alpha}(x,x')$$
$$+ \frac{q}{2r} U_{;\alpha'}(x,x') u^{\alpha'} \partial_{\alpha} u + \frac{q}{2r} U_{;\alpha}(x,x'') + \frac{q}{2r} U_{;\alpha''}(x,x'') u^{\alpha''} \partial_{\alpha} v \tag{2.73a}$$
$$+ \frac{1}{2} q V(x,x') \partial_{\alpha} u - \frac{1}{2} q V(x,x'') \partial_{\alpha} v - \frac{1}{2} q \int_u^v \nabla_{\alpha} V(x, z(\tau)) \, \mathrm{d}\tau \,,$$

$$A^{\mathrm{S}}{}_{\alpha;\beta}(x) = -\frac{q}{2r^2} U_{\alpha\beta'} u^{\beta'} \partial_{\beta} r - \frac{q}{2r_{\mathrm{adv}}^2} U_{\alpha\beta''} u^{\beta''} \partial_{\beta} r_{\mathrm{adv}}$$
$$+ \frac{q}{2r} U_{\alpha\beta';\beta} u^{\beta'} + \frac{q}{2r} U_{\alpha\beta';\gamma'} u^{\beta'} u^{\gamma'} \partial_{\beta} u + \frac{q}{2r_{\mathrm{adv}}} U_{\alpha\beta'';\beta} u^{\beta''}$$
$$+ \frac{q}{2r_{\mathrm{adv}}} U_{\alpha\beta'';\gamma''} u^{\beta''} u^{\gamma''} \partial_{\beta} v + \frac{1}{2} q V_{\alpha\beta'} u^{\beta'} \partial_{\beta} u \tag{2.73b}$$
$$- \frac{1}{2} q V_{\alpha\beta''} u^{\beta''} \partial_{\beta} v - \frac{1}{2} q \int_u^v \nabla_{\beta} V_{\alpha\mu}(x, z(\tau)) u^{\beta}(\tau) \, \mathrm{d}\tau \,,$$

and

$$\gamma^{\mathrm{S}}{}_{\alpha\beta;\gamma}(x) = -\frac{2m}{r^2} U_{\alpha\beta\alpha'\beta'} u^{\alpha'} u^{\beta'} \partial_{\gamma} r - \frac{2m}{r_{\mathrm{adv}}^2} U_{\alpha\beta\alpha''\beta''} u^{\alpha''} u^{\beta''} \partial_{\gamma} r_{\mathrm{adv}}$$
$$+ \frac{2m}{r} U_{\alpha\beta\alpha'\beta';\gamma} u^{\alpha'} u^{\beta'} + \frac{2m}{r} U_{\alpha\beta\alpha'\beta';\gamma'} u^{\alpha'} u^{\beta'} u^{\gamma'} \partial_{\gamma} u$$
$$+ \frac{2m}{r_{\mathrm{adv}}} U_{\alpha\beta\alpha'\beta';\gamma} u^{\alpha'} u^{\beta'} + \frac{2m}{r_{\mathrm{adv}}} U_{\alpha\beta\alpha''\beta'';\gamma''} u^{\alpha''} u^{\beta''} u^{\gamma''} \partial_{\gamma} v \tag{2.73c}$$
$$- 2m \int_u^v \nabla_{\gamma} V_{\alpha\beta\mu\nu}(x, z(\tau)) u^{\mu} u^{\nu} \, \mathrm{d}\tau \,.$$

These expressions form the basis for a calculation of the regularization parameters. They can be found in Eqs. (413), (464) and (527) of [33].

20

2.6 Taylor expansions and world line point

Our goal is the calculation of the singularity structure of the field gradients in Eq. (2.73) near an arbitrary point $\bar{x} = z(\bar{\tau})$ on the world line of the particle. We therefore need to expand the field gradients in a Taylor expansion around $\bar{x}$. Unfortunately the field gradients depend on the field point x not only through its explicit dependence on it, but also through a hidden dependence due to the null geodesic that links x and x' or x''. Changing x will also vary x' and x'', introducing complicated dependencies which are hard to deal with. To disentangle the dependence of the field gradients on x, we expand the potentials U, V as well as r and r_{adv} around the world line point $\bar{x}$. This consolidates the dependence of bi-tensor on the world line to a single point $\bar{x}$, with the dependence on x', x'' being absorbed into displacements on the world line.

2.6.1 Taylor expansion along the world line

Consider a function $p(\tau)$ which is a scalar on the world line. We expand it around a time $\bar{\tau}$ as

$$p(\tau) = p(\bar{\tau}) + \dot{p}(\bar{\tau})\Delta + \frac{1}{2}\ddot{p}(\bar{\tau})\Delta^2 + \frac{1}{6}\dddot{p}(\bar{\tau})\Delta^3 + \frac{1}{24}p^{(4)}(\bar{\tau})\Delta^4 + O(\Delta^5)\,, \quad (2.74)$$

where $\Delta = \tau - \bar{\tau}$ and an overdot denotes a covariant derivative with respect to τ, $\dot{p}(\tau) \equiv \frac{\mathrm{D}p(\tau)}{\mathrm{d}\tau} \equiv p_{;\bar{\alpha}}u^{\bar{\alpha}}$. Evaluating Eq. (2.74) at $\Delta_+ = v - \bar{\tau}$ and $\Delta_- = u - \bar{\tau}$ yields an approximation for p at the advanced and retarded points which is accurate to $O(\Delta^5)$.

2.6.2 Calculation of Δ_+ and Δ_-

We use the special case where p is Synge's world function evaluated at a point on the world line and at the field point, $p(\tau) = \sigma(x, z(\tau))$, to find approximation for $\Delta_\pm$ in terms of $\sigma_{\bar{\alpha}}$. Evaluating $p(\tau)$ at the advanced or retarded points $\tau = u, v$ we have

$$
0 = \sigma(x, \bar{x}) + \sigma_{\bar{\alpha}}(x, \bar{x})u^{\bar{\alpha}}\Delta + \frac{1}{2}\sigma_{\bar{\alpha}\bar{\beta}}(x, \bar{x})u^{\bar{\alpha}}u^{\bar{\beta}}\Delta^2 + \frac{1}{6}\sigma_{\bar{\alpha}\bar{\beta}\bar{\gamma}}(x, \bar{x})u^{\bar{\alpha}}u^{\bar{\beta}}u^{\bar{\gamma}}\Delta^3
$$
$$
+ \frac{1}{24}\sigma_{\bar{\alpha}\bar{\beta}\bar{\gamma}\bar{\delta}}(x, \bar{x})u^{\bar{\alpha}}u^{\bar{\beta}}u^{\bar{\gamma}}u^{\bar{\delta}}\Delta^4 + \frac{1}{120}\sigma_{\bar{\alpha}\bar{\beta}\bar{\gamma}\bar{\delta}\bar{\varepsilon}}(x, \bar{x})u^{\bar{\alpha}}u^{\bar{\beta}}u^{\bar{\gamma}}u^{\bar{\delta}}u^{\bar{\varepsilon}}\Delta^5 + O(\Delta^6)\,,
$$

$$(2.75)$$

where Δ is either Δ_+ or Δ_-. We use Eqs. (2.7) and (2.29) to obtain expansion of Synge's world function and its higher derivatives in terms of $\sigma_{\bar{\alpha}}$. After some algebra we find

$$\sigma = \frac{1}{2}g_{\bar{\alpha}\bar{\beta}}\sigma^{\bar{\alpha}}\sigma^{\bar{\beta}}\,, \tag{2.76a}$$

$$\sigma_{\bar{\alpha}}u^{\bar{\alpha}} \equiv \bar{r}\,, \tag{2.76b}$$

$$\sigma_{\bar{\alpha}\bar{\beta}}u^{\bar{\alpha}}u^{\bar{\beta}} = -1 - \frac{1}{3}R_{u\sigma u\sigma} + \frac{1}{12}R_{u\sigma u\sigma|\sigma} + O(\varepsilon^4)\,, \tag{2.76c}$$

$$\sigma_{\bar{\alpha}\bar{\beta}\bar{\gamma}}(x, \bar{x})u^{\bar{\alpha}}u^{\bar{\beta}}u^{\bar{\gamma}} = -\frac{1}{4}R_{u\sigma u\sigma|u} + O(\varepsilon^3)\,, \tag{2.76d}$$

$$\sigma_{\bar{\alpha}\bar{\beta}\bar{\gamma}\bar{\delta}}(x, \bar{x})u^{\bar{\alpha}}u^{\bar{\beta}}u^{\bar{\gamma}}u^{\bar{\delta}} = 0 + O(\varepsilon^2)\,, \tag{2.76e}$$

and
$$\sigma_{\bar{\alpha}\bar{\beta}\bar{\gamma}\bar{\delta}\bar{\varepsilon}}(x,\bar{x})u^{\bar{\alpha}}u^{\bar{\beta}}u^{\bar{\gamma}}u^{\bar{\delta}}u^{\bar{\varepsilon}} = 0 + O(\varepsilon)\,, \tag{2.76f}$$

where we have introduced the short-hand notation $\bar{r} = \sigma_{\bar{\alpha}}u^{\bar{\alpha}}$, $R_{u\sigma u\sigma} \equiv R_{\bar{\alpha}\bar{\beta}\bar{\gamma}\bar{\delta}}u^{\bar{\alpha}}\sigma^{\bar{\beta}}u^{\bar{\gamma}}\sigma^{\bar{\delta}}$ and $R_{u\sigma u\sigma|u} \equiv R_{\bar{\alpha}\bar{\beta}\bar{\gamma}\bar{\delta};\bar{\varepsilon}}u^{\bar{\alpha}}\sigma^{\bar{\beta}}u^{\bar{\gamma}}\sigma^{\bar{\delta}}u^{\bar{\varepsilon}}$. The notation is unambiguous and can be extended to any number of derivatives in the obvious way. Many variants of this notation will appear in the following.

In order to invert Eq. (2.75) for Δ we make the ansatz
$$\Delta = \Delta_1 + \frac{1}{2}\Delta_2 + \frac{1}{6}\Delta_3 + \frac{1}{24}\Delta_4 + O(\varepsilon^5)\,, \tag{2.77}$$

where $\Delta_n = O(\varepsilon^n)$ and ε is the bookkeeping variable used to keep track of powers of σ_α. Substituting Eq. (2.77) into Eq. (2.75), collecting the coefficients on front of each power of ε, and demanding that the equation holds order by order, we find
$$\Delta_1 = \bar{r} \pm s\,, \tag{2.78a}$$
$$\Delta_2 = 0\,, \tag{2.78b}$$
$$\Delta_3 = \mp R_{u\sigma u\sigma}\frac{(\bar{r} \pm s)^2}{s}\,, \tag{2.78c}$$

and
$$\Delta_4 = \mp \frac{(\bar{r} \pm s)^2}{s}[R_{u\sigma u\sigma|u}(\bar{r} \pm s) - R_{u\sigma u\sigma|\sigma}]\,, \tag{2.78d}$$

where we have introduced yet another short hand for the spatial separation $s \equiv \sqrt{(u_{\bar{\alpha}}u_{\bar{\beta}} + g_{\bar{\alpha}\bar{\beta}})\sigma^{\bar{\alpha}}\sigma^{\bar{\beta}}}$. Inspection shows that the upper sign in Eq. (2.78) is valid for $\Delta = \Delta_+$ and the lower sign is valid for $\Delta = \Delta_-$. We find
$$\Delta_- = (\bar{r} - s) + \frac{(\bar{r} - s)^2}{6s}R_{u\sigma u\sigma} + \frac{(\bar{r} - s)^2}{24s}[R_{u\sigma u\sigma|u}(\bar{r} - s) - R_{u\sigma u\sigma|\sigma}] + O(\varepsilon^5)\,, \quad \text{(2.79a)}$$

and
$$\Delta_+ = (\bar{r} + s) - \frac{(\bar{r} + s)^2}{6s}R_{u\sigma u\sigma} - \frac{(\bar{r} + s)^2}{24s}[R_{u\sigma u\sigma|u}(\bar{r} + s) - R_{u\sigma u\sigma|\sigma}] + O(\varepsilon^5)\,. \quad \text{(2.79b)}$$

2.6.3 Taylor expansions of r and r_{adv}

We obtain expansions for r and r_{adv} by setting $p(\tau) = \sigma_\mu(x, z(\tau))u^\mu$ and expanding around $\bar{\tau}$ as described in section 2.6.1 up to order $O(\Delta^5)$. With this definition for $p(\tau)$ we have $r = p(u)$ and $r_{\text{adv}} = -p(v)$ and since $\sigma_\mu(x, z(\tau))u^\mu = \dot{\sigma}(x, z(\tau))$ the coefficients in a Taylor expansion for r and r_{adv} are (up to a sign) the ones listed in Eq. (2.76). Substituting the coefficients and the expressions for $\Delta_\pm$ we find
$$r = s - \frac{\bar{r}^2 - s^2}{6s}R_{u\sigma u\sigma} - \frac{\bar{r} - s}{24s}\left[(\bar{r} - s)(\bar{r} + 2s)R_{u\sigma u\sigma|u} - (\bar{r} + s)R_{u\sigma u\sigma|\sigma}\right] + O(\varepsilon^5)\,, \quad \text{(2.80a)}$$

and
$$\begin{aligned} r_{\text{adv}} = s &- \frac{\bar{r}^2 - s^2}{6s}R_{u\sigma u\sigma} \\ &- \frac{\bar{r} + s}{24s}\left[(\bar{r} + s)(\bar{r} - 2s)R_{u\sigma u\sigma|u} - (\bar{r} - s)R_{u\sigma u\sigma|\sigma}\right] + O(\varepsilon^5)\,. \end{aligned} \tag{2.80b}$$

2.6.4 Taylor expansions of $\partial_\alpha u$ and $\partial_\alpha v$

At first glance the procedure outlined in section 2.6.1 is not applicable to the terms involving gradients, since they are tensors and cannot therefore be expanded in a Taylor series. However closer inspection reveals that the terms involving gradients are tensors at the field point x only, but are scalars on the world line. The world line indices are saturated by contractions with the four velocity. We therefore define a world line scalar $p_\alpha = \partial_\alpha u$ and proceed as in section 2.6.1. [33] gives expressions for $\partial_\alpha u$ and $\partial_\alpha v$ in term of Synge's world function in his Eq. (145) and the material leading to Eq. (231). We use

$$\partial_\alpha u = -\frac{\sigma_\alpha}{r}, \tag{2.81a}$$

$$\partial_\alpha v = +\frac{\sigma_\alpha}{r_{\text{adv}}}. \tag{2.81b}$$

We therefore require expansions of σ_α on the world line. We define a world line scalar $\sigma_\alpha(\tau) = \sigma_\alpha(x, z(\tau))$ and expand it as

$$
\begin{aligned}
\sigma_\alpha(\tau) = {} & \sigma_\alpha(x, \bar{x}) + \sigma_{\alpha\bar{\beta}}(x, \bar{x})u^{\bar{\beta}}\Delta + \frac{1}{2}\sigma_{\alpha\bar{\beta}\bar{\gamma}}(x, \bar{x})u^{\bar{\beta}}u^{\bar{\gamma}}\Delta^2 \\
& + \frac{1}{6}\sigma_{\alpha\bar{\beta}\bar{\gamma}\bar{\delta}}(x, \bar{x})u^{\bar{\beta}}u^{\bar{\gamma}}u^{\bar{\delta}}\Delta^3 + O(\Delta^4),
\end{aligned} \tag{2.82}
$$

where Δ is either Δ_+ or Δ_-. We use Eq. (2.29) to obtain expansion of the higher derivatives of Synge's world function in terms of $\sigma_{\bar{\alpha}}$. After some algebra we find

$$\sigma_{\alpha\bar{\beta}}u^{\bar{\beta}} = -g^{\bar{\alpha}}{}_\alpha\left(u_{\bar{\alpha}} + \frac{1}{6}R_{\bar{\alpha}\sigma u\sigma}\right) + O(\varepsilon^3), \tag{2.83a}$$

$$\sigma_{\alpha\bar{\beta}\bar{\gamma}}u^{\bar{\beta}}u^{\bar{\gamma}} = \frac{2}{3}g^{\bar{\alpha}}{}_\alpha R_{\bar{\alpha}u\sigma u} + O(\varepsilon^2), \tag{2.83b}$$

$$\sigma_{\alpha\bar{\beta}\bar{\gamma}\bar{\delta}}(x, \bar{x})u^{\bar{\beta}}u^{\bar{\gamma}}u^{\bar{\delta}} = 0 + O(\varepsilon). \tag{2.83c}$$

Evaluating Eq. (2.82) at Δ_- or Δ_+ yields σ_α at the retarded and advanced points, respectively:

$$
\begin{aligned}
\sigma_\alpha(x, x') = g^{\bar{\alpha}}{}_\alpha \Bigg\{ & -\Big[\sigma_{\bar{\alpha}} + (\bar{r} - s)u_{\bar{\alpha}}\Big] \\
& -\left[\frac{1}{6}(\bar{r} - s)R_{\bar{\alpha}\sigma u\sigma} + \frac{(\bar{r} - s)^2}{6s}R_{u\sigma u\sigma}u_{\bar{\alpha}} - \frac{1}{3}(\bar{r} - s)^2 R_{\bar{\alpha}u\sigma u}\right] \\
& +\left[\frac{1}{12}(\bar{r} - s)R_{\bar{\alpha}\sigma u\sigma|\sigma} - \frac{(\bar{r} - s)^2}{24s}\Big((\bar{r} - s)R_{u\sigma u\sigma|u} - R_{u\sigma u\sigma|\sigma}\Big)u_{\bar{\alpha}}\right. \\
& \left. -\frac{1}{24}(\bar{r} - s)^2\Big(3R_{\bar{\alpha}u\sigma u|\sigma} + R_{\bar{\alpha}\sigma u\sigma|u}\Big) + \frac{1}{12}(\bar{r} - s)^3 R_{\bar{\alpha}u\sigma u|u}\right] + O(\varepsilon^5)\Bigg\},
\end{aligned} \tag{2.84}
$$

and

$$\sigma_\alpha(x, x'') = g^{\bar{\alpha}}_{\ \alpha}\left\{-\left[\sigma_{\bar{\alpha}} + (\bar{r}+s)u_{\bar{\alpha}}\right]\right.$$
$$-\left[\frac{1}{6}(\bar{r}+s)R_{\bar{\alpha}\sigma u\sigma} - \frac{(\bar{r}+s)^2}{6s}R_{u\sigma u\sigma}u_{\bar{\alpha}} - \frac{1}{3}(\bar{r}+s)^2 R_{\bar{\alpha}u\sigma u}\right]$$
$$+\left[\frac{1}{12}(\bar{r}+s)R_{\bar{\alpha}\sigma u\sigma|\sigma} + \frac{(\bar{r}+s)^2}{24s}\Big((\bar{r}+s)R_{u\sigma u\sigma|u} - R_{u\sigma u\sigma|\sigma}\Big)u_{\bar{\alpha}}\right.$$
$$\left.\left.-\frac{1}{24}(\bar{r}+s)^2\Big(3R_{\bar{\alpha}u\sigma u|\sigma} + R_{\bar{\alpha}\sigma u\sigma|u}\Big) + \frac{1}{12}(\bar{r}+s)^3 R_{\bar{\alpha}u\sigma u|u}\right] + O(\varepsilon^5)\right\}. \tag{2.85}$$

2.6.5 Taylor expansions of $\partial_\alpha r$ and $\partial_\alpha r_{\mathrm{adv}}$

Expressions for $\partial_\alpha r$ and $\partial_\alpha r_{\mathrm{adv}}$ are displayed in Eqs. (147) and (232) of [33]:

$$\partial_\alpha r = -\sigma_{\alpha'\beta'}u^{\alpha'}u^{\beta'}\frac{\sigma_\alpha}{r} + \sigma_{\alpha\alpha'}u^{\alpha'}, \tag{2.86}$$

$$\partial_\alpha r_{\mathrm{adv}} = -\sigma_{\alpha''\beta''}u^{\alpha''}u^{\beta''}\frac{\sigma_\alpha}{r_{\mathrm{adv}}} - \sigma_{\alpha\alpha''}u^{\alpha''}. \tag{2.87}$$

We note that $\sigma_{\alpha'\beta'}u^{\alpha'}u^{\beta'} = \ddot{\sigma}$ and $\sigma_{\alpha\beta'}u^{\beta'} = \dot{\sigma}_\alpha$ so that the coefficients of Eq. (2.29) can be used in an expansion of $\sigma_{\alpha'\beta'}u^{\alpha'}u^{\beta'}$ as

$$\ddot{\sigma}(\tau) = \ddot{\sigma} + \dddot{\sigma}\Delta + \frac{1}{2}\sigma^{(4)}\Delta^2 + O(\varepsilon^3), \tag{2.88}$$

and those of Eq. (2.82) can be used in an expansion of $\sigma_{\alpha\beta'}u^{\beta'}$ as

$$\dot{\sigma}_\alpha = \dot{\sigma}_\alpha + \ddot{\sigma}_\alpha\Delta + \frac{1}{2}\dddot{\sigma}_\alpha\Delta^2 + O(\varepsilon^3). \tag{2.89}$$

For the advanced point x'' similar considerations apply. We find

$$\sigma_{\alpha\alpha'}u^{\alpha'} = g^{\bar{\alpha}}_{\ \alpha}\left\{-u_{\bar{\alpha}} - \left[\frac{1}{6}R_{\bar{\alpha}\sigma u\sigma} - \frac{2}{3}(\bar{r}-s)R_{\bar{\alpha}u\sigma u}\right] + \left[\frac{1}{12}R_{\bar{\alpha}\sigma u\sigma|\sigma}\right.\right.$$
$$\left.\left.-\frac{1}{12}(\bar{r}-s)\Big(3R_{\bar{\alpha}u\sigma u|\sigma} + R_{\bar{\alpha}\sigma u\sigma|u}\Big) + \frac{1}{4}(\bar{r}-s)^2 R_{\bar{\alpha}u\sigma u|u}\right]\right.$$
$$\left.+ O(\varepsilon^4)\right\}, \tag{2.90a}$$

$$\sigma_{\alpha\alpha''}u^{\alpha''} = g^{\bar{\alpha}}_{\ \alpha}\left\{-u_{\bar{\alpha}} - \left[\frac{1}{6}R_{\bar{\alpha}\sigma u\sigma} - \frac{2}{3}(\bar{r}+s)R_{\bar{\alpha}u\sigma u}\right] + \left[\frac{1}{12}R_{\bar{\alpha}\sigma u\sigma|\sigma}\right.\right.$$
$$\left.\left.-\frac{1}{12}(\bar{r}+s)\Big(3R_{\bar{\alpha}u\sigma u|\sigma} + R_{\bar{\alpha}\sigma u\sigma|u}\Big) + \frac{1}{4}(\bar{r}+s)^2 R_{\bar{\alpha}u\sigma u|u}\right]\right.$$
$$\left.+ O(\varepsilon^4)\right\}, \tag{2.90b}$$

and

$$\sigma_{\alpha'\beta'}u^{\alpha'}u^{\beta'} = -1 - \frac{1}{3}R_{u\sigma u\sigma} + \frac{1}{12}\left[R_{u\sigma u\sigma|\sigma} - 3(\bar{r}-s)R_{u\sigma u\sigma|u}\right] + O(\varepsilon^4), \qquad (2.90a)$$

$$\sigma_{\alpha''\beta''}u^{\alpha''}u^{\beta''} = -1 - \frac{1}{3}R_{u\sigma u\sigma} + \frac{1}{12}\left[R_{u\sigma u\sigma|\sigma} - 3(\bar{r}+s)R_{u\sigma u\sigma|u}\right] + O(\varepsilon^4). \qquad (2.90b)$$

Substituting all of these results into Eqs. (2.86) and (2.86) we find

$$\begin{aligned}
\partial_\alpha r = -\frac{1}{s}g^{\bar{\alpha}}{}_\alpha\Bigg\{&\left[\sigma_{\bar{\alpha}} + \bar{r}u_{\bar{\alpha}}\right] + \left[\frac{1}{6}\bar{r}R_{\bar{\alpha}\sigma u\sigma} - \frac{1}{3}(\bar{r}^2-s^2)R_{\bar{\alpha}u\sigma u} + \frac{\bar{r}^2+s^2}{6s^2}R_{u\sigma u\sigma}\sigma_{\bar{\alpha}}\right.\\
&\left.+ \frac{\bar{r}(\bar{r}^2-s^2)}{6s^2}R_{u\sigma u\sigma}u_{\bar{\alpha}}\right] + \left[-\frac{1}{12}\bar{r}R_{\bar{\alpha}\sigma u\sigma|\sigma} + \frac{1}{8}(\bar{r}^2-s^2)R_{\bar{\alpha}u\sigma u|\sigma}\right.\\
&+ \frac{1}{24}(\bar{r}^2-s^2)R_{\bar{\alpha}\sigma u\sigma|u} - \frac{1}{12}(\bar{r}-s)^2(\bar{r}+2s)R_{\bar{\alpha}u\sigma u|u}\\
&+ \frac{1}{24s^2}\left((\bar{r}-s)(\bar{r}^2+\bar{r}s+4s^2)R_{u\sigma u\sigma|u} - (\bar{r}^2+s^2)R_{u\sigma u\sigma|\sigma}\right)\sigma_{\bar{\alpha}}\\
&\left.+ \frac{\bar{r}-s}{24s^2}\left((\bar{r}-s)(\bar{r}^2+2\bar{r}s+3s^2)R_{u\sigma u\sigma|u} - \bar{r}(\bar{r}+s)R_{u\sigma u\sigma|\sigma}\right)u_{\bar{\alpha}}\right]\\
&+ O(\epsilon^5)\Bigg\}
\end{aligned} \qquad (2.92)$$

and

$$\begin{aligned}
\partial_\alpha r_{\mathrm{adv}} = -\frac{1}{s}g^{\bar{\alpha}}{}_\alpha\Bigg\{&\left[\sigma_{\bar{\alpha}} + \bar{r}u_{\bar{\alpha}}\right] + \left[\frac{1}{6}\bar{r}R_{\bar{\alpha}\sigma u\sigma} - \frac{1}{3}(\bar{r}^2-s^2)R_{\bar{\alpha}u\sigma u} + \frac{\bar{r}^2+s^2}{6s^2}R_{u\sigma u\sigma}\sigma_{\bar{\alpha}}\right.\\
&\left.+ \frac{\bar{r}(\bar{r}^2-s^2)}{6s^2}R_{u\sigma u\sigma}u_{\bar{\alpha}}\right] + \left[-\frac{1}{12}\bar{r}R_{\bar{\alpha}\sigma u\sigma|\sigma} + \frac{1}{8}(\bar{r}^2-s^2)R_{\bar{\alpha}u\sigma u|\sigma}\right.\\
&+ \frac{1}{24}(\bar{r}^2-s^2)R_{\bar{\alpha}\sigma u\sigma|u} - \frac{1}{12}(\bar{r}+s)^2(\bar{r}-2s)R_{\bar{\alpha}u\sigma u|u}\\
&+ \frac{1}{24s^2}\left((\bar{r}+s)(\bar{r}^2-\bar{r}s+4s^2)R_{u\sigma u\sigma|u} - (\bar{r}^2+s^2)R_{u\sigma u\sigma|\sigma}\right)\sigma_{\bar{\alpha}}\\
&\left.+ \frac{\bar{r}+s}{24s^2}\left((\bar{r}+s)(\bar{r}^2-2\bar{r}s+3s^2)R_{u\sigma u\sigma|u} - \bar{r}(\bar{r}-s)R_{u\sigma u\sigma|\sigma}\right)u_{\bar{\alpha}}\right]\\
&+ O(\epsilon^5)\Bigg\}.
\end{aligned} \qquad (2.93)$$

2.6.6 Taylor expansions of the potentials

Taylor expansions of the direct potentials

In section 2.4 we displayed the direct part of the scalar, electromagnetic and gravitational singular Green function, which is given by

$$\begin{aligned}
U(x,\bar{x}) &= \Delta^{1/2}(x,\bar{x})\,,\\
U^\alpha{}_{\bar{\beta}}(x,\bar{x}) &= g^\alpha{}_{\bar{\beta}}(x,\bar{x})\Delta^{1/2}(x,\bar{x})\,,
\end{aligned}$$

and

$$U^{\alpha\beta}{}_{\bar{\gamma}\bar{\delta}}(x,\bar{x}) = g^{(\alpha}{}_{\bar{\gamma}}(x,\bar{x})g^{\beta)}{}_{\bar{\delta}}(x,\bar{x})\Delta^{1/2}(x,\bar{x}) \,,$$

respectively. In order to obtain an expansion for the direct potential we first need an expansion of the van-Vleck determinant $\Delta(x,\bar{x})$. Fortunately this turns out to be a simple expression in vacuum spacetimes. First consider the expansion of $\sigma_{\alpha\bar{\beta}}$ derived in Eq. (2.29). We introduce the auxiliary matrix

$$\Delta^{\bar{\alpha}}{}_{\bar{\beta}} = -g^{\bar{\alpha}}{}_{\alpha}\sigma^{\alpha}{}_{\bar{\beta}} = \delta^{\bar{\alpha}}{}_{\bar{\beta}} + \frac{1}{6}R^{\bar{\alpha}}{}_{\bar{\gamma}\bar{\beta}\bar{\delta}}\sigma^{\bar{\gamma}}\sigma^{\bar{\delta}} - \frac{1}{12}R^{\bar{\alpha}}{}_{\bar{\gamma}\bar{\beta}\bar{\delta};\bar{\varepsilon}}\sigma^{\bar{\gamma}}\sigma^{\bar{\delta}}\sigma^{\bar{\varepsilon}} + O(\varepsilon^4) \,, \qquad (2.94)$$

in terms of which the van-Vleck determinant is given by $\Delta(x,\bar{x}) = \det(\Delta^{\bar{\alpha}}{}_{\bar{\beta}})$. Since this matrix is close to the identity matrix, we expand its determinant as

$$\det(\Delta^{\bar{\alpha}}{}_{\bar{\beta}}) = 1 + \operatorname{tr}(\Delta^{\bar{\alpha}}{}_{\bar{\beta}} - \delta^{\bar{\alpha}}{}_{\bar{\beta}}) + O(\Delta^{\bar{\alpha}}{}_{\bar{\beta}} - \delta^{\bar{\alpha}}{}_{\bar{\beta}})^2 \,. \qquad (2.95)$$

In vacuum spacetimes the Ricci tensor vanishes and therefore

$$\Delta(x,\bar{x}) = 1 + O(\varepsilon^4), \quad \text{in vacuum spacetimes} \,.$$
$$(2.96)$$

This statement still holds for the square root $\Delta^{1/2}$ of Δ implying that

$$U(x,\bar{x}) = 1 + O(\varepsilon^4) \,, \qquad (2.97a)$$
$$U^{\alpha}{}_{\bar{\beta}}(x,\bar{x}) = g^{\alpha}{}_{\bar{\beta}}(x,\bar{x}) + O(\varepsilon^4) \,, \qquad (2.97b)$$

and

$$U^{\alpha\beta}{}_{\bar{\gamma}\bar{\delta}}(x,\bar{x}) = g^{(\alpha}{}_{\bar{\gamma}}(x,\bar{x})g^{\beta)}{}_{\bar{\delta}}(x,\bar{x}) + O(\varepsilon^4) \,. \qquad (2.97c)$$

Scalar case Clearly the Taylor expansion for the direct potential for the scalar case is trivial since U is constant to the order required in the calculation

$$U(\tau) = 1 + O(\varepsilon^4) \,. \qquad (2.98)$$

Electromagnetic case We define world line scalars via $U_{\alpha}(\tau) \equiv U^{\mu}{}_{\alpha}(x,z(\tau))u_{\mu}$, $U_{\alpha\beta}(\tau) \equiv U_{\alpha\mu;\beta}(x,z(\tau))u^{\mu}$ for $U^{\mu}{}_{\alpha}$ and its derivative. Note that $U_{\alpha\mu\nu}(x,z(\tau))u^{\mu}u^{\nu} = \dot{U}_{\alpha}$ and therefore does not require separate treatment. Thus

$$U_{\alpha}(\tau) = U_{\alpha} + \dot{U}_{\alpha}\Delta + \frac{1}{2}\ddot{U}_{\alpha}\Delta^2 + \frac{1}{6}\dddot{U}_{\alpha}\Delta^3 + O(\Delta^4) \,, \qquad (2.99a)$$

and

$$U_{\alpha\beta}(\tau) = U_{\alpha\beta} + \dot{U}_{\alpha\beta}\Delta + \frac{1}{2}\ddot{U}_{\alpha\beta}\Delta^2 + O(\Delta^3) \,, \qquad (2.99b)$$

where all coefficients are to be evaluated on the world line. Repeated use of Eq. (2.30) to handle the derivatives of the parallel propagator hidden in $\dot{U}_{\alpha}$ and $U_{\alpha\beta}$ yields

expressions for the coefficients

$$U_\alpha = g^{\bar\alpha}{}_\alpha u^{\bar\alpha} + O(\varepsilon^4)\,, \tag{2.100a}$$

$$\dot{U}_\alpha = g^{\bar\alpha}{}_\alpha\Big(\frac{1}{2}R_{\bar\alpha uu\sigma} - \frac{1}{6}R_{\bar\alpha uu\sigma|\sigma}\Big) + O(\varepsilon^3)\,, \tag{2.100b}$$

$$\ddot{U}_\alpha = -\frac{1}{3}g^{\bar\alpha}{}_\alpha R_{\bar\alpha u\sigma u|u} + O(\varepsilon^2)\,, \tag{2.100c}$$

$$\dddot{U}_\alpha = 0 + O(\varepsilon)\,, \tag{2.100d}$$

and

$$U_{\alpha\beta} = g^{\bar\alpha}{}_\alpha g^{\bar\beta}{}_\beta\Big(\frac{1}{2}R_{\bar\alpha u\bar\beta\sigma} - \frac{1}{3}R_{\bar\alpha u\bar\beta\sigma|\sigma}\Big) + O(\varepsilon^3)\,, \tag{2.101a}$$

$$\dot{U}_{\alpha\beta} = g^{\bar\alpha}{}_\alpha g^{\bar\beta}{}_\beta\Big(\frac{1}{2}R_{\bar\alpha u\bar\beta u} + \frac{1}{6}R_{\bar\alpha u\bar\beta\sigma|u} - \frac{1}{3}R_{\bar\alpha u\bar\beta u|\sigma}\Big) + O(\varepsilon^2)\,, \tag{2.101b}$$

$$\ddot{U}_{\alpha\beta} = \frac{1}{3}g^{\bar\alpha}{}_\alpha g^{\bar\beta}{}_\beta R_{\bar\alpha u\bar\beta u|u} + O(\varepsilon)\,, \tag{2.101c}$$

where we have introduced yet another variant of the short hand notation of section 2.6.2 for contraction of the Riemann tensor involving free indices $R_{\bar\alpha uu\sigma} \equiv R_{\bar\alpha\bar\beta\bar\gamma\bar\delta}u^{\bar\beta}u^{\bar\gamma}\sigma^{\bar\delta}$.

Gravitational case As done for the electromagnetic case we define world line scalars $U_{\alpha\beta}(\tau) \equiv U^{\mu\nu}{}_{\alpha\beta}(x, z(\tau))u_\mu u_\nu$, $U_{\alpha\beta\gamma}(\tau) \equiv U_{\alpha\beta\mu\nu;\gamma}(x, z(\tau))u^\mu u^\nu$ for $U^{\mu\nu}{}_{\alpha\beta}$ and its derivative at x. Again, the derivative on the world line does not require separate treatment. Thus

$$U_{\alpha\beta}(\tau) = U_{\alpha\beta} + \dot{U}_{\alpha\beta}\Delta + \frac{1}{2}\ddot{U}_{\alpha\beta}\Delta^2 + \frac{1}{6}\dddot{U}_{\alpha\beta}\Delta^3 + O(\Delta^4)\,, \tag{2.102a}$$

$$U_{\alpha\beta\gamma}(\tau) = U_{\alpha\beta\gamma} + \dot{U}_{\alpha\beta\gamma}\Delta + \frac{1}{2}\ddot{U}_{\alpha\beta\gamma}\Delta^2 + O(\Delta^3)\,, \tag{2.102b}$$

where all coefficients are to be evaluated on the world line. Repeated use of Eq. (2.30) to handle the derivatives of the parallel propagator hidden in $\dot{U}_{\alpha\beta}$ and $U_{\alpha\beta\gamma}$ yields expressions for the coefficients

$$U_{\alpha\beta} = g^{\bar\alpha}{}_{(\alpha}g^{\bar\beta}{}_{\beta)}u^{\bar\alpha}u^{\bar\beta} + O(\varepsilon^4)\,, \tag{2.103a}$$

$$\dot{U}_{\alpha\beta} = g^{\bar\alpha}{}_{(\alpha}g^{\bar\beta}{}_{\beta)}\Big(R_{\bar\alpha u\sigma u|u} + \frac{1}{3}R_{\bar\alpha u\sigma u|\sigma}\Big)u_{\bar\beta} + O(\varepsilon^3)\,, \tag{2.103b}$$

$$\ddot{U}_{\alpha\beta} = \frac{2}{3}g^{\bar\alpha}{}_{(\alpha}g^{\bar\beta}{}_{\beta)}R_{\bar\alpha uu\sigma|u}u_{\bar\beta} + O(\varepsilon^2)\,, \tag{2.103c}$$

and

$$\dddot{U}_{\alpha\beta} = 0 + O(\varepsilon)\,, \tag{2.103d}$$

and

$$U_{\alpha\beta\gamma} = g^{\bar\alpha}{}_{(\alpha}g^{\bar\beta}{}_{\beta)}g^{\bar\gamma}{}_\gamma\Big(R_{\bar\beta u\bar\gamma\sigma} + \frac{2}{3}R_{\bar\beta u\bar\gamma s|\sigma}\Big)u_{\bar\alpha} + O(\varepsilon^3)\,, \tag{2.104a}$$

$$\dot{U}_{\alpha\beta\gamma} = g^{\bar\alpha}{}_{(\alpha}g^{\bar\beta}{}_{\beta)}g^{\bar\gamma}{}_\gamma\Big(R_{\bar\beta u\bar\gamma u} - \frac{2}{3}R_{\bar\beta u\bar\gamma u|\sigma} + \frac{1}{3}R_{\bar\beta u\bar\gamma\sigma|u}\Big)u_{\bar\alpha} + O(\varepsilon^2)\,, \tag{2.104b}$$

$$\ddot{U}_{\alpha\beta\gamma} = \frac{2}{3}g^{\bar\alpha}{}_{(\alpha}g^{\bar\beta}{}_{\beta)}g^{\bar\gamma}{}_\gamma R_{\bar\beta u\bar\gamma u|u}u_{\bar\alpha} + O(\varepsilon)\,, \tag{2.104c}$$

where the parenthesis indicate symmetrization over α and β.

The expressions in Eqs. (2.98), (2.99), and (2.102) form Taylor expansions of the direct potentials along the world line, evaluating the at $\tau = v$ and $\tau = u$ respectively yields the direct potentials at the advanced and retarded points x'' and x'.

Taylor expansion of the tail terms

In this section we derive expressions for the tail term V appearing in the expressions for the singular fields Eq. (2.73). As we will see, the scalar and electromagnetic tail term vanishes to the required order if the background spacetime is a vacuum spacetime.

Scalar field The scalar tail term is governed by Eq. (2.50), which in vacuum spacetimes read

$$[V] = 0\,,$$
(2.105a)

$$V_{,\alpha}\sigma^\alpha + \frac{1}{2}(\sigma^\alpha{}_\alpha - 1)V = \frac{1}{2}g^{\mu\nu}\nabla_\mu\nabla_\nu U, \quad \text{on the light cone}\,,$$
(2.105b)

and

$$g^{\mu\nu}\nabla_\mu\nabla_\nu V = 0\,.$$
(2.105c)

From Eq. (2.97a) we have $U = 1 + O(\varepsilon^4)$ and thus $g^{\mu\nu}\nabla_\mu\nabla_\nu U = O(\varepsilon^2)$. The data (initial data and sources) for system Eq. (2.105) therefore vanishes to $O(\varepsilon^2)$ and the trivial solution

$$V(x, x') = 0$$
(2.106)

clearly solves this system. By uniqueness the trivial solution is also the *only* solution and the tail term in Eq. (2.73a) vanishes to second order.

Electromagnetic field The electromagnetic tail term is governed by Eq. (2.57), which in vacuum spacetimes read

$$\left[V^\alpha{}_{\bar{\beta}}\right] = 0\,,$$
(2.107a)

$$V^\alpha{}_{\bar{\beta};\gamma}\sigma^\gamma + \frac{1}{2}(\sigma^\gamma{}_\gamma - 2)V^\alpha{}_{\bar{\beta}} = \frac{1}{2}g^{\mu\nu}\nabla_\mu\nabla_\nu U^\alpha{}_{\bar{\beta}}, \quad \text{on the light cone}\,,$$
(2.107b)

and

$$g^{\mu\nu}\nabla_\mu\nabla_\nu V^\alpha{}_{\bar{\beta}} = 0\,,$$
(2.107c)

where it is not immediately obvious why $V^\alpha{}_{\bar{\beta}}$ vanishes. Given Eqs. (2.30) and (2.97b) it is straightforward to show that

$$g^{\mu\nu}\nabla_\mu\nabla_\nu U^\alpha{}_{\bar{\beta}} = \frac{1}{3}g^\alpha{}_{\bar{\alpha}}R^{\bar{\alpha}}{}_{\bar{\beta}}{}^{\bar{\mu}}{}_{\bar{\nu};\bar{\mu}}\sigma^{\bar{\nu}} + O(\varepsilon^2)\,.$$
(2.108)

We exchange the first and second pair of indices of the Riemann tensor and apply Bianchi's identity, which brings the right hand side to the form

$$g^{\mu\nu}\nabla_\mu\nabla_\nu U^\alpha{}_{\bar{\beta}} = -\frac{1}{3}g^\alpha{}_{\bar{\alpha}}\left(R^{\bar{\mu}}{}_{\bar{\nu}\bar{\mu}}{}^{\bar{\alpha}}{}_{;\bar{\beta}} + R^{\bar{\mu}}{}_{\bar{\nu}\bar{\beta}\bar{\mu}}{}^{;\bar{\alpha}}\right)\sigma^{\bar{\nu}} + O(\varepsilon^2)\,. \tag{2.109}$$

The $O(\varepsilon)$ term vanishes since the contractions of the Riemann tensor vanish in vacuum spacetimes. Therefore we find a result analogous to the scalar field, namely that the trivial solution to Eq. (2.107) is the only one and

$$V^\alpha{}_{\bar{\beta}} = 0 + O(\varepsilon^2) \tag{2.110}$$

vanishes up to second order.

Gravitational field For gravity the situation is slightly different since the right hand side of the light cone differential equation Eq. (2.66b) cannot be shown to vanish even in vacuum spacetimes. However since we only require a solution $V^{\alpha\beta}{}_{\gamma'\delta'}$ up to terms of order $O(\varepsilon^2)$ the wave equation Eq. (2.66d) is identically true. We therefore only consider Eqs. (2.66b) and (2.66c). First consider the term in Eq. (2.66c) involving $\sigma^\varepsilon{}_\varepsilon$. Inspecting the expansion displayed in Eq. (2.29) we find that $\sigma^\varepsilon{}_\varepsilon = 4 + O(\varepsilon^4)$. We use the expansion Eq. (2.30) and argue as in the electromagnetic case that

$$g^{\mu\nu}\nabla_\mu\nabla_\nu U^{\alpha\beta}{}_{\bar{\gamma}\bar{\delta}} = 0 + O(\varepsilon^2)\,. \tag{2.111}$$

Substituting these two results into Eq (2.66c) we find

$$V^{\alpha\beta}{}_{\bar{\gamma}\bar{\delta};\varepsilon}\sigma^\varepsilon + V^{\alpha\beta}{}_{\bar{\gamma}\bar{\delta}} = g^{(\gamma}{}_{\bar{\gamma}}g^{\delta)}{}_{\bar{\delta}}R^\alpha{}_\gamma{}^\beta{}_\delta \tag{2.112}$$

with an initial condition

$$\left[V^{\alpha\beta}{}_{\bar{\gamma}\bar{\delta}}\right] = R^{(\bar{\alpha}}{}_{\bar{\gamma}}{}^{\bar{\beta})}{}_{\bar{\delta}}\,. \tag{2.113}$$

It is straightforward to guess a solution to this system which is correct to $O(\varepsilon^2)$. We find

$$V^{\alpha\beta}{}_{\bar{\gamma}\bar{\delta}} = g^{(\gamma}{}_{\bar{\gamma}}g^{\delta)}{}_{\bar{\delta}}\left(R^\alpha{}_\gamma{}^\beta{}_\delta - \frac{1}{2}R^\alpha{}_\gamma{}^\beta{}_{\delta;\varepsilon}\sigma^\varepsilon + O(\varepsilon^2)\right)\,. \tag{2.114}$$

Our result agrees with that of Anderson, Flanagan, and Ottewill [35] who derive results for $V^{\alpha\beta}{}_{\bar{\gamma}\bar{\delta}}$ to much higher order.

Eq. (2.114) forms the basis for a Taylor expansion of the tail terms along the world line. First however we use the symmetry of $V_{\alpha\beta\bar{\gamma}\bar{\delta}}$ to swap the barred and unbarred points

$$V_{\alpha\beta\bar{\gamma}\bar{\delta}} = g^{\bar{\alpha}}{}_\alpha g^{\bar{\beta}}{}_\beta\left(R_{\bar{\alpha}\bar{\gamma}\bar{\beta}\bar{\delta}} - \frac{1}{2}R_{\bar{\alpha}\bar{\gamma}\bar{\beta}\bar{\delta};\bar{\varepsilon}}\sigma^{\bar{\varepsilon}} + O(\varepsilon^2)\right)\,,$$

and calculate the derivative appearing inside the integral of Eq. (2.73c)

$$V_{\alpha\beta\bar{\gamma}\bar{\delta};\varepsilon} = \frac{1}{2}g^{\bar{\alpha}}{}_\alpha g^{\bar{\beta}}{}_\beta g^{\bar{\varepsilon}}{}_\varepsilon R_{\bar{\alpha}\bar{\gamma}\bar{\beta}\bar{\delta};\bar{\varepsilon}} + O(\varepsilon)\,. \tag{2.115}$$

We then define a world line scalar $V_{\alpha\beta} \equiv V_{\alpha\beta\mu\nu}u^\mu u^\nu$, $V_{\alpha\beta\gamma} \equiv V_{\alpha\beta\mu\nu\gamma}u^\mu u^\nu$ for $V_{\alpha\beta\gamma'\delta'}$ and its derivative. Thus

$$V_{\alpha\beta}(\tau) = V_{\alpha\beta} + \dot{V}_{\alpha\beta}\Delta + O(\Delta^2)\,, \tag{2.116a}$$
$$V_{\alpha\beta\gamma}(\tau) = V_{\alpha\beta\gamma} + O(\Delta)\,, \tag{2.116b}$$

where all coefficients are to be evaluated on the world line. Repeated use of Eq. (2.30) to handle the derivatives of the parallel propagator hidden in $\dot{V}_{\alpha\beta}$ yields expressions for the coefficients

$$V_{\alpha\beta} = g^{\bar\alpha}{}_\alpha g^{\bar\beta}{}_\beta\Big(R_{\bar\alpha u\bar\beta u} - \frac{1}{2}R_{\bar\alpha u\bar\beta u|\sigma}\Big) + O(\varepsilon^2)\,, \tag{2.117a}$$

and

$$\dot{V}_{\alpha\beta} = \frac{1}{2}g^{\bar\alpha}{}_\alpha g^{\bar\beta}{}_\beta R_{\bar\alpha u\bar\beta u|u} + O(\varepsilon)\,, \tag{2.117b}$$

and

$$V_{\alpha\beta\gamma} = \frac{1}{2}g^{\bar\alpha}{}_{(\alpha}g^{\bar\beta}{}_{\beta)}g^{\bar\gamma}{}_\gamma R_{\bar\alpha u\bar\beta u|u} + O(\varepsilon)\,. \tag{2.118}$$

The expressions in Eqs. (2.116) form Taylor expansions of the gravitational tail potentials along the world line, evaluating them at $\tau = v$ and $\tau = u$ respectively yields the tail potentials at the advanced and retarded points x'' and x'. Since to the required order $V_{\alpha\beta\gamma}$ is constant on the world line, the integral term is given by

$$\int_u^v \nabla_\gamma V_{\alpha\beta\mu\nu}(x, z(\tau))u^\mu u^\nu \, \mathrm{d}\tau = (v - u)\frac{1}{2}g^{\bar\alpha}{}_{(\alpha}g^{\bar\beta}{}_{\beta)}g^{\bar\gamma}{}_\gamma R_{\bar\alpha u\bar\beta u|u} + O(\varepsilon^2)\,. \tag{2.119}$$

2.7 Final expressions for the singular field

We use the results displayed in the previous sections to obtain an explicit expansion of the singular field in terms of $\sigma_{\bar\alpha}$ and $g^{\bar\alpha}{}_\alpha$.

Using the results displayed in Eqs. (2.73a), (2.80), (2.98), (2.84), (2.85), (2.90), (2.90a), and (2.106) [all of them], we obtain for the scalar singular field

$$\begin{aligned}
\Phi_\alpha^{\mathrm{S}}(x) = \frac{q}{s^3}g^{\bar\alpha}{}_\alpha\Bigg\{&\Big[\sigma_{\bar\alpha} + \bar{r}u_{\bar\alpha}\Big] \\
&+ \Big[\frac{1}{6}\bar{r}R_{\bar\alpha\sigma u\sigma} - \frac{1}{3}(\bar{r}^2 - s^2)R_{\bar\alpha u\sigma u} + \frac{3\bar{r}^2 - s^2}{6s^2}R_{u\sigma u\sigma}\sigma_{\bar\alpha} + \frac{\bar{r}(\bar{r}^2 - s^2)}{2s^2}R_{u\sigma u\sigma}u_{\bar\alpha}\Big] \\
&+ \Big[-\frac{1}{12}\bar{r}R_{\bar\alpha\sigma u\sigma|\sigma} + \frac{1}{8}(\bar{r}^2 - s^2)R_{\bar\alpha u\sigma u|\sigma} + \frac{1}{24}(\bar{r}^2 - s^2)R_{\bar\alpha\sigma u\sigma|u} \\
&- \frac{1}{12}\bar{r}(\bar{r}^2 - 3s^2)R_{\bar\alpha u\sigma u|u} + \frac{1}{24s^2}\Big(3\bar{r}(\bar{r}^2 - s^2)R_{u\sigma u\sigma|u} - (3\bar{r}^2 - s^2)R_{u\sigma u\sigma|\sigma}\Big)\sigma_{\bar\alpha} \\
&+ \frac{\bar{r}^2 - s^2}{8s^2}\Big((\bar{r}^2 - s^2)R_{u\sigma u\sigma|u} - \bar{r}R_{u\sigma u\sigma|\sigma}\Big)u_{\bar\alpha}\Big] + O(\varepsilon^5)\Bigg\}\,.
\end{aligned}$$

$$\tag{2.120}$$

Using the results displayed in Eqs. (2.73b), (2.80), (2.99), (2.82), (2.84), (2.85), (2.90), (2.90a), and (2.110) [all of them], we obtain for the electromagnetic singular field

$$
\begin{aligned}
A^{\mathrm{S}}_{\alpha;\beta}(x) = qg^{\bar{\alpha}}{}_{\alpha}g^{\bar{\beta}}{}_{\beta}\Bigg\{ & \left[\frac{1}{s^3}u_{\bar{\alpha}}\sigma_{\bar{\beta}} + \frac{\bar{r}}{s^3}u_{\bar{\alpha}}u_{\bar{\beta}}\right] \\
& + \left[\frac{\bar{r}}{6s^3}u_{\bar{\alpha}}R_{\bar{\beta}\sigma u\sigma} + \left(\frac{\bar{r}}{2s^3}\sigma_{\bar{\beta}} + \frac{\bar{r}^2-s^2}{2s^3}u_{\bar{\beta}}\right)R_{\bar{\alpha}uu\sigma} + \frac{\bar{r}^2-s^2}{3s^2}u_{\bar{\alpha}}R_{\bar{\beta}uu\sigma}\right. \\
& \left. + \frac{1}{2s}R_{\bar{\alpha}u\bar{\beta}\sigma} + \frac{3\bar{r}^2-s^2}{6s^5}R_{u\sigma u\sigma}u_{\bar{\alpha}}\sigma_{\bar{\beta}} + \frac{\bar{r}(\bar{r}^2-s^2)}{2s^5}R_{u\sigma u\sigma}u_{\bar{\alpha}}u_{\bar{\beta}} + \frac{\bar{r}}{2s}R_{\bar{\alpha}u\bar{\beta}u}\right] \\
& + \left[-\frac{\bar{r}}{12s^3}u_{\bar{\alpha}}R_{\bar{\beta}\sigma u\sigma|\sigma} - \frac{\bar{r}^2-s^2}{24s^3}u_{\bar{\alpha}}R_{\bar{\beta}\sigma\sigma u|u} - \left(\frac{\bar{r}}{6s^3}\sigma_{\bar{\beta}} + \frac{\bar{r}^2-s^2}{6s^3}u_{\bar{\beta}}\right)R_{\bar{\alpha}uu\sigma|\sigma}\right. \\
& - \frac{\bar{r}^2-s^2}{8s^3}u_{\bar{\alpha}}R_{\bar{\beta}uu\sigma|\sigma} - \frac{1}{3s^2}R_{\bar{\alpha}u\bar{\beta}\sigma|\sigma} + \left(\frac{\bar{r}^2-s^2}{6s^3}\sigma_{\bar{\beta}} + \frac{\bar{r}(\bar{r}^2-3s^2)}{6s^3}u_{\bar{\beta}}\right)R_{\bar{\alpha}uu\sigma|u} \\
& + \frac{\bar{r}(\bar{r}^2-3s^2)}{12s^3}u_{\bar{\alpha}}R_{\bar{\beta}uu\sigma|u} - \frac{\bar{r}}{3s}R_{\bar{\alpha}u\bar{\beta}u|\sigma} + \frac{\bar{r}}{6s}R_{\bar{\alpha}u\bar{\beta}\sigma|u} + \frac{\bar{r}^2+s^2}{6s^3}R_{\bar{\alpha}u\bar{\beta}u|u} \\
& + \left(-\frac{3\bar{r}^2-s^2}{24s^5}R_{u\sigma u\sigma|\sigma} + \frac{\bar{r}(\bar{r}^2-s^2)}{8s^5}R_{u\sigma u\sigma|u}\right)u_{\bar{\alpha}}\sigma_{\bar{\beta}} \\
& \left.\left. + \left(-\frac{\bar{r}(\bar{r}^2-s^2)}{8s^5}R_{u\sigma u\sigma|\sigma} + \frac{(\bar{r}^2-s^2)^2}{8s^5}R_{u\sigma u\sigma|u}\right)u_{\bar{\alpha}}u_{\bar{\beta}}\right]\right\} + O(\varepsilon^2)\,.
\end{aligned}
$$

$$(2.121)$$

Using the results displayed in Eqs. (2.73c), (2.80), (2.102), (2.116), (2.82), (2.84), (2.85), (2.90), (2.90a) and (2.79) [all of them], we obtain for the gravitational singular

field

$$\gamma^{\mathrm{S}}_{\alpha\beta;\gamma}(x)$$

$$
= mg^{\bar{\alpha}}{}_{\alpha}g^{\bar{\beta}}{}_{\beta}g^{\bar{\gamma}}{}_{\gamma}\Bigg\{\Bigg[\Bigg(\frac{u_{\bar{\alpha}}u_{\bar{\beta}}u_{\bar{\gamma}}\bar{r}^4}{2s^5}+\frac{u_{\bar{\alpha}}u_{\bar{\beta}}\sigma_{\bar{\gamma}}\bar{r}^3}{2s^5}-\frac{u_{\bar{\alpha}}u_{\bar{\beta}}u_{\bar{\gamma}}\bar{r}^2}{s^3}-\frac{u_{\bar{\alpha}}u_{\bar{\beta}}\sigma_{\bar{\gamma}}\bar{r}}{2s^3}+\frac{u_{\bar{\alpha}}u_{\bar{\beta}}u_{\bar{\gamma}}}{2s}\Bigg)R_{u\sigma u\sigma|u}
$$

$$
+\Bigg(\frac{4u_{\bar{\beta}}u_{\bar{\gamma}}\bar{r}^3}{3s^3}+\frac{4u_{\bar{\beta}}\sigma_{\bar{\gamma}}\bar{r}^2}{3s^2}-\frac{4u_{\bar{\beta}}u_{\bar{\gamma}}\bar{r}}{s}-\frac{4u_{\bar{\beta}}\sigma_{\bar{\gamma}}}{3s}\Bigg)R_{\bar{\alpha}uu\sigma|u}+\Bigg(\frac{u_{\bar{\alpha}}u_{\bar{\beta}}\bar{r}^3}{3s^3}-\frac{u_{\bar{\alpha}}u_{\bar{\beta}}\bar{r}}{s}\Bigg)R_{\bar{\gamma}uu\sigma|u}
$$

$$
+\Bigg(-\frac{u_{\bar{\alpha}}u_{\bar{\beta}}u_{\bar{\gamma}}\bar{r}^3}{2s^5}-\frac{u_{\bar{\alpha}}u_{\bar{\beta}}\sigma_{\bar{\gamma}}\bar{r}^2}{2s^5}+\frac{u_{\bar{\alpha}}u_{\bar{\beta}}u_{\bar{\gamma}}\bar{r}}{2s^3}+\frac{u_{\bar{\beta}}u_{\bar{\alpha}}\sigma_{\bar{\gamma}}}{6s^3}\Bigg)R_{u\sigma u\sigma|\sigma}
$$

$$
+\Bigg(\frac{2u_{\bar{\gamma}}\bar{r}^2}{s}+\frac{2\sigma_{\bar{\gamma}}\bar{r}}{s}+2u_{\bar{\gamma}}s\Bigg)R_{\bar{\alpha}u\bar{\beta}u|u}+\Bigg(\frac{4u_{\bar{\beta}}\bar{r}^2}{3s^2}+\frac{4su_{\bar{\beta}}}{3}\Bigg)R_{\bar{\alpha}u\bar{\gamma}u|u}
$$

$$
+\Bigg(-\frac{u_{\bar{\alpha}}u_{\bar{\beta}}\bar{r}^2}{6s^3}+\frac{u_{\bar{\alpha}}u_{\bar{\beta}}}{6s}\Bigg)R_{\bar{\gamma}\sigma\sigma u|u}+\Bigg(-\frac{u_{\bar{\alpha}}u_{\bar{\beta}}\bar{r}^2}{2s^3}+\frac{u_{\bar{\alpha}}u_{\bar{\beta}}}{2s}\Bigg)R_{\bar{\gamma}uu\sigma|\sigma}
$$

$$
+\Bigg(\frac{4u_{\bar{\beta}}u_{\bar{\gamma}}\bar{r}^2}{3s^2}-\frac{4u_{\bar{\beta}}\sigma_{\bar{\gamma}}\bar{r}}{s^3}+\frac{4u_{\bar{\beta}}u_{\bar{\gamma}}}{3s}\Bigg)R_{\bar{\alpha}uu\sigma|\sigma}-\frac{8u_{\bar{\beta}}\bar{r}}{3s}R_{\bar{\alpha}u\bar{\gamma}u|\sigma}+\frac{4u_{\bar{\beta}}\bar{r}}{3s}R_{\bar{\alpha}u\bar{\gamma}\sigma|u}
$$

$$
+\Bigg(-\frac{2u_{\bar{\gamma}}\bar{r}}{s}-\frac{\sigma_{\bar{\gamma}}}{s}\Bigg)R_{\bar{\alpha}u\bar{\beta}u|\sigma}-\frac{u_{\bar{\alpha}}u_{\bar{\beta}}\bar{r}}{3s^2}R_{\bar{\gamma}\sigma u\sigma|\sigma}-\frac{8u_{\bar{\beta}}}{3s}R_{\bar{\alpha}u\bar{\gamma}\sigma|\sigma}-2sR_{\bar{\alpha}u\bar{\beta}u|\bar{\gamma}}\Bigg]
$$

$$
+\Bigg[\Bigg(\frac{4u_{\bar{\alpha}}u_{\bar{\beta}}\bar{r}^2}{3s^3}-\frac{4u_{\bar{\alpha}}u_{\bar{\beta}}}{3s}\Bigg)R_{\bar{\gamma}uu\sigma}+\Bigg(\frac{4u_{\bar{\beta}}u_{\bar{\gamma}}\bar{r}^2}{s^3}+\frac{4u_{\bar{\beta}}\sigma_{\bar{\gamma}}\bar{r}}{s^3}-\frac{4u_{\bar{\beta}}u_{\bar{\gamma}}}{s}\Bigg)R_{\bar{\alpha}uu\sigma|\sigma}
$$

$$
+\Bigg(\frac{2u_{\bar{\alpha}}u_{\bar{\beta}}u_{\bar{\gamma}}\bar{r}^3}{s^5}+\frac{2u_{\bar{\alpha}}u_{\bar{\beta}}\sigma_{\bar{\gamma}}\bar{r}^2}{s^5}-\frac{2u_{\bar{\alpha}}u_{\bar{\beta}}u_{\bar{\gamma}}\bar{r}}{s^3}-\frac{2u_{\bar{\alpha}}u_{\bar{\beta}}\sigma_{\bar{\gamma}}}{3s^2}\Bigg)R_{u\sigma u\sigma}+\Bigg(\frac{4u_{\bar{\gamma}}\bar{r}}{s}+\frac{4\sigma_{\bar{\gamma}}}{s}\Bigg)R_{\bar{\alpha}u\bar{\beta}u}
$$

$$
+\frac{4u_{\bar{\beta}}\bar{r}}{s}R_{\bar{\alpha}u\bar{\gamma}u}+\frac{2u_{\bar{\alpha}}u_{\bar{\beta}}\bar{r}}{3s^3}R_{\bar{\gamma}\sigma u\sigma}+\frac{4u_{\bar{\beta}}}{s}R_{\bar{\alpha}u\bar{\gamma}|\sigma}\Bigg]+\Bigg[\frac{4u_{\bar{\alpha}}u_{\bar{\beta}}(u_{\bar{\gamma}}\bar{r}+\sigma_{\bar{\gamma}})}{s^3}\Bigg]\Bigg\}+O(\varepsilon^2)\,.
$$

$$\tag{2.122}$$

2.8 Tetrad components

The original mode sum regularization scheme by Barack, Ori, Mino, Nakano and Tanaka [2] operated on a scalar spherical harmonic decomposition of the self-force four vector. In our approach we introduce tetrad components of the field gradients which are proper scalars and can be decomposed into scalar spherical harmonics in a natural way. We introduce a pseudo-Cartesian tetrad

$$
e^{\alpha}{}_{(0)}=\Bigg[\frac{1}{\sqrt{f}},0,0,0\Bigg],
\tag{2.123a}
$$

$$
e^{\alpha}{}_{(1)}=\Bigg[0,\sqrt{f}\sin\theta\cos\phi,\frac{1}{r}\cos\theta\cos\phi,-\frac{\sin\phi}{r\sin\theta}\Bigg],
\tag{2.123b}
$$

$$
e^{\alpha}{}_{(2)}=\Bigg[0,\sqrt{f}\sin\theta\sin\phi,\frac{1}{r}\cos\theta\sin\phi,\frac{\cos\phi}{r\sin\theta}\Bigg],
\tag{2.123c}
$$

$$
e^{\alpha}{}_{(3)}=\Bigg[0,\sqrt{f}\cos\theta,-\frac{1}{r}\sin\theta,0\Bigg]
\tag{2.123d}
$$

together with the complex combinations

$$
e^{\alpha}{}_{(\pm)}\equiv e^{\alpha}_{(1)}\pm ie^{\alpha}_{(2)}=\Bigg[0,\sqrt{f}\sin\theta e^{\pm i\phi},\frac{1}{r}\cos\theta e^{\pm i\phi},\frac{\pm ie^{\pm i\phi}}{r\sin\theta}\Bigg],
\tag{2.123e}
$$

where $f = 1 - \frac{2M}{r}$ and decompose Φ_α, $A_{\alpha;\beta}$ and $\gamma_{\alpha\beta;\gamma}$ in terms of these.

The pseudo-Cartesian tetrad is orthonormal

$$g_{\alpha\beta}e^{\alpha}{}_{(\mu)}e^{\beta}{}_{(\nu)} = \nu_{(\mu)(\nu)} \,, \tag{2.124}$$

where $\nu_{(\mu)(\nu)} = \mathrm{diag}(-1,1,1,1)$ is the Minkowski metric. With the help of the matrix inverse $\nu^{(\mu)(\nu)}$ of $\nu_{(\mu)(\nu)}$ we define a dual tetrad

$$e^{(\mu)}{}_\alpha \equiv g_{\alpha\beta}\nu^{(\mu)(\nu)}e^{\beta}{}_{(\nu)} \,. \tag{2.125}$$

The tetrad and its dual satisfy a completeness relation

$$e^{\beta}{}_{(\mu)}e^{(\mu)}{}_\alpha = \delta^{\beta}{}_\alpha \,, \quad e^{\alpha}{}_{(\mu)}e^{(\nu)}{}_\alpha = \delta^{(\mu)}{}_{(\nu)} \,. \tag{2.126}$$

We define tetrad components for example for the scalar field gradient Φ_α

$$\Phi_{(\mu)} = \Phi_\alpha e^{\alpha}{}_{(\mu)} \,, \tag{2.127a}$$

$$\Phi_\alpha = \Phi_{(\mu)}e^{(\mu)}{}_\alpha \,, \tag{2.127b}$$

using the completeness relations to guarantee the existence of a unique decomposition.

2.9 Coupling coefficients

The numerical scheme described in section 4 deals with a decomposition of the field into scalar, vector and tensorial harmonics. In order to obtain tetrad components of the field gradient from these, we require coupling coefficients similar to the Clebsch-Gordon coefficients in quantum mechanics.

2.9.1 Scalar coupling coefficients

We require a translation table between the gradient of a scalar spherical harmonic mode decomposition $\nabla_\alpha(\Phi^{\ell m}Y_{\ell m})$ and a spherical harmonic mode decomposition of the tetrad components $\Phi^{\ell m}_{(\mu)}$. We begin by writing down the multipole modes of the tetrad decomposition of the field gradient and gradually substituting for the field gradient

$$
\begin{aligned}
\Phi^{\ell m}_{(\mu)} &= \int \Phi_{(\mu)} \, \bar{Y}^{\ell m} \, \mathrm{d}\Omega \\
&= \int e^{\alpha}{}_{(\mu)} \nabla_\alpha \Phi \bar{Y}^{\ell m} \, \mathrm{d}\Omega \\
&= \int e^{\alpha}{}_{(\mu)} \nabla_\alpha \left(\sum_{\ell',m'} \Phi^{\ell'm'} Y_{\ell'm'} \right) \bar{Y}^{\ell m} \, \mathrm{d}\Omega \\
&= \sum_{\ell',m'} \int \left(e^{a}{}_{(\mu)} \Phi^{\ell'm'}_{,a} Y_{\ell'm'} + e^{A}{}_{(\mu)} \Phi^{\ell'm'} Y_{\ell'm',A} \right) \bar{Y}^{\ell m} \, \mathrm{d}\Omega \\
&= \sum_{\ell',m'} \left(\Phi^{\ell'm'}_{,a} \int e^{a}{}_{(\mu)} Y_{\ell'm'} \bar{Y}^{\ell m} \, \mathrm{d}\Omega + \Phi^{\ell'm'} \int e^{A}{}_{(\mu)} Y_{\ell'm',A} \bar{Y}^{\ell m} \, \mathrm{d}\Omega \right) \\
&\equiv \sum_{\ell',m'} \left(C^{a}_{(\mu)}(\ell m | \ell'm') \Phi^{\ell'm'}_{,a} + C_{(\mu)}(\ell m | \ell'm') \Phi^{\ell'm'} \right) ,
\end{aligned}
\tag{2.128}
$$

where in the third line we used the convention to designate angular indices θ, ϕ by capital Latin letters and use lowercase Latin letters for r and t indices. The coupling coefficients are integrals over three spherical harmonics—one hidden in the angular dependence of the basis vectors—that can be evaluated using the results in chapter 12.6 of [36] as outlined in [23]. After some algebra we find the non-vanishing coefficients

$$C^t_{(0)}(\ell m|\ell'm') = \frac{1}{\sqrt{f}}\,\delta_{\ell\ell'}\delta_{mm'}\,, \tag{2.129a}$$

$$C^r_{(+)}(\ell m|\ell'm') = -\sqrt{\frac{(\ell+m-1)(\ell+m)}{(2l-1)(2l+1)}}\sqrt{f}\delta_{\ell',\ell-1}\delta_{m',m-1}$$
$$+\sqrt{\frac{(\ell-m+1)(\ell-m+2)}{(2l+1)(2l+3)}}\sqrt{f}\delta_{\ell',\ell+1}\delta_{m',m-1}\,, \tag{2.129b}$$

$$C^r_{(-)}(\ell m|\ell'm') = \sqrt{\frac{(\ell-m-1)(\ell-m)}{(2l-1)(2l+1)}}\sqrt{f}\,\delta_{\ell',\ell-1}\delta_{m',m+1}$$
$$-\sqrt{\frac{(\ell+m+1)(\ell+m+2)}{(2l+1)(2l+3)}}\sqrt{f}\delta_{\ell',\ell+1}\delta_{m',m+1}\,, \tag{2.129c}$$

$$C^r_{(3)}(\ell m|\ell'm') = \sqrt{\frac{(\ell-m)(\ell+m)}{(2l-1)(2l+1)}}\sqrt{f}\delta_{\ell',\ell-1}\delta_{m'm}$$
$$+\sqrt{\frac{(\ell-m+1)(\ell+m+1)}{(2l+1)(2l+3)}}\sqrt{f}\delta_{\ell',\ell+1}\delta_{m'm}\,, \tag{2.129d}$$

$$C_{(+)}(\ell m|\ell'm') = \sqrt{\frac{(\ell+m-1)(\ell+m)}{(2l-1)(2l+1)}}\frac{\ell-1}{r}\delta_{\ell',\ell-1}\delta_{m',m-1}$$
$$+\sqrt{\frac{(\ell-m+1)(\ell-m+2)}{(2l+1)(2l+3)}}\frac{\ell+2}{r}\delta_{\ell',\ell+1}\delta_{m',m-1\cdot}\,, \tag{2.129e}$$

$$C_{(-)}(\ell m|\ell'm') = -\sqrt{\frac{(\ell-m-1)(\ell-m)}{(2l-1)(2l+1)}}\frac{\ell-1}{r}\delta_{\ell',\ell-1}\delta_{m',m+1}$$
$$-\sqrt{\frac{(\ell+m+1)(\ell+m+2)}{(2l+1)(2l+3)}}\frac{\ell+2}{r}\delta_{\ell',\ell+1}\delta_{m',m+1\cdot}\,, \tag{2.129f}$$

and

$$C_{(3)}(\ell m|\ell'm') = -\sqrt{\frac{(\ell-m)(\ell+m)}{(2l-1)(2l+1)}}\frac{\ell-1}{r}\delta_{\ell',\ell-1}\delta_{m'm}$$
$$+\sqrt{\frac{(\ell-m+1)(\ell+m+1)}{(2l+1)(2l+3)}}\frac{\ell+2}{r}\delta_{\ell',\ell+1}\delta_{m'm\cdot\cdot}\,. \tag{2.129g}$$

2.9.2   Electromagnetic coupling coefficients

Similar to the scalar case we require coupling coefficients to translate between the modes of the vector potential $A_a^{\ell m}$, $v^{\ell m}$, $\tilde{v}^{\ell m}$ (as defined in section 4.3) and the tetrad components of the Faraday tensor

$$F_{\alpha\beta} = A_{\beta,\alpha} - A_{\alpha,\beta}\,. \tag{2.130}$$

The tetrad components $F_{(\mu)(\nu)}$ are decomposed in terms of scalar spherical harmonics

$$F_{(\mu)(\nu)} = \sum_{\ell,m} F_{(\mu)(\nu)}^{\ell m} Y_{\ell m}\,, \tag{2.131}$$

where each mode is given by

$$F_{(\mu)(\nu)}^{\ell m} = \int F_{(\mu)(\nu)} \bar{Y}_{\ell m}\ \mathrm{d}\Omega\,. \tag{2.132}$$

To obtain expressions for the coupling coefficients we substitute $F_{(\mu)(\nu)} = F_{\alpha\beta} e^{\alpha}{}_{(\mu)} e^{\beta}{}_{(\nu)}$ into Eq. (2.132)

$$\begin{aligned}
F_{(\mu)(\nu)}^{\ell m} &= \int \mathrm{d}\Omega\, F_{(\mu)(\nu)} \bar{Y}^{\ell m} \\
&= \int \mathrm{d}\Omega\, (A_{\beta,\alpha} - A_{\alpha,\beta})\, e^{\alpha}{}_{(\mu)} e^{\beta}{}_{(\nu)} \bar{Y}^{\ell m} \\
&= \int \sum_{\ell',m'} \Big[(A_{b,a} - A_{a,b})\, e^{a}{}_{(\mu)} e^{b}{}_{(\nu)} \bar{Y}^{\ell m} + (A_{b,A} - A_{A,b})\, e^{A}{}_{(\mu)} e^{b}{}_{(\nu)} \bar{Y}^{\ell m} \\
&\qquad\qquad + (A_{B,a} - A_{a,B})\, e^{a}{}_{(\mu)} e^{B}{}_{(\nu)} \bar{Y}^{\ell m} + (A_{B,A} - A_{A,B})\, e^{A}{}_{(\mu)} e^{B}{}_{(\nu)} \bar{Y}^{\ell m} \Big]\ \mathrm{d}\Omega \\
&\equiv \sum_{\ell',m'} \Big[C^{ab}_{(\mu)(\nu)}(\ell'm'|\ell m) \left(A_{b,a}^{\ell'm'} - A_{a,b}^{\ell'm'} \right) + D^{a}_{(\mu)(\nu)}(\ell'm'|\ell m) \left(\partial_a v^{\ell'm'} - A_a^{\ell'm'} \right) \\
&\qquad\qquad + E^{a}_{(\mu)(\nu)}(\ell'm'|\ell m) \partial_a \tilde{v}^{\ell'm'} + E_{(\mu)(\nu)}(\ell'm'|\ell m) \tilde{v}^{\ell'm'} \Big]\,,
\end{aligned} \tag{2.133}$$

which defines the coupling coefficients. It is often possible to express these coupling in coefficients in terms of linear combinations of the coupling coefficients derived in section 3.6 for the scalar field. To simplify the notation of the coupling coefficients we use

$$\gamma^{\ell m} = \sqrt{\frac{(\ell+m)(\ell+m+1)}{(2\ell+1)(2\ell+3)}}\,, \tag{2.134a}$$

$$\epsilon^{\ell m} = \sqrt{\frac{(\ell+m+1)(\ell-m+1)}{(2\ell+1)(2\ell+3)}}\,, \tag{2.134b}$$

as shorthands for recurring combinations of terms. Similarly it proves useful to define lower order "coupling coefficients" for the odd sector, which is absent in the scalar

case.

$$E_{(+)}(\ell'm'|\ell m) = -\frac{i}{r}\sqrt{(\ell - m + 1)(\ell + m)}\delta_{\ell'\ell}\delta_{m'm-1}, \qquad (2.135a)$$

$$E_{(-)}(\ell'm'|\ell m) = -\frac{i}{r}\sqrt{(\ell + m + 1)(\ell - m)}\delta_{\ell'\ell}\delta_{m'm+1}. \qquad (2.135b)$$

In terms of these, the first coefficient for the expansion of $F_{(0)(+)}$ is given by

$$\begin{aligned}
C^{tr}_{(0)(+)}(\ell'm'|\ell m) &= \int Y^{\ell'm'}e^t_{(0)}e^r_{(+)}\bar{Y}^{\ell m}\,d\Omega \\
&= \frac{1}{\sqrt{f}}\int Y^{\ell'm'}e^r_{(+)}\bar{Y}^{\ell m}\,d\Omega \\
&= C^r_{(+)}(\ell'm'|\ell m)/\sqrt{f},
\end{aligned} \qquad (2.136)$$

where $C^r_{(+)}(\ell'm'|\ell m)$ is the scalar coupling coefficient given in Eq. (2.129b). All other combinations of a, b and (μ), (ν) lead to a vanishing $C^{ab}_{(\mu)(\nu)}$. Similarly for the remaining non-vanishing coefficients for the $F_{(0)(+)}$ component

$$D^t_{(0)(+)}(\ell'm'|\ell m) = C_{(+)}(\ell'm'|\ell m)/\sqrt{f}, \qquad (2.137a)$$

$$E^t_{(0)(+)}(\ell'm'|\ell m) = E_{(+)}(\ell'm'|\ell m)/\sqrt{f}. \qquad (2.137b)$$

The coupling coefficients for $F_{(+)(-)}$ contain both even and odd modes. The first non-vanishing one is $D^r_{(+)(-)}(\ell'm'|\ell m)$, which is given by

$$\begin{aligned}
D^r_{(+)(-)}(\ell'm'|\ell m) = {}& \sqrt{f}\gamma^{\ell,-m+1}C_{(-)}(\ell'm'|\ell + 1, m - 1) \\
&- \sqrt{f}\gamma^{\ell-1,m}C_{(-)}(\ell'm'|\ell - 1, m - 1) \\
&+ \sqrt{f}\gamma^{\ell,m+1}C_{(+)}(\ell'm'|\ell + 1, m + 1) \\
&- \sqrt{f}\gamma^{\ell-1,-m}C_{(+)}(\ell'm'|\ell - 1, m + 1)
\end{aligned} \qquad (2.138)$$

while the coefficients coupling to odd modes are

$$\begin{aligned}
E^r_{(+)(-)}(\ell'm'|\ell m) = {}& \sqrt{f}\gamma^{\ell,-m+1}E_{(-)}(\ell'm'|\ell + 1, m - 1) \\
&- \sqrt{f}\gamma^{\ell-1,m}E_{(-)}(\ell'm'|\ell - 1, m - 1) \\
&+ \sqrt{f}\gamma^{\ell,m+1}E_{(+)}(\ell'm'|\ell + 1, m + 1) \\
&- \sqrt{f}\gamma^{\ell-1,-m}E_{(+)}(\ell'm'|\ell - 1, m + 1),
\end{aligned} \qquad (2.139a)$$

$$\begin{aligned}
E_{(+)(-)}(\ell'm'|\ell m) = {}& -2i/r^2(\ell + 1)(\ell + 2)\epsilon^{\ell m}\delta_{\ell'\ell+1}\delta_{m'm} \\
&- 2i/r^2(\ell - 1)\ell\epsilon^{\ell-1,m}\delta_{\ell'\ell-1}\delta_{m'm}.
\end{aligned} \qquad (2.139b)$$

"Piled Higher and Deeper" by Jorge Cham, www.phdcomics.com

Chapter 3

Regularization parameters

3.1 Multipole coefficients

In this section we derive expressions for the *multipole coefficients*, values of the modes of a spherical harmonic decomposition of a scalar function at the north pole of a specific angular coordinate system. The material in this chapter is patterned after the treatment in [18], [15] and [37].

Let α, β be angular coordinates on a sphere in Schwarzschild spacetime. Let $F_{(\mu)}$ be a scalar function, which we envision to be a tetrad component of the force. We introduce multipole coefficients $F_{(\mu)}^{\ell}$ via

$$F_{(\mu)} = \sum_{\ell} F_{(\mu)}^{\ell}, \quad F_{(\mu)}^{\ell} \equiv \sum_{m} F_{(\mu)}^{\ell m}(t, r) Y_{\ell m}(0, ?), \quad F_{(\mu)}^{\ell m} = \int F_{(\mu)} \bar{Y}^{\ell m} \, \mathrm{d}\Omega. \quad (3.1)$$

Here ? stands for an arbitrary angle β since at the north pole $\alpha = 0$ the angle β is irrelevant. Further at the north pole all but the $m = 0$ spherical harmonics vanish (see Eq. (12.6.2) in [36])

$$Y_{\ell m}(0, \beta) = \sqrt{\frac{2\ell + 1}{4\pi}} \delta_{m0}, \quad (3.2)$$

therefore the sum over m in Eq. (3.1) collapses and the multipole coefficients are given by

$$F_{(\mu)}^{\ell} = \sqrt{\frac{2\ell + 1}{4\pi}} F_{(\mu)}^{\ell 0}. \quad (3.3)$$

The spherical harmonic mode $F_{(\mu)}^{\ell 0}$ in turn is given by

$$F_{(\mu)}^{\ell 0} = \int F_{(\mu)} \bar{Y}^{\ell 0} \, d\Omega = \int \left(\int F_{(\mu)} \sqrt{\frac{2\ell + 1}{4\pi}} P_\ell(\cos\alpha) \, d\cos\alpha \right) d\beta \,, \qquad (3.4)$$

where we have substituted

$$Y_{\ell m} = \sqrt{\frac{2\ell + 1}{4\pi} \frac{(\ell - m)!}{(\ell + m)!}} P_\ell^m(\cos\alpha) e^{im\beta} \qquad (3.5)$$

for the spherical harmonic. Clearly then we can evaluate the multipole coefficients as

$$F_{(\mu)}^\ell = \frac{1}{2\pi} \int \underbrace{\left(\frac{2\ell + 1}{2} \int F_{(\mu)}(r, t, \alpha, \beta) P_\ell(\cos\alpha) \, d\cos\alpha \right)}_{\text{Legendre decomposition}} d\beta \,, \qquad (3.6)$$

$$\underbrace{\phantom{F_{(\mu)}^\ell = \frac{1}{2\pi} \int \left(\frac{2\ell + 1}{2} \int F_{(\mu)}(r, t, \alpha, \beta) P_\ell(\cos\alpha) \, d\cos\alpha \right) d\beta}}_{\text{average over } \beta}$$

ie. by first decomposing in terms Legendre polynomials and then averaging over β. Note that on occasion we will reverse the order of the integrals in order to show that certain terms vanish when averaged over β.

3.2 Mode sum regularization

For a singular source term $\rho(x)$, $j_\alpha(x)$ or $T_{\alpha\beta}(x)$ the retarded solution of the wave equations Eqs. (2.44), (2.53) and (2.63) diverges at the position of the particle. Decomposing into scalar, vector and tensorial spherical harmonic modes, however, we find that each mode separately is continuous (but not differentiable) at the position of the particle, denoted

$$x_0 = [t_0, r_0, \frac{\pi}{2}, \varphi_0] \,. \qquad (3.7)$$

The mode-sum regularization procedure of Barack, Ori, Mino, Sasaki and Tanaka [2] first calculates each mode, then regularizes each mode individually and finally sums the modes to retrieve the regularized force. Schematically, using scalar harmonics to decompose the (vector) force on the particle, this means that the force (which corresponds to the field gradient) is decomposed into spherical harmonic modes as follows

$$F_\alpha^{\text{ret}} = \sum_{\ell=0}^\infty \sum_{m=-\ell}^\ell F_\alpha^{\text{ret}, \ell m}(t, r) Y_{\ell m}(\theta, \phi) \,, \qquad (3.8a)$$

$$F_\alpha^{\text{ret}, \ell m}(t, r) = \int F_\alpha^{\text{ret}}(t, r, \theta, \phi) \bar{Y}^{\ell m}(\theta, \phi) \, d\Omega \,. \qquad (3.8b)$$

For each ℓ-mode we form multipole coefficients

$$F_\alpha^{\text{ret}, \ell} \equiv \sum_{m=-\ell}^\ell F_\alpha^{\text{ret}, \ell m} Y_{\ell m}(\tfrac{\pi}{2}, \varphi_0) \qquad (3.9)$$

which are finite at the position of the particle. The regularized self-force is calculated as

$$F_\alpha^{\text{R}} = \sum_\ell \left\{ F_\alpha^{\text{ret},\ell} - q \left[A_\alpha \left(\ell + \frac{1}{2} \right) + B_\alpha + \frac{C_\alpha}{\ell + \frac{1}{2}} + \frac{D_\alpha}{(\ell - \frac{1}{2})(\ell + \frac{3}{2})} + \dots \right] \right\}, \quad (3.10)$$

where the regularization parameter A_α, B_α, C_α and D_α are independent of ℓ. The terms in square brackets in Eq. (3.10) are the multipole coefficients of the singular field. Strictly speaking, only the A_α, B_α and C_α terms are required to regularize the mode sum. The D_α terms correspond to a regular contribution and their sum vanishes identically. Removing the D_α terms, however, results in a sum which converges faster, allowing us to calculate fewer ℓ modes to reach a given accuracy for the self-force. Numerically therefore the inclusion of the D_α terms is advantageous.

Since the singular field gradient modes are discontinuous across the position of the particle we cannot evaluate the analog of Eq. (3.8b) on a sphere containing the position of the particle. We therefore evaluate the integral on a slightly larger sphere of radius $r_0 + \Delta$ and take a one-sided limit $\Delta \to 0^+$ to handle the discontinuity. For similar reasons, we follow Barack [37] and obtain the multipole coefficients of the singular field gradient not at x_0 but at the displaced point $x_0' = [t, r_0 + \Delta, \pi/2, \varphi_0']$ where

$$\varphi_0' = \varphi_0 - c\Delta, \quad c = \frac{r_0 J \dot{r}_0}{(r_0 - 2M)(r_0^2 + J^2)}. \quad (3.11)$$

3.3 Rotation of coordinates

The multipole coefficients of $\Phi_{(\mu)}^\ell$, $A_{(\mu)(\nu)}^\ell$ and $\gamma_{(\mu)(\nu)(\lambda)}^\ell$ are invariant under a rotation of the angles θ and ϕ. This follows from the fact that a rotation $[\theta, \phi] \mapsto [\alpha, \beta]$ maps each spherical harmonic $Y_{\ell m}(\theta, \phi)$ to a linear combination of $Y_{\ell m}(\alpha, \beta)$ coupling terms of different m, but leaving ℓ alone. Since the multipole coefficients result from a summation over m they are unchanged under such a coordinate transformation. Following Mino [15] we use this property to introduce new angular coordinates α, β in which the point $[\frac{\pi}{2}, \varphi_0']$ is rotated to the north pole $[\alpha = 0, \beta = ?]$. Here ? indicates that the value of β is irrelevant. Such a rotation simplifies the calculations significantly since the regularization parameters, which are the multipole coefficients of the singular field gradient evaluated at the location of the particle, can be evaluated at the special point $\alpha = 0$ instead of the generic point $[\theta = \pi/2, \phi = \varphi_0(t)]$. Formally the rotation is described by

$$\sin\theta \cos(\phi - \varphi_0') = \cos\alpha, \quad (3.12a)$$
$$\sin\theta \sin(\phi - \varphi_0') = \sin\alpha \cos\beta, \quad (3.12b)$$
$$\cos\theta = \sin\alpha \sin\beta. \quad (3.12c)$$

3.4 Representation of the displacement vector

The key step of mode sum regularization is to obtain the modes of the singular field gradient on a sphere which does not include the location of the particle. For a particle

located at

$$x_0 = [t, r_0, \pi/2, \varphi_0] \tag{3.13}$$

we use a sphere of slightly large radius $r_0 + \Delta$ and therefore have for the displacement vector w^α

$$w^\alpha = [0, \Delta, \theta - \pi/2, \phi - \varphi_0] \,, \tag{3.14}$$

where the displacement in ϕ is calculated with respect to φ_0 not φ_0' of Eq. (3.12). In terms of the angles α and β defined in section 3.3, the angular components of w^α are given by

$$w^\theta = -\arcsin(\sin\alpha\sin\beta)\,, \quad \text{and} \quad w^\phi = \arcsin\left(\frac{\sin\alpha\cos\beta}{\sqrt{1 - \sin^2\alpha\sin^2\beta}}\right) - c\Delta\,. \tag{3.15}$$

We define an auxiliary variable

$$Q \equiv \sqrt{1 - \cos\alpha} \Leftrightarrow \sin(\alpha) = Q\sqrt{2 - Q^2}\,, \tag{3.16}$$

which is of the same order as α and thus Δ. Expanding Eq. (3.15) we obtain an expansion of w^α in terms of functions globally defined on the sphere

$$w^\theta = -\sqrt{2}Q\sin\beta - \frac{\sqrt{2}}{12}Q^3(1 - 4\cos^2\beta)\sin\beta + O(Q^5)\,, \tag{3.17a}$$

$$w^\phi = -c\Delta + \sqrt{2}Q\cos\beta + \frac{\sqrt{2}}{12}Q^3(9 - 8\cos^2\beta)\cos\beta + O(Q^5)\,. \tag{3.17b}$$

3.5   Squared distance function

The last piece of machinery we need is the leading order term of the squared distance function

$$\tilde{\rho}^2 = g_{\alpha\beta}w^\alpha w^\beta\,, \tag{3.18}$$

where the metric is to be evaluated at the particle's location x_0. Keeping only the leading order term in Q and Δ we find

$$\rho^2 = \frac{r_0^4 E^2}{(r_0 - 2M)^2(r_0^2 + J^2)}\Delta^2 + 2(r_0^2 + J^2)\chi Q^2\,, \tag{3.19a}$$

where

$$\chi \equiv 1 - k\sin^2\beta\,, \quad k \equiv \frac{J^2}{r_0^2 + J^2}\,. \tag{3.19b}$$

Substituting for Q this can be rewritten in the form

$$\rho^2 = 2(r_0^2 + J^2)\chi(\delta^2 + 1 - \cos\alpha)\,, \quad \text{with} \quad \delta^2 \equiv \frac{E^2 r_0^4}{2(r_0^2 + J^2)^2(r_0 - 2M)^2}\frac{\Delta^2}{\chi}\,. \tag{3.20}$$

We use the results displayed in Eq. (3.19) to write the field gradients in terms of ρ, Q, Δ, $\chi\cos\beta$ and $\sin\beta$ such that Q, $\cos\beta$ and $\sin\beta$ occur only linearly, higher powers having been replaced by ρ and χ respectively.

3.6 Scalar field

A calculation of the scalar regularization parameters begins with Eq. (2.120). We introduce tetrad components of the field gradient using the tetrad of section 2.8

$$\Phi^{\mathrm{S}}_{(\mu)} \equiv \Phi^{\mathrm{S}}_{\alpha} e^{\alpha}{}_{(\mu)} , \tag{3.21}$$

which permits a clean calculation of the regularization parameters using only scalar spherical harmonics.

Using the symbolic manipulator GRTensor II which runs under Maple we substitute Eqs. (2.31), (2.38), (2.39), (2.43), (3.17), $w^t = 0$, $w^r = \Delta$ and (3.19) into Eq. (3.21). The resulting expression is much to long to be displayed here, containing several hundred thousand terms. Instead we list its overall structure in terms of Δ, ρ, and Q, $\cos\beta$, $\sin\beta$.

$$\Phi^{\mathrm{S}}_{(\mu)} = \Phi^{\mathrm{S}}_{(\mu),-2} + \Phi^{\mathrm{S}}_{(\mu),-1} + \Phi^{\mathrm{S}}_{(\mu),0} + \Phi^{\mathrm{S}}_{(\mu),1} + O(\varepsilon^2) , \tag{3.22a}$$

$$\Phi^{\mathrm{S}}_{(\mu),-2} = O(\Delta/\rho^3) + O(Q\cos\beta/\rho^3) , \tag{3.22b}$$

$$\begin{aligned}\Phi^{\mathrm{S}}_{(\mu),-1} &= O(1/\rho) + O(Q\cos\beta\Delta/\rho^3) + O(\Delta^2/\rho^3) \\ &\quad + O(Q\cos\beta\Delta^3/\rho^5) + O(\Delta^4/\rho^5) ,\end{aligned} \tag{3.22c}$$

$$\begin{aligned}\Phi^{\mathrm{S}}_{(\mu),0} &= O(Q\cos\beta/\rho) + O(\Delta/\rho) + O(Q\cos\beta\Delta^2/\rho^3) + O(\Delta^3/\rho^3) \\ &\quad + O(Q\cos\beta\Delta^4/\rho^5) + O(\Delta^5/\rho^5) + O(Q\cos\beta\Delta^6/\rho^7) + O(\Delta^7/\rho^7) ,\end{aligned} \tag{3.22d}$$

and

$$\begin{aligned}\Phi^{\mathrm{S}}_{(\mu),+1} &= O(\rho) + O(Q\cos\beta\Delta/\rho) + O(\Delta^2/\rho) + O(Q\cos\beta\Delta^3/\rho^3) + O(\Delta^4/\rho^3) \\ &\quad + O(Q\cos\beta\Delta^5/\rho^5) + O(\Delta^6/\rho^5) + O(Q\cos\beta\Delta^7/\rho^7) \\ &\quad + O(\Delta^8/\rho^7) + O(Q\cos\beta\Delta^9/\rho^9) + O(\Delta^{10}/\rho^9) ,\end{aligned} \tag{3.22e}$$

where $O(\ )$ stands for terms that involve only a particular combination of Δ, ρ, and Q, $\cos\beta$, $\sin\beta$ with coefficients that might depend on χ, r_0, $\dot{r}_0$, E, J, etc. Of the terms listed in Eq. (3.22) only a handful survive the multipole decomposition and do not vanish for $\Delta \to 0$. Based on the results of Appendix B, we can formulate a set of rules as to which terms vanish:

- All terms containing isolated occurrences of $\cos\beta$ vanish since the average in Eq. (B.2) is zero.

- All terms of the form Δ^n/ρ^m with $n + 2 > m$, m odd vanish. This follows from Eqs. (B.5) and (B.6). A term $1/\rho^m$ gives rise to a coefficient $\mathcal{A}^{-k-1/2}$ involving δ^{-2m+2} which in turn is proportional to Δ^{-2m+2} overwhelming the term Δ^n.

These two rules eliminate almost all of the terms in Eq. (3.22), the only ones surviving being

$$\Phi^{\mathrm{S}}_{(\mu),-2} = O(\Delta/\rho^3) , \tag{3.23a}$$

$$\Phi^{\mathrm{S}}_{(\mu),-1} = O(1/\rho) , \tag{3.23b}$$

and

$$\Phi^{\mathrm{S}}_{(\mu),+1} = O(\rho) \,. \tag{3.23c}$$

Note that there is no $\Phi^{\mathrm{S}}_{(\mu),0}$ term anymore; such a term would correspond to a C regularization parameter and cannot occur if the procedure is well defined [1]. We introduce the notation $(x)_\ell$ for the multipole coefficient of a term x and use the results of Eq. (3.6), Eq. (B.5) and (B.2) to find the multipole coefficients of the terms listed in Eq. (3.23)

$$\left(\Delta/\rho^3\right)_\ell = \left(\ell + \frac{1}{2}\right) \frac{r_0 - 2M}{Er_0^3} \operatorname{sign}(\Delta) + O(\Delta) \,, \tag{3.24a}$$

$$\left(\chi^{-p}/\rho\right)_\ell = \frac{F(p + \frac{1}{2}, \frac{1}{2}; 1; k)}{\sqrt{r_0^2 + J^2}} + O(\Delta) \,, \tag{3.24b}$$

and

$$\left(\chi^{-p}\rho\right)_\ell = -\frac{\sqrt{r_0^2 + J^2}F(p - \frac{1}{2}, \frac{1}{2}; 1; k)}{(l - \frac{1}{2})(l + \frac{3}{2})} + O(\Delta) \,, \tag{3.24c}$$

where $\operatorname{sign}(\Delta)$ is equal to $+1$ if $\Delta > 0$ and to -1 if $\Delta < 0$. Finally we express the hypergeometric functions in terms of (rescaled) complete elliptic integrals

$$\mathcal{E} \equiv \frac{2}{\pi} \int_0^{\pi/2} (1 - k \sin^2 \psi)^{1/2} \, d\psi = F(-\tfrac{1}{2}, \tfrac{1}{2}; 1; k) \,, \tag{3.25a}$$

and

$$\mathcal{K} \equiv \frac{2}{\pi} \int_0^{\pi/2} (1 - k \sin^2 \psi)^{-1/2} \, d\psi = F(\tfrac{1}{2}, \tfrac{1}{2}; 1; k) \tag{3.25b}$$

in which $k \equiv J^2/(r_0^2 + J^2)$. We identify the regularization parameters $A_{(\mu)}$, $B_{(\mu)}$, $C_{(\mu)}$, and $D_{(\mu)}$ defined by

$$F^{\mathrm{S}}_{(\mu)} \equiv \sum_\ell \left[\left(\ell + \frac{1}{2}\right) A_{(\mu)} + B_{(\mu)} + \frac{C_{(\mu)}}{\ell + \frac{1}{2}} + \frac{D_{(\mu)}}{(\ell - \frac{1}{2})(\ell + \frac{3}{2})} + \dots \right] \,, \tag{3.26}$$

and find

$$A_{(0)} = \frac{\dot{r}_0}{\sqrt{f_0}(r_0^2 + J^2)} \operatorname{sign}(\Delta) \,, \tag{3.27a}$$

and

$$A_{(+)} = -e^{i\varphi_0} \frac{E}{\sqrt{f_0}(r_0^2 + J^2)} \operatorname{sign}(\Delta) \,. \tag{3.27b}$$

We also find

$$B_{(0)} = -\frac{Er_0\dot{r}_0}{\sqrt{f_0}(r_0^2 + J^2)^{3/2}} \mathcal{E} + \frac{Er_0\dot{r}_0}{2\sqrt{f_0}(r_0^2 + J^2)^{3/2}} \mathcal{K} \,, \tag{3.28a}$$

$$B_{(+)} = e^{i\varphi_0} \left(B^c_{(+)} - iB^s_{(+)} \right) \,, \tag{3.28b}$$

$$\begin{aligned} B^c_{(+)} = {} & \left[\frac{r_0\dot{r}_0^2}{\sqrt{f_0}(r_0^2 + J^2)^{3/2}} + \frac{\sqrt{f_0}}{2r_0\sqrt{r_0^2 + J^2}} \right] \mathcal{E} \\ & - \left[\frac{r_0\dot{r}_0^2}{2\sqrt{f_0}(r_0^2 + J^2)^{3/2}} + \frac{\sqrt{f_0} - 1}{r_0\sqrt{r_0^2 + J^2}} \right] \mathcal{K} \,, \end{aligned} \tag{3.28c}$$

and

$$B_{(+)}^s = -\frac{(2-\sqrt{f_0})\dot{r}_0}{2J\sqrt{r_0^2+J^2}\sqrt{f_0}}\mathcal{E} + \frac{(2-\sqrt{f_0})\dot{r}_0}{2J\sqrt{r_0^2+J^2}\sqrt{f_0}}\mathcal{K},. \tag{3.28d}$$

We also find

$$C_{(\mu)} = 0 \tag{3.29}$$

and

$$D_{(0)} = -\left[\frac{Er_0^3(r_0^2-J^2)\dot{r}_0^3}{2\sqrt{f_0}(r_0^2+J^2)^{7/2}}\right.$$
$$\left.+ \frac{E(r_0^7+30Mr_0^6-7J^2r_0^5+114MJ^2r_0^4+104MJ^4r_0^2+36MJ^6)\dot{r}_0}{16r_0^4\sqrt{f_0}(r_0^2+J^2)^{5/2}}\right]\mathcal{E}$$
$$+ \left[\frac{Er_0^3(5r_0^2-3J^2)\dot{r}_0^3}{16\sqrt{f_0}(r_0^2+J^2)^{7/2}} + \frac{E(r_0^5+16Mr_0^4-3J^2r_0^3+42MJ^2r_0^2+18MJ^4)\dot{r}_0}{16r_0^2\sqrt{f_0}(r_0^2+J^2)^{5/2}}\right]\mathcal{K}, \tag{3.30a}$$

and

$$D_{(+)} = e^{i\varphi_0}\left(D_{(+)}^c - iD_{(+)}^s\right),$$
$$\tag{3.30b}$$

$$D_{(+)}^c = \left[\frac{r_0^3(r_0^2-J^2)\dot{r}_0^4}{2\sqrt{f_0}(r_0^2+J^2)^{7/2}} - \frac{r_0\dot{r}_0^2}{4(r_0^2+J^2)^{3/2}}\right.$$
$$+ \frac{(3r_0^7+6Mr_0^6-J^2r_0^5+31MJ^2r_0^4+26MJ^4r_0^2+9MJ^6)\dot{r}_0^2}{4r_0^4\sqrt{f_0}(r_0^2+J^2)^{5/2}}$$
$$+ \frac{(3r_0^7+8Mr_0^6+J^2r_0^5+26MJ^2r_0^4+22MJ^4r_0^2+8MJ^6)\sqrt{f_0}}{16r_0^6(r_0^2+J^2)^{3/2}}$$
$$\left.- \frac{r_0^3+2Mr_0^2+4MJ^2}{8r_0^4\sqrt{r_0^2+J^2}}\right]\mathcal{E} + \left[-\frac{r_0^3(5r_0^2-3J^2)\dot{r}_0^4}{16\sqrt{f_0}(r_0^2+J^2)^{7/2}} + \frac{r_0\dot{r}_0^2}{8(r_0^2+J^2)^{3/2}}\right.$$
$$- \frac{(7r_0^5+12Mr_0^4-J^2r_0^3+46MJ^2r_0^2+18MJ^4)\dot{r}_0^2}{16r_0^2\sqrt{f_0}(r_0^2+J^2)^{5/2}}$$
$$\left.- \frac{(7r_0^5+6Mr_0^4+6J^2r_0^3+12MJ^2r_0^2+4MJ^4)\sqrt{f_0}}{16r_0^4(r_0^2+J^2)^{3/2}} + \frac{3}{8r_0\sqrt{r_0^2+J^2}}\right]\mathcal{K}, \tag{3.30c}$$

$$D_{(+)}^s = \left[\frac{r_0^2(r_0^2-7J^2)(\sqrt{f_0}-2)\dot{r}_0^3}{16J\sqrt{f_0}(r_0^2+J^2)^{5/2}}\right.$$
$$- \frac{(2r_0^7+Mr_0^6+5J^2r_0^5+10MJ^2r_0^4+29MJ^4r_0^2+14MJ^6)\dot{r}_0}{8r_0^5J(r_0^2+J^2)^{3/2}}$$
$$\left.+ \frac{(r_0^5-Mr_0^4+4J^2r_0^3-5MJ^2r_0^2+2MJ^4)\dot{r}_0}{4r_0^3J\sqrt{f_0}(r_0^2+J^2)^{3/2}}\right]\mathcal{E} + \left[-\frac{r_0^2(r_0^2-3J^2)(\sqrt{f_0}-2)\dot{r}_0^3}{16J\sqrt{f_0}(r_0^2+J^2)^{5/2}}\right.$$
$$+ \frac{(4r_0^5+2Mr_0^4+7J^2r_0^3+10MJ^2r_0^2+14MJ^4)\dot{r}_0}{16r_0^3J(r_0^2+J^2)^{3/2}}$$
$$\left.- \frac{(2r_0^3-2Mr_0^2+5J^2r_0-8MJ^2)\dot{r}_0}{8r_0J\sqrt{f_0}(r_0^2+J^2)^{3/2}}\right]\mathcal{K}. \tag{3.30d}$$

Finally we use the regularization parameters to regularize the retarded field gradient

$$\Phi^{\mathrm{R}}_{(\mu)} = \sum_{\ell} \left\{ \Phi^{\mathrm{ret}}_{(\mu),\ell} - q \left[A_{(\mu)} \left(\ell + \frac{1}{2} \right) + B_{(\mu)} + \frac{C_{(\mu)}}{\ell + \frac{1}{2}} + \frac{D_{(\mu)}}{(\ell - \frac{1}{2})(\ell + \frac{3}{2})} + \cdots \right] \right\}. \quad (3.31)$$

3.7 Electromagnetic field

A calculation of the scalar regularization parameters begins with Eq. (2.121). We introduce tetrad components of the Faraday tensor using the tetrad of section 2.8

$$F^{\mathrm{S}}_{(\mu)(\nu)} \equiv \left(A^{\mathrm{S}}_{\beta;\alpha} - A^{\mathrm{S}}_{\alpha;\beta} \right) e^{\alpha}{}_{(\mu)} e^{\beta}{}_{(\nu)}, \quad (3.32)$$

which permits a clean calculation of the regularization parameters using only scalar spherical harmonics.

As in section 3.6 we use the symbolic manipulator GRTENSOR II which runs under MAPLE to substitute Eqs. (2.31), (2.38), (2.39), (2.43), (3.17), $w^t = 0$, $w^r = \Delta$ and (3.19) into Eq. (3.32). The overall structure of the resulting expression in terms of Δ, ρ, and Q, $\cos\beta$, $\sin\beta$ is

$$F^{\mathrm{S}}_{(\mu)(\nu)} = F^{\mathrm{S}}_{(\mu)(\nu),-2} + F^{\mathrm{S}}_{(\mu)(\nu),-1} + F^{\mathrm{S}}_{(\mu)(\nu),0} + F^{\mathrm{S}}_{(\mu)(\nu),1} + O(\varepsilon^2), \quad (3.33\mathrm{a})$$

$$F^{\mathrm{S}}_{(\mu)(\nu),-2} = O(\Delta/\rho^3) + O(Q\cos\beta/\rho^3), \quad (3.33\mathrm{b})$$

$$F^{\mathrm{S}}_{(\mu)(\nu),-1} = O(1/\rho) + O(Q\cos\beta\Delta/\rho^3) + O(\Delta^2/\rho^3) \\ + O(Q\cos\beta\Delta^3/\rho^5) + O(\Delta^4/\rho^5), \quad (3.33\mathrm{c})$$

$$F^{\mathrm{S}}_{(\mu)(\nu),0} = O(Q\cos\beta/\rho) + O(\Delta/\rho) + O(Q\cos\beta\Delta^2/\rho^3) + O(\Delta^3/\rho^3) \\ + O(Q\cos\beta\Delta^4/\rho^5) + O(\Delta^5/\rho^5) + O(Q\cos\beta\Delta^6/\rho^7) + O(\Delta^7/\rho^7), \quad (3.33\mathrm{d})$$

and

$$F^{\mathrm{S}}_{(\mu)(\nu),+1} = O(\rho) + O(Q\cos\beta\Delta/\rho) + O(\Delta^2/\rho) + O(Q\cos\beta\Delta^3/\rho^3) \\ + O(\Delta^4/\rho^3) + O(Q\cos\beta\Delta^5/\rho^5) + O(\Delta^6/\rho^5) + O(Q\cos\beta\Delta^7/\rho^7) \quad (3.33\mathrm{e}) \\ + O(\Delta^8/\rho^7) + O(Q\cos\beta\Delta^9/\rho^9) + O(\Delta^{10}/\rho^9),$$

where $O(\ )$ stands for terms that involve only a particular combination of Δ, ρ, and Q, $\cos\beta$, $\sin\beta$ with coefficients that might depend on χ, r_0, $\dot{r}_0$, E, J, etc. Using the rules listed in section 3.6 we eliminate all but a handful of terms

$$F^{\mathrm{S}}_{(\mu)(\nu),-2} = O(\Delta/\rho^3), \quad (3.34\mathrm{a})$$

$$F^{\mathrm{S}}_{(\mu)(\nu),-1} = O(1/\rho), \quad (3.34\mathrm{b})$$

and

$$F^{\mathrm{S}}_{(\mu)(\nu),+1} = O(\rho). \quad (3.34\mathrm{c})$$

As for the scalar case there is no $F^{\mathrm{S}}_{(\mu)(\nu),0}$ term anymore. Using the results of Eq. (3.6), Eq. (B.5) and (B.2) we obtain the multipole coefficients of the remaining terms and

after re-expanding the resulting hypergeometric functions in terms of the elliptic integrals of section (3.6) we obtain regularization parameters

$$A_{(0)(+)} = \text{sign}(\Delta)\left[\frac{i\dot{r}_0 J}{r_0 \mathfrak{f}a^2} - \frac{1}{r_0^2}\right]e^{i\varphi_0},$$

(3.35a)

$$B_{(0)(+)} = \left\{\left[-\frac{iE(J^2 - r_0^2)\dot{r}_0}{a^3\pi\mathfrak{f}J} + \frac{E(2-\mathfrak{f})}{\pi\mathfrak{f}ar_0}\right]\mathcal{E} - \frac{ir_0^2 E\dot{r}_0}{a^3 J\mathfrak{f}\pi}\mathcal{K}\right\}e^{i\varphi_0},$$

(3.35b)

$$D_{(0)(+)}$$
$$= \left\{\left[\frac{iEr_0^2(-14r_0^2 J^2 + J^4 + r_0^4)\dot{r}_0^3}{8\pi J\mathfrak{f}a^7} - \frac{(-r_0\mathfrak{f}J^2 + 2r_0 J^2 + 7r_0^3\mathfrak{f} - 14r_0^3)E\dot{r}_0^2}{8a^5\mathfrak{f}\pi}\right.\right.$$
$$+ i\left(8MJ^8 - 14MJ^6 r_0^2 - 3r_0^5 J^4 - 80MJ^4 r_0^4 + 4J^4 r_0^5\mathfrak{f} - 7r_0^7 J^2 - 68Mr_0^6 J^2 + 4r_0^9\right.$$
$$\left.- 26Mr_0^8 - 4r_0^9\mathfrak{f}\right)E\dot{r}_0\bigg/\left(8r_0^5 a^5\mathfrak{f}J\pi\right)$$
$$- \left(8Mr_0\mathfrak{f}J^6 - 8r_0^3 MJ^4 + 38J^4 r_0^3\mathfrak{f} - 2r_0^6 J^2 - 16Mr_0^5 J^2 + 3J^2 r_0^6\mathfrak{f} + 54J^2 r_0^5\mathfrak{f}\right.$$
$$\left.\left.+ 20r_0^7\mathfrak{f} + 5r_0^8\mathfrak{f} - 6r_0^8\right)E\bigg/\left(8r_0^7 a^3\mathfrak{f}\pi\right)\right]\mathcal{E}$$
$$+ \left[\frac{iEr_0^4(7J^2 - r_0^2)\dot{r}_0^3}{8\pi J\mathfrak{f}a^7} - \frac{(2-\mathfrak{f})r_0^3 E\dot{r}_0^2}{2a^5\mathfrak{f}\pi}\right.$$
$$+ \frac{(4Mr_0\mathfrak{f}J^4 + 20J^2 r_0^3\mathfrak{f} + 8Mr_0^3 J^2 + 14r_0^5 M\mathfrak{f} - 2r_0^6 + 12Mr_0^5 + r_0^6\mathfrak{f})E}{8r_0^5 a^3\mathfrak{f}\pi}$$
$$\left.\left.- \frac{i(2MJ^6 - 9Mr_0^2 J^4 - 2J^2 r_0^5\mathfrak{f} - 20Mr_0^4 J^2 - 2r_0^7\mathfrak{f} + 2r_0^7 - 13Mr_0^6)E\dot{r}_0}{4r_0^3 a^5\mathfrak{f}J\pi}\right]\mathcal{K}\right\}e^{i\varphi_0},$$

(3.35c)

$$A_{(+)(-)} = \text{sign}(\Delta)\frac{2iEJ}{a^2 r_0\mathfrak{f}}e^{i\varphi_0},$$

(3.35d)

$$B_{(+)(-)} = -2i\left\{\left[-\frac{(r_0^2 - J^2)\dot{r}_0^2}{a^3\pi J\mathfrak{f}} + \frac{-J^2 r_0\mathfrak{f} + 2r_0 J^2 + 2r_0^3 - 2r_0^3\mathfrak{f}}{r_0^3 aJ\pi}\right]\mathcal{E}\right.$$
$$\left.+ \left[\frac{r_0^2\dot{r}_0^2}{a^3\mathfrak{f}J\pi} - \frac{2(1-\mathfrak{f})}{aJ\pi}\right]\mathcal{K}\right\}e^{i\varphi_0},$$

(3.35e)

$$D_{(+)(-)} = -2i\left\{\left[-\frac{r_0^2(-14r_0^2J^2 + J^4 + r_0^4)\dot{r}_0^4}{8\mathfrak{f}\pi Ja^7}\right.\right.$$
$$-\left(4M\mathfrak{f}J^8 - 7Mr_0^2\mathfrak{f}J^6 + 2J^4r_0^5\mathfrak{f} + 2J^4r_0^4M - J^4r_0^5 - 43J^4r_0^4\mathfrak{f}M - 7J^2r_0^7\mathfrak{f}\right.$$
$$\left.- 27J^2Mr_0^6\mathfrak{f} - 11Mr_0^8\mathfrak{f} - r_0^9\mathfrak{f} + r_0^9 - 2r_0^8M\right)r_0^{1/2}\dot{r}_0^2 \Big/\left(4r_0^5a^5J\mathfrak{f}\pi\right)$$
$$-\left(8M\mathfrak{f}J^8 - 8J^6Mr_0^2 + 30Mr_0^2\mathfrak{f}J^6 - 2J^4r_0^5 + 10J^4r_0^4\mathfrak{f}M - 24J^4r_0^4M + 3J^4r_0^5\mathfrak{f}\right.$$
$$\left.\left.- 28J^2Mr_0^6 + J^2r_0^7\mathfrak{f} - 28J^2Mr_0^6\mathfrak{f} - 20Mr_0^8\mathfrak{f} - 12r_0^8M\right)\Big/\left(8r_0^7a^3J\pi\right)\right]\mathcal{E}$$
$$+\left[-\frac{r_0^4(7J^2 - r_0^2)\dot{r}_0^4}{8\mathfrak{f}\pi Ja^7} + \left(4M\mathfrak{f}J^6 - 16J^4Mr_0^2 + 4r_0^2\mathfrak{f}MJ^4 - 18J^2r_0^4\mathfrak{f}M\right.\right.$$
$$\left.- 28J^2r_0^4M - J^2\mathfrak{f}r_0^5 - 12r_0^6M - 20r_0^6\mathfrak{f}M\right)\Big/\left(8r_0^5a^3J\pi\right)$$
$$+\left(2M\mathfrak{f}J^6 - 9r_0^2\mathfrak{f}MJ^4 + J^2r_0^5 - 2J^2r_0^4M - 5J^2\mathfrak{f}r_0^5 - 14J^2r_0^4\mathfrak{f}M - 2r_0^6M\right.$$
$$\left.\left.\left.+ r_0^7 - 11r_0^6\mathfrak{f}M - \mathfrak{f}r_0^7\right)\dot{r}_0^2\Big/\left(4r_0^{5/2}a^5J\mathfrak{f}\pi\right)\right]\mathcal{K}\right\}e^{i\varphi_0},$$

$$(3.35\text{f})$$

where $\mathfrak{f} = \sqrt{\frac{r_0 - 2M}{r_0}}$, $a^2 = r_0^2 + J^2$.

Finally we use the regularization parameters to regularize the retarded Faraday tensor

$$F^{\text{R}}_{(\mu)(\nu)} = \sum_\ell\left\{F^{\text{ret}}_{(\mu)(\nu),\ell} - q\left[A_{(\mu)(\nu)}\left(\ell + \frac{1}{2}\right) + B_{(\mu)(\nu)} + \frac{C_{(\mu)(\nu)}}{\ell + \frac{1}{2}} + \frac{D_{(\mu)(\nu)}}{(\ell - \frac{1}{2})(\ell + \frac{3}{2})} + \cdots\right]\right\}.$$

$$(3.36)$$

3.8 Gravitational field

A calculation of the scalar regularization parameters begins with Eq. (2.122). For the gravitational case we deviate slightly from the procedure introduced in sections 3.6 and 3.7 and calculate regularization parameters not for the field gradient $\gamma_{\alpha\beta;\gamma}$ but instead for the force acting on the particle [33]

$$F_\alpha = k_\alpha{}^{\beta\gamma\delta}\gamma_{\alpha\beta\gamma}, \tag{3.37a}$$
$$k_\alpha{}^{\beta\gamma\delta} = \frac{1}{2}u^\beta u^\gamma \delta_\alpha{}^\delta + \frac{1}{4}g^{\beta\gamma}\delta^{\alpha\delta} + \frac{1}{4}u_\alpha g^{\beta\gamma}u^\delta - \delta^{\alpha\beta}u^\gamma u^\delta - \frac{1}{2}u_\alpha u^\beta u^\gamma u^\delta. \tag{3.37b}$$

The projector $k_\alpha{}^{\beta\gamma\delta}$ in Eq. (3.37) involves the four velocity u^α of the particle, which is only defined on the world line. In order to be able to evaluate the singular force away from the world line we must extend u^α away from the world line. For a first order calculation of the self-force, all extensions which smoothly approach the four velocity on the world line are equivalent. We choose the simplest one and rigidly extend u^α

away from the world line; this means that the contravariant components u^α expressed in Schwarzschild coordinates are kept constant as we move away from the world line.

Our reason for choosing to regularize F_α instead of $\gamma_{\alpha\beta;\gamma}$ is purely based in convenience of calculation, there are fewer components to F_α than there are to $\gamma_{\alpha\beta;\gamma}$.

We introduce tetrad components of the force using the tetrad of section 2.8

$$F^{\mathrm{S}}_{(\mu)} \equiv F^{\mathrm{S}}_{\alpha} e^{\alpha}{}_{(\mu)} , \qquad (3.38)$$

which permits a clean calculation of the regularization parameters using only scalar spherical harmonics.

As in section 3.6 we use the symbolic manipulator GRTensor II which runs under MAPLE to substitute Eqs. (2.31), (2.38), (2.39), (2.43), (3.17), $w^t = 0$, $w^r = \Delta$ and (3.19) into Eq. (3.38). The resulting expression is very much to long to be displayed here, containing several hundred thousand terms. Instead we list its overall structure in terms of Δ, ρ, and Q, $\cos\beta$, $\sin\beta$.

$$F^{\mathrm{S}}_{(\mu)} = F^{\mathrm{S}}_{(\mu),-2} + F^{\mathrm{S}}_{(\mu),-1} + F^{\mathrm{S}}_{(\mu)(\nu),0} + F^{\mathrm{S}}_{(\mu),1} + O(\varepsilon^2) , \qquad (3.39\text{a})$$

$$F^{\mathrm{S}}_{(\mu),-2} = O(\Delta/\rho^3) + O(Q\cos\beta/\rho^3) , \qquad (3.39\text{b})$$

$$\begin{aligned} F^{\mathrm{S}}_{(\mu),-1} = {} & O(1/\rho) + O(Q\cos\beta\Delta/\rho^3) + O(\Delta^2/\rho^3) \\ & + O(Q\cos\beta\Delta^3/\rho^5) + {+}O(\Delta^4/\rho^5) , \end{aligned} \qquad (3.39\text{c})$$

$$\begin{aligned} F^{\mathrm{S}}_{(\mu),0} = {} & O(Q\cos\beta/\rho) + O(\Delta/\rho) + O(Q\cos\beta\Delta^2/\rho^3) + O(\Delta^3/\rho^3) \\ & + O(Q\cos\beta\Delta^4/\rho^5) + O(\Delta^5/\rho^5) + O(Q\cos\beta\Delta^6/\rho^7) + O(\Delta^7/\rho^7) , \end{aligned} \qquad (3.39\text{d})$$

and

$$\begin{aligned} F^{\mathrm{S}}_{(\mu),+1} = {} & O(\rho) + O(Q\cos\beta\Delta/\rho) + O(\Delta^2/\rho) + O(Q\cos\beta\Delta^3/\rho^3) + O(\Delta^4/\rho^3) \\ & + O(Q\cos\beta\Delta^5/\rho^5) + O(\Delta^6/\rho^5) + O(Q\cos\beta\Delta^7/\rho^7) \\ & + O(\Delta^8/\rho^7) + O(Q\cos\beta\Delta^9/\rho^9) + O(\Delta^{10}/\rho^9) , \end{aligned} \qquad (3.39\text{e})$$

where $O(\ )$ stands for terms that involve only a particular combination of Δ, ρ, and Q, $\cos\beta$, $\sin\beta$ with coefficients that might depend on χ, r_0, $\dot{r}_0$, E, J etc. Using the rules listed in section 3.6 we eliminate all but a handful of terms

$$F^{\mathrm{S}}_{(\mu),-2} = O(\Delta/\rho^3) , \qquad (3.40\text{a})$$

$$F^{\mathrm{S}}_{(\mu),-1} = O(1/\rho) , \qquad (3.40\text{b})$$

and

$$F^{\mathrm{S}}_{(\mu),+1} = O(\rho) . \qquad (3.40\text{c})$$

As for the scalar case there is no $F^{\mathrm{S}}_{(\mu)(\nu),0}$ term anymore. Using the results of Eq. (3.6), Eq. (B.5) and (B.2) we obtain the multipole coefficients of the remaining terms and after re-expanding the resulting hypergeometric functions in terms of the elliptic

integrals of section (3.6) we obtain regularization parameters

$$A_{(0)} = \frac{\dot{r}}{\text{sign}(\Delta)a^2\mathfrak{f}}\,,$$

(3.41a)

$$B_{(0)} = \frac{2J^2\dot{r}}{r_0a^3\pi\mathfrak{f}E}\mathcal{E} + \frac{r_0}{a^3\mathfrak{f}\pi E\dot{r}}\mathcal{K}\,,$$

(3.41b)

$$\begin{aligned}
D_{(0)} = &\left[\frac{r_0(34r_0^2J^2 + 11J^4 + 15r_0^4)E\dot{r}^3}{4\pi a^7\mathfrak{f}}\right.\\
&\left. + \left(192r_0^9 + 876MJ^8 + 48r_0J^8 + 2114Mr_0^4J^4 + 651J^2r_0^7 + 426J^6r_0^3\right.\right.\\
&\left.\left. + 2332J^6Mr_0^2 + 706Mr_0^6J^2 + 861J^4r_0^5\right)E\dot{r}\Big/\left(24\pi a^5\mathfrak{f}r_0^4J^2\right)\right]\mathcal{E}\\
&+ \left[-\frac{r_0(15r_0^4 + 35r_0^2J^2 + 12J^4)E\dot{r}^3}{8\pi a^7\mathfrak{f}} + \left(-192r_0^7 - 555r_0^5J^2 - 608Mr_0^4J^2\right.\right.\\
&\left.\left. - 579J^4r_0^3 - 1126Mr_0^2J^4 - 204J^6r_0 - 542J^6M\right)E\dot{r}\Big/\left(24a^5\pi\mathfrak{f}r_0^2J^2\right)\right]\mathcal{K}\,,
\end{aligned}$$

(3.41c)

$$A_{(+)} = -\frac{E}{\text{sign}(\Delta)a^2\mathfrak{f}}e^{i\varphi_0}\,,$$

(3.41d)

$$\begin{aligned}
B_{(+)} = &\left\{\left[-\frac{i[(r_0^2 + 2J^2)\mathfrak{f} + 2r_0^2]\dot{r}}{r_0^2a\mathfrak{f}\pi J} - \frac{2J^2\dot{r}^2}{r_0\pi\mathfrak{f}a^3} + \frac{r_0 - 2M}{ar_0^2\pi\mathfrak{f}}\right]\mathcal{E}\right.\\
&\left. + (-\frac{i(2 - \mathfrak{f})\dot{r}}{a\mathfrak{f}\pi J} - \frac{r_0\dot{r}^2}{\pi\mathfrak{f}a^3} + \frac{2r_0\mathfrak{f} + 4M - 2r_0}{ar_0^2\pi\mathfrak{f}})\mathcal{K}\right\}e^{i\varphi_0}\,,
\end{aligned}$$

(3.41e)

and

$$D_{(+)} = \left\{ \left[\frac{i[(-38J^4 + 15r_0^4 - 31r_0^2 J^2)\mathfrak{f} - 16J^4 - 30r_0^4 - 62r_0^2 J^2]\dot{r}^3}{8J\mathfrak{f}\pi a^5} \right.\right.$$

$$+ i\left[(-96r_0^9 - 330J^2 r_0^7 - 225Mr_0^6 J^2 - 480J^4 r_0^5 - 624Mr_0^4 J^4 - 261J^6 r_0^3\right.$$

$$-723J^6 Mr_0^2 - 24r_0 J^8 - 306MJ^8)\mathfrak{f} - 2r_0^2 J^2(27r_0^5 + 31Mr_0^4 + 30r_0^3 J^2 + 113Mr_0^2 J^2$$

$$\left. - 6J^4 r_0 + 100MJ^4)\right]\dot{r}\Big/\left(12a^3 r_0^5 \mathfrak{f}\pi J^3\right) - \frac{r_0(34r_0^2 J^2 + 11J^4 + 15r_0^4)\dot{r}^4}{4a^7\pi\mathfrak{f}}$$

$$+ \left[18r_0^3 J^2 a^2(5r_0^2 + 4J^2)\mathfrak{f} - 218Mr_0^6 J^2 - 498J^4 r_0^5 - 96r_0^9 - 393J^2 r_0^7\right.$$

$$\left. - 1214J^6 Mr_0^2 - 24r_0 J^8 - 946Mr_0^4 J^4 - 201J^6 r_0^3 - 438MJ^8\right]\dot{r}^2\Big/\left(12r_0^4 a^5\pi\mathfrak{f}J^2\right)$$

$$+ \left[-2r_0^3 a^2(27r_0^3 + 106Mr_0^2 + 36r_0 J^2 + 88J^2 M)\mathfrak{f} + (-2M + r_0)(81r_0^7 - 256Mr_0^6\right.$$

$$\left.\left. + 195r_0^5 J^2 - 866Mr_0^4 J^2 + 120J^4 r_0^3 - 886Mr_0^2 J^4 - 264J^6 M)\right]\Big/\left(24a^3\pi\mathfrak{f}r_0^7\right)\right]\mathcal{E}$$

$$+ \left[\frac{i[(-15r_0^4 + r_0^2 J^2 + 12J^4)\mathfrak{f} + 24J^4 + 62r_0^2 J^2 + 30r_0^4]\dot{r}^3}{8J\mathfrak{f}\pi a^5}\right.$$

$$+ i\left[(192r_0^7 + 564r_0^5 J^2 + 450Mr_0^4 J^2 + 633J^4 r_0^3 + 890Mr_0^2 J^4 + 252J^6 r_0 + 458J^6 M)\mathfrak{f}\right.$$

$$\left. + 2J^2(54r_0^5 + 62Mr_0^4 + 75r_0^3 J^2 + 56Mr_0^2 J^2 + 12J^4 r_0 + 12MJ^4)\right]\dot{r}\Big/\left(24a^3 r_0^3\mathfrak{f}\pi J^3\right)$$

$$+ \frac{r_0(15r_0^4 + 35r_0^2 J^2 + 12J^4)\dot{r}^4}{8a^7\pi\mathfrak{f}} + \left[-18r_0 J^2 a^2(5r_0^2 + 4J^2)\mathfrak{f} + 192r_0^7 + 633r_0^5 J^2\right.$$

$$\left. + 428Mr_0^4 J^2 + 669J^4 r_0^3 + 922Mr_0^2 J^4 + 204J^6 r_0 + 542J^6 M\right]\dot{r}^2\Big/\left(24r_0^2 a^5\pi\mathfrak{f}J^2\right)$$

$$+ \left[6r_0 a^2(11r_0^3 + 68Mr_0^2 - 4r_0 J^2 + 92J^2 M)\mathfrak{f} - (-2M + r_0)(93r_0^5 - 158Mr_0^4\right.$$

$$\left.\left. + 138r_0^3 J^2 - 236Mr_0^2 J^2 + 48J^4 r_0 - 84MJ^4)\right]\Big/\left(24a^3\pi\mathfrak{f}r_0^5\right)\right]\mathcal{K}\right\}e^{i\varphi_0}.$$

$$(3.41\text{f})$$

"Piled Higher and Deeper" by Jorge Cham, `www.phdcomics.com`

Chapter 4

Numerical method

In this chapter we describe the numerical methods we used to calculate the retarded fields for the scalar and electromagnetic case. In this thesis we did not obtain numerical results for the gravitational case, however the methods described here should be applicable to the gravitational case as well.

4.1 Particle motion

Following Darwin [38] we introduce the dimensionless semi-latus rectum p and the eccentricity e such that for a bound orbit around a Schwarzschild black hole of mass M,

$$r_1 = \frac{pM}{1+e}, \quad r_2 = \frac{pM}{1-e} \tag{4.1}$$

are the radial positions of the periastron and apastron, respectively. Without loss of generality, we confine the motion of the particle to the equatorial plane $\theta = \frac{\pi}{2}$. Energy per unit mass and angular momentum per unit mass are then given by

$$E^2 = \frac{(p-2-2e)(p-2+2e)}{p\,(p-3-e^2)}, \quad J^2 = \frac{p^2 M^2}{p-3-e^2}, \tag{4.2}$$

which are linked to the components of u_α as $u_t = -E$, $u_\phi = J$. Together with these definitions it is useful to introduce an orbital parameter χ such that along the trajectory of the particle,

$$r(\chi) = \frac{pM}{1+e\cos\chi}, \tag{4.3}$$

where χ is single-valued along the orbit. We can then write down first-order differential equations for $\chi(t)$ and the azimuthal angle $\varphi(t)$ of the particle,

$$\frac{d\chi}{dt} = \frac{(p-2-2e\cos\chi)(1+e\cos\chi)^2}{(Mp^2)}\sqrt{\frac{p-6-2e\cos\chi}{(p-2-2e)(p-2+2e)}}\,, \qquad (4.4a)$$

$$\frac{d\varphi}{dt} = \frac{(p-2-2e\cos\chi)(1+e\cos\chi)^2}{p^{3/2}M\sqrt{(p-2-2e)(p-2+2e)}}\,, \qquad (4.4b)$$

which are equivalent to the geodesic equation

$$u^\beta \nabla_\beta u^\alpha = 0\,. \qquad (4.5)$$

We use the embedded Runge-Kutta-Fehlberg (4, 5) algorithm provided by the GNU SCIENTIFIC LIBRARY routine gsl_odeiv_step_rkf45 and an adaptive step-size control to evolve the position of the particle forward in time. Intermediate values of the particle's position are found using a Hermite interpolation of the nearest available calculated positions.

Below, quantities bearing a subscript "0" (for example $f_0 = 1 - 2M/r_0$) are evaluated at the particle's position; they are functions of τ only.

4.2 Scalar field

Our task is to numerically solve the scalar wave equation Eq. (2.44)

$$g^{\alpha\beta}\nabla_\alpha\nabla_\beta\Phi(x) = -4\pi\rho(x)\,,$$

with a source term

$$\rho(x) = q\int_\gamma \delta^4(x,z)\,d\tau\,.$$

For numerical purposes it is convenient to define $\psi_{\ell m}$ by

$$\Phi(x) = \sum_{\ell=0}^{\infty}\sum_{m=-\ell}^{\ell}\frac{1}{r}\psi_{\ell m}Y^{\ell m}\,, \qquad (4.6)$$

where $Y_{\ell m}$ are the usual scalar spherical harmonics. After substituting in Eq. (2.44), this yields a reduced wave equation for the multipole moments $\psi_{\ell m}$:

$$-\partial_t^2\psi_{\ell m} + \partial_{r^*}^2\psi_{\ell m} - V_\ell\psi_{\ell m} = -4\pi q\frac{f_0}{r_0 E}\bar{Y}_{\ell m}(\pi/2,\varphi_0)\delta(r^*-r_0^*)\,, \qquad (4.7)$$

where

$$V_\ell = f\left(\frac{2M}{r^3} + \frac{\ell(\ell+1)}{r^2}\right)\,, \qquad (4.8)$$

and an overbar denotes complex conjugation.

In order to numerically solve Eq. (4.7) we use the fourth-order finite difference scheme introduced by Lousto [5], with some modifications to suit our needs. We choose to implement a fourth-order convergent code because the accuracy obtained with a second order scheme, while much easier to achieve, is inadequate for precision determination of the self-force.

From now on, we will suppress the subscripts ℓ and m on V_ℓ and $\psi_{\ell m}$ for convenience of notation.

Inspecting Eq. (4.7) we see that the wave equation consists of three parts: the wave-operator term $(\partial_{r^*}^2 - \partial_t^2)\psi$ and the potential term $V\psi$ on the left-hand side, and the source term on the right-hand side of the equation. Of these, the wave operator turns out to be easiest to handle, and the source term does not create a substantial difficulty. The term involving the potential V turns out to be the most difficult one to handle.

Following Lousto we introduce a staggered grid with step sizes $\Delta t = \frac{1}{2}\Delta r^* \equiv h$, which follows the characteristic lines of the wave operator in Schwarzschild spacetime; see Fig. 4.1 for a sketch of a typical grid cell. The basic idea behind the method is to integrate the wave equation over a unit cell of the grid, which nicely deals with the Dirac-δ source term on the right-hand side. To this end, we introduce the Eddington-Finkelstein null coordinates $v = t + r^*$ and $u = t - r^*$ and use them as integration variables.

4.2.1 Differential operator

Rewriting the wave operator in terms of u and v, we find $-\partial_t^2 + \partial_{r^*}^2 = -4\partial_u\partial_v$, which allows us to evaluate the integral involving the wave operator exactly. We find

$$\iint_{\text{cell}} -4\partial_u\partial_v\psi \; \mathrm{d}u \; \mathrm{d}v = -4[\psi(t+h,r^*)+\psi(t-h,r^*)-\psi(t,r^*-h)-\psi(t,r^*+h)]. \quad (4.9)$$

4.2.2 Source term

If we integrate over a cell traversed by the particle, then the source term on the right-hand side of the equation will have a non-zero contribution. Writing the source term as $G(t,r^*)\delta\big(r^* - r_0^*(t)\big)$ with

$$G(t,r^*) = -4\pi q\frac{f}{Er}\bar{Y}_{\ell m}(\pi/2,\varphi_0)\,, \quad (4.10)$$

we find

$$\iint_{\text{cell}} G\delta\big(r^* - r_0^*(t)\big) \; \mathrm{d}u \; \mathrm{d}v = -\frac{8\pi q}{E} \int_{t_1}^{t_2} \frac{f_0(t)}{r_0(t)}\bar{Y}_{\ell m}\big(\pi/2,\varphi_0(t)\big) \; \mathrm{d}t\,, \quad (4.11)$$

where t_1 and t_2 are the times at which the particle enters and leaves the cell, respectively. While we do not have an analytic expression for the trajectory of the particle (except when the particle follows a circular orbit), we can numerically integrate the

first-order ordinary differential equations that govern the particle's motion to a precision that is much higher than that of the partial differential equation governing ψ. In this sense we treat the integral over the source term as exact. To evaluate the integral we adopt a four-point Gauss-Legendre scheme, which has an error of order h^8.

4.2.3   Potential term

The most problematic term—from the point of view of implementing an approximation of sufficiently high order in h—turns out to be the term $V\psi$ in Eq. (4.7). Since this term does not contain a δ-function, we have to approximate the double integral

$$\iint\limits_{\text{cell}} V\psi \; \mathrm{d}u \; \mathrm{d}v \tag{4.12}$$

up to terms of order h^6 for a generic cell in order to achieve an overall $O(h^4)$ convergence of the scheme.

Here we have to treat cells traversed by the particle ("sourced" cells) differently from the generic ("vacuum") cells. While much of the algorithm can be transferred from the vacuum cells to the sourced cells, some modifications are required. We will describe each case separately in the following subsections.

Vacuum case

To implement Lousto's scheme to evolve the field across the vacuum cells, we use a double Simpson rule to compute the integral Eq. (4.12). We introduce the notation

$$g(t, r^*) = V(r^*)\,\psi(t, r^*) \tag{4.13}$$

and label our points in the same manner (see Fig. 4.1) as in [5]:

$$\iint\limits_{\text{cell}} g \; \mathrm{d}u \; \mathrm{d}v = \left(\frac{h}{3}\right)^2 [g_1 + g_2 + g_3 + g_4 + 4(g_{12} + g_{24} + g_{34} + g_{13}) + 16g_0] + O(h^6). \tag{4.14}$$

Here, for example, g_1 is the value of g at the grid point labelled 1, and g_{12} is the value of g at the off-grid point labelled 12, etc. Deviating from Lousto's scheme, we choose to calculate g_0 using an expression different from that derived in [5]. Unlike Lousto's approach, our expression exclusively involves points that are within the past light cone of the current cell. We find

$$g_0 = \frac{1}{16}[8V_4\,\psi_4 + 8V_1\,\psi_1 + 8V_2\,\psi_2 - 4V_6\,\psi_6 - 4V_5\,\psi_5 \tag{4.15}$$
$$+ V_{10}\,\psi_{10} + V_7\,\psi_7 - V_9\,\psi_9 - V_8\,\psi_8] + O(h^4).$$

In order to evaluate the term in parentheses in Eq. (4.14), we again use a variant of the equations given in [5]. Lousto's equations (33) and (34),

$$g_{13} + g_{12} = V(r_0^* - h/2)\,(\psi_1 + \psi_0)\left[1 - \frac{1}{2}\left(\frac{h}{2}\right)^2 V(r_0^* - h/2)\right] + O(h^4), \tag{4.16a}$$

$$g_{24} + g_{34} = V(r_0^* + h/2)\,(\psi_0 + \psi_4)\left[1 - \frac{1}{2}\left(\frac{h}{2}\right)^2 V(r_0^* + h/2)\right] + O(h^4) \tag{4.16b}$$
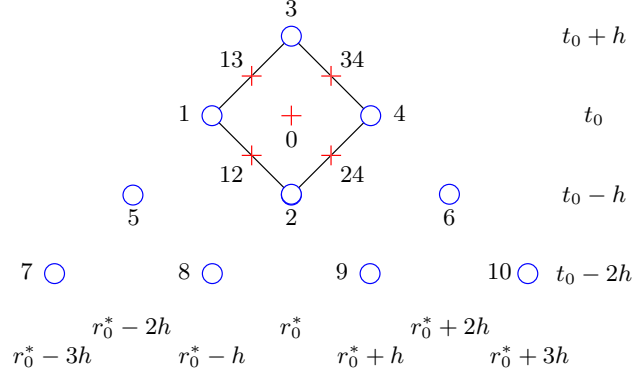
Figure 4.1: Points used to calculate the integral over the potential term for vacuum cells. Grid points are indicated by blue circles while red cross-hairs indicate points in between two grid points. We calculate field values at points that do not lie on the grid by employing the second-order finite-difference scheme described in [5].

contain isolated occurrences of ψ_0, the value of the field at the central point. Since Eq. (4.15) only allows us to find $g_0 = V_0\psi_0$, finding ψ_0 would involve a division by V_0, which will be numerically unstable very close to the event horizon where $V_0 \approx 0$. Instead we choose to express the potential term appearing in the square brackets as a Taylor series around r_0^*. This allows us to eliminate the isolated occurrences of ψ_0, and we find

$$
\begin{aligned}
g_{13} + g_{12} + g_{24} + g_{34} = {}& 2V(r_0^*)\,\psi_0\left[1 - \frac{1}{2}\left(\frac{h}{2}\right)^2 V(r_0^*)\right] \\
&+ V(r_0^* - h/2)\,\psi_1\left[1 - \frac{1}{2}\left(\frac{h}{2}\right)^2 V(r_0^* - h/2)\right] \\
&+ V(r_0^* + h/2)\,\psi_4\left[1 - \frac{1}{2}\left(\frac{h}{2}\right)^2 V(r_0^* + h/2)\right] \\
&+ \frac{1}{2}[V(r_0^* - h/2) - 2V(r_0^*) + V(r_0^* + h/2)](\psi_1 + \psi_4) + O(h^4)\,.
\end{aligned}
$$
(4.17)

Because of the $(\frac{h}{3})^2$ factor in Eq. (4.14), this allows us to reach the required $O(h^6)$ convergence for a generic vacuum cell. This—given that there is a number of order $N = 1/h^2$ of such cells—yields the desired overall $O(h^4)$ convergence of the full algorithm, at the end of the N steps required to finish the simulation.

Sourced cells

For vacuum cells, the algorithm described above is the complete algorithm used to evolve the field forward in time. For cells traversed by the particle, however, we have to reconsider the assumptions used in deriving Eqs. (4.15) and (4.17). When deriving Eq. (4.17) we have employed the second-order evolution finite-difference scheme (see [5]), in which the single step equation

$$
\psi_3 = -\psi_2 + \left(1 - \frac{h^2}{2}V_0\right)(\psi_1 + \psi_4)
$$
(4.18)

55

is accurate only to $O(h^3)$ for cells traversed by the particle. For these cells, therefore, the error term in Eq. (4.17) is $O(h^3)$ instead of $O(h^4)$. As there is a number of order $N' = 1/h$ of cells that are traversed by the particle in a simulation run, the overall error—after including the $(\frac{h}{3})^2$ factor in Eq. (4.14)—is of order h^4. We can therefore afford this reduction of the convergence order in Eq. (4.17)

Equation (4.15), however, is accurate only to $O(h)$ for cells traversed by the particle. Again taking the $(\frac{h}{3})^2$ factor into account, this renders the overall scheme $O(h^2)$. Figure 4.2 shows the cells affected by the particle's traversal and the reduced order
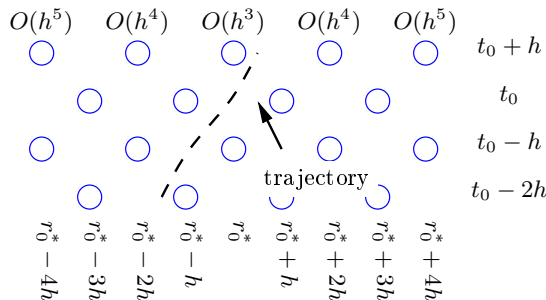

Figure 4.2: Cells affected by the passage of the particle, showing the reduced order of the single step equation

of the single step equation for each cell. Cells whose convergence order is $O(h^5)$ or higher do not need modifications, since there is only a number $N' = 1/h$ of such cells in the simulation. We are therefore concerned about cells neighbouring the particle's trajectory and those traversed by the particle.

Cells neighbouring the particle   These cells are not traversed by the particle, but the particle might have traversed cells in their past light-cone, which are used in the calculation of g_0 in Eq. (4.15). For these cells, we use a one-dimensional Taylor expansion of $g(t, r^*)$ within the current time-slice $t = t_0$,

$$
\begin{aligned}
g_0 = \frac{1}{16}[& 5V(r_0^* - h)\,\psi(t_0, r_0^* - h) + 15V(r_0^* - 3h)\,\psi(t_0, r_0^* - 3h) \\
& - 5V(r_0^* - 5h)\,\psi(t_0, r_0^* - 5h) + V(r_0^* - 7h)\,\psi(t_0, r_0^* - 7h)] + O(h^4)
\end{aligned}
\tag{4.19}
$$

for the cell on the left-hand side, and

$$
\begin{aligned}
g_0 = \frac{1}{16}[& 5V(r_0^* + h)\,\psi(t_0, r_0^* + h) + 15V(r_0^* + 3h)\,\psi(t_0, r_0^* + 3h) \\
& - 5V(r_0^* + 5h)\,\psi(t_0, r_0^* + 5h) + V(r_0^* + 7h)\,\psi(t_0, r_0^* + 7h)] + O(h^4)
\end{aligned}
\tag{4.20}
$$

for the cell on the right-hand side, where (t_0, r_0^*) is the centre of the cell traversed by the particle. Both of these are more accurate than is strictly necessary; we would need error terms of order h^3 to achieve the desired overall $O(h^4)$ convergence of the scheme. Keeping the extra terms, however, improves the numerical convergence slightly.

Cells traversed by the particle We choose not to implement a fully explicit algorithm to handle cells traversed by the particle, because this would increase the complexity of the algorithm by a significant factor. Instead we use an iterative approach to evolve the field using the integrated wave equation

$$-4(\psi_3 + \psi_2 - \psi_1 - \psi_4) - \iint\limits_{\text{cell}} V\,\psi\,\mathrm{d}u\,\mathrm{d}v = -\frac{8\pi q}{E}\int_{t_1}^{t_2} \frac{f_0(t)}{r_0(t)}\bar{Y}_{\ell m}\big(\pi/2, \varphi_0(t)\big)\,\mathrm{d}t\,. \quad (4.21)$$

In this equation the integral involving the source term can be evaluated to any desired accuracy at the beginning of the iteration, because the motion of the particle is determined by a simple system of ordinary differential equations, which are easily integrated with reliable numerical methods. It remains to evaluate the integral over the potential term, which we do iteratively. Schematically the method works as follows:

- Make an initial guess for ψ_3 using the second-order finite-difference scheme. This guess is correct up to terms of $O(h^3)$.

- Match a second-order piecewise interpolation polynomial to the six points that make up the past light-cone of the future grid point, including the future point itself.
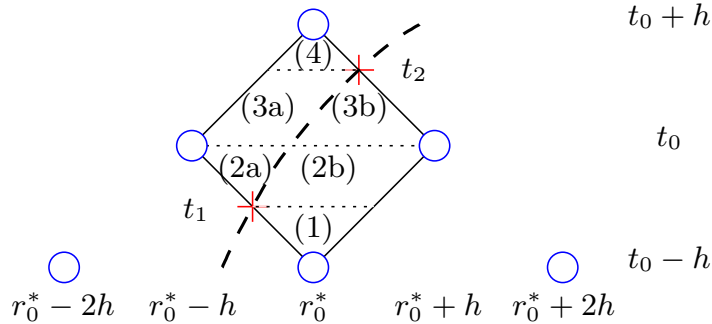

Figure 4.3: Typical cell traversal of the particle. We split the domain into sub-parts indicated by the dotted line based on the time the particle enters (at t_1) and leaves (at t_2) the cell. The integral over each sub-part is evaluated using an iterated two-by-two point Gauss-Legendre rule.

- Use this approximation for ψ to numerically calculate

$$\iint\limits_{\text{cell}} V\,\psi\,\mathrm{d}u\,\mathrm{d}v\,,$$

using two-by-two point Gauss-Legendre rules for the six sub-parts indicated in Fig. 4.3.

- Update the future value of the field and repeat the process until the iteration has converged to a required degree of accuracy.

4.2.4   Initial values and boundary conditions

As is typical for numerical simulations, we have to pay careful attention to specifying initial data and appropriate boundary conditions. These aspects of the numerical method are highly non-trivial problems in full numerical relativity, but they can be solved or circumvented with moderate effort in the present work.
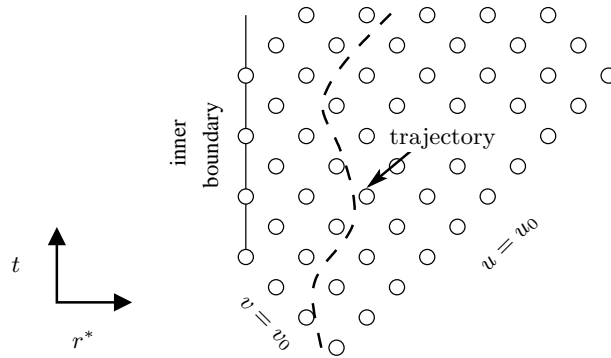
Initial data

Figure 4.4: Numerical domain evolved during the simulation. We impose an inner boundary condition close to the black whole where we can implement it easily to the accuracy of the underlying floating point format. Far away from the black hole, we evolve the full domain of dependence of the initial data domain without imposing boundary conditions.

In this work we use a characteristic grid consisting of points lying on characteristic lines of the wave operator to evolve ψ forward in time. As such, we need to specify characteristic initial data on the lines $u = u_0$ and $v = v_0$ shown in Fig. 4.4. We choose not to worry about specifying "correct" initial data, but instead arbitrarily choose ψ to vanish on $u = u_0$ and $v = v_0$:

$$\psi(u = u_0, v) = \psi(u, v = v_0) = 0 \,. \tag{4.22}$$

This is equivalent to adding spurious initial waves in the form of a homogeneous solution of Eq. (4.7) to the correct solution. This produces an initial wave burst that moves away from the particle with the speed of light, and quickly leaves the numerical domain. Any remaining tails of the spurious initial data decay as $t^{-(2\ell+2)}$ as shown in [39] and become negligible after a short time. We conclude that the influence of the initial-wave content on the self-force becomes negligible after a time of the order of the light-crossing time of the particle's orbit.

Boundary conditions

On the analytical side we would like to impose ingoing boundary conditions at the event horizon $r^* \to -\infty$ and outgoing boundary conditions at spatial infinity $r^* \to \infty$, ie.

$$\lim_{r^* \to -\infty} \partial_u \psi = 0 \,, \quad \lim_{r^* \to \infty} \partial_v \psi = 0 \,. \tag{4.23}$$

Because of the finite resources available to a computer we can only simulate a finite region of the spacetime, and are faced with the reality of implementing boundary conditions at finite values of r^*. Two solutions to this problem present themselves:

1. choose the numerical domain to be the domain of dependence of the initial data surface. Since the effect of the boundary condition can only propagate forward in time with at most the speed of light, this effectively hides any influence of the boundary. This is what we choose to do in order to deal with the outer boundary condition.

2. implement boundary conditions sufficiently "far out" so that *numerically* there is no difference between imposing the boundary condition there or at infinity. Since the boundary conditions depend on the vanishing of the potential $V(r)$ appearing in the wave equation, this will happen once $1 - 2M/r \approx 0$. Near the horizon $r \approx 2M(1 + \exp(r^*/2M))$, so this will happen—to numerical accuracy— for modestly large (negative) values of $r^* \approx -73\,M$. We choose to implement the ingoing waves condition $\partial_u \psi_{\ell m} = 0$ or

$$\psi(t + h, r^*) = \psi(t, r^* - h) \tag{4.24}$$

here.

4.2.5   Implementation

Putting the results described in the preceding sections together we arrive at explicit evolution equations to evolve ψ from one time slice to the next one.

Vacuum cells

Cells not traversed by the particle are evolved using Eqs. (4.9), (4.14) – (4.17). Explicitly written out, we use

$$
\begin{aligned}
\psi_3 = -\psi_2 &+ \left[1 - \frac{1}{4}\left(\frac{h}{3}\right)^2 (V_0 + V_1) + \frac{1}{16}\left(\frac{h}{3}\right)^4 V_0 (V_0 + V_1)\right]\psi_1 \\
&+ \left[1 - \frac{1}{4}\left(\frac{h}{3}\right)^2 (V_0 + V_4) + \frac{1}{16}\left(\frac{h}{3}\right)^4 V_0 (V_0 + V_4)\right]\psi_4 \\
&- \left[1 - \frac{1}{4}\left(\frac{h}{3}\right)^2 V_0\right]\left(\frac{h}{3}\right)^2 (g_{12} + g_{24} + g_{34} + g_{13} + 4g_0),
\end{aligned}
\tag{4.25}
$$

where g_0 is given by Eq. (4.15) and the sum $g_{12} + g_{24} + g_{34} + g_{13}$ is given by Eq. (4.17).

Cells next to the particle

Vacuum cells close to the current position of the particle require a different approach to calculate g_0, since the cells in their past light cone could have been traversed by the particle. We use Eqs. (4.19) and (4.20) to find g_0 in this case. Other than this modification, the same algorithm as for generic vacuum cells is used.

Cells traversed by the particle

We evolve cells traversed by the particle using the iterative algorithm described in Sec. 4.2.3. Here

$$\psi_3 = -\psi_1 + \psi_2 + \psi_4 - \frac{1}{4} \iint_{\text{cell}} V\,\psi \; \mathrm{d}u \; \mathrm{d}v + \frac{2\pi q}{E} \int_{t_1}^{t_2} \frac{f_0(t)}{r_0(t)} \bar{Y}_{\ell m}(\pi/2, \pi_0(t)) \; \mathrm{d}t \,, \quad (4.26)$$

where the initial guess for the iterative evolution of $\iint_{\text{cell}} V\psi \, \mathrm{d}u \, \mathrm{d}v$ is obtained using the second order finite-difference scheme of Lousto and Price [4],

$$\psi_3 = -\psi_1 + \left[1 - \frac{h^2}{2} V_0 \right] [\psi_2 + \psi_4] + \frac{2\pi q}{E} \int_{t_1}^{t_2} \frac{f_0(t)}{r_0(t)} \bar{Y}_{\ell m}(\pi/2, \pi_0(t)) \; \mathrm{d}t \,. \quad (4.27)$$

Successive iterations use a four-point Gauss-Legendre rule to evaluate the integral of $V\psi$; this requires a second-order polynomial interpolation of the current field values as described in Appendix D.1.

4.2.6 Extraction of the field data at the particle

In order to extract the value of the field and its first derivatives at the position of the particle, we again use a polynomial interpolation at the points surrounding the particle's position. Using a fourth-order polynomial, as described in Appendix D.1, we can estimate ψ, $\partial_t \psi_t$, and $\partial_{r^*} \psi$ at the position of the particle up to errors of order h^4. The $O(h^4)$ accuracy we achieve by using a fourth-order piecewise polynomial shows up clearly in a regression plot such as Fig. 4.7.

4.2.7 Numerical tests

In this section we present the tests we have performed to validate our numerical evolution code. In order to check the fourth-order convergence rate of the code, we perform regression runs with increasing resolution for both a vacuum test case, where we seeded the evolution with a Gaussian wave packet, and a case where a particle is present.

Convergence tests: Vacuum

As a first test of the validity of our numerical code we estimate the convergence order by removing the particle and performing regression runs for several resolutions. We use a Gaussian wave packet as initial data,

$$\psi(u = u_0, v) = \exp(-[v - v_p]^2/[2\sigma^2]) \,, \qquad (4.28\text{a})$$
$$\psi(u, v = v_0) = 0 \,, \qquad (4.28\text{b})$$

where $v_p = 75\,M$ and $\sigma = 10\,M$, $v_0 = -u_0 = 6\,M + 2\,M \ln 2$, and we extract the field values at $r^* = 20\,M$. Several such runs were performed, with varying resolution of 2, 4, 8, 16, and 32 grid points per M. Figure 4.5 shows $\psi(2h) - \psi(h)$ rescaled by appropriate powers of 2, so that in the case of fourth-order convergence the curves would lie on top of each other. As can be seen from the plots, they do, and the vacuum portion of the code is indeed fourth-order convergent.
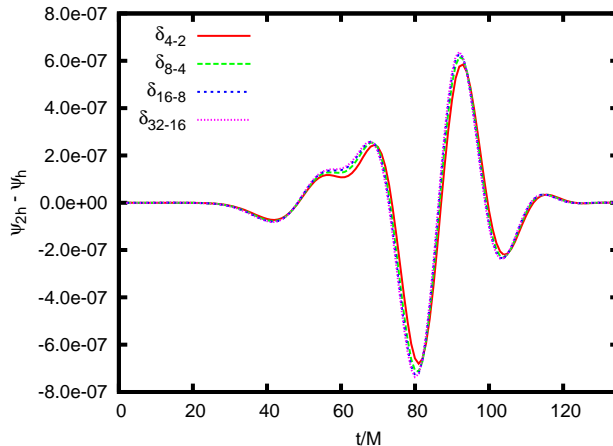
Figure 4.5: Convergence test of the numerical algorithm in the vacuum case. We show differences between simulations using different step sizes $h = 0.5\,M$ (ψ_2), $h = 0.25\,M$ (ψ_4), $h = 0.125\,M$ (ψ_8), $h = 0.0625\,M$ (ψ_{16}), and $h = 0.03125\,M$ (ψ_{32}). Displayed are the rescaled differences $\delta_{4-2} = \psi_4 - \psi_2$, $\delta_{8-4} = 2^4(\psi_8 - \psi_4)$, $\delta_{16-8} = 4^4(\psi_8 - \psi_4)$, and $\delta_{32-16} = 8^4(\psi_8 - \psi_4)$ for the real part of the $\ell = 2$, $m = 2$ mode at $r^* \approx 20\,M$. The maximum value of the field itself is of the order of 0.1, so that the errors in the field values are roughly five orders of magnitude smaller than the field values themselves. We can see that the convergence is in fact of fourth-order, as the curves lie nearly on top of each other, with only the lowest resolution curve δ_{4-2} deviating slightly.

Convergence tests: Particle

While the convergence test described in section 4.2.7 clearly shows that the desired convergence is achieved for vacuum evolution, it does not test the parts of the code that are used in the integration of the inhomogeneous wave equation. To test these we perform a second set of regression runs, this time using a non-zero charge q. We extract the field at the position of the particle, thus also testing the implementation of the extraction algorithm described in section 4.2.6. For this test we choose the $\ell = 6$, $m = 4$ mode of the field generated by a particle on a mildly eccentric geodesic orbit with $p = 7$, $e = 0.3$. As shown in Fig. 4.6 the convergence is still of fourth order, but the two curves no longer lie precisely on top of each other at all times. The region before $t \approx 100\,M$ is dominated by the initial wave burst and therefore does not scale as expected, yielding two very different curves. In the region $300\,M \lesssim t \lesssim 400\,M$ the two curves lie on top of each other, as expected for a fourth-order convergent finite-difference scheme. In the region between $t \approx 200\,M$ and $t \approx 300\,M$, however, the dashed curves have slightly smaller amplitudes than the solid one, indicating an order of convergence different from (but close to) four.

To explain this behaviour we have to examine the terms that contribute significantly to the error in the simulation. The numerical error is almost completely dominated by that of the approximation of the potential term $\iint_{\text{cell}} V\psi \, \mathrm{d}u \, \mathrm{d}v$ in the integrated wave equation. For vacuum cells the error in this approximation scales as h^6, where h is the step size. For cells traversed by the particle, on the other hand,
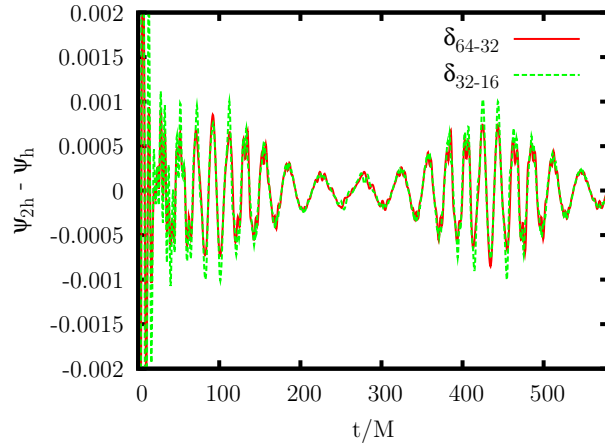
61

Figure 4.6: Convergence test of the numerical algorithm in the sourced case. We show differences between simulations using different step sizes of 4 (ψ_4), 8 (ψ_8), 16 (ψ_{16}), and 32 (ψ_{32}) cells per M. Displayed are the rescaled differences $\delta_{8-4} = \psi_8 - \psi_4$, etc. (see caption of Fig. 4.5 for definitions) of the field values at the position of the particle for a simulation with $\ell = 6$, $m = 4$ and $p = 7$, $e = 0.3$. We see that the convergence is approximately fourth-order.
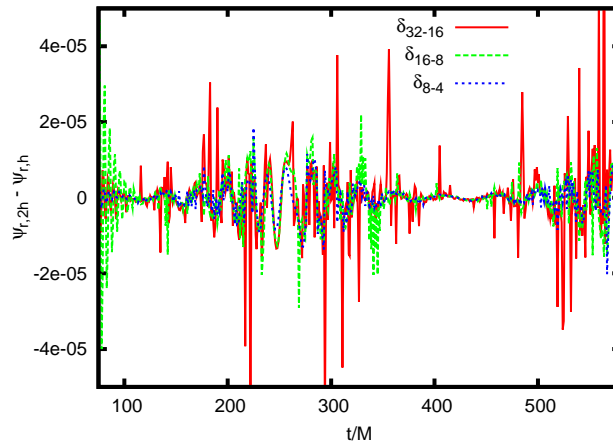

Figure 4.7: Convergence test of the numerical algorithm in the sourced case. We show differences between $\partial_r \Phi$ for simulations using different step sizes of 4 ($\Phi_{r,4}$), 8 ($\Phi_{r,8}$), 16 ($\Phi_{r,16}$), and 32 ($\Phi_{r,32}$) cells per M. Displayed are the rescaled differences $\delta_{8-4} = \Phi_{r,8} - \Phi_{r,4}$ etc. of the values at the position of the particle for a simulation with $\ell = 6$, $m = 4$ and $p = 7$, $e = 0.3$. Although there is much noise caused by the piecewise polynomials used to extract the data, we can see that the convergence is approximately fourth-order.

the approximation error depends also on the difference $t_2 - t_1$ of the times at which the particle enters and leaves the cell. This difference is bounded by h but does not necessarily scale as h. For example, if a particle enters a cell at its very left, then scaling h by $\frac{1}{2}$ would not change $t_2 - t_1$ at all, thus leading to a scaling behaviour that differs from expectation.

To investigate this further we conducted test runs of the simulation for a particle on a circular orbit at $r = 6\,M$. In order to observe the expected scaling behaviour, we have to make sure that the particle passes through the tips of the cell it traverses. When this is the case, then $t_2 - t_1 \equiv h$ and a plot similar to the one shown in Fig. 4.6 shows the proper scaling behaviour. As a further test we artificially reduced the convergence order of the *vacuum* scheme to two by implementing the second-order scheme described in [5]. By keeping the algorithm that deals with sourced cells unchanged, we reduced the relative impact on the numerical error. This, too, allows us to recover the expected (second-order) convergence. Figures 4.8 and 4.9 illustrate the effects of the measures taken to control the convergence behaviour.
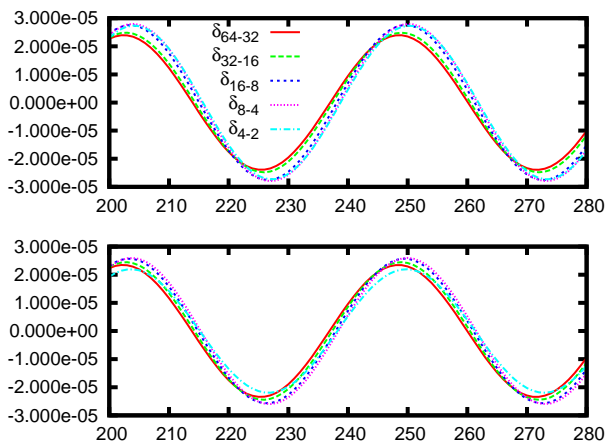

Figure 4.8: Behaviour of convergence tests for a particle in circular orbit at $r = 6\,M$. We show differences between simulations of the $\ell = 2$, $m = 2$ multipole moment using different step sizes of 2 (ψ_2), 4 (ψ_4), 8 (ψ_8), 16 (ψ_{16}), 32 (ψ_{32}) and 64 (ψ_{64}) cells per M. Displayed are the real part of the rescaled differences $\delta_{4-2} = (\psi_4 - \psi_2)$ etc. of the field values at the position of the particle, defined as in Fig. 4.5. The values have been rescaled so that—for fourth order convergence—the curves should all coincide. The upper panel corresponds to a set of simulations where the particle traverses the cells away from their tips. The curves do not coincide perfectly with each other, seemingly indicating a failure of the convergence. The lower panel was obtained in a simulation where the particle was carefully positioned so as to pass through the tips of each cell it traverses. This set of simulations passes the convergence test more convincingly.
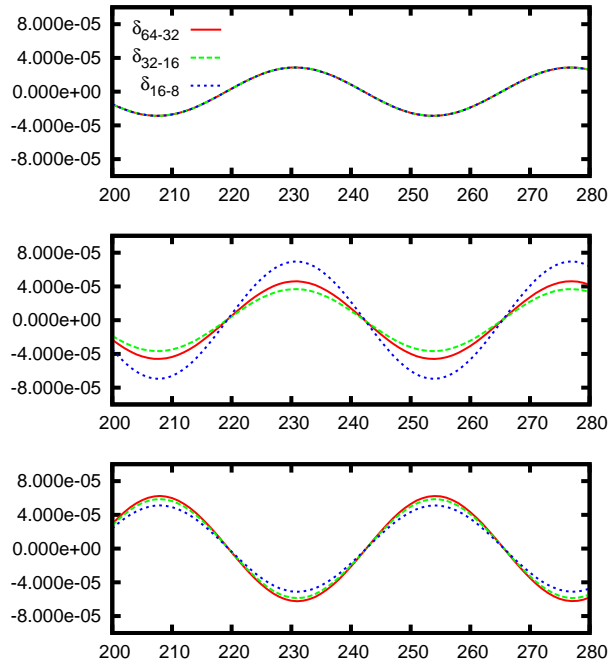
63

Figure 4.9: Behaviour of convergence tests for a particle in circular orbit at $r = 6\,M$. We show differences between simulations of the $\ell = 2$, $m = 2$ multipole moment using different step sizes of 8 (ψ_8), 16 (ψ_{16}), 32 (ψ_{32}), and 64 (ψ_{64}) cells per M. Displayed are the real part of the rescaled differences $\delta_{16-8} = \psi_{16} - \psi_8$ etc. of the field values at the position of the particle, defined as in Fig. 4.5. The values have been rescaled so that—for second order convergence—the curves should all coincide. The upper two panels correspond to simulations where the second order finite-difference scheme was used throughout. For the topmost one, care was taken to ensure that the particle passes through the tip of each cell it traverses, while in the middle one no such precaution was taken. Clearly the curves in the middle panel do not coincide with each other, indicating a failure of the second-order convergence of the code. The lower panel was obtained in a simulation using the mixed-order algorithm described in the text. While the curves still do not coincide precisely, the observed behaviour is much closer to the expected one than for the purely second order finite-difference scheme.

4.3 Electromagnetic field: Faraday tensor method

Our task is to numerically solve the Maxwell equations

$$g^{\beta\gamma}\nabla_\gamma F_{\alpha\beta}(x) = 4\pi j_\alpha(x)\,, \tag{4.29a}$$
$$\nabla_{[\gamma}F_{\alpha\beta]}(x) = 0\,, \tag{4.29b}$$
$$j_\alpha(x) = q\int_\gamma u_\alpha(\tau)\delta_4(x, z(\tau))\,\mathrm{d}\tau\,. \tag{4.29c}$$

We use vector spherical harmonics $Z_A^{\ell m} = \partial_A Y^{\ell m}$ and $X_A^{\ell m} = \epsilon_A{}^B \partial_B Y^{\ell m}$ as introduced in [40] and decompose the vector potential A_α and the current density j_α as

$$A_a(t, r, \theta, \phi) = A_a^{\ell m}(t, r)Y_{\ell m}(\theta, \phi)\,, \tag{4.30a}$$
$$j_a(t, r, \theta, \phi) = j_a^{\ell m}(t, r)Y_{\ell m}(\theta, \phi) \qquad \text{for } a = t, r\,, \tag{4.30b}$$
$$A_A(t, r, \theta, \phi) = v_{\ell m}(t, r)Z_A^{\ell m}(\theta, \phi) + \tilde{v}_{\ell m}(t, r)X_A^{\ell m}(\theta, \phi)\,, \tag{4.30c}$$
$$j_A(t, r, \theta, \phi) = j_{\ell m}^{\text{even}}(t, r)Z_A^{\ell m}(\theta, \phi) + j_{\ell m}^{\text{odd}}(t, r)X_A^{\ell m}(\theta, \phi) \qquad \text{for } A = \theta, \phi\,, \tag{4.30d}$$

where a summation over ℓ and m is implied. Substituting these into Eq. (2.53) we arrive at two decoupled sets of equations for the even ($A_a^{\ell m}$, $v_{\ell m}$) and odd ($\tilde{v}_{\ell m}$) modes

$$-f\frac{\partial^2 A_t^{\ell m}}{\partial r^2} + f\frac{\partial^2 A_r^{\ell m}}{\partial t \partial r} - \frac{2f}{r}\frac{\partial A_t^{\ell m}}{\partial r} + \frac{2f}{r}\frac{\partial A_r^{\ell m}}{\partial t} - \frac{\ell(\ell+1)}{r^2}\frac{\partial v^{\ell m}}{\partial t} + \frac{\ell(\ell+1)}{r^2}A_t^{\ell m} \tag{4.31a}$$
$$= 4\pi j_t^{\ell m}\,,$$

$$f^{-1}\frac{\partial^2 A_r^{\ell m}}{\partial t^2} - f^{-1}\frac{\partial^2 A_t^{\ell m}}{\partial t \partial r} - \frac{\ell(\ell+1)}{r^2}\frac{\partial v^{\ell m}}{\partial r} + \frac{\ell(\ell+1)}{r^2}A_r^{\ell m} = 4\pi j_r^{\ell m}\,, \tag{4.31b}$$

$$-f\frac{\partial^2 v^{\ell m}}{\partial t^2} + f^{-1}\frac{\partial^2 v^{\ell m}}{\partial t^2} - \frac{2M}{r^2}\frac{\partial v^{\ell m}}{\partial r} + f\frac{\partial A_r^{\ell m}}{\partial r} - f^{-1}\frac{\partial A_t^{\ell m}}{\partial t} + \frac{2M}{r^2}\tilde{v}^{\ell m} = 4\pi j_{\ell m}^{\text{even}}\,, \tag{4.31c}$$

$$-f\frac{\partial^2 \tilde{v}^{\ell m}}{\partial t^2} + f^{-1}\frac{\partial^2 \tilde{v}^{\ell m}}{\partial t^2} - \frac{2M}{r^2}\frac{\partial \tilde{v}^{\ell m}}{\partial r} + \frac{\ell(\ell+1)}{r^2}\tilde{v}^{\ell m} = 4\pi j_{\ell m}^{\text{odd}}\,, \tag{4.31d}$$

where

$$j_t^{\ell m} = -\frac{qf}{r_0^2}\bar{Y}^{\ell m}(\frac{\pi}{2}, \varphi_0)\delta(r - r_0)\,, \tag{4.32a}$$

$$j_r^{\ell m} = \frac{q\dot{r}_0}{Er_0^2}\bar{Y}^{\ell m}(\frac{\pi}{2}, \varphi_0)\delta(r - r_0)\,, \tag{4.32b}$$

$$j_{\ell m}^{\text{even}} = -\frac{imqfJ}{\ell(\ell+1)Er_0^2}\bar{Y}^{\ell m}(\frac{\pi}{2}, \varphi_0)\delta(r - r_0)\,, \tag{4.32c}$$

$$j_{\ell m}^{\text{odd}} = -\frac{qfJ}{\ell(\ell+1)Er_0^2}\partial_\theta\bar{Y}^{\ell m}(\frac{\pi}{2}, \varphi_0)\delta(r - r_0)\,. \tag{4.32d}$$

In the equations above an overbar denotes complex conjugation, an overdot denotes differentiation with respect to τ.

The three even mode equations Eq. (4.31a) – Eq. (4.31c) are not yet amenable to a numerical treatment, as they are highly coupled. In order to obtain a more convenient set of equation we define the auxiliary fields

$$\psi^{\ell m} \equiv -r^2 \left(\frac{\partial A_t^{\ell m}}{\partial r} - \frac{\partial A_r^{\ell m}}{\partial t} \right), \tag{4.33a}$$

$$\chi^{\ell m} \equiv f \left(A_r^{\ell m} - \frac{\partial v^{\ell m}}{\partial r} \right), \tag{4.33b}$$

$$\xi^{\ell m} \equiv A_t^{\ell m} - \frac{\partial v^{\ell m}}{\partial t}, \tag{4.33c}$$

which, up to the scaling factors, are just the tr, $r\phi$ and $t\phi$ components of the Faraday tensor

$$F_{tr} = \sum_{\ell,m} \frac{\psi^{\ell m}}{r^2} Y^{\ell m}, \tag{4.34a}$$

$$F_{tA} = \sum_{\ell,m} (-\xi^{\ell m} Z_A^{\ell m} + \tilde{v}_{,t}^{\ell m} X_A^{\ell m}), \tag{4.34b}$$

$$F_{rA} = \sum_{\ell,m} (\frac{\chi^{\ell m}}{f} Z_A^{\ell m} + \tilde{v}_{,r}^{\ell m} X_A^{\ell m}), \tag{4.34c}$$

$$\begin{aligned} F_{\theta\phi} &= \sum_{\ell,m} \tilde{v}_{\ell m} (X_{\phi,\theta}^{\ell m} - X_{\theta,\phi}^{\ell m}) \\ &= -\sum_{\ell,m} \ell(\ell+1)\tilde{v}_{\ell m} \sin(\theta) Y^{\ell m}. \end{aligned} \tag{4.34d}$$

Importantly, the relations in Eq. (4.33) can be arithmetically inverted to yield the Faraday tensor components appearing in Eq. (2.133)

$$A_{r,t}^{\ell' m'} - A_{t,r}^{\ell' m'} = \frac{\psi^{\ell m}}{r^2}, \tag{4.35a}$$

$$\partial_t v^{\ell' m'} - A_t^{\ell' m'} = -\xi^{\ell m}, \tag{4.35b}$$

and

$$\partial_r v^{\ell' m'} - A_r^{\ell' m'} = -\frac{\chi^{\ell m}}{f}, \tag{4.35c}$$

We then form linear combinations of derivatives of Eqs.(4.31a) – (4.31c). We use $[\partial_r(r^2(4.31\text{b})) - \partial_t(r^2(4.31\text{a}))]$ for $\psi^{\ell m}$ and find

$$\frac{\partial^2 \psi^{\ell m}}{\partial r^{*2}} - \frac{\partial^2 \psi^{\ell m}}{\partial t^2} - \frac{\ell(\ell+1)}{r^3} \psi^{\ell m} = S_{[\psi]}, \tag{4.36a}$$

$$S_{[\psi]} = 4\pi f \left[\frac{\partial r^2 j_t^{\ell m}}{\partial r} - \frac{\partial r^2 j_r^{\ell m}}{\partial t} \right]. \tag{4.36b}$$

Similarly we use $[f(4.31b) - \partial_r(f(4.31c))]$ for χ and $[(4.31a) - \partial_t(4.31c)]$ for ξ. We find

$$\frac{\partial^2 \chi^{\ell m}}{\partial r^{*2}} - \frac{\partial^2 \chi^{\ell m}}{\partial t^2} - \frac{\ell(\ell+1)(r-2M)}{r^3}\chi^{\ell m} = S_{[\chi]}, \tag{4.37a}$$

$$S_{[\chi]} = 4\pi f\left[\frac{\partial f j_{\ell m}^{\text{even}}}{\partial r} - f j_r^{\ell m}\right], \tag{4.37b}$$

$$\frac{\partial^2 \xi^{\ell m}}{\partial r^{*2}} - \frac{\partial^2 \xi^{\ell m}}{\partial t^2} - \frac{\ell(\ell+1)(r-2M)}{r^3}\xi^{\ell m} - \frac{2(r-3M)(r-2M)}{r^5}\psi^{\ell m} = S_{[\xi]}, \tag{4.37a}$$

$$S_{[\xi]} = 4\pi f\left[\frac{\partial f j_{\ell m}^{\text{even}}}{\partial t} - f j_t^{\ell m}\right]. \tag{4.37b}$$

Eqs. (4.36) – (4.37a) are still partially coupled, however the coupling is in the form of a staggering, which allows us to first solve for $\psi^{\ell m}$ and use this result in the calculation of $\xi^{\ell m}$. On the other hand, the source terms appearing on the right hand side contain derivatives of δ resulting in fields that are discontinuous at the location of the particle. Lousto's scheme is designed to cope with precisely this situation.

We note that the three fields $\psi^{\ell m}$, $\chi^{\ell m}$ and $\xi^{\ell m}$ are not independent of each other; in fact knowledge of $\psi^{\ell m}$ is sufficient to reconstruct $\chi^{\ell m}$ and $\xi^{\ell m}$. Eq. (4.31a) can be rearranged to yield

$$\xi^{\ell m} = -\frac{f}{\ell(\ell+1)}\frac{\partial \psi^{\ell m}}{\partial r} - \frac{4\pi}{\ell(\ell+1)}j_t^{\ell m}, \tag{4.39a}$$

and similarly from Eq. (4.31b)

$$\chi^{\ell m} = -\frac{1}{\ell(\ell+1)}\frac{\partial \psi^{\ell m}}{\partial t} - \frac{4\pi f}{\ell(\ell+1)}j_r^{\ell m}, \tag{4.39b}$$

showing that knowledge of $\psi^{\ell m}$ is sufficient to reconstruct the even multipole components of the Faraday tensor. In this work, however, we choose to solve for $\chi^{\ell m}$ and $\xi^{\ell m}$ directly, rather than numerically differentiate $\psi^{\ell m}$ to obtain them. The gain in speed by reducing the number of equations does not seem to offset the additional time required to calculate $\psi^{\ell m}$ accurately enough to obtain good approximations for its derivatives at the location of the particle. In this approach Eqs. (4.39a) and (4.39b) are treated as constraints that the dynamical variables have to satisfy.

Finally we derive explicit expressions for the source terms $S_{[\cdot]}$ on the right hand sides of the field equations

$$S_{[\cdot]} = G_{[\cdot]}(t)f_0\delta(r-r_0) + F_{[\cdot]}(t)f\delta'(r-r_0), \tag{4.40a}$$

$$G_{[\psi]}(t) = -\frac{4\pi q}{E^2}f_0\left(\ddot{r}_0 - \frac{im\dot{r}_0 J}{r_0^2}\right)\bar{Y}_{\ell m}(\frac{\pi}{2},\varphi_0), \tag{4.40b}$$

$$F_{[\psi]}(t) = 4\pi q f_0\left(\frac{\dot{r}_0^2}{E^2} - 1\right)\bar{Y}_{\ell m}(\frac{\pi}{2},\varphi_0), \tag{4.40c}$$

$$G_{[\chi]}(t) = -\frac{4\pi q\dot{r}_0}{Er_0^2}f_0\bar{Y}_{\ell m}(\frac{\pi}{2},\varphi_0), \tag{4.40d}$$

$$F_{[\chi]}(t) = -\frac{4\pi q J im}{E\ell(\ell+1)r_0^2}f_0^2\bar{Y}_{\ell m}(\frac{\pi}{2},\varphi_0), \tag{4.40e}$$

$$G_{[\xi]}(t) = -4\pi q \left\{ \frac{Jim}{E^2\ell(\ell+1)r_0^2}\left[\left(\frac{2M}{r_0^2}-\frac{2f_0}{r_0}\right)\dot{r}_0 - \frac{imJ}{r_0^2}\right] - \frac{1}{r_0^2} \right\} f_0 \bar{Y}_{\ell m}(\frac{\pi}{2},\varphi_0), \quad (4.40\text{f})$$

$$F_{[\xi]}(t) = \frac{4\pi q Jim\dot{r}_0}{E^2\ell(\ell+1)r_0^2} f_0^2 \bar{Y}_{\ell m}(\frac{\pi}{2},\varphi_0). \quad (4.40\text{g})$$

We note that the coefficient functions $G_{[\cdot]}$ and $F_{[\cdot]}$ are independent of r (but do contain terms in $r_0(t)$), an observation we will later use to simplify Lousto's expression for the source terms.

4.3.1 Constraint equations

The full set of Maxwell equations consists of the inhomogeneous equations Eq. (4.29a) as well as the homogeneous constraints Eq. (4.29b) which have to be satisfied by a solution to Eq. (4.29a). Introducing a vector potential A_α implies that the constraints are identically satisfied since they reduce to the Bianchi identities for the second derivatives of A_α. When solving for the components of the Faraday tensor directly there is no a priory guarantee that a solution to Eq. (4.36) – (4.37a), and (4.31d) satisfies Eq. (4.29b). It turns out, however, that a decomposition into spherical harmonics is sufficient to ensure that all but one of the constraints are identically satisfied. The one that is not identically true is the $tr\phi$ (or $tr\theta$) equation, which in terms of $\psi^{\ell m}$, $\chi^{\ell m}$ and $\xi^{\ell m}$ reads

$$\frac{\psi^{\ell m}}{r^2} - \frac{\chi^{\ell m}_{,t}}{f} + \xi^{\ell m}_{,r} = 0. \quad (4.41)$$

If the fields satisfy the sourced Maxwell equations Eqs. (4.31a), (4.31b), then Eq. (4.41) is just the evolution equation for $\psi^{\ell m}$. Thus Eq. (4.41) is valid whenever $\psi^{\ell m}$ satisfies the consistency relations Eq. (4.39a) and (4.39b).

Analytically then, the situation is clear. Given a set of initial conditions for $\psi^{\ell m}$, $\chi^{\ell m}$ and $\xi^{\ell m}$ which satisfy the sourced Maxwell equations initially, a solution to the system of Eq. (4.36) – (4.37a), (4.31d) satisfies the sourced equations at all later times. Given this, the homogeneous Maxwell equations are also satisfied at all times and the reduced system is equivalent to the original set of Maxwell equations.

Numerically we monitor but do not enforce Eq. (4.39a) and (4.39b). Section 4.3.5 displays results for the constraint violations for our set of sample results.

Discretization—even sector

Lousto's method is directly applicable to terms of the form $-\frac{\partial^2\psi}{\partial t^2} + \frac{\partial^2\psi}{\partial r^{*2}}$, $V(r)\psi$ (ie. the wave operator and potential terms) on the left hand side of the equation and the source terms $S_\alpha(t)$ on the right hand side. Here ψ is used as a placeholder for any of $\psi^{\ell m}$, $\chi^{\ell m}$ or $\xi^{\ell m}$; $V(r)$ is an expression depending only on r and $S(t)$ is one of the

right hand side expressions in Eqs. (4.36) – (4.37a). We discretize these terms as

$$\iint\limits_{\text{cell}} \mathrm{d}u \ \mathrm{d}v \ \left(-\frac{\partial^2 \psi}{\partial t^2} + \frac{\partial^2 \psi}{\partial r^{*2}} \right) = -4 \left[\psi_3 + \psi_2 - \psi_1 - \psi_4 \right],$$

(4.42a)

$$\iint\limits_{\text{cell}} \mathrm{d}u \ \mathrm{d}v \ V(r)\psi = \begin{cases} h^2(\psi_1 + \psi_2 + \psi_3 + \psi_4)V_0 + O(h^4) & \text{vacuum cells} \\ (A_1\psi_1 + A_2\psi_2 + A_3\psi_3 + A_4\psi_4)V_0 + O(h^3) & \text{sourced cells} \end{cases}$$

(4.42b)

and

$$\iint\limits_{\text{cell}} \mathrm{d}u \ \mathrm{d}v \ S_\alpha(t) = 2\int_{t_1}^{t_2} G(t, r_0(t)) \ \mathrm{d}t \pm \frac{2F(t_1, r_0(t_1))}{1 - 2M/r(t_1)}[1 \mp \dot{r}_0(t_1)/E]^{-1}$$
$$\pm \frac{2F(t_2, r_0(t_2))}{1 - 2M/r(t_2)}[1 \pm \dot{r}_0(t_2)/E]^{-1},$$

(4.43)

where $u = t - r^*$, $v = t + r^*$ are null coordinates, $\psi_1, \ldots, \psi_4$ refer to values of the field at the points labelled 1,...,4 in Fig. 4.1, $h = \Delta_t = \Delta_{r^*}/2$ is the step size, V_0 is the value of the potential at the centre of the cell, $A_1, \ldots, A_4$ are the areas indicated in Fig. 4.1 and t_1 and t_2 are the times at which the particle enters and leaves the cell, respectively.

Discretization—odd sector

When written in terms of r^*, Eq. (4.31d), which governs the odd modes $\tilde{v}^{\ell m}$, reads

$$\frac{\partial^2 \tilde{v}^{\ell m}}{\partial r^{*2}} - \frac{\partial^2 \tilde{v}^{\ell m}}{\partial t^2} - \frac{\ell(\ell+1)(r-2M)}{r^3}\tilde{v}^{\ell m} = -4\pi f j_{\tilde{v}}^{\ell m}, \qquad (4.44\text{a})$$

$$j_{\tilde{v}}^{\ell m} = -\frac{qJ}{\ell(\ell+1)Er_0^2}\partial_\theta \bar{Y}^{\ell m}(\frac{\pi}{2}, \varphi_0)\delta(r^* - r_0^*). \qquad (4.44\text{b})$$

Eq. (4.44a) is of precisely the same form as the scalar wave equation discussed in section 4.2. We re-use the fourth order numerical code described there with $V = \frac{\ell(\ell+1)(r-2M)}{r^3}$, $S = 4\pi \frac{qfJ}{\ell(\ell+1)Er_0^2}\partial_\theta \bar{Y}^{\ell m}(\frac{\pi}{2}, \varphi_0)$. This yields accurate results for $\tilde{v}$ and its derivatives.

4.3.2 Initial values and boundary conditions

We follow the approach described in section 4.2.4 and do not specify physical initial data or an outer boundary condition. We arbitrarily choose the fields to vanish on the characteristic slices $u = u_0$ and $v = v_0$

$$\psi(u = u_0) = \psi(v = v_0) = 0, \qquad (4.45)$$

thereby adding a certain amount of spurious waves to the solution which show up as an initial burst.

We implement ingoing wave boundary conditions near the event horizon, sufficiently close so that *numerically* $r \approx 2M$, that is the potential terms in Eqs. (4.36) – (4.37a) vanish. This happens at $r^* \approx -73\,M$ and we implement the ingoing waves condition $\partial_u \psi_{\ell m} = 0$ there. Near the outer boundary this is not possible, since the potential decays only slowly. Instead we choose to evolve the full domain of dependence of the initial data surface there, hiding the effects of the boundary.

4.3.3 Extraction of the field data at the particle

We use a straightforward one-sided extrapolation of field values to the right of the particle's position to extract values for ψ and $\partial_{r^*}\psi$. Specifically we fit a fourth order polynomial

$$p(x) = \sum_{n=0}^{4} \frac{c_i}{n!} x^n \,, \tag{4.46}$$

where $x = r^* = r_0^*$ to the five points to the right of the particle's current position and extract ψ and $\partial_{r^*}\psi$ as c_0 and c_1, respectively. In order to calculate $\frac{\partial \psi(t_0, r_0^*)}{\partial t}$ we follow [41] and calculate $\frac{\mathrm{d}\psi(t, r^*(t))}{\mathrm{d}t}$ on the world line of the particle. Since this can be calculated using either the field values on the world line

$$\frac{\mathrm{d}\psi(t, r^*(t))}{\mathrm{d}t} = \frac{\psi(t+h, r^*(t+h)) - \psi(t-h, r^*(t-h))}{2h} + O(h^2)\,, \tag{4.47}$$

or as

$$\frac{\mathrm{d}\psi(t, r^*(t))}{\mathrm{d}t} = \frac{\partial \psi}{\partial t} + \frac{\partial \psi}{\partial r^*}\frac{\mathrm{d}r_0^*}{\mathrm{d}t}\,, \tag{4.48}$$

where both $\frac{\partial \psi}{\partial r^*}$ and $\frac{\mathrm{d}r_0^*}{\mathrm{d}t} = \frac{\dot{r}_0}{E}$ are known, this allows us to find

$$\frac{\partial \psi}{\partial t} = \frac{\mathrm{d}\psi(t, r^*(t))}{\mathrm{d}t} - \frac{\partial \psi}{\partial r^*}\frac{\mathrm{d}r_0^*}{\mathrm{d}t}\,. \tag{4.49}$$

We repeat this procedure to the left of the particle. As a check for the extraction procedure, we compare the difference between the right hand and left hand values $[\psi] = \psi_{\mathrm{right}} - \psi_{\mathrm{left}}$ with the analytically calculated jump conditions of appendix D.2.1. Similarly we check that the numerical solution satisfies the first order Maxwell equations Eq. (4.29a), (4.29b). In particular we check whether the numerical solutions obtained for χ and ξ directly are consistent with Eqs. (4.39b) and (4.39a), which give them in terms of derivatives of ψ.

4.3.4 Numerical tests

In this section we present the tests we performed to validate our numerical evolution code. First, in order to check the second-order convergence rate of the code, we perform regression runs with increasing resolution. As a second test, we compute the regularized self-force for several different combinations of orbital elements p and e and check that the multipole coefficients decay with ℓ as expected. This provides a very sensitive check on the overall implementation of the numerical scheme as well as the analytical calculations that lead to the regularization parameters.

Convergence tests

We performed regression runs for our second-order convergent code using a non-zero charge q and an eccentric orbit. We extract the field at the position of the particle, thus also testing the implementation of the extraction algorithm described in section 4.3.3. We choose the $\ell = 6$, $m = 4$ mode of the field generated by a particle on a mildly eccentric geodesic orbit with $p = 7$, $e = 0.3$. As shown in Fig. 4.10 the convergence is roughly of second order. In the region $200\,M \lesssim t \lesssim 350\,M$ the two
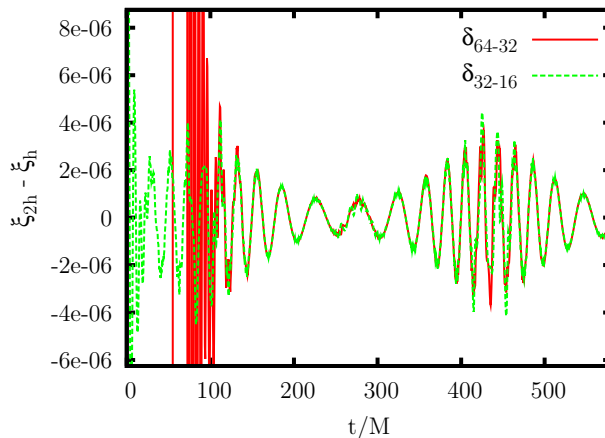

Figure 4.10: Convergence test of the numerical algorithm in the sourced case. We show differences between simulations using different step sizes of 16, 32 and 64 cells per M. Displayed are the rescaled differences $\delta_{32-16} = \xi(h = 1/32M) - \xi(h = 1/16M)$ etc. of the field values at the position of the particle for a simulation with $\ell = 6$, $m = 4$ and $p = 7$, $e = 0.3$. We see that the convergence is approximately second-order. The curves are rescaled in such a way as to provide an estimate for the error of the highest resolution run compared to the real ($h \equiv 0$) solution.

curves lie on top of each other, as expected for a second-order convergent scheme. In the region from $400\,M$ to $450\,M$ there is some difference between the two lines, caused by cell crossing effects similar to those discussed in section 4.2.7.

4.3.5 Constraint violations

We monitor but do not enforce Eq. (4.39a) and (4.39b). This could in principle lead to the generation of growing modes similar to the gauge violating modes in the vector potential method of section 4.4.1. In the case of the first order constraints, however, we generally find that violations of the constraints are at least three orders of magnitude smaller than the field quantities themselves. Figures 4.11 and 4.12 compare ξ obtained from its evolution equations to that obtained from Eq. (4.39a) and (4.39b).
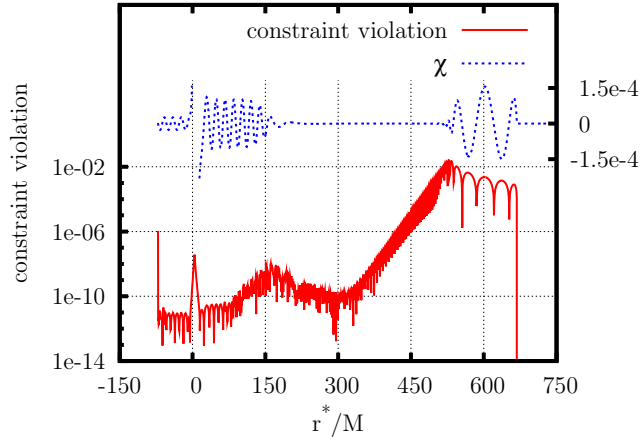
Figure 4.11: Violations of the constraint $Z_\xi = \xi + \frac{1}{\ell(\ell+1)}\frac{\partial\psi}{\partial t} = 0$ in the vacuum region away from the location of particle. We plot the ratio of the magnitudes of $\log_{10}|Z_\chi|$ and χ respectively as obtained from the evolution equations on a spatial slice at $t = 600\,M$. For this slightly eccentric orbit ($p = 7.0$, $e = 0.3$) using a stepsize $h = 1/512M$ the errors in the $\ell = 2$, $m = 2$ mode are at least three orders of magnitude smaller than the field values. The exponentially growing signal between $300M \lesssim r^* \lesssim 500$ is a remnant of the initial data pulse travelling outward.
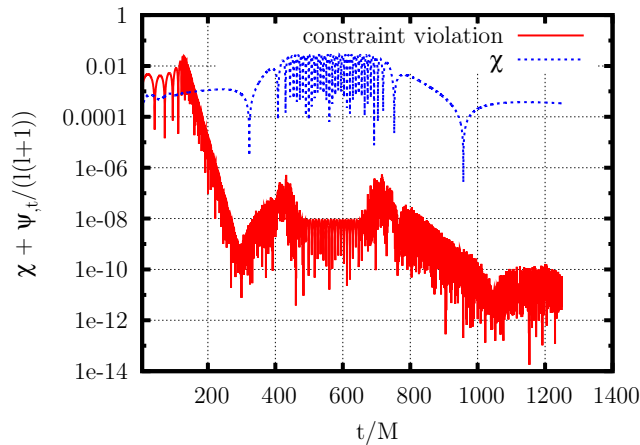

Figure 4.12: Violations of the constraint $Z_\chi = \chi + \frac{1}{\ell(\ell+1)}\frac{\partial\psi}{\partial t} = 0$ at the location of the particle as a function of time. We display χ and $\log_{10}|Z_\chi|$ for the $\ell = 5$, $m = 3$ mode of a particle on an eccentric orbit with $p = 7.8001$, $e = 0.9$ with stepsize $h = 1/2048\,M$. During the time $400\,M \lesssim t \lesssim 800\,M$ the particle is in the whirl phase. The exponentially decaying signal before $t \approx 250M$ is the initial data pulse.

4.3.6 Monopole mode

For the electromagnetic field, the monopole mode $\ell = 0$ is non-radiative. The vector harmonics $Z_A^{\ell m}$ and $X_A^{\ell m}$ cannot be defined in this case and the only surviving multipole mode is ψ. For the monopole case Eq. (4.36) reduces to a wave equation in flat space

$$\frac{\partial^2 \psi}{\partial r^{*2}} - \frac{\partial^2 \psi}{\partial t^2} = 4\pi f \left[\frac{\partial (r^2 j_t^{0,0})}{\partial r} - \frac{\partial (r^2 j_r^{0,0})}{\partial t} \right], \tag{4.50}$$

which is simple enough so that we can solve it analytically. A straightforward calculation shows that

$$\psi(r^*) = -\sqrt{4\pi} q \theta(r^* - r_0^*) \tag{4.51}$$

satisfies Eq. (4.50) and corresponds to no outgoing radiation $(\partial_t - \partial_{r^*})\psi = 0$ at the event horizon and no ingoing radiation $(\partial_t + \partial_{r^*})\psi = 0$ at spatial infinity. The interpretation of this result is clear: inside of the particle's orbit at $r^* = r_0^*(\tau)$ there is no charge, and outside the total charge is equal to q.

4.4 Alternative calculation using the vector potential

In this section we describe a variant of the numerical calculation discussed above that uses the vector potential instead of the Faraday tensor. To this end we decompose the vector potential and the sources in terms of vectorial spherical harmonics as in Eq. (4.30) and substitute into the Maxwell equations for the vector potential in the Lorenz gauge $g^{\alpha\beta} A_{\alpha;\beta} = 0$ Eq. (2.53). We arrive at two decoupled sets of equations for the even $(A_a^{\ell m}, v_{\ell m})$ and odd $(\tilde{v}_{\ell m})$ modes, namely Eqs. (4.31a) – (4.31d), which when written in terms of r^* read

$$-\frac{\partial^2 A_t^{\ell m}}{\partial t^2} + \frac{\partial^2 A_t^{\ell m}}{\partial r^{*2}} + \frac{2M}{r^2} \left(\frac{\partial A_{r^*}^{\ell m}}{\partial t} - \frac{\partial A_t^{\ell m}}{\partial r^*} \right) - \ell(\ell+1)\frac{r-2M}{r^3} A_t^{\ell m} \tag{4.52a}$$
$$= -4\pi(r-2M)j_t^{\ell m}$$

$$-\frac{\partial^2 A_{r^*}^{\ell m}}{\partial t^2} + \frac{\partial^2 A_{r^*}^{\ell m}}{\partial r^{*2}} + \frac{2M}{r^2} \left(\frac{\partial A_t^{\ell m}}{\partial t} - \frac{\partial A_{r^*}^{\ell m}}{\partial r^*} \right)$$
$$- \left(\ell(\ell+1)\frac{r-2M}{r^3} + 2\frac{(r-2M)^2}{r^4} \right) A_{r^*}^{\ell m} \tag{4.52b}$$
$$+ \ell(\ell+1)\frac{(r-2M)^2}{r^4} v_{\ell m} = -4\pi(r-2M)j_{r^*}^{\ell m} - \frac{\partial^2 v_{\ell m}}{\partial t^2} + \frac{\partial^2 v_{\ell m}}{\partial r^{*2}}$$
$$- \ell(\ell+1)\frac{r-2M}{r^3} v_{\ell m} + 2\frac{(r-2M)}{r^3} A_{r^*}^{\ell m} = -4\pi\frac{r-2M}{r} j_v^{\ell m}$$

$$-\frac{\partial^2 \tilde{v}_{\ell m}}{\partial t^2} + \frac{\partial^2 \tilde{v}_{\ell m}}{\partial r^{*2}} - \ell(\ell+1)\frac{r-2M}{r^3} \tilde{v}_{ellm} = -4\pi\frac{r-2M}{r} j_{\tilde{v}}^{\ell m}, \tag{4.52c}$$

where $j_\alpha^{\ell m}$ is defined as in Eq. (4.32) in the main text.

We discretize the set of reduced equations Eqs.(4.36) – (4.37a) using Lousto's second order method as described in section 4.3. Since the source terms on the right hand side are less singular for the vector potential than they are for the Faraday tensor, we do not have to distinguish between sourced and vacuum cell in the integral over the potential terms.

Terms containing first derivatives $\frac{\partial \psi}{\partial t}$, $\frac{\partial \psi}{\partial r^*}$, where now and in the remainder of the section ψ stands for any one of $A_t^{\ell m}$, $A_{r^*}^{\ell m}$, $v^{\ell m}$ or $\tilde{v}^{\ell m}$, were not treated in [4], but, for generic vacuum cells, can be handled in a straightforward manner

$$\iint_{\text{cell}} \mathrm{d}u \; \mathrm{d}v \, V(r) \frac{\partial \psi}{\partial t} = 2h(\psi_3 - \psi_2)V_0 + O(h^4) \tag{4.53a}$$

$$\iint_{\text{cell}} \mathrm{d}u \; \mathrm{d}v \, V(r) \frac{\partial \psi}{\partial r^*} = 2h(\psi_4 - \psi_1)V_0 + O(h^4) \,. \tag{4.53b}$$

This fails for cells traversed by the particle, since the field is only continuous across the world line but not differentiable. For these cells we take recourse to Lousto's original scheme, which has to deal with a similar issue, and use

$$\iint_{\text{cell}} \mathrm{d}u \; \mathrm{d}v \, V(r) \frac{\partial \psi}{\partial t} = \left(A_1 \partial_t \psi_1 + A_2 \partial_t \psi_2 + A_3 \partial_t \psi_3 + A_4 \partial_t \psi_4 \right) V_0 + O(h^3) \,, \tag{4.54a}$$

$$\iint_{\text{cell}} \mathrm{d}u \; \mathrm{d}v \, V(r) \frac{\partial \psi}{\partial r^*} = \left(A_1 \partial_{r^*} \psi_1 + A_2 \partial_{r^*} \psi_2 + A_3 \partial_{r^*} \psi_3 + A_4 \partial_{r^*} \psi_4 \right) V_0 + O(h^3) \,, \tag{4.54b}$$

where $A_1, \ldots, A_4$ are the subareas indicated in Fig. 4.1 and $\partial_t \psi_1$, $\ldots$, $\partial_t \psi_4$, $\partial_{r^*} \psi_1$, $\ldots$, $\partial_{r^*} \psi_4$ are zeroth order accurate approximations to the derivatives in the subareas. We calculate these using grid points outside of the cell on the same side of the world line as the corresponding subarea, for example

$$\partial_{r^*} \psi_1 = \frac{\psi(t, r^* - h) - \psi(t, r^* - 3h)}{2h} + O(h) \,. \tag{4.55}$$

4.4.1 Gauge condition

In contrast to the scalar field, the electromagnetic vector potential has to satisfy a gauge condition

$$Z \equiv g^{\alpha\beta} A_{\alpha;\beta} = 0 \,. \tag{4.56}$$

Analytically the gauge condition is preserved by the evolution equations, so that it is sufficient to impose it in the initial data. Numerically, however, small violations of the gauge condition due to numerical errors can be amplified exponentially and come to dominate the solution. To handle this situation we introduce a gauge damping scheme as described in [19]. That is we add a term of the form

$$\frac{4M}{r^2} Z = \frac{4M}{r^2} \left(-\frac{1}{r - 2M} \frac{\partial A_t}{\partial t} + \frac{1}{r - 2M} \frac{\partial A_{r^*}}{\partial r^*} + \frac{1}{r^2} A_{r^*} - \frac{\ell(\ell+1)}{r^2} v \right) \tag{4.57}$$

to the t components of the evolution equations Eqs. (2.53), which dampens out violations of the gauge condition. This choice proved to be numerically stable for the radiative ($\ell > 0$) modes but unstable for the monopole ($\ell = 0$) mode.

4.4.2 Monopole mode

The monopole mode of the electromagnetic field is non-radiative. This makes its behaviour sufficiently different from that of the radiative ($\ell > 0$) modes that the approach outlined earlier fails. In this case Eq. (2.53) reduces to a set of coupled equations for $A_a^{0,0}$ only. Rather than solving the system of equations directly for $A_t^{0,0}$ and $A_{r*}^{0,0}$ we use the analytical result for the F_{tr} component of the Faraday tensor derived in section 4.3.6. This proves to be sufficient to reconstruct the combination $A_{r,t}^{0,0} - A_{t,r}^{0,0}$ appearing in Eq. (2.133).

4.4.3 Initial values and boundary conditions

We handle the problem of initial data and boundary conditions the same way as in the scalar case described in section 4.2.4. We arbitrarily choose the fields to vanish on the characteristic slices $u = u_0$ and $v = v_0$

$$A_\alpha(u = u_0) = A_\alpha(v = v_0) = 0\,, \tag{4.58}$$

thereby adding a certain amount of spurious waves to the solution which show up as an initial burst. Gauge violations in this initial data are damped out along with those arising during the evolution.

We implement ingoing wave boundary conditions near the event horizon and choose a numerical domain that covers the full domain of dependence of the the initial data near the outer boundary.

4.4.4 Extraction of the field data at the particle

In order to extract the value of the field and its first derivatives at the position of the particle, we use a variant of the extraction scheme described in section 4.2.6. We introduce a piecewise polynomial

$$p(x) = \begin{cases} c_0 + c_1 x + \frac{c_3}{2}x^2 & \text{if } x < 0 \\ c_0' + c_1' x + \frac{c_3'}{2}x^2 & \text{if } x > 0 \end{cases} \tag{4.59}$$

in $x \equiv r^* - r_0^*$ on the current slice. Its coefficients to the left and right of the world line are linked by jump conditions $c_n = c_n' + [\partial_{r*}^n \psi]$ listed in Appendix D.2.2. Fitting this polynomial to the three grid points closest to the particle, we extract approximations for $\psi(t_0, r_0^*)$ and $\frac{\partial\psi(t_0,r_0^*)}{\partial r^*}$ which are just the coefficients c_0, c_1 respectively. Once we have obtained these, we proceed as in section 4.3.3 following [41] to obtain values for $\frac{\partial\psi(t_0,r_0^*)}{\partial t}$.

4.4.5 Convergence tests

We performed regression runs for our second-order convergent code using a non-zero charge q and an eccentric orbit. We extract the field at the position of the particle, thus also testing the implementation of the extraction algorithm described

in section 4.4.4. We choose the $\ell = 6$, $m = 4$ mode of the field generated by a particle on a mildly eccentric geodesic orbit with $p = 7$, $e = 0.3$. As shown in Fig. 4.13 the convergence is roughly of second order. In the region $200\,M \lesssim t \lesssim 350\,M$ the
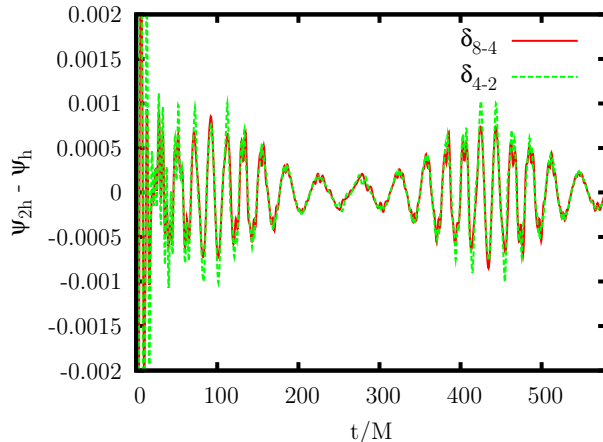

Figure 4.13: Convergence test of the numerical algorithm in the sourced case. We show differences between simulations using different step sizes of 4, 8 and 16 cells per M. Displayed are the rescaled differences $\delta_{8-4} = A_{r*}^{\ell m}(h = 1/8M) - A_{r*}^{\ell m}(h = 1/4M)$ etc. of the field values at the position of the particle for a simulation with $\ell = 6$, $m = 4$ and $p = 7$, $e = 0.3$. We see that the convergence is approximately second-order.

two curves lie on top of each other, as expected for a second-order convergent finite-difference scheme. In the region from $400\,M$ to $450\,M$ there is some difference between the two lines, caused by cell crossing effects similar to those discussed in section 4.2.7.

4.4.6 Gauge violations

Unlike the scalar field, the vector potential has to satisfy a gauge condition. The gauge condition Eq. (4.56) is not dynamical; it is not part of the evolution system. Instead the wave equation Eq. (2.53) propagates the Lorenz condition forward in time. Therefore if the initial conditions $A_\mu(t = 0)$, $A_{\mu,t}(t = 0)$ satisfy the Lorenz condition, so will the vector potential A_μ at any later time. However, the evolution of Z might be unstable, meaning that small deviations from the exact solution, which will occur in any numerical scheme, are amplified and grow exponentially. This is the reason for using the gauge damping scheme introduced in section 4.4.1, which modifies the evolution equations such that violations of the gauge condition are dynamically damped, ie. Z is driven towards zero. Plotting the gauge condition versus time as in Fig. 4.14, we find that any gauge violations are damped away quickly and the simulations settles to a steady state.

4.4.7 Comparison to direct calculation of the Faraday tensor

Using the vector potential code described above we can reproduce the results obtained from the Faraday tensor method. The differences are small, with the Faraday tensor
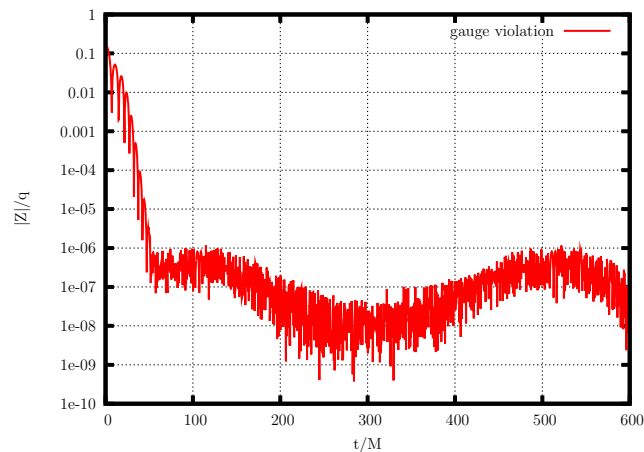
Figure 4.14: Gauge violation $Z = A^\alpha{}_{;\alpha} = 0$ for the $\ell = 3$, $m = 1$ mode of the vector potential sourced by a particle on an eccentric orbit $p = 7.2$, $e = 0.5$ at the location of the particle. The gauge violations are quickly damped away even at he position of the source, where the discretization errors are worst.

code generally yielding more accurate results since the costly numerical differentiation that is necessary in the vector potential calculation is not required.
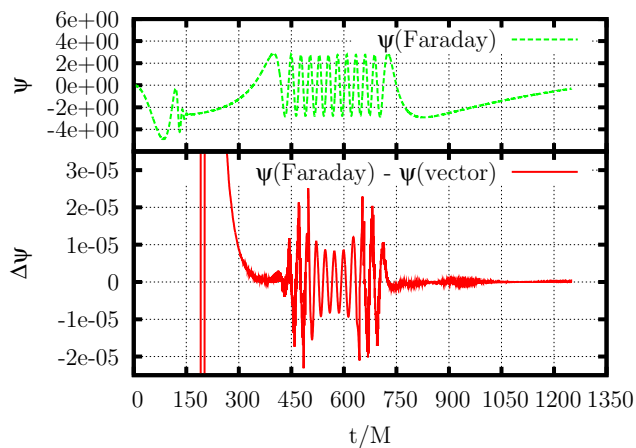
Figure 4.15: Differences between $F_{tr}^{\ell m}$ calculated using the vector potential and calculated using the Faraday tensor method for $\ell = 2$, $m = 2$ mode of field for the zoom-whirl orbit shown in 5.5. Displayed are the difference and the actual field. The stepsizes were $h = 1.041\bar{6} \times 10^{-2} M$ and $h = 1/512M$ for the vector potential calculation and the Faraday tensor calculation respectively.

"Piled Higher and Deeper" by Jorge Cham, `www.phdcomics.com`

Chapter 5

Self force

In this chapter we display results for the self-force calculation of the scalar and electromagnetic field.

5.1 Scalar field

For the scalar field we display results for the numerically calculated multipole coefficients as well as the self-force obtained from these.

5.1.1 High-ℓ behaviour of the multipole coefficients

Inspection of Eq. (3.26) reveals that a plot of $\Phi_{(\mu)\ell}$ as a function of ℓ (for a given value of t) should display a linear growth in ℓ for large ℓ. Removing the $A_{(\mu)}$ term should produce a constant curve, removing the $B_{(\mu)}$ term (given that $C_{(\mu)} = 0$) should produce a curve that decays as ℓ^{-2}, and finally, removing the $D_{(\mu)}$ term should produce a curve that decays as ℓ^{-4}. It is a powerful test of the numerical method to check whether these expectations are borne out by the numerical data. Fig. 5.1 plots the remainders as obtained from our numerical simulation, demonstrating the expected behaviour. It displays, on a logarithmic scale, the absolute value of $\operatorname{Re}\Phi^{\mathrm{R}}_{(+)\ell}$, the real part of the $(+)$ component of the self-force. The orbit is eccentric ($p = 7.2$, $e = 0.5$), and all components of the self-force require regularization. The first curve (in triangles) shows the unregularized multipole coefficients that increase linearly in ℓ, as confirmed by fitting a straight line to the data. The second curve (in squares)
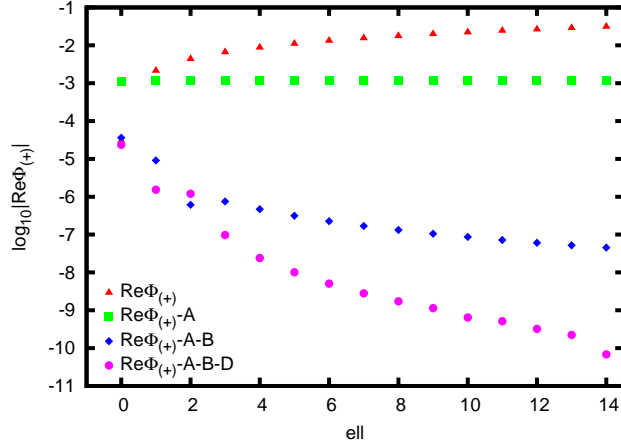
Figure 5.1: Multipole coefficients of the dimensionless self-force $\frac{M^2}{q} \operatorname{Re} \Phi^{\mathrm{R}}_{(+)}$ for a particle on an eccentric orbit ($p = 7.2$, $e = 0.5$). The coefficients are extracted at $t = 500\,M$ along the trajectory shown in Fig. 5.3. The plots show several stages of the regularization procedure, with a closer description of the curves to be found in the text.

shows partially regularized coefficients, obtained after the removal of $(\ell + 1/2)A_{(\mu)}$; this clearly approaches a constant value for large ℓ. The curve made up of diamonds shows the behaviour after removal of $B_{(\mu)}$; because $C_{(\mu)} = 0$, it decays as ℓ^{-2}, a behaviour that is confirmed by a fit to the $\ell \geq 5$ part of the curve. Finally, after removal of $D_{(\mu)}/[(\ell - \frac{1}{2})(\ell + \frac{3}{2})]$ the terms of the sum decrease in magnitude as ℓ^{-4} for large values of ℓ, as derived in [18]. Each one of the last two curves would result in a converging sum, but the convergence is much faster after subtracting the $D_{(\mu)}$ terms. We thereby gain more than 2 orders of magnitude in the accuracy of the estimated sum.

Figure 5.1 provides a sensitive test of the implementation of both the numerical and analytical parts of the calculation. Small mistakes in either one will cause the difference in Eq. (3.26) to have a vastly different behaviour.

5.1.2   Self-force on a circular orbit

For the case of a circular orbit, the regularization parameters $A_{(0)}$, $B_{(0)}$, and $D_{(0)}$ all vanish identically, so that the (0) (or alternatively the t) component of the self-force does not require regularization. Figure 5.2 thus shows only one curve, with the magnitude of the multipole coefficients decaying exponentially with increasing ℓ.

As a final test, in Table 5.1 we compare our result for the self-force on a particle in a circular orbit at $r = 6M$ to those obtained in [23, 32] using a frequency-domain code. For a circular orbit, a calculation in the frequency domain is more efficient, and we expect the results of [23, 32] to be much more accurate than our own results. This fact is reflected in the number of multipole coefficients we can reliably extract from the numerical data before being limited by the accuracy of the numerical method: the frequency-domain calculation found usable multipole coefficients up to $\ell = 20$,
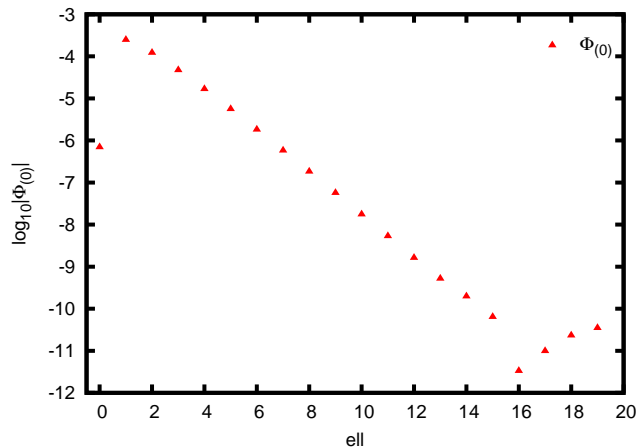
Figure 5.2: Multipole coefficients of $\Phi^{\mathrm{R}}_{(0)}$ for a particle on a circular orbit. Note that $\Phi^{\mathrm{R}}_{(0)\ell}$ is linked to Φ^{R}_t via $\Phi^{\mathrm{R}}_t = \sqrt{f_0}\Phi^{\mathrm{R}}_{(0)}$. The multipole coefficients decay exponentially with ℓ until $\ell \approx 16$, at which point numerical errors start to dominate.

	This work: time-domain	Previous work: frequency-domain [23]	Diaz-Rivera et. al. [32]
$\frac{M^2}{q}\Phi^{\mathrm{R}}_t$	3.60339×10^{-4}	$3.60907254 \times 10^{-4}$	
$\frac{M^2}{q}\Phi^{\mathrm{R}}_r$	1.6767×10^{-4}	1.67730×10^{-4}	1.6772834×10^{-4}
$\frac{M}{q}\Phi^{\mathrm{R}}_\phi$	-5.30424×10^{-3}	$-5.30423170 \times 10^{-3}$	

Table 5.1: Results for the self-force on a scalar particle with scalar charge q on a circular orbit at $r_0 = 6M$. The first column lists the results as calculated in this work using time-domain numerical methods, while the second and third columns list the results as calculated in [23, 32] using frequency-domain methods. For the t and ϕ components the number of digits is limited by numerical round off error. For the r component the number of digits is limited by the truncation error of the sum of multipole coefficients.

whereas our data for $\Phi^{\mathrm{R}}{}_{(0)\ell}$ is dominated by noise by the time ℓ reaches 16. Figure 5.2 shows this behaviour.

5.1.3 Accuracy of the numerical method

Several figures of merit can be used to estimate the accuracy of numerical values for the self-force.

An estimate for the truncation error arising from truncating the summation in Eq. (3.26) at some ℓ_{max} can be calculated by considering the behaviour of the remaining terms for large ℓ. Detweiler, Messaritaki, and Whiting [18] showed that the remaining terms scale as ℓ^{-4} for large ℓ. They find the functional form of the terms to be

$$\frac{E\mathcal{P}_{3/2}}{(2\ell - 3)(2\ell - 1)(2\ell + 3)(2\ell + 5)}, \tag{5.1}$$

where $\mathcal{P}_{3/2} = 36\sqrt{2}$. We fit a function of this form to the tail end of a plot of the multipole coefficients to find the coefficient E in Eq. (5.1). Extrapolating to $\ell \to \infty$ we find that the truncation error is

$$\epsilon = \sum_{\ell=\ell_{\mathrm{max}}}^{\infty} [\text{Eq. (5.1)}] = \frac{12\sqrt{2}E\ell_{\mathrm{max}}}{(2\ell_{\mathrm{max}} + 3)(2\ell_{\mathrm{max}} + 1)(2\ell_{\mathrm{max}} - 1)(2\ell_{\mathrm{max}} - 3)} \tag{5.2}$$

where ℓ_{max} is the value at which we truncate the summation. For all but the special case of the (0) component for a circular orbit, for which all regularization parameters vanish identically, we use this approach to calculate an estimate for the truncation error.

A second source of error lies in the numerical calculation of the retarded solution to the wave equation. This error depends on the step size h used to evolve the field forward in time. For a numerical scheme of a given convergence order, we can estimate this discretization error by extrapolating the differences of simulations using different step sizes down to $h = 0$. This is what was done in the graphs shown in Sec. 4.2.7.

We display results for mildly eccentric orbits. High eccentricity causes $\partial_r \Phi$ (displayed in Fig. 4.7) to be plagued by high frequency noise produced by effects similar to those described in Sec. 4.2.7. This makes it impossible to reliably estimate the discretization error for these orbits. We do not expect this to be very different for highly eccentric orbits.

Finally we compare our final results for the self-force F_α to "reference values". For circular orbits, frequency-domain calculations are much more accurate than our time-domain computations. We thus compare our results to the results obtained in [23]. Table 5.2 lists typical values for the various errors listed above.

5.1.4 Mildly eccentric orbit

We choose a particle on an eccentric orbit with $p = 7.2$, $e = 0.5$ which starts at $r = pM/(1 - e^2)$, halfway between periastron and apastron. The field is evolved for $1000\,M$, corresponding to about 6 angular and two radial periods with a resolution

error estimation	mildly eccentric orbit
truncation error ($\frac{M^2}{q}\Phi_{(+)}$)	$\approx 2 \times 10^{-3}\%$
discretization error ($\frac{M^2}{q}\partial_r\Phi_{\ell m}$)	$\approx 10^{-5}\%$
comparison with reference values	circular orbit
$\frac{M^2}{q^2}F_t$	0.2%
$\frac{M^2}{q^2}F_r$	0.04%
$\frac{M}{q^2}F_\phi$	$2 \times 10^{-4}\%$

Table 5.2: Estimated values for the various errors in the components of the self-force as described in the text. We show the truncation and discretization errors for a mildly eccentric orbit and the total error for a circular orbit. The truncation error is calculated using a plot similar to the one shown in Fig. 5.7. The discretization error is estimated using a plot similar to that in Fig. 4.7 for the $\ell = 2$, $m = 2$ mode, and the total error is estimated as the difference between our values and those of [23]. We use $p = 7.2$, $e = 0.5$ for the mildly eccentric orbit and $p = 6$ for the circular orbit. Note that we use the tetrad component $\Phi_{(+)}$ for the truncation error and the vector component $\partial_r\Phi$ for the discretization error. Both are related by the translation table Eqs. (2.129), we expect corresponding errors to be comparable for $\Phi_{(+)}$ and $\partial_r\Phi$.

of 16 grid points per M, both in the t and r^* directions, for $\ell = 0$. Higher values of ℓ (and thus m) require a corresponding increase in the number of grid points to achieve the same fractional accuracy. Multipole coefficients for $0 \leq \ell \leq 15$ are calculated and used to reconstruct the regularized self-force F_α along the geodesic. Figure 5.4 shows the result of the calculation. For the choice of parameters used to calculate the force
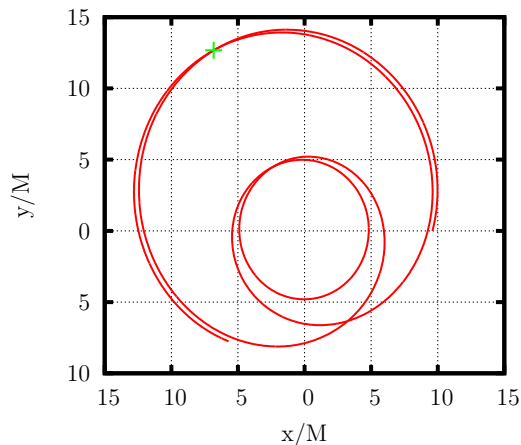

Figure 5.3: Trajectory of a particle with $p = 7.2$, $e = 0.5$. The cross-hair indicates the point where the data for Fig. 5.1 was extracted.

shown in Fig. 5.4, the error bars corresponding to the truncation error (which are already much larger than than the discretization error) would be of the order of the line thickness and have not been drawn.
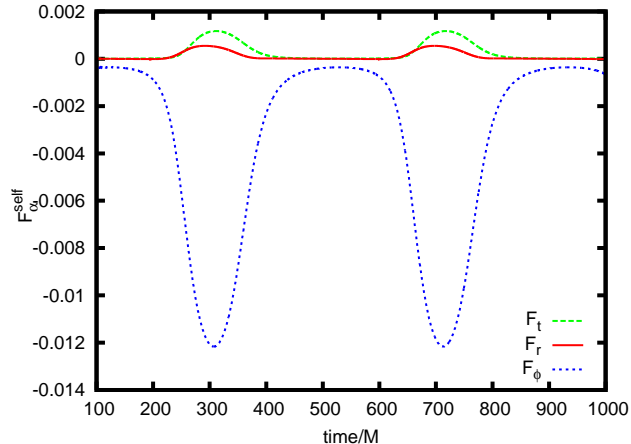
Figure 5.4: Regularized dimensionless self-force $\frac{M^2}{q^2}F_t$, $\frac{M^2}{q^2}F_r$ and $\frac{M}{q^2}F_\phi$ on a particle on an eccentric orbit with $p = 7.2$, $e = 0.5$.

Already for this small eccentricity, we see that the self-force is most important when the particle is closest to the black hole (ie. for $200\,M \lesssim t \lesssim 400\,M$ and $600\,M \lesssim t \lesssim 800\,M$); the self-force acting on the particle is very small once the particle has moved away to $r \approx 15\,M$.

Following for example the treatment of Wald [34], Appendix C, it is easy to see that the rates of change $\dot{E}$ and $\dot{J}$ (per unit proper time) are directly related to components of the acceleration a_α (and therefore force) experienced by the particle via

$$\dot{E} = -a_t\,, \quad \dot{J} = a_\phi\,. \tag{5.3}$$

The self-force shown in Fig. 5.4 therefore confirms our naïve expectation that the self-force should decrease both the energy and angular momentum of the particle as radiation is emitted. Interestingly, the r component of the force is always positive, pointing away from the black hole. The decay of the orbit is driven by losses of energy and angular momentum, not by the self-force pushing the particle towards to black hole.

5.1.5 Zoom-whirl orbit

Highly eccentric orbits are of most interest as sources of gravitational radiation. For nearly parabolic orbits with $e \lesssim 1$ and $p \gtrsim 6 + 2e$, a particle revolves around the black hole a number of times, moving on a nearly circular trajectory close to the event horizon ("whirl phase") before moving away from the black hole ("zoom phase"). During the whirl phase the particle is in the strong field region of the black hole, emitting a copious amount of radiation. Figures 5.5 and 5.6 show the trajectory of a particle and the force on such an orbit with $p = 7.8001$, $e = 0.9$ for an simulation which spans about one radial period and about 11 angular periods. Even more so than for the mildly eccentric orbit discussed in Sec. 5.1.4, the self-force (and thus the amount of radiation produced) is much larger while the particle is close to the black
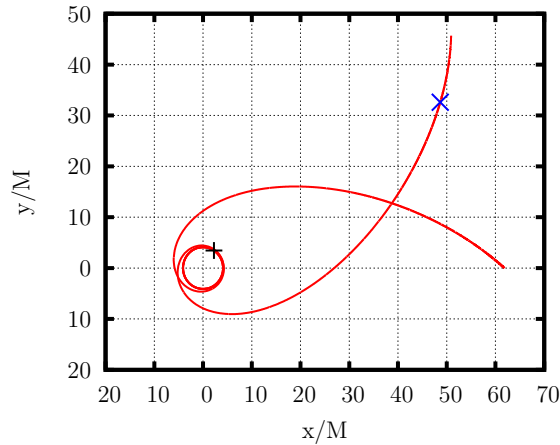
Figure 5.5: Trajectory of a particle on a zoom-whirl orbit with $p = 7.8001$, $e = 0.9$. The cross-hairs indicate the positions where the data shown in Fig. 5.7 and 5.8 was extracted.
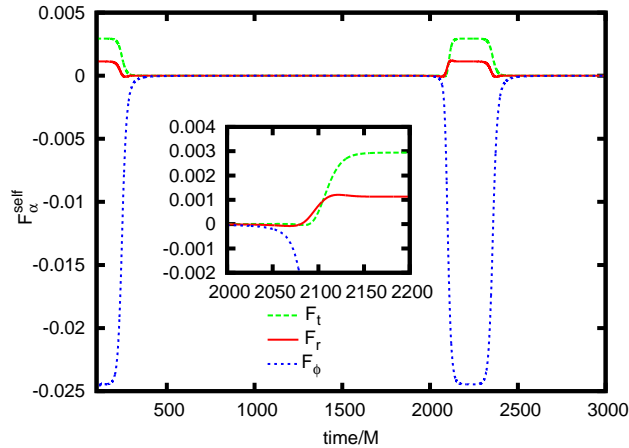

Figure 5.6: Self-force acting on a particle. Shown is the dimensionless self-force $\frac{M^2}{q^2}F_t$, $\frac{M^2}{q^2}F_r$ and $\frac{M}{q^2}F_\phi$ on a zoom-whirl orbit with $p = 7.8001$, $e = 0.9$. The inset shows a magnified view of the self-force when the particle is about to enter the whirl phase. No error bars showing an estimate error are shown, as the errors shown for example in Table 5.2 are to small to show up on the graph. Notice that the self-force is essentially zero during the zoom phase $500\,M \lesssim t \lesssim 2000\,M$ and reaches a constant value very quickly after the particle enters into the whirl phase.

hole than when it zooms out.

It is instructive to have a closer look at the force acting on the particle when it is within the zoom phase, and also when it is moving around the black hole on the nearly circular orbit of the whirl phase. In Fig. 5.7 and Fig. 5.8 we show plots of $\Phi_{(0)\ell}$ vs. ℓ after the removal of the $A_{(\mu)}$, $B_{(\mu)}$, and $D_{(\mu)}$ terms. While the particle is still zooming in toward the black hole, $\Phi_{(0)\ell}$ behaves exactly as for the mildly eccentric orbit described in Sec. 5.1.4 over the full range of ℓ plotted; ie. the magnitude of each term scales as ℓ^0, ℓ^{-2} and ℓ^{-4}, after removal of the $A_{(\mu)}$, $B_{(\mu)}$, and $D_{(\mu)}$ terms respectively. Close to the black hole, on the other hand, the particle moves along
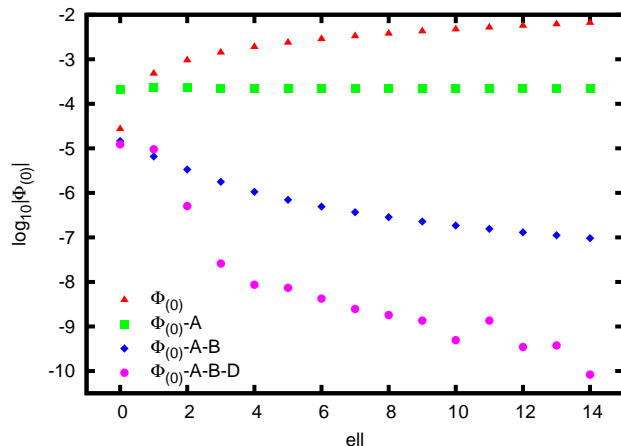

Figure 5.7: Multipole coefficients of $\frac{M^2}{q} \operatorname{Re} \Phi_{(0)}^{\mathrm{R}}$ for a particle on a zoom-whirl orbit ($p = 7.8001$, $e = 0.9$). The coefficients are extracted at $t = 2000\,M$ as the particle is about to enter the whirl phase. As $\dot{r}$ is non-zero, all components of the self-force require regularization and we see that the dependence of the multipole coefficients on ℓ is as predicted by Eq. 3.26. After the removal of the regularization parameters $A_{(\mu)}$, $B_{(\mu)}$, and $D_{(\mu)}$ the remainder is proportional to ℓ^0, ℓ^{-2} and ℓ^{-4} respectively.

a nearly circular trajectory. If the orbit were perfectly circular for all times, ie. $\dot{r} \equiv 0$, then the (0) component would not require regularization at all, and the multipole coefficients would decay exponentially, resulting in a straight line on the semi-logarithmic plot shown in Fig. 5.8. As the real orbit is not precisely circular, curves eventually deviate from a straight line. Removal of the $A_{(\mu)}$ term is required almost immediately (beginning with $\ell \approx 3$), while the $D_{(\mu)}$ term starts to become important only after $\ell \approx 11$. This shows that there is a smooth transition from the self-force on a circular orbit, which does not require regularization of the t and ϕ components, to that of a generic orbit, for which all components of the self-force require regularization.

5.2 Electromagnetic field—Faraday tensor

For the electromagnetic field we display results for the numerically calculated multipole coefficients as well as the self-force calculated from these.
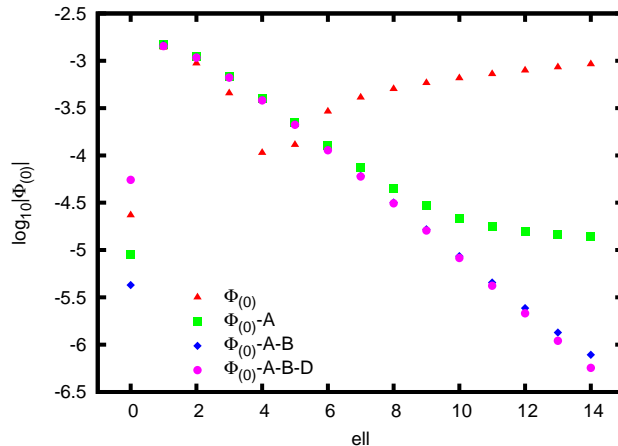
Figure 5.8: Multipole coefficients of $\mathrm{Re}\,\Phi_{(0)}^{\mathrm{R}}$ for a particle on a zoom-whirl orbit ($p = 7.8001$, $e = 0.9$). The coefficients are extracted at $t = 2150\,M$ while the particle is in the whirl phase. The orbit is nearly circular at this time, causing the dependence on ℓ after removal of the regularization parameters to approximate that of a true circular orbit.

5.2.1 High-ℓ behaviour of the multipole coefficients

Inspection of Eq. (3.36) reveals that a plot of $F_{(\mu)(\nu)}^{\ell}$ as a function of ℓ (for a given value of t) should display a linear growth in ℓ for large ℓ. Removing the $A_{(\mu)(\nu)}$ term should produce a constant curve, removing the $B_{(\mu)(\nu)}$ term (given that $C_{(\mu)(\nu)} = 0$) should produce a curve that decays as ℓ^{-2}, and finally, removing the $D_{(\mu)(\nu)}$ term should produce a curve that decays as ℓ^{-4}. It is a powerful test of the overall implementation to check whether the numerical data behaves as expected. Fig. 5.9 plots the remainders as obtained from our numerical simulation, demonstrating the expected behaviour. It displays, on a logarithmic scale, the absolute value of $\mathrm{Im}\,F_{(+)(-)\ell}^{\mathrm{R}}$, the imaginary part of the $(+)(-)$ component of the Faraday tensor. The orbit is eccentric ($p = 7.2$, $e = 0.5$), and all components of the self-force require regularization. The first curve (in triangles) shows the unregularized multipole coefficients that increase linearly in ℓ, as confirmed by fitting a straight line to the data. The second curve (in squares) shows partially regularized coefficients, obtained after the removal of $(\ell + 1/2)A_{(\mu)(\nu)}$; this clearly approaches a constant for large values of ℓ. The curve made up of diamonds shows the behaviour after removal of $B_{(\mu)(\nu)}$; because $C_{(\mu)(\nu)} = 0$, it decays as ℓ^{-2}, a behaviour that is confirmed by a fit to the $\ell \geq 5$ part of the curve. Finally, after removal of $D_{(\mu)(\nu)}/[(\ell - \frac{1}{2})(\ell + \frac{3}{2})]$ the terms of the sum decrease in magnitude approximately as $\ell^{-4.5}$. This differs from the expected behaviour of ℓ^{-4} as derived in [18]; we expect this to be due to the fact that we truncated the series at $\ell = 15$, which seems to be not large enough to show the asymptotic behaviour. Extending the range to very high values of ℓ proved to be very difficult, since the finite-difference scheme is only second order convergent, so that the numerical errors become dominant by the time the asymptotic behaviour begins to emerge.

Each one of the last two curves would result in a converging sum, but the conver-
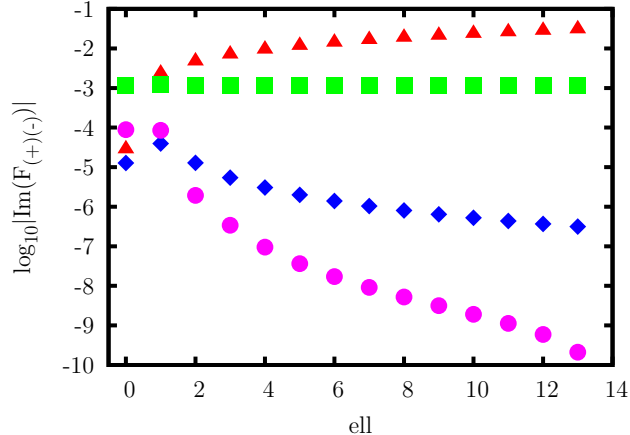
Figure 5.9: Multipole coefficients of the dimensionless Faraday tensor component $\frac{M^2}{q} \operatorname{Im} F^{\mathrm{R}}_{(+)(-)}$ for a particle on an eccentric orbit ($p = 7.2$, $e = 0.5$). The coefficients are extracted at $t = 500\,M$ along the trajectory shown in Fig. 5.3. The plots show several stages of the regularization procedure, with a closer description of the curves to be found in the text.

gence is faster after subtracting the $D_{(\mu)(\nu)}$ terms. We thereby gain about one order of magnitude in the accuracy of the estimated sum.

Figure 5.9 provides a sensitive test of the implementation of both the numerical and analytical parts of the calculation. Small mistakes in either one will cause the difference in Eq. (3.36) to have a vastly different behaviour.

5.2.2 Accuracy of the numerical method

In this work we are less demanding with the numerical accuracy then we were section 4.2, where we describe a very high accuracy numerical code. Implementing this code is very tedious even for the scalar case, and much more so for the electromagnetic case treated here. Therefore we implemented a simpler method that allows us to access the physics of the problem without being bogged down in technical problems due to a complicated numerical method.

An estimate for the truncation error arising from cutting short the summation in Eq. (3.36) at some ℓ_{max} can be calculated by considering the behaviour of the remaining terms for large ℓ as done in Eqs. (5.1) and (5.2).

A second source of error lies in the numerical calculation of the retarded solution to the wave equation. This error depends on the step size h used to evolve the field forward in time. For a numerical scheme of a given convergence order, we can estimate this discretization error by extrapolating from simulations using different step sizes down to $h = 0$. This is what was done in the graphs shown in Sec. 4.3.4.

We display results for the mildly eccentric orbit show in Fig. 5.3 with data extracted at $t = 500\,M$ ie. at the instant shown in Fig. 5.9. At this moment, the multipole coefficients of $F^{\mathrm{R}}_{(+)}$ decay as expected, but for example the $F^{\mathrm{R}}_{(0)}$ component decays faster. We choose an orbit of low eccentricity as high eccentricity causes the

spatial derivatives to be plagued by high frequency noise, as discussed in section 4.2.7. This makes it impossible to reliably estimate the discretization error for these orbits.

Table 5.3 lists typical values for the errors listed above.

error estimation	mildly eccentric orbit
truncation error $[\frac{M^2}{q^2}\mathrm{Re}(F^{\mathrm{R}}_{(+)})]$	$\approx 5 \times 10^{-2}\%$
discretization error $[\frac{M^2}{q}\partial_r A_t]$	$\approx 10^{-1}\%$

Table 5.3: Estimated values for the various errors in the components of the self-force as described in the text. We show the truncation and discretization errors for the mildly eccentric orbit ($p = 7.2$, $e = 0.5$). The truncation error is calculated using a plot similar to the one shown in Fig. 5.9. The discretization error is estimated using a plot similar to that in Fig. 4.10 for the $\ell = 2$, $m = 2$ mode.

5.2.3 Mildly eccentric orbit

We choose a particle on an eccentric orbit with $p = 7.2$, $e = 0.5$ which starts at $r = pM/(1 - e^2)$, halfway between periastron and apastron. The field is evolved for $600\,M$, corresponding to about 5 angular and two radial periods, with a resolution of 32 grid points per M, both in the t and r^* directions, for $\ell = 0$. Higher values of ℓ (and thus m) require a corresponding increase in the number of grid points used to achieve the same fractional accuracy. Multipole coefficients for $0 \le \ell \le 15$ are calculated and used to reconstruct the regularized self-force F_α along the geodesic. Figure 5.10 shows the result of the calculation. For the choice of parameters used to
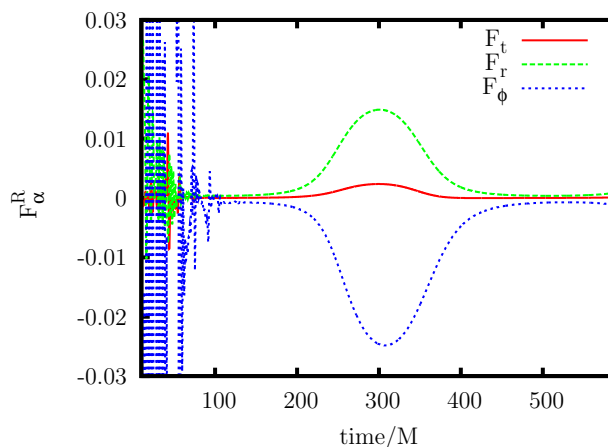

Figure 5.10: Regularized dimensionless self-force $\frac{M^2}{q^2}F_t$, $\frac{M^2}{q^2}F_r$ and $\frac{M}{q^2}F_\phi$ on a particle on an eccentric orbit with $p = 7.2$, $e = 0.5$.

calculate the force shown in Fig. 5.10, the error bars corresponding to the truncation error (which are already much larger than than the discretization error) would be of the order of the line thickness and have not been drawn.

Already for this small eccentricity, we see that the self-force is most important when the particle is closest to the black hole (ie. for $200\,M \lesssim t \lesssim 400\,M$); the self-force acting on the particle is very small once the particle has moved away to $r \approx 15\,M$.

Out observation from the scalar self-force still apply, namely that the self-force is decreasing energy and angular momentum, but also somewhat counter-intuitively is pointing away from the black hole.

5.2.4 Zoom-whirl orbit

Highly eccentric orbits are of most interest as sources of gravitational radiation. For nearly parabolic orbits with $e \lesssim 1$ and $p \gtrsim 6 + 2e$, a particle revolves around the black hole a number of times, moving on a nearly circular trajectory close to the event horizon ("whirl phase"), before moving away from the black hole ("zoom phase"). During the whirl phase the particle is in the strong field region of the black hole, emitting a copious amount of radiation. Figures 5.5 and 5.11 show the trajectory of a particle and the force on such an orbit with $p = 7.8001$, $e = 0.9$. Even more
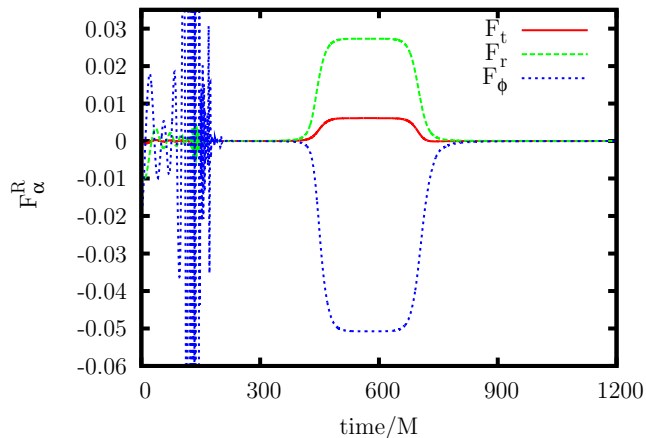

Figure 5.11: Self-force acting on a particle. Shown is the dimensionless self-force $\frac{M^2}{q^2}F_t$, $\frac{M^2}{q^2}F_r$ and $\frac{M}{q^2}F_\phi$ on a zoom-whirl orbit with $p = 7.8001$, $e = 0.9$. No error bars showing an estimate error are shown, as the errors shown are to small to show up on the graph. Notice that the self-force is essentially zero during the zoom phase $900\,M \lesssim t \lesssim 1200\,M$ and reaches a constant value very quickly after the particle enters into the whirl phase.

so than for the mildly eccentric orbit discussed in Sec. 5.2.3, the self-force (and thus the amount of radiation produced) is much larger while the particle is close to the black hole than when it zooms out. The force graph is very similar to that obtained for the scalar self-force in the scalar case in section 5.1.5, however the overshooting behaviour at the onset and near the end of the whirl phase is not as pronounced.

In Fig. 5.13 and Fig. 5.12 we show plots of $F^\ell_{(0)}$ constructed from $F^\ell_{(\mu)(\nu)}$ after the removal of the $A_{(\mu)(\nu)}$, $B_{(\mu)(\nu)}$, and $D_{(\mu)(\nu)}$ terms. We observe a behaviour very
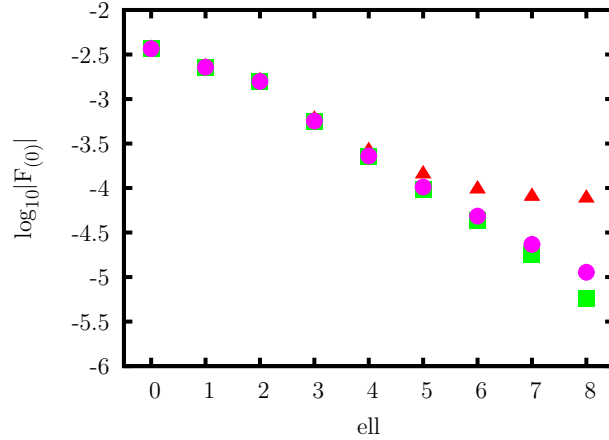
Figure 5.12: Multipole coefficients of $\frac{M^2}{q} \operatorname{Re} F_{(0)}^{\mathrm{R}}$ for a particle on a zoom-whirl orbit ($p = 7.8001$, $e = 0.9$). The coefficients are extracted at $t = 525\,M$ when the particle is deep within the whirl phase. Here $\dot{r} \approx 0$ and the behaviour of $F_{(\mu),\ell}^{\mathrm{R}}$ is very close to that for a circular orbit, requiring very little regularization. Red triangles are used for the unregularized multipole coefficients $F_{(0),\ell}$, squares, diamonds and disks are used for the partly regularized coefficients after the removal of the $A_{(0)}$, $B_{(0)}$ and $D_{(0)}$ terms respectively.
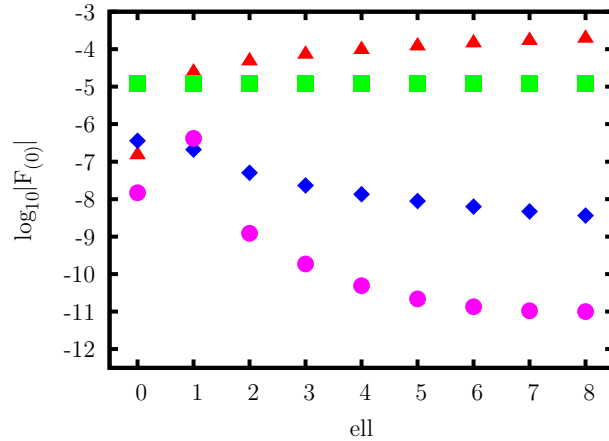
Figure 5.13: Multipole coefficients of $\frac{M^2}{q} \operatorname{Re} F_{(0)}^{\mathrm{R}}$ for a particle on a zoom-whirl orbit ($p = 7.8001$, $e = 0.9$). The coefficients are extracted at $t = 1100\,M$ when the particle is far away from the black hole. As $\dot{r}$ is non-zero, all components of the self-force require regularization and we see that the dependence of the multipole coefficients on ℓ is as predicted by Eq. 3.36. After the removal of the regularization parameters $A_{(\mu)(\nu)}$, $B_{(\mu)(\nu)}$, and $D_{(\mu)(\nu)}$ the remainder is proportional to ℓ^0, ℓ^{-2} and ℓ^{-4} respectively.

similar to that described in section 5.1.5 on the scalar self-force. While the particle is whirling around the black hole, the multipole coefficients behave very similar to those of a circular orbit. Only for high values of ℓ is the inclusion of the $D_{(0)}$ terms required . During the zoom phase on the other hand all components of the self-force require regularization right away.

5.2.5 Effects of the conservative self-force

Non-geodesic motion

To obtain expressions for E and J under the influence of the self-force, we follow the discussion in [32]. We retain the symbols E and J to denote the t and ϕ components of u_α even though these components are no longer constants of motion

$$u_\alpha = [-E(\tau), \dot{r}/f, 0, J(\tau)].\qquad(5.4)$$

Following for example the treatment of Wald [34], Appendix C, it is easy to see that the rates of change $\dot{E}$ and $\dot{J}$ (per unit proper time) are given by

$$\dot{E} = -\frac{F_t}{m}, \quad \dot{J} = \frac{F_\phi}{m},\qquad(5.5)$$

where F_α is the force experienced by the particle. The normalization condition for the four velocity reads

$$-1 = u^\alpha u_\alpha = -\frac{E^2}{f} + \frac{\dot{r}^2}{f} + \frac{J^2}{r^2},\qquad(5.6)$$

and the r-component of the geodesic equation is

$$\frac{F^r}{m} = \ddot{r} - \frac{M\dot{r}^2}{(r-2M)r} - \frac{(r-2M)J^2}{r^4} + \frac{ME^2}{(r-2M)r},\qquad(5.7)$$

where F^r is the radial component of the force, which we imagine to be the self-force $F^r_{\text{self}} = qF^r{}_\mu u^\mu$. Solving Eq. (5.6) and (5.7) for E^2 and J^2 we find

$$E^2 = \left[\dot{r}^2 + \frac{(r-2M)r\ddot{r}}{r-3M} + \frac{(r-2M)^2}{(r-3M)r}\right] - \frac{(r-2M)r}{r-3M}\frac{F^r}{m},\qquad(5.8a)$$

$$J^2 = \left[\frac{r^4\ddot{r}}{r-3M} + \frac{Mr^2}{r-3M}\right] - \frac{r^4}{r-3M}\frac{F^r}{m},\qquad(5.8b)$$

where the terms in square brackets are the geodesic expressions of energy and angular momentum. Eqs. (5.8a) and (5.8b) are reformulations of the normalization condition Eq. (5.6) and the radial equation of motion Eq. (5.7); no new physics is present. The new aspect lies in interpreting them to give energy and angular momentum of the orbit once its *true* radial motion and the radial force have been specified. This is unusual in that ordinarily, in the geodesic context, we would use the constants of motion E and J and the expression for the force to obtain equations governing the radial motion. Here we have turned the procedure around.

For small perturbing force of order ε we expand Eqs. (5.8a) and (5.8b) in terms of the perturbation strength around a given geodesic and find

$$E = E_0 + \Delta E \approx E_0 - \frac{(r - 2M)r}{2(r - 3M)E_0} \frac{F^r}{m} + O(\varepsilon^2), \tag{5.9a}$$

$$J = J_0 + \Delta J \approx J_0 - \frac{r^4}{2(r - 3M)J_0} \frac{F^r}{m} + O(\varepsilon^2). \tag{5.9b}$$

Here r is the true position of the particle r including the effect of the force, it differs from the geodesic unperturbed position r_0. Further,

$$E_0 = \sqrt{\dot{r}^2 + \frac{(r - 2M)r\ddot{r}}{(r - 3M)} + \frac{(r - 2M)^2}{(r - 3M)r}}, \tag{5.10a}$$

$$J_0 = \sqrt{\frac{r^2(r^2\ddot{r} + M)}{r - 3M}} \tag{5.10b}$$

are energy and angular momentum of the true trajectory. We stress that E_0 and J_0 are not the geodesic values for energy and angular momentum. They are of the correct form but are evaluated using the *accelerated* values for r, $\dot{r}$ and $\ddot{r}$ (instead of the geodesic values r_0, $\dot{r}_0$, etc.) and therefore contain terms of order ε. Quantities multiplying F^r can be evaluated on the unperturbed geodesic since F^r is already of order ε, so r could be replaced by r_0. In this work however, we fix the radial motion completely, either by forcing the particle to move on a circular orbit of given r or by specifying its radial motion by other means. Therefore we know the particle's true (since we enforce it) trajectory, but the corresponding unperturbed geodesic.

The fractional changes $\Delta E/E_0$ and $\Delta J/J_0$, withrespect to the "accelerated" energy and angular momentum, are given by

$$\Delta E/E_0 = -\frac{(r_0 - 2M)r_0}{2(r_0 - 3M)E_0^2} \frac{F^r}{m} + O(\varepsilon^2), \tag{5.11a}$$

$$\Delta J/J_0 = -\frac{r_0^4}{2(r_0 - 3M)J_0^2} \frac{F^r}{m} + O(\varepsilon^2). \tag{5.11b}$$

Once the perturbations in E and J are known, we calculate the change in the angular frequency

$$\Omega \equiv \frac{d\varphi_0}{dt} = \frac{r - 2M}{r^3} \frac{J}{E}. \tag{5.12}$$

For small perturbing force we expand in powers of the perturbation strength

$$\Omega = \frac{r_0 - 2M}{r_0^3} \frac{J_0}{E_0} \left[1 - \left(\frac{r_0^4}{2(r_0 - 3M)J_0^2} - \frac{(r_0 - 2M)r_0}{2(r_0 - 3M)E_0^2} \right) \frac{F^r}{m} \right] + O(\varepsilon^2). \tag{5.13}$$

The relative change $\Delta\Omega/\Omega_0$ is given by

$$\Delta\Omega/\Omega_0 = -\left(\frac{r_0^4}{2(r_0 - 3M)J_0^2} - \frac{(r_0 - 2M)r}{2(r_0 - 3M)E_0^2} \right) \frac{F^r}{m} + O(\varepsilon^2). \tag{5.14}$$

Conservative self-force

Before we give an expression for the conservative self-force, we have to introduce the concept of an advanced force. In analogy to the retarded Green function we define an advanced Green function $G_-(x, \bar{x})$ as in Eq. (2.47). It has support on and inside the future light cone of the field point x. A self-force defined in terms of $G_-(x, \bar{x})$ depends on the entire future history of the particle. Numerically we find the advanced force by running the simulation backwards in time. That is we start the evolution on the very last time slice and evolve backwards in time until we reach the slice corresponding to $t = 0$. We reverse the boundary condition at the event horizon to be outgoing radiation only $(\partial_t + \partial_{r*})\psi = 0$ and adjust the outer boundary so as to simulate only the backwards domain of dependence of the initial slice. We do not change the trajectory of the particle. We do not change the regularization parameters, since they depend only on the local behaviour of the field and are insensitive to the boundary conditions far away.

With this preliminary work in place we follow the literature (see for example [42]) and define the dissipative part of the self-force to be the half-retarded minus half-advanced force and the conservative part to be the half-retarded plus half-advanced force

$$F_\alpha^{\text{diss}} \equiv \frac{1}{2}\left(F_\alpha^{\text{ret}} - F_\alpha^{\text{adv}}\right), \tag{5.15a}$$

$$F_\alpha^{\text{cons}} \equiv \frac{1}{2}\left(F_\alpha^{\text{ret}} + F_\alpha^{\text{adv}}\right). \tag{5.15b}$$

The conservative force is the time reversal invariant part of the self-force. It does not affect the radiated energy or angular momentum fluxes $\dot{E}$ and $\dot{J}$; it shifts the values of E and J away from their geodesic values, affecting the orbital motion and the phase of the emitted waves.

Circular orbits

The effect of the conservative self-force is most clearly observed for circular orbits, where the unperturbed angular frequency Ω_0 as well as the shift due to the perturbation are constant in time.

For a particle in circular motion the self-force is constant in time and it turns out that the radial component is entirely conservative whereas the t and ϕ components are entirely dissipative. For any circular orbit $\dot{r} = \ddot{r} = 0$ and E_0, J_0 are given by

$$E_0 = \frac{r_0 - 2M}{\sqrt{r_0(r_0 - 3M)}}, \tag{5.16a}$$

$$J_0 = r_0\sqrt{\frac{M}{r_0 - 3M}}. \tag{5.16b}$$

Substituting these into Eq. (5.13) we find

$$\Omega = \sqrt{\frac{M}{r_0^3} - \frac{(r_0 - 3M)}{2mM}\sqrt{\frac{M}{r_0}}F_r} + O(\varepsilon^2), \tag{5.17}$$

where the first term is just the angular frequency for an unperturbed geodesic at radius r_0. The fractional change $\Delta\Omega/\Omega_0$ is then

$$\frac{\Delta\Omega}{\Omega_0} = -\frac{(r_0 - 3M)r_0}{2mM}F_r + O(\varepsilon^2). \tag{5.18}$$

Similarly the fractional changes in E and J: $\Delta E/E_0$ and $\Delta J/J_0$ are given by

$$\Delta E/E_0 = -\frac{r_0 - 2M}{2m}\sqrt{\frac{r_0}{r_0 - 3M}}F_r, \tag{5.19a}$$

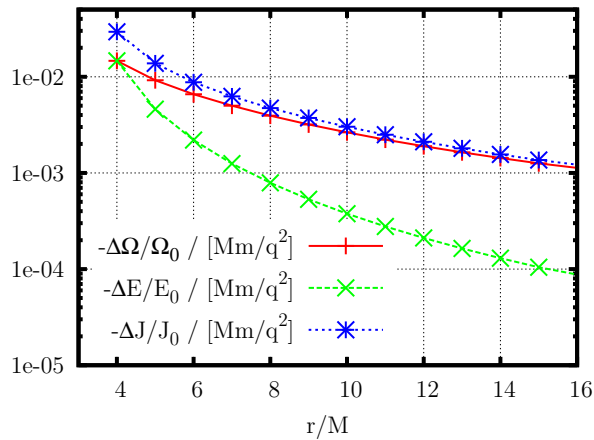$$\Delta J/J_0 = -\frac{(r_0 - 2M)r_0^2}{2m}\sqrt{\frac{1}{M(r_0 - 3M)}}F_r. \tag{5.19b}$$

Figure 5.14: Fractional change $\Delta\Omega/\Omega_0$ induced by the presence of the conservative self-force. The effect of the self-force is to move the radius of the orbit outward, decreasing its angular frequency.

Figure 5.14 shows the fractional change in Ω_0, E and J as a function of the orbit's radius r_0. Each of Ω_0, E and J is decreased by the self-force, only slightly so for large orbits $r \gg M$ but up to several percent of the charge to mass ratio $\frac{q^2}{Mm}$ for orbits close to the black hole. Since their effect on the phase of the waveform accumulates secularly even such a small effect will become quite noticeable in one radiation reaction time.

Eccentric orbits

For eccentric orbits the self-force is no longer constant in time and we have to numerically calculate both the retarded and the advanced self-force in order to construct the conservative self-force.
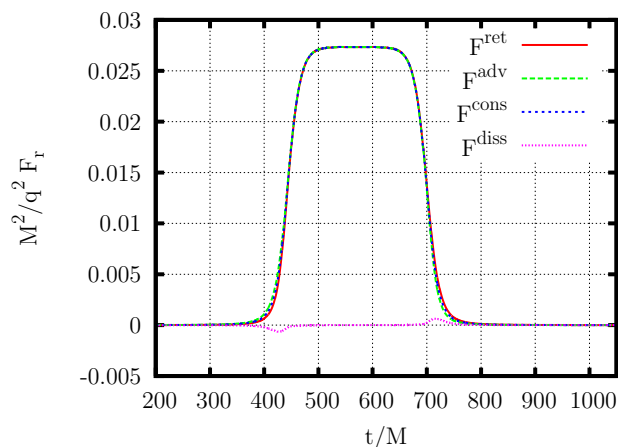
Figure 5.15: r component of the dimensionless self-force acting on a particle on a zoom-whirl orbit ($p = 7.8001$, $e = 0.9$) around a Schwarzschild black hole. Shown are the retarded (solid, red), advanced (dashed, green), conservative (dotted, blue) and dissipative (finely dotted, pink) force acting on the particle.

Figure 5.16: ϕ component of the dimensionless self-force acting on a particle on a zoom-whirl orbit ($p = 7.8001$, $e = 0.9$) around a Schwarzschild black hole. Shown are the retarded (solid, red), advanced (dashed, green), conservative (dotted, blue) and dissipative (finely dotted, pink) force acting on the particle.
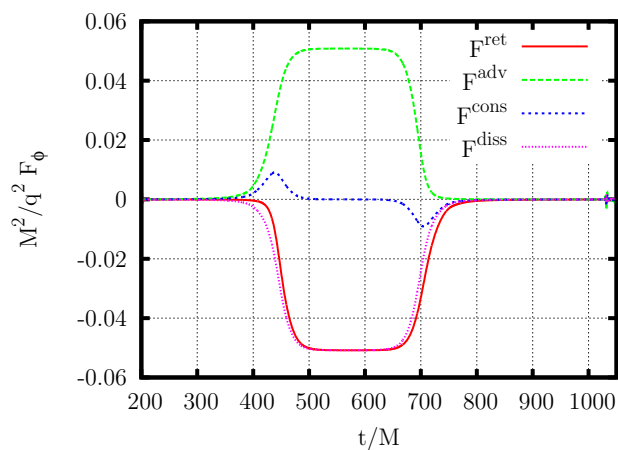
Conservative force on zoom-whirl orbits   We calculate the conservative self-force on a zoom-whirl orbit with $p = 7.8001$, $e = 0.9$. Figs. 5.15 and 5.16 display the breakdown of the self-force into retarded and advanced, and conservative and dissipative parts for a particle on a zoom-whirl orbit. In both plots the force is very weak when the particle is in the zoom phase $t \lesssim 400\,M$ or $t \gtrsim 800\,M$ and nearly constant while the particle is in the whirl phase $400\,M \lesssim t \lesssim 800\,M$. Inspection of the behaviour of the r component reveals that it is almost exclusively conservative, with only a tiny dissipative effect when the particle enters or leaves the whirl phase. This result is consistent with the observation that the particle moves on a nearly circular trajectory while in the whirl phase, for which the radial component is precisely conservative. Similarly the ϕ component is almost entirely dissipative, with only a small conservative contribution when the particle enters or leaves the whirl phase, its maximum coinciding with that of $\ddot{r}$ (not shown on the graph).

We calculate the relative changes in E, J and Ω under the influence of the self-force using Eqs. (5.11a), (5.11b), (5.14). Fig. 5.17 displays the relative changes $\Delta E/E_0$,
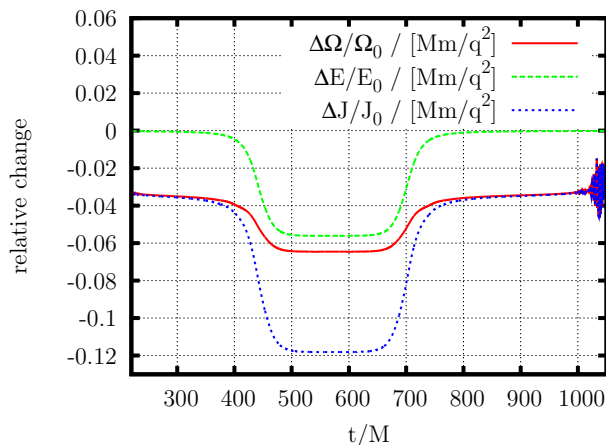

Figure 5.17: Relative change in Ω, E, J for a particle on a zoom-whirl orbit due to the electromagnetic self-force.

$\Delta J/J_0$ and $\Delta\Omega/\Omega_0$ for a particle on a zoom whirl orbit $p = 7.8001$, $e = 0.9$. The change in E, J and Ω is strongest (and negative) in the whirl phase when $r \approx 4.1M$. It is consistent with the shift experienced by a particle on a circular orbit at $4.1M$.

Retardation of the self-force   For a scalar charge moving in a weak gravitational field Poisson [43] showed that the self-force is delayed with respect to the particle motion by twice the light travel time from the particle to the central body. In a spacetime where the central body is compact the treatment of [43] is no longer directly applicable, but we still expect some retardation in the self-force when compared to the particle's motion. To study this effect, we calculate the self-force on an eccentric orbit with $p = 78$, $e = 0.9$; this orbit is ten times larger than the zoom-whirl orbit discussed earlier. The large orbit was chosen so as to be able to clearly see any possible retardation which might not be visible if the particle's orbit is deep within the strong

field region close to the black hole. Figures 5.18 and 5.19 display plots of the r and
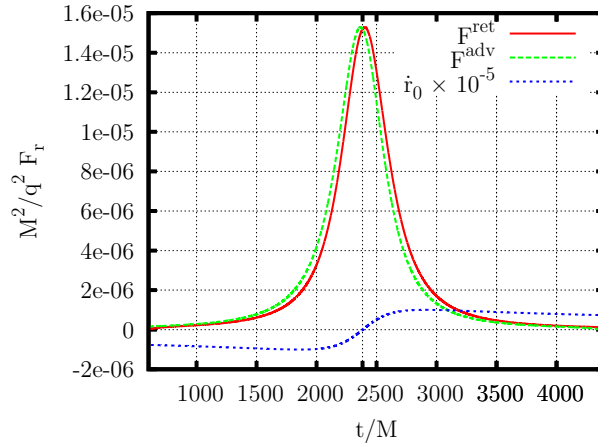

Figure 5.18: r component of the dimensionless self-force acting on a particle on an orbit with $p = 78$, $e = 0.9$. Shown are the retarded and advanced forces as well as $\dot{r}$. The vertical line at $t \approx 2383\,M$ marks the time of closest approach to the black hole.
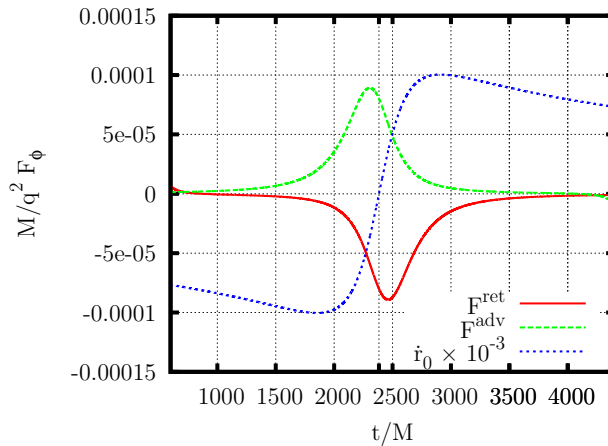
Figure 5.19: ϕ component of the dimensionless self-force acting on a particle on an orbit with $p = 78$, $e = 0.9$. Shown are the retarded and advanced forces as well as $\dot{r}$. The vertical line at $t \approx 2383\,M$ marks the time of closest approach to the black hole.

ϕ components of the self-force acting on the particle close to periastron. Shown are the retarded and advanced forces as well as the particle's radial velocity $\dot{r}$. Without considering retardation we expect the self-force to be strongest when the particle is closest to the black hole, when $\dot{r} = 0$, as evident in Fig. 5.15. Clearly for the r component displayed in Fig. 5.18 the retarded and advanced forces both peak at a time very close to the zero crossing of $\dot{r}$, suggesting very little time delay in the r component of the self-force. In Fig. 5.19 on the other hand the retarded and advanced forces peak away from the time of closest approach $t_{\min}$. Inspection of the graph shows that the delay (advance) between the time of closest approach and the peak in the retarded

(advanced) force is compatible with a delay of $\Delta t_{\min} \approx 2(r_{\min} - 3.0\,M) \approx 74\,M$. Using a delay of $\Delta t \approx 2[r_0(t) - 3.0\,M]$ and plotting $F_\phi^{\text{ret}}(t + \Delta t)$ and $-F_\phi^{\text{adv}}(t - \Delta t)$ versus t, we see in Fig. 5.20 that both curves visually lie on top of each other, and the maximum is located at $t_{\min}$. This suggests that the dissipative part of the self-force is largely due to radiation that travels into the strong field region close to the black hole and is scattered back to the particle. The time delay can then be loosely interpreted as the time it takes the signal to travel to the light ring around the black hole and back to the particle. This interpretation is loose for two reasons. First it is r^* and not r that is associated with the light travel time. Using r^*, however, does not lead to a better overlap of the curves once a suitable constant offset is chosen. Second, for the zoom-whirl orbit shown in Fig. 5.11 the (shallow) maximum in the self-force is offset by only $\Delta t \approx 2(r_0(t) - 1.0\,M)$, which leads to a reasonable overlap of the two curves. Interestingly using r^* instead of r yields a worse overlap. For very large orbits such as $p = 780$, $e = 0.9$, it is impossible to distinguish the small constant offset from the dominant $2r_0(t)$ contribution.

5.2.6 Weak field limit

As a last application we use our code to compare the numerical self-force in the weak field region to the self-force calculated using the weak field expression

$$\boldsymbol{f}_{\text{self}} = \lambda_c \frac{q^2}{m} \frac{M}{r^3} \hat{\boldsymbol{r}} + \lambda_{rr} \frac{2}{3} \frac{q^2}{m} \frac{\mathrm{d}\boldsymbol{g}}{\mathrm{d}t}\,, \quad \boldsymbol{g} = -\frac{M}{r^2} \hat{\boldsymbol{r}}\,, \tag{5.20}$$

of [42, 44]. Here boldface symbols are used for three vectors, a hat indicates a vector which is normalized using the flat space spatial metric $\delta_{\alpha\beta}$. λ_c and λ_{rr} are labels for the conservative and dissipative parts of the self-force respectively. $\boldsymbol{g}$ is the Newtonian gravitational acceleration around a spherical mass of mass M. The radial coordinate r is the isotropic coordinate $\bar{r}$, not the areal coordinate r_{SW} used in the remainder of the paper.

This identification of r with the isotropic coordinate is not unique, but is motivated by the fact that the Newtonian limit of the Schwarzschild metric is

$$g_{\alpha\beta}\,\mathrm{d}x^\alpha\,\mathrm{d}x^\beta = -(1 + 2\Phi)\,\mathrm{d}t^2 + (1 - 2\Phi)\left(\mathrm{d}\bar{r}^2 + \bar{r}^2\,\mathrm{d}\theta^2 + \bar{r}^2\sin^2\theta\,\mathrm{d}\phi^2\right), \tag{5.21}$$

where $\Phi(\bar{r}) = -\frac{M}{\bar{r}}$. This in turn is most easily derived by linearizing the isotropic metric

$$g_{\alpha\beta}\,\mathrm{d}x^\alpha\,\mathrm{d}x^\beta = -\frac{\left(1 - \frac{M}{r\bar{r}}\right)^2}{\left(1 + \frac{M}{r\bar{r}}\right)^2}\,\mathrm{d}t^2 + \left(1 + \frac{M}{r\bar{r}}\right)^4 \left(\mathrm{d}\bar{r}^2 + \bar{r}^2\,\mathrm{d}\theta^2 + \bar{r}^2\sin^2\theta\,\mathrm{d}\phi^2\right) \tag{5.22}$$

in M. $\bar{r}$ is linked to the Schwarzschild areal radius r_{SW} by

$$r = \bar{r}\left(1 + \frac{M}{2\bar{r}}\right)^2. \tag{5.23}$$

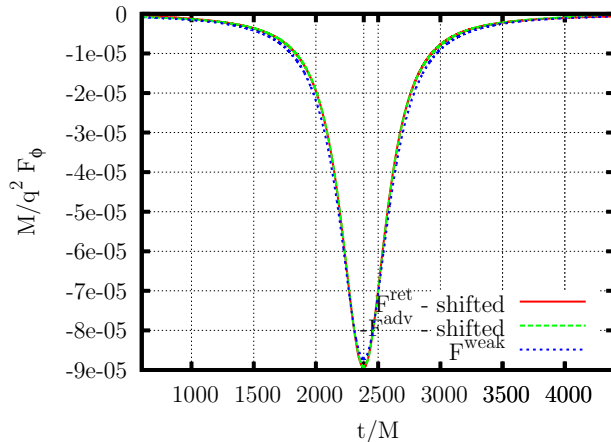Far away from the black hole r_{SW} and $\bar{r}$ are identical.

Figure 5.20: ϕ component of the retarded (solid red line) and (dashed green line) negative advanced self-forces acting on a particle with $p = 78$, $e = 0.9$. The forces have been shifted by $\Delta t \approx 2[r_0(t) - 3.0\,M]$. Also shown is the self-force calculated using the weak field expression Eq. 5.20 (blue dotted line).

We calculate the self-force for a particle on an eccentric orbit with $e = 0.9$ and $p = 78$ or $p = 780$. Fig. 5.20 shows the retarded and (negative) advanced forces shifted by $\Delta t \approx 2[r_0(t) - 3.0\,M]$ as well as the analytic force calculated using Eq. (5.20). At this distance there are still noticeable differences between the (shifted) retarded field and the weak field expression. One reason for this lies in the choice of a suitable r coordinate to correspond to the r coordinate in the weak field expression. We use the areal Schwarzschild r, but the isotropic coordinate $\bar{r}$ or even the tortoise r^* could be used. Neither one yields a better agreement between the two curves.

For $p = 780$ using a shift of $\Delta t = 2r_0(t)$ the agreement between numerical data and analytic expression is excellent as is evident in Fig. 5.21. At this distance r, $\bar{r}$ and r^* are indistinguishable.

Investigating the difference between numerical and analytic self-force, we plot both for a set of circular orbit with $6 \leq p \leq 75$. Fig. 5.22 displays the analytic and numerical self-forces. The analytic values were calculated using the isotropic radius $\bar{r}$, taking care to account for the different normalizations of $\hat{r}$, $\hat{\phi}$ and $\left(\frac{\partial}{\partial \bar{r}}\right)^{\alpha}$ and $\left(\frac{\partial}{\partial \phi}\right)^{\alpha}$. The agreement between the weak field expression Eq. (5.20) and the numerical results is surprisingly good close to the black hole down to $p = 6$.

5.3 Electromagnetic field—vector potential

Using the vector potential code described in Section 4.4 we can reproduce the results obtained from the Faraday tensor method discussed in section 5.2. The differences are small, with the Faraday tensor code generally yielding more accurate results since the costly numerical differentiation that is necessary in the vector potential calculation is not required. Nevertheless we can reproduce for example the correct decay behaviour
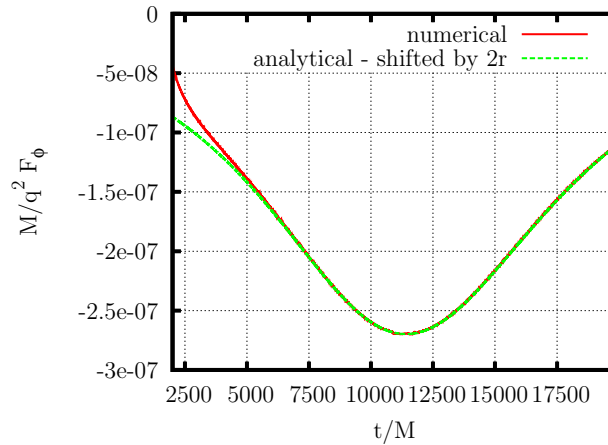
Figure 5.21: ϕ component of the retarded self-force acting on a particle on an orbit with $p = 780$, $e = 0.9$ close to periastron. Shown are the numerical (solid, red) and shifted analytical (dashed, green) forces. The agreement between numerical and analytical calculation is excellent, the discrepancy for $t \lesssim 7500\,M$ is due to initial data contamination.
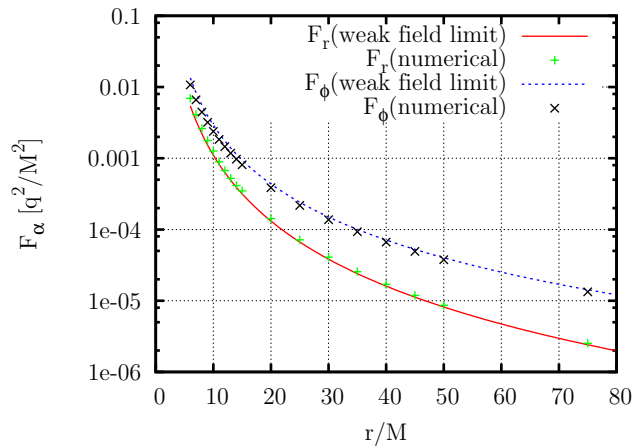
Figure 5.22: Comparison of analytic and numerical self-forces on circular orbits at different radii. Shown are the r and ϕ components of the self-force calculated numerically (crosses) and analytically using Eq. (5.20).

101

of the multipole coefficients for a zoom-whirl orbit as shown in Fig. 5.23.
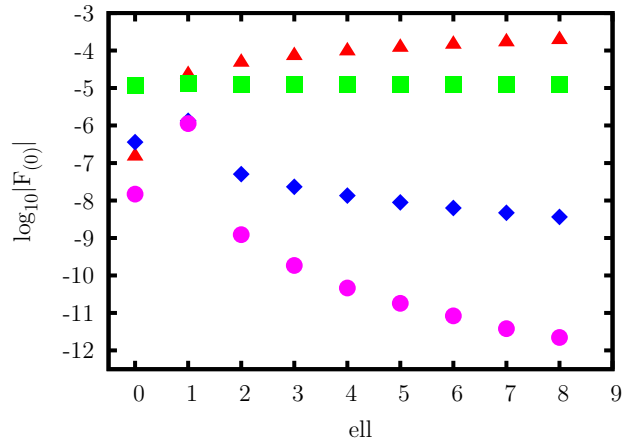
Figure 5.23: Multipole coefficients of $\frac{M^2}{q} \operatorname{Re} F_{(0)}^R$ for a particle on a zoom-whirl orbit ($p = 7.8001$, $e = 0.9$), calculated using a stepsize of $h = 0.125M$ for the $\ell = 1$ modes and increasing the resolution linearly with ℓ for $\ell > 1$. The coefficients are extracted at $t = 1100\,M$ when the particle is deep within the zoom phase. Red triangles are used for the unregularized multipole coefficients $F_{(0),\ell}$, squares, diamonds and disks are used for the partly regularized coefficients after the removal of the $A_{(0)}$, $B_{(0)}$ and $D_{(0)}$ terms respectively.
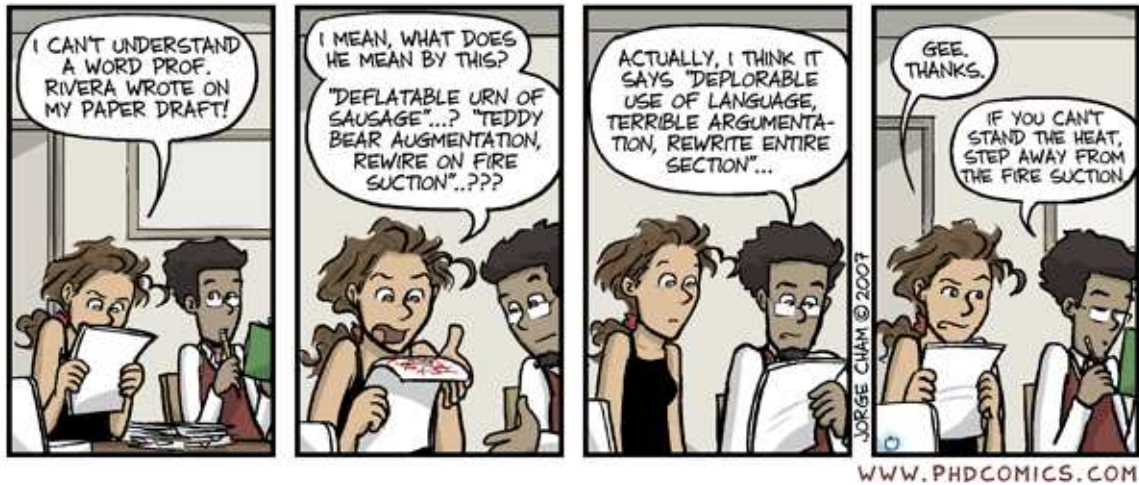
"Piled Higher and Deeper" by Jorge Cham, www.phdcomics.com

Chapter 6

Conclusions and Future Directions

6.1 Summary

Chapter 2 introduced the theoretical framework this thesis is based on. In particular Green functions in curved spacetime were introduced and regularized equations of motion for a point particle were presented.

Chapter 3 introduced the concepts behind the calculation of the regularization parameters used in the mode-sum scheme of [2]. We calculated the regularization parameters A, B and D along a geodesic for scalar, electromagnetic and massive perturbations of Schwarzschild spacetime.

Chapter 4 introduced the fourth and second order characteristic evolution schemes that we used to solve the scalar and electromagnetic wave equations. We discussed the issues of gauge violations and constraint equations that have to be dealt with in the electromagnetic case. We also displayed convergence plots showing that our numerical code reaches the desired convergence order.

In chapter 5 we displayed results for the scalar and electromagnetic self-force for a selection of orbits including highly eccentric orbits. For the electromagnetic self-force, we investigated the effect of the conservative force on the constants of motion.

6.2   Conclusions

For both the scalar and the electromagnetic self-force we find that the self-force is strongest when the particle is closest to the black hole. In particular we find that for zoom-whirl orbits during the whirl phase the self-force is nearly constant and very close to that of a particle on a circular orbit of the same radius. However there are also qualitative differences between the two self-forces. In the scalar case we observed an overshooting of the self-force when the particle enters or leaves the whirl phase. This effect is much weaker in the electromagnetic case, making it hard to observe at all.

For the electromagnetic field we find that the numerical results agree with weak field expressions derived for example in [43] for sufficiently large distances $r \gtrsim 400\,M$ away from the black hole. We also find that the analytic expressions neglect the retardation of the self-force with respect to the particle motion that is present in the numerical data. Only when delayed by $\Delta t \approx 2r_0(t)$ does the analytical result match the numerical self-force.

We calculated the effects of the conservative electromagnetic self-force on circular orbits, where it reduces the angular frequency of the orbit and thus affects the phasing of the observed waves. We find this effect to be much stronger in the electromagnetic case than in the scalar case discussed by [32]. In particular during the nearly circular whirl phase of a zoom-whirl orbit we find that the fractional change in Ω is approximately $0.06\,\frac{q^2}{mM}$. Since there are approximately 4 revolutions in each whirl phase, any waveform ignoring the effect of the conservative self-force picks up a relative phase error of $0.24\,\frac{q^2}{Mm}$ per radial orbit. Since this error accumulates over time it will rapidly become out of phase with the true waveform. This statement however is not directly transferable to the gravitational case since the radius r_0 of the orbit is not a gauge invariant quantity. Therefore we cannot distinguish between changes in Ω due to effects of the self-force and due to gauge choices. To obtain a meaningful measure of the effect of the gravitational self-force we need to compare two gauge invariant quantities, for example Ω and the gauge invariant u^t of [45].

6.3   Future outlook

A straightforward continuation of the work presented in this thesis lies in the application of the methods developed here to the case of a gravitational perturbation of a Schwarzschild black hole. The treatment presented for the vector potential of the electromagnetic field in particular is easily generalized to accommodate a gravitational perturbation described in the Lorenz gauge.

A technical improvement would be the implementation of a fourth order accurate finite difference scheme to handle the coupled system of equations governing electromagnetic or gravitational perturbations. Sago [46] has recently implemented such a scheme, based on the work for the scalar case presented here.

Finally a more ambitious future project is the implementation of a self-consistent (but entirely first order in the perturbation strength q) algorithm to update the

particle's motion based on the calculated self-force. Such an approach would require changes in a number of steps in the method used in this work. First the equation of motion for the particle is no longer the geodesic equation, instead an acceleration term has to be included on the right hand side. This affects the regularization parameters which were calculated under the assumption of geodesic motion, appendix E illustrates such a calculation. In a practical implementation it is no longer possible to calculate each ℓ, m mode independently of the others. At each timestep the regularized force has to be calculated from all the modes in order to update the motion of the particle which serves as a source for the field. This makes the numerical implementation of such a scheme technically more complicated, although it is not fundamentally different from the current implementation. In a practical implementation one is also forced to consider the demands on computing power. The current implementation comfortably runs on ordinary desktop machines, each mode requiring several hours to calculate. However all 45 modes that contribute for $\ell \leq 8$ would require too much computing time on a single machine. Some parallelization technique other than the current trivial parallelization will need to be used.

"Piled Higher and Deeper" by Jorge Cham, www.phdcomics.com

Appendix A

Notation

Throughout the thesis a large number of symbols are be used. While we introduce each symbol when it is first used, there might be use for a central location where all the definitions are presented. This chapter therefore collects some of the definitions in one place. As we are re-using some of the symbols in the the text, there is a certain amount of context sensitivity to the meaning of (some) symbols; we will try to point out these cases.

Throughout the thesis we will deal with a Schwarzschild background spacetime of mass M, whose metric $g_{\alpha\beta}$ is given by the line element

$$
\begin{aligned}
\mathrm{d}s^2 &= -\left(1 - \frac{2M}{r}\right)\mathrm{d}t^2 + \left(1 - \frac{2M}{r}\right)^{-1}\mathrm{d}r^2 + r^2(\mathrm{d}\theta^2 + \sin^2\theta\,\mathrm{d}\phi^2) \\
&= -\left(1 - \frac{2M}{r}\right)\left[\mathrm{d}t^2 + \mathrm{d}(r^*)^2\right] + r^2(\mathrm{d}\theta^2 + \sin^2\theta\,\mathrm{d}\phi^2)\,,
\end{aligned}
\tag{A.1}
$$

where the first line uses Schwarzschild coordinates t, r, θ and ϕ while the second one employs the tortoise coordinate

$$
r^* = r + 2M\ln\left(1 - \frac{r}{2M}\right).
\tag{A.2}
$$

Occasionally we will employ the Eddington-Finkelstein null coordinates

$$
u = t - r^*, \quad v = t + r^*,
\tag{A.3}
$$

which are connected to the characteristic lines of the wave operator.

We denote the covariant derivative compatible with the metric as

$$\nabla_\alpha v^\beta \equiv \partial_\alpha v^\beta + \Gamma^\beta{}_{\alpha\gamma} v^\gamma , \tag{A.4}$$

where

$$\Gamma^\alpha{}_{\beta\gamma} = \frac{1}{2} g^{\alpha\mu} (\partial_\gamma g_{\mu\beta} + \partial_\beta g_{\gamma\mu} - \partial_\mu g_{\beta\gamma}) \tag{A.5}$$

are the Christoffel symbols. We will also use a semicolon ";" for the same purpose and a comma "," to denote an ordinary partial derivative. $R^\alpha{}_{\beta\gamma\delta}$ is the Riemann tensor defined such that

$$\omega_{\alpha;\beta\gamma} = \omega_{\alpha;\gamma\beta} + R^\mu{}_{\alpha\beta\gamma} \omega_\mu , \tag{A.6}$$

$R_{\alpha\beta} = R^\mu{}_{\alpha\mu\beta}$ is the Ricci tensor and finally $R = R^\mu{}_\mu$ is the Ricci scalar.

We are interested in the motion of a point particle of mass m possibly carrying a scalar or electromagnetic charge q moving along a geodesic $\gamma : \tau \mapsto z(\tau)$. Here τ is the proper time along the world line and $u^\alpha = \frac{dz^\alpha}{d\tau}$ is its four velocity. Due to the existence of timelike and angular Killing vectors in Schwarzschild spacetime, the t and ϕ components of the u_α are conserved. Furthermore, without loss of generality we restrict the particle to move in the equatorial plane $\theta = \pi/2$. Therefore the components of the four velocity are explicitly given by

$$u^\alpha = [E/f_0, \dot{r}_0, 0, J/r_0^2] , \tag{A.7}$$

where E is the conserved energy, J the conserved angular momentum and $\dot{r}_0 \equiv \frac{dr_0}{d\tau}$ is the radial velocity component. We use the convention that terms bearing a subscript "0" refer to the location of the particle, denoted by

$$x_0 = \left[t_0, r_0, \frac{\pi}{2}, \varphi_0\right] . \tag{A.8}$$

We use an overdot to denote covariant derivatives along the world line,

$$\dot{v}^\alpha \equiv \frac{Dv^\alpha}{d\tau} \equiv u^\beta \nabla_\beta v^\alpha . \tag{A.9}$$

We make extensive use of bi-tensorial expressions involving Synge's world function $\sigma(x, \bar{x})$ and its various derivatives $\nabla_\alpha \sigma(x, \bar{x}) \equiv \sigma_\alpha$, $\nabla_{\bar{\alpha}} \sigma(x, \bar{x}) \equiv \sigma_{\bar{\alpha}}$. Initially x and $\bar{x}$ denote two arbitrary points. When dealing with Green functions, x will be the *field point* and the $\bar{x}$ will be *source point*. When dealing with expansions along the world line, $\bar{x}$ will be on the world line, whereas x will be a point away from the world line. When dealing with the singular Green function we will also introduce the retarded point x' and the advanced point x'' which lie on the intersection of the world line γ and the past and future light cones of x, respectively. When writing bi-tensors, we will denote indices at $\bar{x}$ using barred letters $\bar{\alpha}$, $\bar{\beta}$, etc. We will denote indices at x' using primed letters α', β', etc. We will denote indices at x'' using doubly primed letters α'', β', etc. We will denote indices at x using plain letters α, β, etc. We will use μ, ν, etc. to denote indices at generic points on a world line, either between x and $\bar{x}$ or on γ or for dummy indices that are summed over.

We introduce a short hand notation for contractions between the Riemann tensor, its derivatives and either u^μ or σ^μ such that for example

$$R_{u\sigma u\sigma|\sigma} \equiv R_{\bar\alpha\bar\beta\bar\gamma\bar\delta;\bar\varepsilon} u^{\bar\alpha}\sigma^{\bar\beta}u^{\bar\gamma}\sigma^{\bar\delta}\sigma^{\bar\varepsilon}\,. \tag{A.10}$$

We use

$$[T_{\mu\nu}(x,\bar x)] \equiv \lim_{x\to\bar x} T_{\mu\nu}(x,\bar x) \tag{A.11}$$

to denote the coincidence limit of a bi-tensor $T_{\mu\nu}(x,\bar x)$ as well as to denote jumps of field derivatives across the world line

$$[\partial_u^n\partial_v^m\psi] \equiv \lim_{\epsilon\to 0^+}[\partial_u^n\partial_v^m\psi(t_0, r_0^* + \epsilon) - \partial_u^n\partial_v^m\psi(t_0, r_0^* - \epsilon)]\,. \tag{A.12}$$

No danger of confusing the two uses should arise.

We use ε as a bookkeeping variable to track the order of distance measure between two points x and $\bar x$. A term X is said to be $O(\varepsilon^n)$ if $\lim_{x\to\bar x}\frac{X}{|x-\bar x|^n}$ is a number of order unity.

We use Φ, A_μ and $\gamma_{\mu\nu}$ to denote a scalar field, the electromagnetic potential, and a gravitational perturbation. For the electromagnetic case only we use $F_{\mu\nu} \equiv \left(A_{\nu,\mu} - A_{\mu,\nu}\right)$ to denote the Faraday tensor.

We define the angular metric Ω_{AB} on the two sphere by

$$\Omega_{AB}\,\mathrm{d}\theta^A\,\mathrm{d}\theta^B = \mathrm{d}\theta^2 + \sin^2\theta\,\mathrm{d}\phi^2\,, \tag{A.13}$$

where $\theta^A = \theta, \phi$. Its compatible covariant derivative $|$ is such that

$$\Omega_{AB|C} = 0\,. \tag{A.14}$$

The inverse metric Ω^{AB} is the matrix inverse of Ω_{AB}, not the tensor $g^{AC}g^{BD}\Omega_{CD}$. The Riemann tensor

$$R^{(2)}_{ABCD} = (\Omega_{AC}\Omega_{BD} - \Omega_{AD}\Omega_{BC}) \tag{A.15}$$

is used to commute covariant derivatives on the two sphere only.

We denote angular indices by capital Latin letters A, B, ... and indices in the t, r directions by lowercase Latin letters a, b, ...

We use the scalar, vector and (odd) tensor harmonics of Regge and Wheeler [40], which are given by

$$Z_A^{\ell m} \equiv Y^{\ell m}_{,A}\,, \quad X_A^{\ell m} \equiv \epsilon^B{}_A Y^{\ell m}_{,B}\,, \tag{A.16a}$$

$$X_{AB}^{\ell m} \equiv X^{\ell m}_{A|B} - X^{\ell m}_{B|A}\,, \tag{A.16b}$$

where $Y^{\ell m}$ are the usual scalar spherical harmonics of [47] and ϵ_{AB} is the Levi-Civita tensor on the two sphere. We use ℓ, m to label the spherical harmonics, but also use m for the mass of the perturbing object; which meaning is intended for m will be clear from the context.

Appendix B

Angular integration

In this appendix we reproduce those results of Appendices C and D of [18] which we use in the main part of the thesis.

B.1 β integration

In calculating the regularization parameters, the only non-vanishing β dependence is in terms of the form χ^{-p} where

$$\chi \equiv 1 - k \sin^2 \beta, \quad k \equiv \frac{J^2}{r_0^2 + J^2}. \tag{B.1}$$

Averaging this term over the range $-\pi \ldots \pi$ we find

$$\left\langle \chi^{-p} \right\rangle = \frac{1}{2\pi} \int_{-\pi}^{\pi} (1 - k \sin^2 \beta)^{-p} \, \mathrm{d}\beta = \frac{2}{\pi} \int_0^{\pi/2} (1 - k \sin^2 \beta)^{-p} \, \mathrm{d}\beta = F(p, \tfrac{1}{2}; 1; k), \tag{B.2}$$

where $F(a, b; c; z)$ are the hypergeometric functions. If p is an odd half integer, as is the case for our calculation, then the hypergeometric functions appearing can be reduced to a linear combination of complete elliptic integrals

$$\frac{2}{\pi} \mathcal{K} \equiv F(\tfrac{1}{2}, \tfrac{1}{2}; 1; k), \tag{B.3a}$$

and

$$\frac{2}{\pi} \mathcal{E} \equiv F(-\tfrac{1}{2}, \tfrac{1}{2}; 1; k). \tag{B.3b}$$

We note that χ is symmetric around the origin $\beta = 0$ and $\beta = \pi/2$. Because of this, products of powers of χ with $\sin \beta$, $\sin \beta \cos \beta$ (antisymmetric around $\beta = 0$), or $\cos \beta$ (antisymmetric around $\beta = \pi/2$) vanish when averaged over the an interval of length 2π.

B.2   Legendre polynomial expansions

The dependence on α is more complex. The terms that appear in the regularization calculation are of the form

$$(\delta^2 + 1 - u)^{p/2}, \text{ where } u = \cos\alpha \text{ and } \delta \to 0. \tag{B.4}$$

Detweiler et. al. [18] use the generating function of the Legendre polynomials to derive an expansion in terms of Legendre polynomials

$$(\delta^2 + 1 - u)^{p/2} = \sum_{\ell=0}^{\infty} \mathcal{A}_\ell^p(\delta) P_\ell(u). \tag{B.5}$$

They show that for $\delta \to 0$

$$\mathcal{A}_\ell^{-1/2} = \sqrt{2} + O(\ell\delta), \quad \mathcal{A}_\ell^{-k-1/2} = \frac{2\ell + 1}{\delta^{2k-1}(2k - 1)}(1 + O(\ell\delta)), \, k \geq 1, \tag{B.6a}$$

and

$$\mathcal{A}^{k+1/2} = \frac{(-1)^{k+1}2^{k+3/2}[(2k + 1)!!]^2(2\ell + 1)}{\prod_{i=0}^{2k+2}(2\ell - 2k + 2i - 1)}, \, k \geq 0. \tag{B.6b}$$

Appendix C

Spherical harmonics

In this section we list the vector and tensor harmonics used to decompose the Faraday tensor. The material presented here follows the treatment of Martel [48].

C.1 Metric on the two-sphere

We define the angular metric Ω_{AB} on the two sphere by

$$\Omega_{AB}\, \mathrm{d}\theta^A\, \mathrm{d}\theta^B = \mathrm{d}\theta^2 + \sin^2\theta\, \mathrm{d}\phi^2\,, \tag{C.1}$$

where $\theta^A = \theta, \phi$. Its compatible covariant derivative $|$ is such that

$$\Omega_{AB|C} = 0\,. \tag{C.2}$$

The inverse metric Ω^{AB} is the matrix inverse of Ω_{AB}, not the tensor $g^{AC}g^{BD}\Omega_{CD}$. The Riemann tensor

$$R^{(2)}_{ABCD} = (\Omega_{AC}\Omega_{BD} - \Omega_{AD}\Omega_{BC}) \tag{C.3}$$

is used to commute covariant derivatives on the two sphere only. Note that $R^{(2)}_{ABCD}$ is not just the restriction of the four dimensional Riemann tensor $R_{\alpha\beta\gamma\delta}$ to the two-sphere just as Ω_{AB} is not just the restriction of the full metric $g_{\alpha\beta}$ to the sphere.

C.2 Scalar harmonics

The vector and tensor harmonics are based on ordinary scalar spherical harmonics $Y_{\ell m}$. We follow [47] and define the spherical harmonics to be

$$Y_{\ell m}(\theta, \phi) = (-1)^\ell \sqrt{\frac{2\ell+1}{4\pi}\frac{(\ell-m)!}{(\ell+m)!}}P_\ell^m(\cos\theta)e^{im\phi}\,, \tag{C.4}$$

where $P_\ell^m(x)$ are the associated Legendre polynomials. We adopt he sign convention of [47]

$$\bar{Y}_{\ell m} = (-1)^\ell Y_{\ell,-m}\,. \tag{C.5}$$

The spherical harmonics are the eigenfunctions of the angular part of the Laplacian operator and satisfy the eigenvalue equation

$$\frac{1}{\sin\theta}\frac{\partial}{\partial\theta}\left(\sin\theta\frac{\partial Y_{\ell m}}{\partial\theta}\right) + \frac{1}{\sin^2\theta}\frac{\partial^2 Y_{\ell m}}{\partial\phi^2} + \ell(\ell+1)Y_{\ell m} = 0\,. \tag{C.6}$$

In terms of the covariant derivative | this can be written as

$$\Omega^{AB}Y_{|AB}^{\ell m} + \ell(\ell+1)Y_{\ell m} = 0\,. \tag{C.7}$$

The spherical harmonics form an orthonormal set of basis functions on the sphere

$$\int Y_{\ell m}\bar{Y}_{\ell'm'}\;\mathrm{d}\Omega = \delta^{\ell\ell'}\delta^{mm'}\,. \tag{C.8}$$

Any scalar function on the sphere can be decomposed into spherical harmonic modes via

$$f(\theta,\phi) = \sum_{\ell=0}^{\infty}\sum_{m=-\ell}^{\ell}f^{\ell m}Y_{\ell m}(\theta,\phi)\,, \quad f^{\ell m} \equiv \int f(\theta,\phi)\bar{Y}^{\ell m}\;\mathrm{d}\Omega\,. \tag{C.9}$$

C.3 Vector spherical harmonics

The vector harmonics come in two flavours: even and odd. Even modes transform as polar vector components under an inversion of the coordinates, while odd modes transform as axial vector components. We use the vector harmonics of Regge and Wheeler[40] which are defined by

$$Z_A^{\ell m} \equiv Y_{|A}^{\ell m}\,, \quad X_A^{\ell m} \equiv \epsilon_A{}^B Y_{|B}^{\ell m}\,, \tag{C.10}$$

where ϵ_{AB} is the Levi-Civita tensor on the sphere ($\epsilon_{\theta\phi} = \sin\theta$). $Z_A^{\ell m}$ are even vector harmonics and $X_A^{\ell m}$ are odd vector harmonics. The set $\{Z_A^{\ell m}, X_A^{\ell m}\}$ forms an orthogonal, but not orthonormal basis for vectors defined on a two-sphere. We find

$$\int \Omega^{AB}Z_A^{\ell m}\bar{X}_B^{\ell'm'}\;\mathrm{d}\Omega = 0\,, \tag{C.11a}$$

$$\int \Omega^{AB}Z_A^{\ell m}\bar{Z}_B^{\ell'm'}\;\mathrm{d}\Omega = \ell(\ell+1)\delta^{\ell\ell'}\delta^{mm'}\,, \tag{C.11b}$$

and

$$\int \Omega^{AB}X_A^{\ell m}\bar{X}_B^{\ell'm'}\;\mathrm{d}\Omega = \ell(\ell+1)\delta^{\ell\ell'}\delta^{mm'}\,, \tag{C.11c}$$

where we have explicitly spelled out the inverse metric Ω^{AB} used to contract vectors on the two-sphere.

Using the defining equations Eq. (C.10) it is straightforward to show that the even and odd vector harmonics satisfy

$$\Omega^{AB}Z_{A|B}^{\ell m} + \ell(\ell+1)Y^{\ell m} = 0\,, \tag{C.12a}$$

$$\Omega^{AB}X_{A|B}^{\ell m} = 0\,, \tag{C.12b}$$

$$\epsilon ABX_{A|B}^{\ell m} + 2\ell(\ell+1)Y^{\ell m} = 0\,, \tag{C.12c}$$

respectively. Similarly for second derivatives

$$\Omega^{AB} Z^{\ell m}_{A|BC} + \ell(\ell+1) Z^{\ell m}_C = 0 , \tag{C.13a}$$

$$\Omega^{BC} Z^{\ell m}_{A|BC} - [1 - \ell(\ell+1)] Z^{\ell m}_A = 0 , \tag{C.13b}$$

$$\Omega^{AB} X^{\ell m}_{A|BC} = 0 , \tag{C.13c}$$

$$\Omega^{BC} X^{\ell m}_{A|BC} - [1 - \ell(\ell+1)] X^{\ell m}_A = 0 , \tag{C.13d}$$

$$\Omega^{AC} X^{\ell m}_{A|BC} - X^{\ell m}_B = 0 . \tag{C.13e}$$

Any vector valued function on the two-sphere can be decomposed into even and odd vector spherical harmonic moments

$$v_A(\theta, \phi) = \sum_{\ell=0}^{\infty} \sum_{m=-\ell}^{\ell} v_{\ell m} Z^{\ell m}_A + \tilde{v}_{\ell m} X^{\ell m}_A , \tag{C.14a}$$

$$v_{\ell m} \equiv \frac{1}{\ell(\ell+1)} \int \Omega^{AB} v_A(\theta, \phi) Z^{\ell m}_B \, \mathrm{d}\Omega , \tag{C.14b}$$

$$\tilde{v}_{\ell m} \equiv \frac{1}{\ell(\ell+1)} \int \Omega^{AB} v_A(\theta, \phi) X^{\ell m}_B \, \mathrm{d}\Omega , \tag{C.14c}$$

where the contraction is calculated using the metric on the two-sphere.

C.3.1 (Antisymmetric) tensor harmonics

It is useful to define an antisymmetric tensor harmonic

$$X^{\ell m}_{AB} = X^{\ell m}_{A|B} - X^{\ell m}_{B|A} , \tag{C.15}$$

satisfying

$$\Omega^{AB} X^{\ell m}_{AB} = 0 = \Omega^{BC} X^{\ell m}_{BC|A} , \tag{C.16}$$

and

$$\Omega^{BC} X^{\ell m}_{AB|C} = -\ell(\ell+1) X^{\ell m}_A . \tag{C.17}$$

The tensorial harmonics are normalized as

$$\int \Omega^{AC} \Omega^{BD} X^{\ell m}_{AB} \bar{X}^{\ell'm'}_{CD} \, \mathrm{d}\Omega = 2[\ell(\ell+1)]^2 \delta_{\ell\ell'} \delta_{mm'} . \tag{C.18}$$

Appendix D

Jump Conditions

In this appendix we derive the jump conditions linking the field values to the left and to the right of the particle.

D.1 Scalar case

In two places in the numerical simulation we introduce *piecewise polynomials* to approximate the scalar field $\psi_{\ell m}$ across the world line. By a piecewise polynomial we mean a polynomial of the form

$$
p(t, r^*) = \begin{cases} \displaystyle\sum_{n,m=0}^{N} \frac{c_{nm}}{n!\, m!} u^n v^m & \text{if } r^*(u, v) > r_0^* \\ \displaystyle\sum_{n,m=0}^{N} \frac{c'_{nm}}{n!\, m!} u^n v^m & \text{if } r^*(u, v) < r_0^* \end{cases}, \tag{D.1}
$$

where $u = t - r^*$, $v = t + r^*$ are characteristic coordinates, r_0^* is the position of the particle at the time $t(u, v)$, and N is the order of the polynomial, which for our purposes is $N = 4$ or less. The two sets of coefficients c_{nm} and c'_{nm} are not independent of each other, but are linked via jump conditions that can be derived from the wave equation [Eq. (4.7)]. To do so, we rewrite the wave equation in the characteristic coordinates u and v and reintroduce the integral over the world line on the right-hand side,

$$
-4\partial_u \partial_v \psi - V\psi = \int_\gamma \hat{S}(\tau) \delta(u - u_p) \delta(v - v_p)\, \mathrm{d}\tau, \tag{D.2}
$$

where $\hat{S}(\tau) = -8\pi q \frac{\bar{Y}_{\ell m}(\pi/2, \varphi_p(\tau))}{r_p(\tau)}$ is the source term and quantities bearing a subscript p are evaluated on the world line at proper time τ.

Here and in the following we use the notation

$$
[\partial_u^n \partial_v^m \psi] = \lim_{\epsilon \to 0^+} [\partial_u^n \partial_v^m \psi(t_0, r_0^* + \epsilon) - \partial_u^n \partial_v^m \psi(t_0, r_0^* - \epsilon)] \tag{D.3}
$$

to denote the jump in $\partial_u^n \partial_v^m \psi$ across the world line. First, we notice that the source term does not contain any derivatives of the Dirac δ-function, causing the solution

ψ to be continuous. This means that the zeroth-order jump vanishes: $[\psi] = 0$. Our task is then to find the remaining jump conditions at the point (t_0, r_0^*) for $n, m \leq 4$. Alternatively, instead of crossing the world line along a line $t = t_0 = \text{const}$ we can also choose to cross along lines of $u = u_0 = \text{const}$ or $v = v_0 = \text{const}$, noting that for a line of constant v the coordinate u runs from $u_0 + \epsilon$ to $u_0 - \epsilon$ to cross from the left to the right of the world line. Figure D.1 provides a clearer description of the paths taken.
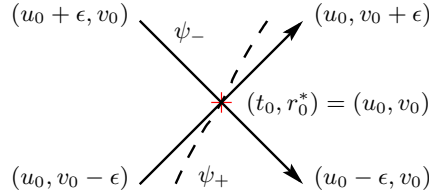

Figure D.1: Paths taken in the calculation of the jump conditions. (u_0, v_0) denotes an arbitrary but fixed point along the world line γ. The wave equation is integrated along the lines of constant u or v indicated in the sketch. Note that in order to move from the domain on the left to the domain on the right, u has to run from $u_0 + \epsilon$ to $u_0 - \epsilon$. Where appropriate we label quantities connected to the domain on the left by a subscript "$-$" and quantities connected to the domain on the right by "$+$".

In order to find the jump $[\partial_u \psi]$ we integrate the wave equation along the line $u = u_0$ from $v_0 - \epsilon$ to $v_0 + \epsilon$

$$-4 \int_{v_0 - \epsilon}^{v_0 + \epsilon} \partial_u \partial_v \psi \, dv - \int_{v_0 - \epsilon}^{v_0 + \epsilon} V\psi \, dv = \int_\gamma \hat{S}(\tau)\delta(u_0 - u_p) \int_{v_0 - \epsilon}^{v_0 + \epsilon} \delta(v - v_p) \, dv \, d\tau , \quad (D.4)$$

which, after involving $\int_{v_0 - \epsilon}^{v_0 + \epsilon} \delta(v - v_p) \, dv = \theta(v_p - v_0 + \epsilon)\theta(v_0 - v_p + \epsilon)$ and $\delta(g(x)) = \delta(x - x_0)/|g'(x_0)|$, yields

$$[\partial_u \psi] = -\frac{1}{4}\frac{f_0}{E - \dot{r}_0}\hat{S}(\tau_0) , \quad (D.5)$$

where the overdot denotes differentiation with respect to proper time τ.

Similarly, after first taking a derivative of the wave equation with respect to v and integrating from $u_0 + \epsilon$ to $u_0 - \epsilon$, we obtain

$$-4 \int_{u_0 + \epsilon}^{u_0 - \epsilon} \partial_u \partial_v^2 \psi \, du - \int_{u_0 + \epsilon}^{u_0 - \epsilon} V\psi \, du = \int_\gamma \hat{S}(\tau) \int_{u_0 + \epsilon}^{u_0 - \epsilon} \delta(u - u_p) \, du \, \delta'(v_0 - v_p) \, d\tau . \quad (D.6)$$

We find

$$[\partial_v^2 \psi] = \frac{1}{4}\frac{f_0}{E + \dot{r}_0}\frac{d}{d\tau}\left[\frac{f_p}{E + \dot{r}_p}\hat{S}(\tau)\right]_{|\tau = \tau_0} . \quad (D.7)$$

Systematically repeating this procedure we find expressions for the jumps in all the derivatives that are purely in the u or v direction. Table D.1 lists these results. Jump conditions for derivatives involving both u and v are obtained directly from the

$$[\psi] = 0 \,, \tag{D.8a}$$

$$[\partial_u \psi] = -\frac{1}{4}\bar{\xi}_0^{-1}\hat{S}(\tau_0) \,, \tag{D.8b}$$

$$[\partial_v \psi] = \frac{1}{4}\xi_0^{-1}\hat{S}(\tau_0) \,, \tag{D.8c}$$

$$[\partial_u^2 \psi] = -\frac{1}{4}\bar{\xi}_0^{-1}\frac{\mathrm{d}}{\mathrm{d}\tau}\left(\bar{\xi}_p^{-1}\hat{S}(\tau)\right)_{|\tau=\tau_0} \,, \tag{D.8d}$$

$$[\partial_v^2 \psi] = \frac{1}{4}\xi_0^{-1}\frac{\mathrm{d}}{\mathrm{d}\tau}\left(\xi_p^{-1}\hat{S}(\tau)\right)_{|\tau=\tau_0} \,, \tag{D.8e}$$

$$[\partial_u^3 \psi] = \frac{1}{4}V\xi_0\bar{\xi}_0^{-1}[\partial_u\psi] - \frac{1}{4}\bar{\xi}_0^{-1}\frac{\mathrm{d}}{\mathrm{d}\tau}\left[\bar{\xi}_p^{-1}\frac{\mathrm{d}}{\mathrm{d}\tau}\left(\bar{\xi}_p^{-1}\hat{S}(\tau)\right)\right]_{|\tau=\tau_0} \,, \tag{D.8f}$$

$$[\partial_v^3 \psi] = \frac{1}{4}V\bar{\xi}_0\xi_0^{-1}[\partial_v\psi] + \frac{1}{4}\xi_0^{-1}\frac{\mathrm{d}}{\mathrm{d}\tau}\left[\xi_p^{-1}\frac{\mathrm{d}}{\mathrm{d}\tau}\left(\xi_p^{-1}\hat{S}(\tau)\right)\right]_{|\tau=\tau_0} \,, \tag{D.8g}$$

$$[\partial_u^4 \psi] = -\frac{1}{4}\left[-\frac{1}{2}\bar{\xi}_0^{-1}V\frac{\ddot{r}_0}{E} + \frac{1}{2}\bar{\xi}_0^{-1}V\frac{\mathrm{d}}{\mathrm{d}\tau}\left(\frac{f_p}{E}\xi_p^2\bar{\xi}_p^{-1}\right)_{|\tau=\tau_0} + 3\xi_0\bar{\xi}_0^{-1}\partial_u V\right.$$
$$\left. + \xi_0^2\bar{\xi}_0^{-2}\partial_v V\right][\partial_u\psi] \tag{D.8h}$$
$$+ \frac{1}{2}\xi_0\bar{\xi}_0^{-1}V[\partial_u^2\psi] - \frac{1}{4}\bar{\xi}_0^{-1}\frac{\mathrm{d}}{\mathrm{d}\tau}\left(\bar{\xi}_p^{-1}\frac{\mathrm{d}}{\mathrm{d}\tau}\left\{\bar{\xi}_p^{-1}\frac{\mathrm{d}}{\mathrm{d}\tau}\left[\bar{\xi}_p^{-1}\hat{S}(\tau)\right]\right\}\right)_{|\tau=\tau_0} \,,$$

$$[\partial_v^4 \psi] = \frac{1}{4}\left[-\frac{1}{2}\xi_0^{-1}V\frac{\ddot{r}_0}{E} + \frac{1}{2}\xi_0^{-1}V\frac{\mathrm{d}}{\mathrm{d}\tau}\left(\frac{f_p}{E}\bar{\xi}_p^2\xi_p^{-1}\right)_{|\tau=\tau_0} + 3\bar{\xi}_0\xi_0^{-1}\partial_v V\right.$$
$$\left. + \bar{\xi}_0^2\xi_0^{-2}\partial_u V\right][\partial_v\psi] \tag{D.8i}$$
$$- \frac{1}{2}\bar{\xi}_0\xi_0^{-1}V[\partial_v^2\psi] - \frac{1}{4}\xi_0^{-1}\frac{\mathrm{d}}{\mathrm{d}\tau}\left(\xi_p^{-1}\frac{\mathrm{d}}{\mathrm{d}\tau}\left\{\xi_p^{-1}\frac{\mathrm{d}}{\mathrm{d}\tau}\left[\xi_p^{-1}\hat{S}(\tau)\right]\right\}\right)_{|\tau=\tau_0} \,.$$

Table D.1: Jump conditions for the derivatives purely in the u or v directions. $\dot{r}$ and $\ddot{r}$ are the particle's radial velocity and acceleration, respectively. They are obtained from the equation of motion for the particle. $\bar{\xi} \equiv \frac{E-\dot{r}}{f}$ and $\xi \equiv \frac{E+\dot{r}}{f}$ were introduced for notational convenience. Quantities bearing a subscript p are evaluated on the particle's world line, while quantities bearing a subscript 0 are evaluated at the particle's current position. Derivatives of V with respect to either u or v are evaluated as $\partial_u V = -\frac{1}{2}f\partial_r V$ and $\partial_v V = \frac{1}{2}f\partial_r V$, respectively.

wave equation [Eq. (D.2)]. We see that

$$[\partial_u \partial_v \psi] = 0 \,, \tag{D.9}$$

and taking an additional derivative with respect to u on both sides reveals that

$$[\partial_u^2 \partial_v \psi] = -\frac{1}{4} V [\partial_u \psi] \,. \tag{D.10}$$

Systematically repeating this procedure we can find jump conditions for each of the mixed derivatives by evaluating

$$[\partial_u^{n+1} \partial_v^{m+1} \psi] = -\frac{1}{4} [\partial_u^n \partial_v^m (V \psi)] \,, \tag{D.11}$$

where $n, m \geq 0$ and derivatives of V with respect to either u or v are evaluated as $\partial_u V = -\frac{1}{2} f \partial_r V$ and $\partial_v V = \frac{1}{2} f \partial_r V$, respectively.

The results of Table D.1 and Eq. (D.11) allow us to express the coefficients of the left-hand polynomial in Eq. (D.1) in terms of the jump conditions and the coefficients of the right-hand side:

$$c'_{nm} = c_{nm} - [\partial_u^n \partial_v^m \psi] \,. \tag{D.12}$$

For $N = 4$ this leaves us with 25 unknown coefficients c_{nm} which can be uniquely determined by demanding that the polynomial match the value of the field on the 25 grid points surrounding the particle. When we are interested in integrating the polynomial, as in the case of the potential term in the fourth-order finite-difference scheme, we do not need all these terms. Instead, in order to calculate for example the integral $\iint_{\text{cell}} V \psi \, du \, dv$ up to terms of order h^5, as is needed to achieve overall $O(h^4)$ convergence, it is sufficient to include only terms such that $n + m \leq 2$, thus reducing the number of unknown coefficients to 6. In this case Eq. (D.1) becomes

$$p(t, r^*) = \begin{cases} \displaystyle\sum_{m+n \leq 2} \frac{c_{nm}}{n! \, m!} u^n v^m & \text{if } r^*(u, v) > r_0^* \\ \displaystyle\sum_{m+n \leq 2} \frac{c'_{nm}}{n! \, m!} u^n v^m & \text{if } r^*(u, v) < r_0^* \end{cases} \,. \tag{D.13}$$

The six coefficients can then be determined by matching the polynomial to the field values at the six grid points which lie within the past light cone of the grid point whose field value we want to calculate.

D.2 Electromagnetic case

D.2.1 Faraday tensor calculation

Since the source term in Eqs. (4.36) – (4.37a) contains a term proportional to $\delta'(r^* - r_0^*)$, the field is discontinuous across the world line of the particle. We only calculate jump conditions in the r^* direction up to $[\partial_{r^*} \psi]$, which we find by substituting the ansatz

$$\psi = \psi_<(t, r^*) \theta(r_0^* - r^*) + \psi_>(t, r^*) \theta(r^* - r_0^*) \tag{D.14}$$

into Eqs. (4.36) – (4.37a) and its t and r^* derivatives. Demanding in each step that the singularity structure on the left hand side matches that of the sources (and their derivatives) on the right hand side yields the jump conditions

$$[\psi] = \frac{F_\psi}{f_0[(\partial_t r_0^*)^2 - 1]} \,, \tag{D.15a}$$

and

$$[\partial_{r^*}\psi] = -\frac{G_\psi}{(\partial_t r_0^*)^2 - 1} - \frac{\partial_t^2 r_0^* \left[3 \left(\partial_t r_0^*\right)^2 + 1\right] F_\psi}{f_0 \left[(\partial_t r_0^*)^2 - 1\right]^3} + 2\frac{\partial_t r_0^* \, \partial_t \left(F_\psi/f_0\right)}{[(\partial_t r_0^*)^2 - 1]^2} \,, \tag{D.15b}$$

where ψ stands for either one of ψ, χ, or ξ.

D.2.2 Vector potential calculation

Since the source term in Eq. (2.53) is singular, the field is only continuous across the world line of the particle, but not smooth. For our purposes we only need the jump conditions in the r^* direction up to $[\partial_{r^*}^2\psi]$, which we find by substituting the ansatz

$$A_a^{\ell m}(t, r^*) = A_{a,<}^{\ell m}(t, r^*)\theta(r_0^* - r^*) + A_{a,>}^{\ell m}(t, r^*)\theta(r^* - r_0^*) \,, \tag{D.16a}$$

$$v^{\ell m}(t, r^*) = v_<^{\ell m}(t, r^*)\theta(r_0^* - r^*) + v_>^{\ell m}(t, r^*)\theta(r^* - r_0^*) \,, \tag{D.16b}$$

$$\tilde{v}^{\ell m}(t, r^*) = \tilde{v}_<^{\ell m}(t, r^*)\theta(r_0^* - r^*) + \tilde{v}_>^{\ell m}(t, r^*)\theta(r^* - r_0^*) \tag{D.16c}$$

into Eqs. (4.52a) – (4.52c) and its t and r^* derivatives. Demanding in each step that the singularity structure on the left hand side matches that of the sources (and their derivatives) on the right hand side yields the jump conditions

$$\left[A_a^{\ell m}\right] = \left[w^{\ell m}\right] = 0 \,, \tag{D.17a}$$

$$\left[\partial_{r^*} A_a^{\ell m}\right] = \frac{E^2}{E^2 - \dot{r}_0^2} S_a \,, \tag{D.17b}$$

$$\left[\partial_{r^*} w^{\ell m}\right] = \frac{E^2}{E^2 - \dot{r}_0^2} S_{\text{even/odd}} \,, \tag{D.17c}$$

$$\left[\partial_{r^*}^2 A_a^{\ell m}\right] = \left(\frac{2ME^4}{r_0^2(E^2 - \dot{r}_0^2)^2} - f_0\frac{(3\dot{r}_0^2 + E^2)E^2\ddot{r}_0}{(E^2 - \dot{r}_0^2)^3}\right) S_a \\ + \frac{2ME^3\dot{r}_0}{r_0^2(E^2 - \dot{r}_0^2)^2} S_b - f_0\frac{2E^2\dot{r}_0}{(E^2 - \dot{r}_0^2)^2} \dot{S}_a \,, \tag{D.17d}$$

$$\left[\partial_{r^*}^2 w^{\ell m}\right] = -f_0\frac{(3\dot{r}_0^2 + E^2)E^2\ddot{r}_0}{(E^2 - \dot{r}_0^2)^3} S_{\text{even/odd}} - f_0\frac{2E^2\dot{r}_0}{(E^2 - \dot{r}_0^2)^2} \dot{S}_{\text{even/odd}} \,, \tag{D.17e}$$

where $a, b \in \{t, r^*\}, a \neq b, w \in \{v, \tilde{v}\}$.

Appendix E

Regularization parameters for accelerated motion

Clearly a calculation of the self-force that only allows for geodesic motion of the particle is not fully consistent. The self-force affects the motion of the particle so that it never moves on a geodesic at all. Thankfully the effects of the self-force are small, of the order of $\frac{q^2}{M^2}$, so that the short term deviations from geodesic motion are also small. Since the effect of the self-force accumulates secularly, however, a geodesic treatment of the particle's motion will certainly be invalid for times of the order of the radiation reaction time. A formalism capable of handling the self-force experienced by a particle on an accelerated world line is needed to handle the long term evolution of the particle.

It turns out that the formalism described in chapter 2 requires only minor changes to accommodate a non-zero acceleration. The key issue is that acceleration terms only occur in expansions along the world line as described in section 2.6. Expansions away from the world line are always done along auxiliary geodesics so that for example the coordinate expansions of $\sigma_{\bar{\alpha}}$ and $g^{\bar{\alpha}}{}_{\alpha}$ do not change. The only expressions that require changes turn out to be the expansions of $\Delta_{\pm}$ in Eq. (2.79) as well as those for σ and σ_{α} in Eqs. (2.76) and (2.82). Following the steps outlined in section 2.6.1 and using

$$a_\mu \equiv u_{\mu;\nu} u^\nu \,, \quad \dot{a}_\mu \equiv a_{\mu;\nu} u^\nu \,, \quad \ldots \tag{E.1}$$

we find

$$\sigma(\tau) = \sigma(\bar{\tau}) + \dot{\sigma}(\bar{\tau})\Delta + \frac{1}{2}\ddot{\sigma}(\bar{\tau})\Delta^2 + \frac{1}{6}\dddot{\sigma}(\bar{\tau})\Delta^3$$
$$+ \frac{1}{24}\sigma^{(4)}(\bar{\tau})\Delta^4 + \frac{1}{120}\sigma^{(5)}(\bar{\tau})\Delta^5 + O(\Delta^6) \,, \tag{E.2a}$$

$$\sigma = \frac{1}{2}\sigma_{\bar{\alpha}}\sigma^{\bar{\alpha}} \,, \tag{E.2b}$$

$$\dot{\sigma} = \sigma_{\bar{\alpha}} u^{\bar{\alpha}} \,, \tag{E.2c}$$

$$\ddot{\sigma} = -1 - \frac{1}{3}R_{u\sigma u\sigma} + \frac{1}{12}R_{u\sigma u\sigma|\sigma} + \sigma_{\bar{\alpha}} a^{\bar{\alpha}} + O(\varepsilon^4) \,, \tag{E.2d}$$

$$\dddot{\sigma} = -\frac{1}{4}R_{u\sigma u\sigma|u} - R_{a\sigma u\sigma} + \sigma_{\bar{\sigma}} \dot{a}^{\bar{\alpha}} + O(\varepsilon^3) \,, \tag{E.2e}$$

$$\sigma^{(4)} = -R_{auu\sigma} + u_{\bar{\alpha}}\dot{a}^{\bar{\alpha}} + \sigma_{\bar{\alpha}}\ddot{a}^{\bar{\alpha}} + O(\varepsilon^2)\,, \tag{E.2f}$$

and

$$\sigma^{(5)} = -5a_{\bar{\alpha}}\dot{a}^{\bar{\alpha}} + O(\varepsilon)\,, \tag{E.2g}$$

where we have introduced the notation

$$R_{auu\sigma} \equiv R_{\bar{\alpha}\bar{\beta}\bar{\gamma}\bar{\delta}}a^{\bar{\alpha}}u^{\bar{\beta}}u^{\bar{\gamma}}\sigma^{\bar{\delta}} \tag{E.3}$$

to denote contractions of the Riemann tensor with the acceleration. Note that the normalization condition $u^\mu u_\mu = -1$ implies that a^μ and u^μ are perpendicular $a^\mu u_\mu = 0$; we have used this to simplify the last relation in Eq. (E.2).

Substituting these expressions into Eq. (2.75) and solving for the coefficients $\Delta_1,\ldots,\Delta_4$ we find for $\Delta_\pm$

$$
\begin{aligned}
\Delta_- = {} & [\bar{r} - s] - \left[\frac{a_\sigma(\bar{r}-s)^2}{2s}\right] + \left[\frac{(\bar{r}-s)^3(a_\sigma)^2(3s+\bar{r})}{8s^3}\right.\\
& + \frac{(\bar{r}-s)^3(\dot{a}_u(s-\bar{r}) - 4\dot{a}_\sigma)}{24s} + \left.\frac{(\bar{r}-s)^2 R_{u\sigma u\sigma}}{6s}\right] + \Bigg[\\
& -\frac{(\bar{r}-s)^4(a_\sigma)^3(5s^2 + 4\bar{r}s + \bar{r}^2)}{16s^5} - \frac{(\bar{r}-s)^4}{48s^3}\Big(2\dot{a}_a s^3 + 5s^2 a_\sigma \dot{a}_u - 2s^2 \dot{a}_a \bar{r} \\
& \qquad\qquad - 4sa_\sigma \bar{r}\dot{a}_u - 16 sa_\sigma \dot{a}_\sigma - a_\sigma \bar{r}^2 \dot{a}_u - 4a_\sigma \bar{r}\dot{a}_\sigma\Big) \\
& -\frac{(\bar{r}-s)^3}{24s^3}\Big(s^3 R_{auu\sigma} + s^3\ddot{a}_\sigma - 4s^2 R_{a\sigma u\sigma} - s^2\ddot{a}_\sigma \bar{r} - s^2 R_{auu\sigma}\bar{r} + 6R_{u\sigma u\sigma}a_\sigma s \\
& \quad + 2R_{u\sigma u\sigma}a_\sigma \bar{r}\Big) - \frac{(\bar{r}-s)^2(R_{u\sigma u\sigma|\sigma} + R_{u\sigma u\sigma|u}s - R_{u\sigma u\sigma|u}\bar{r})}{24s}\Bigg] + O(\varepsilon^5)\,,
\end{aligned}
\tag{E.4a}
$$

and

$$
\begin{aligned}
\Delta_+ = {} & [\bar{r} + s] + \left[\frac{a_\sigma(\bar{r}+s)^2}{2s}\right] + \left[\frac{(\bar{r}+s)^3(a_\sigma)^2(3s-\bar{r})}{8s^3}\right.\\
& + \frac{(\bar{r}+s)^3(\dot{a}_u(s+\bar{r}) + 4\dot{a}_\sigma)}{24s} - \left.\frac{(\bar{r}+s)^2 R_{u\sigma u\sigma}}{6s}\right] \\
& + \left[\frac{(\bar{r}+s)^4(a_\sigma)^3(5s^2 - 4\bar{r}s + \bar{r}^2)}{16s^5} - \frac{(\bar{r}+s)^4}{48s^3}\Big(2\dot{a}_a s^3 - 5s^2 a_\sigma \dot{a}_u + 2s^2 \dot{a}_a \bar{r}\right.\\
& \qquad\qquad - 4sa_\sigma \bar{r}\dot{a}_u - 16 sa_\sigma \dot{a}_\sigma + a_\sigma \bar{r}^2 \dot{a}_u + 4a_\sigma \bar{r}\dot{a}_\sigma\Big) \\
& -\frac{(\bar{r}+s)^3}{24s^3}\Big(s^3 R_{auu\sigma} + s^3\ddot{a}_\sigma + 4s^2 R_{a\sigma u\sigma} + s^2\ddot{a}_\sigma \bar{r} + s^2 R_{auu\sigma}\bar{r} + 6R_{u\sigma u\sigma}a_\sigma s \\
& \quad - 2R_{u\sigma u\sigma}a_\sigma \bar{r}\Big) - \frac{(\bar{r}+s)^2(-R_{u\sigma u\sigma|\sigma} + R_{u\sigma u\sigma|u}s + R_{u\sigma u\sigma|u}\bar{r})}{24s}\Bigg] + O(\varepsilon^5)\,,
\end{aligned}
\tag{E.4b}
$$

where we have introduced the notation $a_\sigma \equiv a^{\bar{\alpha}}\sigma_{\bar{\alpha}}$ and its variants. It has already been used for contractions involving the Riemann tensor earlier.

Similarly we find coefficients for the expansion of σ_α along the world line as in Eq. (2.82). We find

$$\dot{\sigma}_\alpha = -g^{\bar{\alpha}}{}_\alpha \left(u_{\bar{\alpha}} + \frac{1}{6} R_{\bar{\alpha}\sigma u\sigma} - \frac{1}{12} R_{\bar{\alpha}\sigma u\sigma\sigma} \right) + O(\varepsilon^4) \,, \tag{E.5a}$$

$$\ddot{\sigma}_\alpha = -g^{\bar{\alpha}}{}_\alpha \left(\frac{2}{3} R_{\bar{\alpha}uu\sigma} - \frac{1}{4} R_{\bar{\alpha}uu\sigma|\sigma} - \frac{1}{12} R_{\bar{\alpha}\sigma\sigma u|u} - a_{\bar{\alpha}} - R_{\alpha\sigma a\sigma} \right) + O(\varepsilon^3) \,, \tag{E.5b}$$

$$\dddot{\sigma}_\alpha = -g^{\bar{\alpha}}{}_\alpha \left(\frac{1}{2} R_{\bar{\alpha}uu\sigma} + R_{\bar{\alpha}ua\sigma} + R_{\bar{\alpha}au\sigma} - \dot{a}_{\bar{\alpha}} \right) + O(\varepsilon^2) \,, \tag{E.5c}$$

and

$$\sigma_\alpha^{(4)} = -g^{\bar{\alpha}}{}_\alpha \left(R_{\bar{\alpha}uau} + \ddot{a}_{\bar{\alpha}} \right) + O(\varepsilon) \,. \tag{E.5d}$$

Eqs. (E.2), (E.4) and (E.5) are valid for arbitrary values of a_α. In a self-force calculation, the acceleration is small and we only keep terms that are first order or lower in the acceleration or its derivatives. This simplifies the calculations tremendously, since not only terms quadratic in the acceleration vanish, but also contractions between u_α and $\dot{a}_\alpha$ or $\ddot{a}_\alpha$. This follows because the identity

$$0 = u^\alpha a_\alpha \tag{E.6}$$

yields, after taking a derivative with respect to τ on both sides,

$$0 = \frac{\mathrm{D}}{\mathrm{d}\tau} \left(u^\alpha a_\alpha \right) = a^\alpha a_\alpha + u^\alpha \dot{a}_\alpha = u^\alpha \dot{a}_\alpha + O(\mu^2) \,, \tag{E.7}$$

where μ is a bookkeeping parameter that keeps track of powers of a_α.

As an example we calculate the regularization parameters for the scalar field, including first order acceleration terms. We proceed exactly as in section 3.6 substituting Eqs. (E.2), (E.4) and (E.5) for Eqs. (2.76), (2.79) and (2.82) where appropriate.

First we find the gradient of the singular field to be

$$
\begin{aligned}
\Phi^{\rm S}_\alpha = q^2 g^{\bar\alpha}{}_\alpha \Bigg(\Bigg\{ &\Bigg[\Bigg(-\frac{5\bar{r}(\bar{r}-s)^2(\bar{r}+s)^2}{4s^7} R_{u\sigma u\sigma} a_\sigma + \frac{\bar{r}(3\bar{r}^4 - 10s^2\bar{r}^2 + 15s^4)}{24s^5}\ddot{a}_\sigma \\
&+ \frac{\bar{r}(3\bar{r}^4 - 10s^2\bar{r}^2 + 15s^4)}{24s^5} R_{auu\sigma} + \frac{(\bar{r}-s)^2(\bar{r}+s)^2}{2s^5} R_{a\sigma u\sigma} \Bigg) u_{\bar\alpha} \\
&+ \Bigg(-\frac{(\bar{r}-s)(\bar{r}+s)(-s^2+5\bar{r}^2)}{4s^7} R_{u\sigma u\sigma} a_\sigma + \frac{(\bar{r}-s)^2(\bar{r}+s)^2}{8s^5}\ddot{a}_\sigma \\
&+ \frac{(\bar{r}-s)^2(\bar{r}+s)^2}{8s^5} R_{auu\sigma} + \frac{(\bar{r}-s)\bar{r}(\bar{r}+s)}{2s^5} R_{a\sigma u\sigma} \Bigg) \sigma_{\bar\alpha} - \frac{(\bar{r}-s)^2(\bar{r}+s)^2}{2s^5} a_\sigma R_{\bar\alpha uu\sigma} \\
&- \frac{(\bar{r}-s)\bar{r}(\bar{r}+s)}{4s^5} a_\sigma R_{\bar\alpha\sigma u\sigma} + \frac{(\bar{r}-s)^2(\bar{r}+s)^2}{4s^5} a_{\bar\alpha} R_{u\sigma u\sigma} \\
&+ \frac{-6s^2\bar{r}^2 + \bar{r}^4 - 3s^4}{24s^3} R_{\bar\alpha uau} + \frac{\bar{r}(-3s^2+\bar{r}^2)}{6s^3} R_{\bar\alpha uas} + \frac{\bar{r}(-3s^2+\bar{r}^2)}{6s^3} R_{\bar\alpha aus} \\
&+ \frac{(\bar{r}-s)(\bar{r}+s)}{12s^3} R_{\bar\alpha\sigma as} + \frac{-6s^2\bar{r}^2 + \bar{r}^4 - 3s^4}{24s^3}\ddot{a}_{\bar\alpha} \Bigg]\epsilon \\
&+ \Bigg[-\frac{(\bar{r}-s)^2(\bar{r}+s)^2}{2s^5}\dot{a}_\sigma u_{\bar\alpha} - \frac{(\bar{r}-s)\bar{r}(\bar{r}+s)}{2s^5}\dot{a}_\sigma\sigma_{\bar\alpha} + \frac{\bar{r}(-3s^2+\bar{r}^2)}{6s^3}\dot{a}_{\bar\alpha} \Bigg] \\
&+ \Bigg[-\frac{3(\bar{r}-s)\bar{r}(\bar{r}+s)}{2s^5} a_\sigma u_{\bar\alpha} - \frac{(-s^2+3\bar{r}^2)}{2s^5} a_\sigma\sigma_{\bar\alpha} + \frac{(\bar{r}-s)(\bar{r}+s)}{2s^3} a_{\bar\alpha} \Bigg]\epsilon^{-1} \Bigg\}\mu \\
&+ \Bigg[\Bigg(\frac{(\bar{r}-s)^2(\bar{r}+s)^2}{8s^5} R_{u\sigma u\sigma|u} - \frac{(\bar{r}-s)\bar{r}(\bar{r}+s)}{8s^5} R_{u\sigma u\sigma|\sigma} \Bigg) u_{\bar\alpha} \\
&+ \Bigg(\frac{(\bar{r}-s)\bar{r}(\bar{r}+s)}{8s^5} R_{u\sigma u\sigma|u} - \frac{(-s^2+3\bar{r}^2)}{24s^5} R_{u\sigma u\sigma|\sigma} \Bigg) \sigma_{\bar\alpha} - \frac{(\bar{r}-s)(\bar{r}+s)}{24s^3} R_{\bar\alpha\sigma\sigma u|u} \\
&- \frac{(\bar{r}-s)(\bar{r}+s)}{8s^3} R_{\bar\alpha uu\sigma|\sigma} - \frac{\bar{r}}{12s^3} R_{\bar\alpha\sigma u\sigma|\sigma} + \frac{\bar{r}(-3s^2+\bar{r}^2)}{12s^3} R_{\bar\alpha uu\sigma|u} \Bigg]\epsilon \\
&+ \Bigg[\frac{(\bar{r}-s)\bar{r}(\bar{r}+s)}{2s^5} R_{u\sigma u\sigma} u_{\bar\alpha} + \frac{(-s^2+3\bar{r}^2)}{6s^5} R_{u\sigma u\sigma}\sigma_{\bar\alpha} + \frac{(\bar{r}-s)(\bar{r}+s)}{3s^3} R_{\bar\alpha uu\sigma} \\
&+ \frac{\bar{r}}{6s^3} R_{\bar\alpha\sigma u\sigma} \Bigg] + \Bigg[\frac{\bar{r}u_{\bar\alpha} + \sigma_{\bar\alpha}}{s^3} \Bigg]\epsilon^{-2} \Bigg).
\end{aligned}
$$

$$\text{(E.8)}$$

We submit the expression in Eq. (E.8) to the multipole decomposition procedure outlined in section 3.6. After a lengthy calculation we find the regularization parameters to be

$$
A_{(0)} = \frac{\sqrt{r_0}\dot{r}_0\,\mathrm{sign}(\Delta)}{\sqrt{r_0 - 2\bar{M}(r_0^2 + J^2)}}, \tag{E.9a}
$$

$$
A_{(+)} = -\frac{E\sqrt{r_0}\,\mathrm{sign}(\Delta)}{\sqrt{r_0 - 2\bar{M}(r_0^2 + J^2)}}e^{i\varphi_0}, \tag{E.9b}
$$

as well as

$$B_{(0)} = \left[\left(-\frac{r_0^{5/2}(J^2 - r_0^2)Ea_\phi}{(r_0^2 + J^2)^{3/2}\pi J\sqrt{r_0 - 2M}} + \frac{\sqrt{r_0 - 2M}a_t}{\sqrt{(r_0^2 + J^2)r_0}\pi}\right)\mu\right.$$
$$\left. - \frac{2r_0^{3/2}\dot{r}_0 E}{(r_0^2 + J^2)^{3/2}\pi\sqrt{r_0 - 2M}}\right]\mathcal{E} \quad \text{(E.10a)}$$
$$+ \left[-\frac{r_0^{9/2}Ea_\phi}{(r_0^2 + J^2)^{3/2}(r_0 - 2M)^{1/2}J\pi}\mu + \frac{r_0^{3/2}\dot{r}_0 E}{(r_0^2 + J^2)^{3/2}\pi\sqrt{r_0 - 2M}}\right]\mathcal{K},$$

$$B_{(+)} = \left\{\left[\left(\frac{(J^2 - r_0^2)r_0^{5/2}\dot{r}_0 a_\phi}{\sqrt{r_0 - 2M}J(r_0^2 + J^2)^{3/2}\pi} - \frac{\sqrt{r_0}a_r}{\sqrt{r_0^2 + J^2}\sqrt{r_0 - 2M}\pi}\right.\right.\right.$$
$$\left. + \frac{ia_\phi}{\sqrt{r_0^2 + J^2}r_0^3\pi J^2}\right)\mu - \frac{i(\sqrt{r_0 - 2M} - 2\sqrt{r_0})\dot{r}_0}{\sqrt{r_0 - 2M}\pi J\sqrt{r_0^2 + J^2}^{1/2}}$$
$$\left. + \frac{2r_0^{3/2}E^2}{(r_0^2 + J^2)^{3/2}\pi\sqrt{r_0 - 2M}} - \frac{\sqrt{r_0 - 2M}}{\sqrt{r_0^2 + J^2}r_0^{3/2}\pi}\right]\mathcal{E} \quad \text{(E.10b)}$$
$$+ \left[\left(\frac{a_\phi\dot{r}_0}{(r_0^2 + J^2)^{3/2}\sqrt{r_0 - 2M}r_0^{9/2}J\pi} - \frac{ia_\phi}{\sqrt{r_0^2 + J^2}r_0^3\pi J^2}\right)\mu\right.$$
$$+ \frac{i(\sqrt{r_0 - 2M} - 2\sqrt{r_0}\dot{r}_0)}{\pi\sqrt{r_0 - 2M}\sqrt{r_0^2 + J^2}J} - \frac{r_0^{3/2}E^2}{(r_0^2 + J^2)^{3/2}\pi\sqrt{r_0 - 2M}}$$
$$\left.\left. + \frac{2r_0 - \sqrt{r_0(r_0 - 2M)}}{r_0^2\pi\sqrt{r_0^2 + J^2}}\right]\mathcal{K}\right\}e^{i\varphi_0}.$$

The C terms vanish as they did for the geodesic case.

While we did obtain expressions for the D terms, they are much to long to be displayed even in an appendix. Comparing them to the B terms we find that the D terms depend not just on the acceleration, but also on its first and second derivatives with respect to proper time.

These regularization parameters agree with the results obtained in [16] for a radially infalling particle.
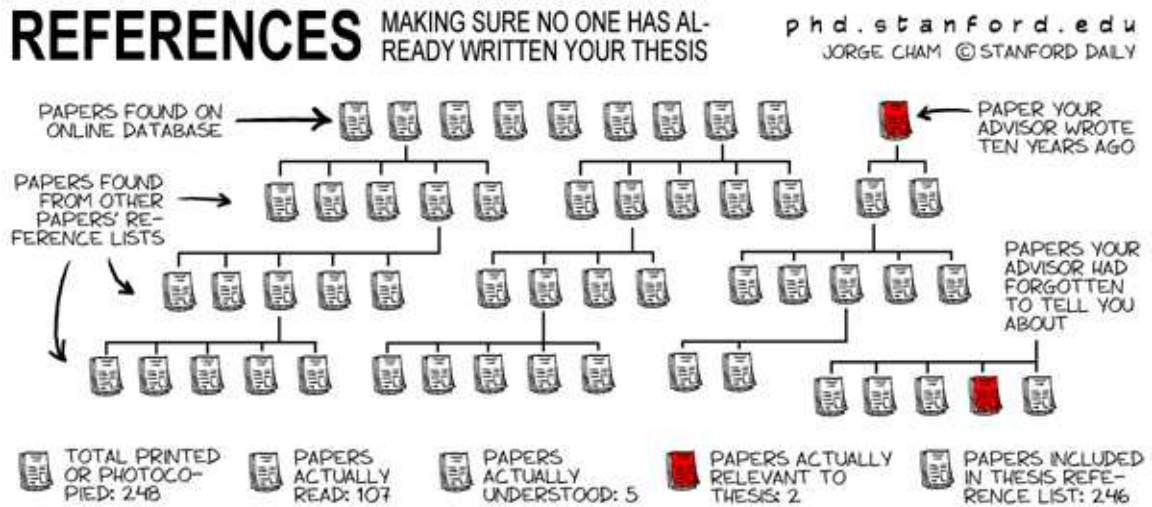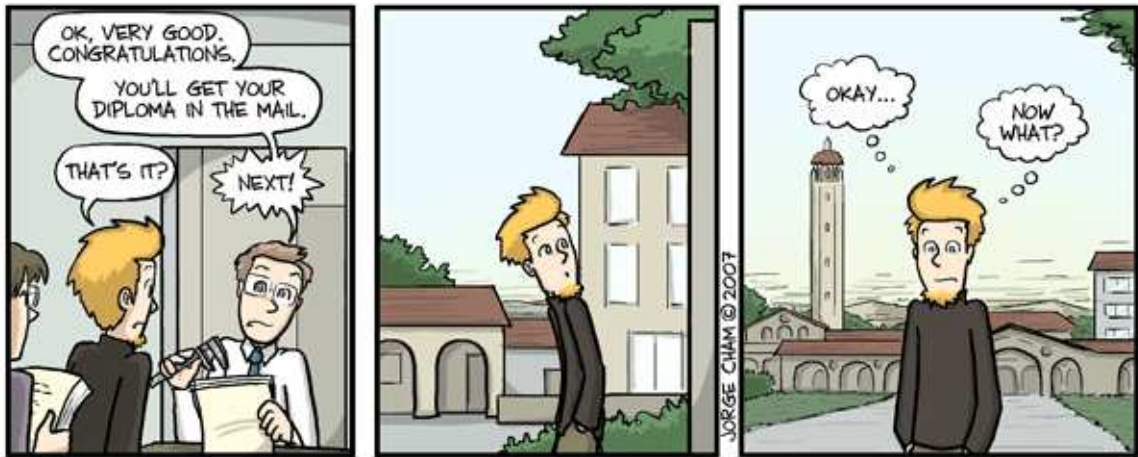
"Piled Higher and Deeper" by Jorge Cham, www.phdcomics.com

Bibliography

[1] Leor Barack and Amos Ori. Mode sum regularization approach for the self-force in black hole spacetime. *Phys. Rev. D*, 61(6):061502, Feb 2000.

[2] Leor Barack, Yasushi Mino, Hiroyuki Nakano, Amos Ori, and Misao Sasaki. Calculating the gravitational self force in Schwarzschild spacetime. *Phys. Rev. Lett.*, 88:091101, 2002.

[3] Steven Detweiler and Bernard F. Whiting. Self-force via a Green's function decomposition. *Phys. Rev. D*, 67:024025, 2003.

[4] Carlos O. Lousto and Richard H. Price. Understanding initial data for black hole collisions. *Phys. Rev. D*, 56(10):6439–6457, Nov 1997.

[5] Carlos O. Lousto. A time-domain fourth-order-convergent numerical algorithm to integrate black hole perturbations in the extreme-mass- ratio limit. *Class. Quant. Grav.*, 22:S543–S568, 2005.

[6] Max Abraham. Prinzipien der dynamik des elektrons. *Annalen der Physik*, 315:105–179, 1903.

[7] H.A. Lorentz. Electromagnetic phenomena in a system moving with any velocity smaller than that of light. *Proc. Acad. Science Amsterdam*, 6:809–831, 1904.

[8] P.A.M. Dirac. Classical theory of radiating electrons. *Proc. R. Soc. London, Ser. A*, 167:148, 1938.

[9] B.S. DeWitt and R.W. Brehme. Radiation damping in a gravitational field. *Ann. Phys. (N.Y.)*, 9:220–259, 1960.

[10] J.M. Hobbs. A vierbein formalism for radiation damping. *Ann. Phys. (N.Y.)*, 47:141–165, 1968.

[11] Yasushi Mino, Misao Sasaki, and Takahiro Tanaka. Gravitational radiation reaction to a particle motion. *Phys. Rev. D*, 55(6):3457–3476, Mar 1997.

[12] Theodore C. Quinn and Robert M. Wald. Axiomatic approach to electromagnetic and gravitational radiation reaction of particles in curved spacetime. *Phys. Rev. D*, 56(6):3381–3394, Sep 1997.

[13] Chad R. Galley and B. L. Hu. Self-force on extreme mass ratio inspirals via curved spacetime effective field theory. 2008.

[14] Abraham I. Harte. Self-forces from generalized Killing fields. 2008.

[15] Yasushi Mino, Hiroyuki Nakano, and Misao Sasaki. Covariant self-force regularization of a particle orbiting a Schwarzschild black hole: Mode decomposition regularization. *Prog. Theor. Phys.*, 108:1039–1064, 2003.

[16] Leor Barack. Self-force on a scalar particle in spherically-symmetric spacetime via mode-sum regularization: Radial trajectories. *Phys. Rev. D*, 62:084027, 2000.

[17] Lior M. Burko. Self force on particle in orbit around a black hole. *Phys. Rev. Lett.*, 84:4529, 2000.

[18] Steven Detweiler, Eirini Messaritaki, and Bernard F. Whiting. Self-force of a scalar field for circular orbits about a schwarzschild black hole. *Phys. Rev. D*, 67(10):104016, May 2003.

[19] Leor Barack and Carlos O. Lousto. Perturbations of Schwarzschild black holes in the Lorenz gauge: Formulation and numerical implementation. *Phys. Rev. D*, 72:104026, 2005.

[20] Leor Barack and Norichika Sago. Gravitational self force on a particle in circular orbit around a Schwarzschild black hole. *Phys. Rev.*, D75:064021, 2007.

[21] Leor Barack and Darren A. Golbourn. Scalar-field perturbations from a particle orbiting a black hole using numerical evolution in 2+1 dimensions. *Phys. Rev.*, D76:044020, 2007.

[22] Tobias S. Keidl, John L. Friedman, and Alan G. Wiseman. On finding fields and self-force in a gauge appropriate to separable wave equations. *Phys. Rev.*, D75:124009, 2007.

[23] Roland Haas and Eric Poisson. Mode-sum regularization of the scalar self-force: Formulation in terms of a tetrad decomposition of the singular field. *Phys. Rev. D*, 74(4):044009, 2006.

[24] Roland Haas. Scalar self-force on eccentric geodesics in Schwarzschild spacetime: a time-domain computation. *Phys. Rev. D*, 75:124011, 2007.

[25] The LISA web site is located at `http://lisa.jpl.nasa.gov/`.

[26] The LIGO, VIRGO, GEO and TAMA sites are located at `http://www.ligo.caltech.edu/`, `http://www.virgo.infn.it/`, `http://www.geo600.uni-hannover.de/` and `http://tamago.mtk.nao.ac.jp/` respectively.

[27] Scott A. Hughes. LISA sources and science. 2007.

[28] Niel J. Cornish. Detection Strategies for Extreme Mass Ratio Inspirals. 2008.

[29] Steve Drasco and Scott A. Hughes. Gravitational wave snapshots of generic extreme mass ratio inspirals. *Phys. Rev.*, D73:024027, 2006.

[30] Steve Drasco. Strategies for observing extreme mass ratio inspirals. *Class. Quant. Grav.*, 23:S769–S784, 2006.

[31] Ian Vega and Steven Detweiler. Regularization of fields for self-force problems in curved spacetime: foundations and a time-domain application. *Phys. Rev. D*, 77:084008, 2008.

[32] Luz Maria Diaz-Rivera, Eirini Messaritaki, Bernard F. Whiting, and Steven Detweiler. Scalar field self-force effects on orbits about a schwarzschild black hole. *Physical Review D (Particles, Fields, Gravitation, and Cosmology)*, 70(12):124018, 2004.

[33] Eric Poisson. The motion of point particles in curved spacetime. *Living Reviews in Relativity*, 7(6), 2004.

[34] Robert M. Wald. *General relativity*. University of Chicago Press, Chicago, 1984.

[35] Warren G. Anderson, Eanna E. Flanagan, and Adrian C. Ottewill. Quasi-local contribution to the gravitational self- force. *Phys. Rev. D*, 71:024036, 2005.

[36] George B. (George Brown) Arfken and Hans-Jurgen Weber. *Mathematical methods for physicists*. Elsevier Academic Press, Amsterdam ; Burlington, MA, 2005.

[37] Leor Barack and Amos Ori. Regularization parameters for the self force in Schwarzschild spacetime. I: Scalar case. *Phys. Rev. D*, 66:084022, 2002.

[38] C. G. Darwin. The gravity field of a particle. *Proc. R. Soc. A*, 249(1257):180–194, Jan 1959.

[39] Richard H. Price. Nonspherical perturbations of relativistic gravitational collapse. i. scalar and gravitational perturbations. *Phys. Rev. D*, 5(10):2419–2438, May 1972.

[40] Tullio Regge. Stability of a Schwarzschild singularity. *Phys. Rev.*, 108:1063–1069, 1957.

[41] Norichiga Sago. Talk in 10th Capra meeting at UAH (2007).

[42] Adam Pound and Eric Poisson. Multi-scale analysis of the electromagnetic self-force in a weak gravitational field. *Phys. Rev. D*, 77:044012, 2008.

[43] Michael J. Pfenning and Eric Poisson. Scalar, electromagnetic, and gravitational self-forces in weakly curved spacetimes. *Phys. Rev. D*, 65:084001, 2002.

[44] Cécile DeWitt-Morette and Bryce Seligman Dewitt. *Relativite, groups et topologie = Relativity, groups and topology : lectures delivered at les Houches during the 1963 session of the Summer School of.* Gordon and Breach, New York, 1964.

[45] Steven Detweiler. A consequence of the gravitational self-force for circular orbits of the Schwarzschild geometry. *Phys. Rev.*, D77:124026, 2008.

[46] Norichiga Sago. Talk in 11th Capra meeting in Orléans (2008).

[47] John David Jackson. *Classical electrodynamics.* Wiley, New York ; Chichester [England], 1999.

[48] Karl Martel. Gravitational waveforms from a point particle orbiting a Schwarzschild black hole. *Phys. Rev. D*, 69:044025, 2004.

"Piled Higher and Deeper" by Jorge Cham, www.phdcomics.com